Investigating the role and regulation of human mitochondrial poly(A) polymerase

William Casey Wilson

Wellcome Trust Centre for Mitochondrial Research

Institute for Ageing and Health

Newcastle University

Thesis submitted to Newcastle University in candidature for the degree of Doctor of Philosophy

October 2013

Abstract

Polyadenylation by the mitochondrial poly(A) polymerase (mtPAP) is a crucial step of post-transcriptional modification in mammalian gene expression. In human mitochondria, polyadenylation is required for completion of seven UAA stop codons following complete processing of the major polycistronic RNA unit. Patients homozygous for a 1432A>G mutation in the *PAPD1* gene, which encodes mtPAP, suffer from symptoms consistent with mitochondrial disease including autosomal-recessive spastic ataxia and optic atrophy. The principal defect of the 1432A>G mutation is short adenylate tails on mt-mRNAs. Fibroblast lines from patients harboring the 1432A>G *PAPD1* mutation were established, and analysis of mitochondrial gene expression showed non-uniform dysregulation. For mt-mRNAs and translation products, there is a mix of depletion, stabilization and no effect, leading to major deficits at steady-state protein levels and of respiratory complexes. To confirm the pathological nature of the mutation, a complementation experiment was performed, which showed that expression of the WT *PAPD1* gene rescued the mutant phenotype. To assess whether catalytic activity was altered in the mutant enzyme, *in vitro* polyadenylation assays with WT and N478D recombinant mtPAP were undertaken. The N478D mtPAP was found to generate the short oligo(A) tails as observed *in vivo*. In addition, the presence of the LRPPRC/SLIRP complex increased the maximal poly(A) extensions generated by both WT and mutant mtPAP. Finally, experiments were undertaken to identify factors potential interacting with mtPAP. The major interacting factor was found to be ATAD3, a protein reported to be involved with multiple mitochondrial processes involving DNA and translation machinery in the form of nucleoids or mitoribosomes respectively. In summary, these investigations provide insights into the impact and regulation of mitochondrial polyadenylation, and contribute towards unraveling the complexities of post-transcriptional maturation in human mitochondrial gene expression.

Acknowledgements

I would first like to thank my supervisors, Bob and Zosia, for taking me on as a student. Throughout my studies, they have provided mentorship and support, not just at the critical junctures, but whenever I knocked on their office door to share new results or general thoughts. Through them, I have had the opportunity to create a strong foundation on which to build a scientific career, and for that I am immensely grateful.

I absolutely have to thank the current and previous members of the Lightowlers lab: Martin, Paul, Ola, Francesco, Alina, Agata, Abdulraheem, Marysia, Kyle, Rawaa, Monika, Fei, Nicole, and Tran. All of you made the lab feel like a family. I enjoyed coming to work every day, and you all are a big reason for that. It is easy to work hard, and for long hours, when you feel like you're just spending time with friends. We struggled and persevered together. Thank you all so much. I will miss you!

I would also like to thank the rest of the mitochondrial research group. I don't think anyone could ask for a nicer, more fun, or more wonderful group of people to spend a few years with. Everyone has shown incredible tolerance for my occasional braggadocio and outlandish journal club emails!

I would especially like to thank Martin Meagher and Paul Smith, as they became my first and best friends in Newcastle, and helped make moving half-way across the world from home a lot easier.

I am incredibly grateful for my fantastic collaborators: Professor Andrew Crosby, Professor Nils Larsson, Dr. Henrik Spahr, Professor Liang Tong, Dr. Jeong Ho Chang, Professor Rick Lewis, Dr. Lorraine Hewitt, Dr. Arnaud Basal, Professor Jean-Claude Martinou, Alexis Jourdain, Dr. Francesco Bruni, and Dr. Hue-Tran Hornig-Do. All of their incredible work, research input, and helpful discussions have been critical for the project. They deserve massive amounts of credit. Of course, this project could not have been undertaken without the participation of the patients. Their contribution is invaluable.

I would very much like to thank my funding sources, The Pathological Society of Great Britain and Ireland, and Newcastle University.

Finally, I would like to thank my family. They have never been shy about saying how proud they are of me, and I hope the work I have done here is worthy of that pride. I love them very much, and while I will be sad to leave England, I am looking forward to being a little closer to home.

Table of Contents

List of Figures

List of Tables

Abbreviations

^{32}P: Phosphate 32 radioactive isotope

^{35}S: Sulfur 35 radioactive isotope

CO, COX: Cytochrome *c* Oxidase

SDHA: Succinate dehydrogenase subunit A

aa: amino acid

ATP: adenosine triphosphate

ADP: adenosine diphosphate

Amp: ampicillin

APS: ammonium persulfate

BN: Blue native

BSA: bovine serum albumin

CBB: Coomassie brilliant blue

CIAA: 24:1 chloroform: isoamylalcohol

CMV: cytomegalovirus

cpm: counts per minute

C-terminus: carboxy-terminus

CYB: cytochrome *b*

DEPC: diethyl pyrocarbonate

dH2O: distilled water

D-Loop: displacement loop

DMEM: Dulbecco's modified Eagle's medium

DMSO: Dimethyl sulfoxide

DNA: deoxyribonucleic acid

dNTP: deoxynucleotide triphosphate

dsDNA: double-stranded DNA

DTT: dithiothreitol

Dulbecco's A-PBS: Calcium and magnesium-free phosphate buffered saline

E. *coli*: *Escherichia coli*

EDTA: Ethylenediaminetetraacetic acid

EGTA: Ethylene glycol-bis(2-aminoethylether)-*N,N,N′,N′*-tetraacetic acid

EtOH: ethanol

FAD: flavin adenine dinucleotide (oxidized)

$FADH_2$: flavin adenine dinucleotide (reduced)

FBS: Fetal calf serum

GAL: galactose

Glu: glucose

GST: Glutathione S-transferase

dGTP: Deoxyguanosine triphosphate

hrs: hours

HEK293: Flp-In™ T-REx™ HEK293 Human embryonic kidney cells

HRP: Horseradish peroxidase

HSP: Heavy strand promoter

H-strand: Heavy strand

IAA: Isoamyl alcohol

IgG: Immunoglobulin G

IMM: Inner mitochondrial membrane

IMS: intermembrane space

IP: immunoprecipitation

IPTG**:** Isopropyl β-D-thiogalactoside

JC1: 5,5′,6,6′-Tetrachloro-1,1′,3,3′-tetraethyl-imidacarbocyanine iodide

kDa: kilodalton

kb: kilobase

LB: Luria-Bertani media

LC MS/MS: liquid chromatography tandem mass spectrometry

LRPPRC: leucine-rich pentatricopeptide repeat containing protein

LSP: Light strand promoter

L-strand: light strand

LVPAPD1: lentiviral vector containing a copy of WT PAPD1 gene

min: minutes

MOPS: morpholinopropanesulfonic acid

MPAT: mitochondrial poly(A) tail assay

mRNA: messenger RNA

mt: mitochondrial

mt-mRNA: mitochondrial mRNA

mtDNA: mitochondrial DNA

mtPAP: human mitochondrial poly(A) polymerase

NAD+: nicotinamide adenine dinucleotide (oxidized)

NADH: nicotinamide adenine dinucleotide (reduced)

NEAA: Non-essential amino acids

ND: NADH dehydrogenase

nDNA: nuclear DNA

NP-40: octylphenoxypolyethoxyethanol (NP-40)

nt: nucleotides

N-terminus: amino-terminus

OD: optical density

OMM: Outer mitochondrial membrane

ORF: open reading frame

Ori_H: origin of heavy-strand replication

Ori_L: origin or light-strand replication

OXPHOS: oxidative phosphorylation

PAPD1: Gene encoding human mitochondrial poly(A) polymerase

PAGE: polyacrylamide gel electrophoresis

PBS: phosphate-buffered saline

PCR: polymerase chain reaction

P_i: inorganic phosphate

PI: Protease inhibitor cocktail

PMSF: phenylmethylsulfonyl fluoride

PNK: polynucleotide kinase

Poly(A): polyadenylation

PVDF: polyvinylidene difluoride

RISC: RNA-induced silencing complex

RNA: ribonucleic acid

ROS: reactive oxygen species

rpm: revolutions per minute

rRNA: ribosomal RNA

RT: Room temperature

Sec: seconds

SDHA: Succinate dehydrogenase subunit A

SDS: sodium dodecyl sulfate

siRNA: small interfering RNA

S/N: supernatant

SOC: super optimal broth with added magnesium and glucose

SSC: Saline sodium citrate buffer

ssDNA: single-stranded DNA

SSPE: saline sodium phosphate EDTA buffer

T_a: annealing temperature

TAE: tris acetate EDTA buffer

Taq: DNA polymerase from *Thermus aquaticus*

TBS: tris-buffered saline

TBST: tris-buffered saline with 0.1% Tween-20

TEMED: N,N,N',N'-Tetramethylethylenediamine

Tet: tetracycline

TOM20: translocase of the outer mitochondrial membrane

tRNA: transfer RNA

Tris: 2-Amino-2-hydroxymethyl-propane-1,3-diol

Triton X-100**:** 4-(1,1,3,3-Tetramethylbutyl)phenyl-polyethylene glycol

Tween 20: Polyethylene glycol sorbitan monolaurate

UTR: untranslated region

UV: ultraviolet

vol: volume

WT: wild-type

Chapter 1

Introduction

1.1 Mitochondria - General Background

Eukaryotic cells have long benefitted from the acquisition of the mitochondrial organelle from its prokaryotic ancestry. Its numerous functions in mammalian cells include carrying out oxidative phosphorylation, housing the Krebs cycle, playing a central role in apoptotic cell death pathways, calcium homeostasis, and the most highly conserved function: biogenesis of iron-sulfur clusters. Other than the nucleus, it is the only organelle in human cells that contains its own genome (mtDNA), encoding its own proteins, rRNA, and tRNAs. As my research has focused exclusively on human mitochondria any references to mitochondria in this thesis will be human-oriented unless specified otherwise.

Mitochondria exhibit a filamentous and reticular structure. The word mitochondrion comes from the Greek words *mitos* and *chondrion*, which mean thread and granule, respectively. Visible by both light and electron microscopy, the organelles range from 0.2-0.8um in length and 0.5-2um in width (Kaasik *et al.*, 2007). The number of mitochondria present in cells is usually closely related to their metabolic demand. Thus highly energetic tissues such as brain, skeletal muscle, cardiac muscle, and liver are especially enriched in mitochondrial mass (Veltri *et al.*, 1990). The genetic material of the organelle, mitochondrial DNA is a double-stranded, circular molecule encoding genes that are not represented in the nucleus and are located within the organelle. Each cell can contain hundreds to thousands of copies of mtDNA molecules, with oocytes harboring at least 100,000 copies (Satoh and Kuroiwa, 1991; Chinnery *et al.*, 2000; Craven *et al.*, 2010).

Over the course of evolution, much of the mitochondrial genomic burden was transferred to the nuclear genome. As a result, there remain only 13 polypeptides, 2 rRNAs, and 22 tRNAs encoded in mtDNA. All the encoded proteins are components of the complexes involved in oxidative phosphorylation. The remaining subunits of the complexes are encoded in the nuclear DNA, synthesized in the cytosol, and transported into mitochondria after translation is complete (Schatz, 1996). This is also the case for all other proteins operating in and constituting the mitochondria that are not encoded in mtDNA, including RNA and DNA polymerases, nucleases, and membrane proteins. Knowing that the estimated number of proteins necessary for a functional organelle is

approximately 1500, and that the mtDNA only encodes 13 proteins, it is approximated that mitochondria contribute ~0.1% of their own total proteome content (Taylor *et al.*, 2003). The mitochondrion is unique from all other human organelles in the necessity of this dual genome support required for function. This is in notable contrast to plants where in addition to mitochondria, chloroplasts contain their own DNA, and import proteins encoded by the nucleus for proper functioning (Soll and Schleiff, 2004).

1.2 Evolutionary origins of mitochondria in eukaryotes

Mitochondria have been evolving within eukaryotic cells ever since the initial endosymbiotic event took place 1.5 billion years ago (Brocks *et al.*, 1999; Gray *et al.*, 1999). Over this time, many changes have occurred during the complex transition from discrete organism to cellular organelle. There are many mitochondrial variants in eukaryotic cells, from human mitochondria that produce approximately 95% of cellular ATP, mitochondria-like organelles that generate ATP from alterative electron acceptors such as NO_3 (Kobayashi *et al.*, 1996) to the mitosomes of *E. cuniculi* that scavenge ATP from the cytosol of their 'host' (Tsaousis *et al.*, 2008). The diverse spectrum of mitochondria-like organelles can broadly be categorized into three groups: classical mitochondria, hydrogenosomes, and mitosomes. Hydrogenosomes are anaerobic, lacking respiratory complexes and generating ATP through H_2 production. This is accomplished with alternatives to mitochondrial metabolic enzymes. For example, decarboxylating pyruvate using pyruvate:ferredoxin oxidoreductase instead of pyruvate dehydrogenase (Hackstein *et al.*, 1999). While hydrogenosomes can be viewed as the anaerobic counterpart to mitochondria, they notably differ in that most of them do not harbor their own genetic material. Mitosomes also lack organellar DNA and they do not produce ATP. However, all three types of mitochondria-like organelles carry out the crucial cellular activity of iron-sulfur cluster formation. While broad groupings may allow for easy comparison and contrast between the degrees of metabolic engagement of these related organelles, it certainly underplays the range of forms they exhibit. Hydrogenosome-like organelles have been identified in metazoans that live exclusively in conditions lacking molecular oxygen (Danovaro *et al.*, 2010).

The ancestor of modern human mitochondria is thought to be an α-proteobacteria (Andersson *et al.*, 1998), although many facets of the proto-mitochondria acquisition by the host cell are unresolved, including where in the phylogenetic tree of α-proteobacteria the actual endosymbiont is located. The exact conditions that initiated the endosymbiotic

event are also controversial. Moreover, disagreement exists over whether the host cell had at that point acquired a nucleus (Mans *et al.*, 2004), or was exhibiting a less compartmentalized structure (Martin 2005).

The conventional view on the symbiotic relationship exhibited by the proto-mitochondria is based on the benefits of ATP provided by aerobic respiration. The ATP/ADP transport system is not bacterially derived, but instead is a member of a larger eukaryotic transport family. Thus, it would be difficult for the host cell to immediately take advantage of the newfound ATP source (Karlberg *et al.*, 2000). A possible explanation of the immediate benefit of the endosymbiont is a reduction in local oxygen tension via respiration (Kurland and Andersson, 2000). At the time of the endosymbiotic event, oxygen in the Earth's atmosphere was increasing, potentially creating a toxicity crisis for life forms not adapted to the high levels of oxidative exposure (Des Marais, 1998; Brocks *et al.*, 1999). Anaerobic organisms would be at a disadvantage in this setting. So acquisition of the endosymbiont to the host cell would provide substantial benefits in the form of protection from a relatively harsh oxidative environment.

Over the course of evolution with the host cell, the majority of genes from proto-mitochondria have either been lost or transferred to the nucleus. This mixture of gene loss or transfer makes estimations of the size of the proto-mitochondrial genome difficult. The modern mitochondrial proteome results from expression of a mixture of genes derived from ancestral α-proteobacteria, mitochondrial genes transferred to the nucleus, and novel eukaryotic genes. There is wide variation of gene loss/transfer between modern α-proteobacterial descendents, with some losing their entire genome (most hydrogenosomes and all mitosomes) and others keeping a subset of genes encoded on mtDNA (Hackstein *et al.*, 2006). The mammalian mitochondrial proteome is becoming increasingly well characterized, with more than 1,100 proteins identified (Rabilloud *et al.*, 1998; Catherman *et al.*, 2013; Lotz *et al.*, 2013). Of the identified mitochondrial proteins, approximately two-thirds have bacterial origins, with the remaining proteins rising from the eukaryotic genome (Szklarczyk and Huynen, 2010). In contrast to the mitochondrial proteome, mtDNA appears to have a monophyletic origin (Andersson *et al.*, 1998). The continued existence of mtDNA represents a major investment of resources for the eukaryotic cells, as the persisting mitochondrial genome necessitates dedicated gene expression machinery. While requiring less maintenance than the nuclear genome, the investment in retaining mtDNA is still substantial enough that there is likely to be significant benefit to the cell. This may be tied into the fact that oxidative phosphorylation cannot occur without a subset of respiratory chain complex components

being produced inside the mitochondrion. Possible reasons for this are debated, but two proposed theories are the "hydrophobicity theory" (von Heijne, 1986) and the "co-location for redox regulation theory" (Allen and Raven, 1996). The first theory proposes that certain genes have been retained in the mitochondrial genome due to the high degree of hydrophobicity of their protein products, which would make transport from the cytosol across the mitochondrial membranes difficult. The second theory proposes that having specific genes housed in the mitochondrial genome allows for the direct regulation of expression of those genes, based on the redox state of mitochondria. Both theories argue for a spatial advantage of producing mitochondrial gene products within the organelle, versus cytosolic translation followed by import.

1.3. Structure and dynamics of the mitochondrion

The morphology of mitochondria is dynamic, constantly undergoing fission and fusion. The organelle is present as a reticular network, and varies in distribution throughout the cell (Figure 1.1). Although previously thought to possess a discrete and

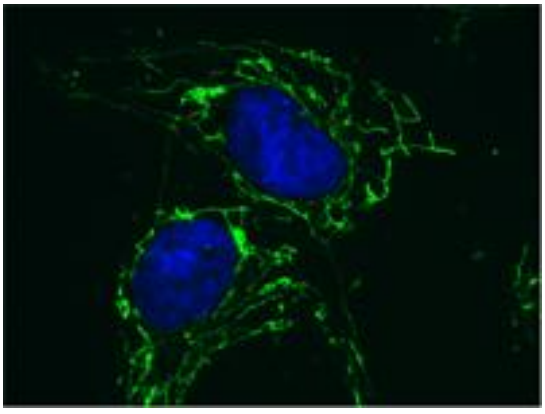

Figure 1.1. The reticulum structure of mitochondria
Human fibroblast mitochondria stained with anti-Complex V (ATPase β) antibodies (green), the nucleus is stained with DAPI (blue), and visualized by fluorescent microscopy. Image used with permission of MitoSciences, Inc.

static structure, mitochondria are currently appreciated as a population of organelles that are able to migrate throughout the cell, undergo processes of fusion and fission, and turnover in a regulated manner. This facilitates their function by enabling recruitment to subcellular compartments, content exchange between mitochondria, morphology changes, and mitochondrial quality control (Chan, 2006).

There are five mitochondrial compartments; the outer membrane (OMM), the intermembrane space (IMS), the inner membrane (IMM), cristae and the mitochondrial

matrix. The outer membrane encloses the organelle, and is more permissive to the transport of molecules due to an array of transporters and channels. The ratio of protein to lipids differs between the two membranes of mitochondria, with the inner membrane exhibiting a 3:1 ratio, and a 1:1 ratio for the outer membrane (Hoch, 1992; Gohil and Greenberg, 2009). Mitochondrial membranes are particularly enriched in phospholipids. This phospholipid composition also differs between membranes. The inner membrane is composed of a higher percent of unsaturated fatty acids, including the signature mitochondrial lipid, cardiolipin. The presence of cardiolipin in the outer membrane has been a controversial topic but recent studies in yeast have shown evidence of cardiolipin located in the outer membrane (Gebert *et al.*, 2009). The total phospholipid composition of mitochondria consists of approximately 40% phosphatidylcholine, 30% phosphatidylethanolamine, 10-15% cardiolipin/phosphatidylinositol, and 5% phosphatidic acid/phosphatidylserine (Colbeau *et al.*, 1971; Osman *et al.*, 2011). More common membrane lipids, such as sterols and sphingolipids, which are important components of the endoplasmic reticulum, Golgi apparatus, lysosome membranes, are only found in trace amounts in mitochondrial membranes (van Meer *et al.*, 2008).

Both membranes house an array of protein machinery. These include porin (also known as voltage-dependent anion channel, VDAC), and the translocases of the outer/inner membrane (TOM/TIM) complexes. The machinery that facilitates fusion and fission are also present, with the major known players being the mitofusins (MFN1/MFN2) on the outer membrane and OPA1 on the inner membrane. Critical mediators of mitophagy are also present on the outer membrane (Liu *et al.*, 2012). The outer membrane is much more permeable to ions and small molecules than the inner membrane that strictly controls what crosses into the matrix.

Areas of the inner membrane exhibit highly folded structures termed "cristae", allowing for a larger surface area on which enzymatic reactions can take place. The complexes of the electron transport chain span the matrix side of the IMM and include transmembrane regions. Within the matrix, the majority of biochemical reactions specific to mitochondria occur. These include oxidative phosphorylation as well as the citric acid cycle, with pyruvate generated by glycolysis in the cytosol being imported into the matrix to fuel the reactions. The matrix also houses the mitochondrial gene expression machinery: mtDNA, mt-tRNAs, mt-mRNAs, mitoribosomes, and replication and transcription enzymes.

1.4 The electron transport chain and oxidative phosphorylation

One of the main functions of human mitochondria is the generation of ATP via oxidative phosphorylation (OXPHOS). Four protein complexes embedded in the inner mitochondrial membrane, namely NADH dehydrogenase (complex I), succinate dehydrogenase (complex II), coenzyme Q:cytochrome *c* reductase (complex III), and cytochrome *c* oxidase (complex IV). With the exception of complex II, all have subunits that are encoded in the mitochondrial genome. Together with the ATP synthase, Complex

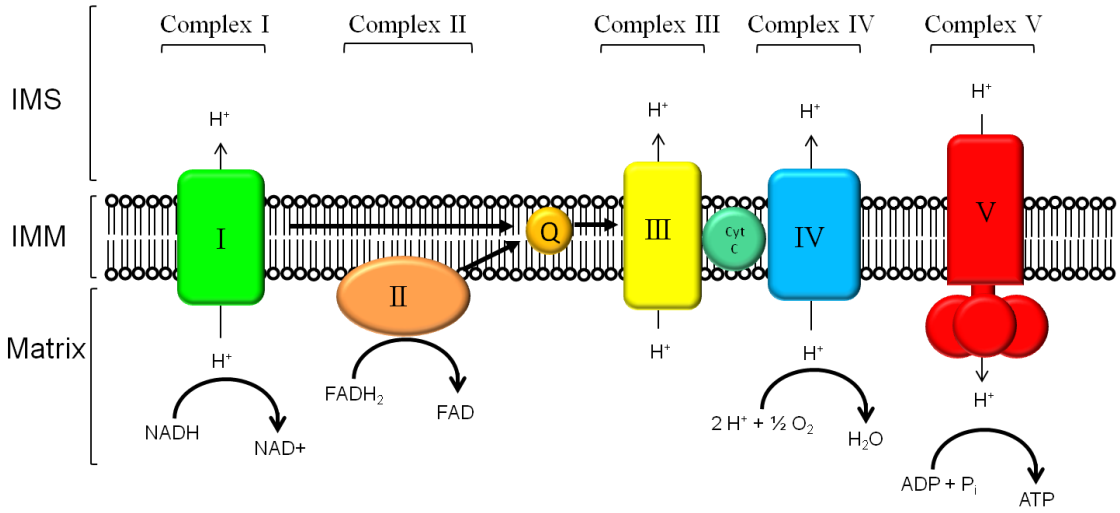

Figure 1.2 The electron transport chain
The five complexes involved in oxidative phosphorylation are shown situated in the inner mitochondrial membrane (IMM). The respiratory complexes and ATP synthase are illustrated with different colors: green (complex I), beige (complex II), orange (coenzyme Q), yellow (complex III), cytochrome *c* (cyan), blue (complex IV), and red (ATP synthase). Coenzyme Q is labeled as "Q", and cytochrome *c* is labeled "Cyt c". Proton translocation, as well as chemical reactions are shown next to the complexes. Other abbreviations are NAD: nicotinamide-adenine dinucleotide; FAD: flavin-adenine dinucleotide; ADP: adenine diphosphate; P_i: inorganic phosphate; ATP: adenine triphosphate; IMS: intermembrane space.

V, these complexes carry out oxidative phosphorylation. The process couples ATP generation with oxidation of NADH and $FADH_2$ (Figure 1.2).

The feeding of electrons into the ETC comes from chemical reactions making up the Krebs cycle. Pyruvate, generated from sugars via glycolysis in the cytosol, is decarboxylated by pyruvate dehydrogenase into acetyl-CoA. Acetyl-CoA is then used as the starting molecule for the Krebs cycle. The complete oxidation of one acetyl-CoA molecule produces three NADH and one $FADH_2$, which carry the electrons to be input into the ETC.

Electrons enter into the chain through complex I with the oxidation of NADH, and complex II oxidizes succinate in the Krebs cycle reducing FAD+ to $FADH_2$. Oxidation of NADH and $FADH_2$ reduce Coenzyme Q (CoQ), which transfers electrons to complex III.

Complexes I, III, and IV pump protons through the IMM as electrons flow along redox centers in the chain, creating an electrochemical gradient across the IMM. Oxygen is the terminal electron acceptor of the ETC, and is reduced to water by complex IV. The resulting gradient forces the protons that have built up in the intermembrane space back across the IMM and into the matrix through a fifth complex, ATP synthase. This movement of protons through ATP synthase energetically drives the conversion of ADP and inorganic phosphate to ATP. The ATP is then transported out of mitochondria via the adenine nucleotide translocator (ANT).

The individual respiratory complexes of the ETC are incorporated into larger "supercomplexes", structures composed of complexes I, II, III, IV, and the mobile electron carriers, Cyt *c*, and CoQ. This structural organization has been proposed to stabilize the individual complexes, and enhance respiration through intimately coordinated electron flow. This interdependence is illustrated where a depletion of one complex can cause activity levels of another complex levels to drop (Acin-Perez *et al.*, 2008).

1.5 The mitochondrial genome

At just 16,569 base pairs, the human mitochondrial genome is a fraction of the size of the nuclear genome. The encoded proteins, rRNAs, and tRNAs, however, are essential for mitochondrial gene expression. Over the course of the estimated 1500 million years (Sicheritz-Pontén *et al.*, 1998) of evolving in synchrony with the eukaryotic nuclear genome, the mitochondrial genome has become reduced from the full complement of genes necessary to support an independent organism to a total of just 37 genes. All other genes were either lost over time or transferred to the nuclear genome through a variety of proposed mechanisms, such as gene transfer agents (GTAs) (McDaniel *et al.*, 2010), transformation (Williams *et al.*, 1997), or transduction (Jiang and Paul, 1998). Further evidence of the relationship to ancient α-proteobacteria is found in the genes that still remain in the mitochondrial DNA, via their similarity to some modern day α-proteobacterial genomes (Andersson *et al.*, 1998; Georgiades and Raoult, 2011).

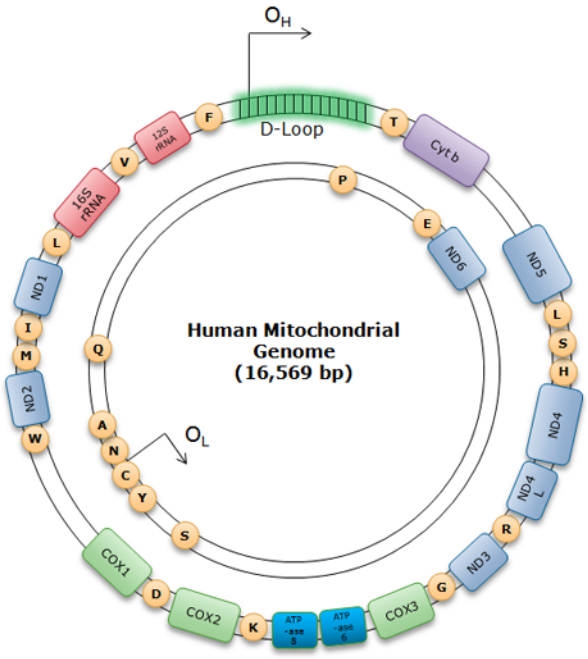

Figure 1.3 The human mitochondrial genome
Genes and rRNAs are labeled with their names, and tRNAs are represented by circles with their single letter amino acid codes. The heavy and light strands are shown as separate rings. Genes belonging to specific respiratory complexes or rRNA are shown as boxes and labeled as follows: rRNA (red), complex I (blue), complex III (violet), complex IV (green), complex V (cyan). Origins of the heavy and light strand are shown with arrows marking their initiation sites and directions.

In contrast to many mtDNA genomes, such as yeast and plants (Lang *et al.*, 1999), human mtDNA possesses an economical and highly compact organization. It is also unlike the human nuclear genome as human mtDNA has very few non-coding regions and many genes are only separated by a few base pairs. The sole exception is an approximately 1100bp section of mtDNA termed the displacement loop, or "D-Loop". The D-Loop houses elements involved in regulating mtDNA replication and transcription initiation. It also possesses an uncommon triple-stranded helix structure. There are no introns in human mtDNA, making splicing machinery within the organelle unnecessary. Many protein-coding genes are separated by tRNA genes, but *MTCOI*, *RNA14*, *MTND5/MTND6* and *MTCYB* are exceptions.

The mtDNA molecule is double-stranded, and contains two separate origins of replication, each dedicated to one strand. The strands are referred to as the heavy (H-) strand and the light (L-) strand, due to their separation in cesium chloride gradients resulting from the guanine nucleotide bias of the heavy strand. Only the *MTND6* gene and eight tRNA genes are located on the L-strand, all other mitochondrial-encoded genes are found on the H-strand (Figure 1.3). The origin of replication for the H-strand is located in the D-Loop, while the origin of replication for the L-strand is between the tRNA asparagine and cysteine genes.

There are three promoters for the initiation of transcription, which occurs in a bi-directional fashion. Two are located on the H-strand, termed HSP1 and HSP2, with the

third found on the L-strand (LSP) (Montoya *et al.*, 1982). HSP1 and LSP are housed in the D-Loop region, while HSP2 is located past the tRNA phenylalanine gene, upstream to the 5' end of the 12S rRNA.

Within an individual cell, it is possible for variants of mtDNA to exist, a condition termed heteroplasmy. When pathological mutations or DNA deletions occur in these variants, mitochondrial dysfunction can result (Holt *et al.*, 1990). The severity of the clinical presentation can be dependent on the ratio of wildtype to altered mtDNA (Chinnery *et al.*, 1997). Thus, heteroplasmy does not necessarily result in a clinically pathological condition (Kirches *et al.*, 2001), but can lead to increasingly severe mitochondrial biochemical dysfunction if the percentage of the mtDNA population becomes too high (Rossignol *et al.*, 1999). This is termed "the threshold effect", and occurs in the range of 70-90% mutant heteroplasmy (Rossignol *et al.*, 1999). However, certain mutations, such as those in tRNA genes, can be functionally dominant and require <25% heteroplasmy levels to exert pathological effects. (Sacconi *et al.*, 2008).

mtDNA molecules are organized into discrete nucleoprotein units, called nucleoids. The number of mtDNA molecules per nucleoid has been contested, ranging from one to ten (Iborra *et al.*, 2004; Bogenhagen *et al.*, 2008; Kukat *et al.*, 2011). The exact complement of proteins packaged with the mtDNA has also been disputed, however the minimum necessary is the mitochondrial transcription factor A (TFAM). The number of TFAM molecules bound to the mtDNA has been estimated at approximately one per 20bp (Kukat *et al.*, 2011). There are many other factors associated with the nucleoids, such as those involved in replication and transcription machinery, but the exact definition of nucleoid components and nucleoid-associated factors is still being refined. A recurring issue is the conflicting composition of nucleoids and their associated factors based on different preparation methods (He *et al.*, 2007; Bogenhagen *et al.*, 2008).

1.6 Replication of mitochondrial DNA

The major factors involved in mtDNA replication are a mitochondria-specific DNA polymerase called POLG (polymerase gamma), the helicase TWINKLE, and the mitochondrial single-strand binding protein (mtSSB). POLG is a heterotrimer, composed of a catalytic subunit (POLGA), and two accessory subunits (POLGB). TWINKLE is a 5'-3' DNA helicase, and forms a stable hexamer or heptamer (Ziebarth *et al.*, 2010). As its name suggests, mtSSB binds ssDNA, and is involved with stabilization and protection of the single strand during replication. The minimal complement of replication factors

necessary for reconstituting mtDNA replication *in vitro* are POLG and TWINKLE, and these proteins together are capable of synthesizing 2kb of ssDNA (Korhonen *et al.*, 2004). With mtSSB added in, synthesis is stimulated to over 16kb (Korhonen *et al.*, 2004). *In vivo*, the mitochondrial RNA polymerase (POLRMT) is necessary for replication of each strand, by generating RNA primers that initiate DNA synthesis (Fuste *et al.*, 2010; Wanrooij *et al.*, 2010).

There are currently at least two proposed theories on the mechanism of replication for mtDNA, and a third, particularly controversial theory. They are termed the "asynchronous strand displacement model", and the "strand coupled bidirectional replication model". In the first model, mtDNA replication occurs in an asymmetric fashion where the synthesis of DNA is initiated at the H-strand origin within the D-loop via RNA primers, then proceeds unidirectionally downstream. After about two-thirds of the H-strand has been replicated, the origin on the L-strand is exposed to the replication machinery, and synthesis of the L-strand begins in the opposite direction (Shadel and Clayton, 1997).

In the second model, bidirectional replication of both strands is initiated from a region not far downstream from the H-strand origin of replication, followed by progression of the dual replication fork structure around the mtDNA molecule (Bowmaker *et al.*, 2003). In this scenario, the D-Loop's triple-stranded structure acts to stall or arrest replication, facilitating the movement of the replication fork downstream. Evidence exists for both models, with the possibility that both types of replication can occur under different physiological conditions. Mitochondrial DNA replication illustrates a complex process, and our understanding of the exact mechanism is far from complete.

The third model proposed, the controversial RITOLS (ribonucleotide incorporation throughout the lagging strand) model, although recently referred to as the "bootlace model" (Reyes *et al.*, 2013). This model postulates that RNA transcripts are hybridized to the displaced strand during replication in order to stabilize and protect the exposed ssDNA. The role here of mtSSB proteins are minimized. This RNA incorporation may also serve regulatory roles in replication (Yasukawa *et al.*, 2006). However, this model is particularly contested.

1.7 Mitochondrial transcription

The mitochondrial transcription machinery is entirely nuclear-encoded. During transcription, recruitment of a mitochondrial specific, single subunit RNA polymerase, POLRMT, is assisted by two transcription factors, TFAM and TFB2M. Two transcription factor B proteins exist, the other being TFB1M. Both have been reported to have transcription factor activity *in vitro (Falkenberg et al., 2002)*, but only TFB2M was shown to be absolutely required for transcription. Both factors are related to rRNA methyltransferases, and TFB1M has been shown to be necessary for methylation of two adenines near the 3' end of the 12S rRNA (Metodiev *et al.*, 2009). TFB2M is a much less efficient methyltransferase (Cotney and Shadel, 2006), lending credence to its role as more of a transcription factor. *In vivo*, several other accessory factors are involved in transcription, such as transcription elongation factor of mitochondria (TEFM) (Minczuk *et al.*, 2011), and MRPL12 (Z. Wang *et al.*, 2007).

From the HSP2 promoter on the H-strand and LSP promoter on the L-strand, mtDNA is transcribed fully into two large, polycistronic precursor RNA transcripts that encompass all the genes on the two respective strands. In addition, a third transcript is transcribed from the HSP1 promoter on the H-strand that starts at the phenylalanine mt-tRNA gene and terminates at the 3' end of the 16S rRNA gene (Figure 1.4). This particular transcription event is also initiated 50-100 times more often than that on the larger H-strand transcript (Montoya *et al.*, 1982; Mercer *et al.*, 2011).

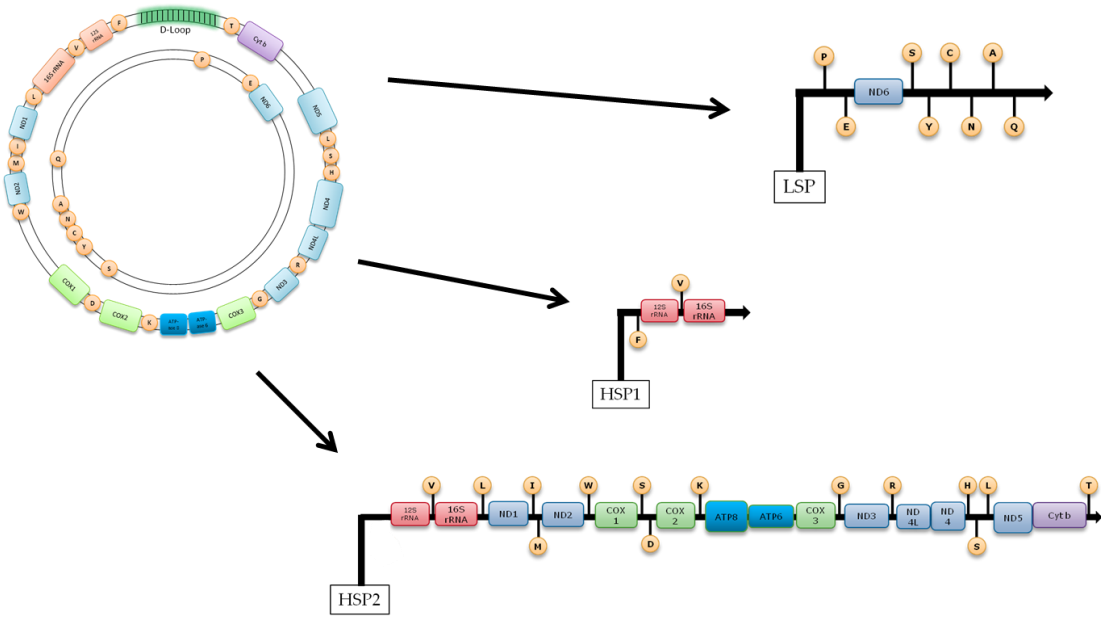

Figure 1.4. Representation of precursor mt-RNA polycistronic units.
The three polycistronic RNA transcription products generated from mtDNA are shown. The same labeling and coloring scheme is used as in Figure 1.3.

Mapping the precise termination site for the transcripts of the longer polycistronic units has been more problematic. The known mitochondrial transcription termination factor mTERF1, has shown binding that mediates termination of the shorter HSP1-initiated RNA within the $tRNA^{LEU}$ gene (Kruse *et al.*, 1989; Asin-Cayuela *et al.*, 2005). MTERF1 functions in a bi-directional manner, particularly with POLRMT transcribing in the direction of the L-strand (Asin-Cayuela *et al.*, 2005). MTERF1 has also been reported to aid in transcription initiation by binding the HSP1 promoter in addition to the $tRNA^{LEU}$ gene. This would cause a "looping out" of the DNA, and facilitate recycling of the active transcription apparatus (M. Martin *et al.*, 2005). Along this line, MTERF1 has been posited to be involved with transcription initiation from the HSP2 promoter as well. Three MTERF1 paralogues exist, with MTERF2 and 3 also reported to be involved in transcriptional processes (Park *et al.*, 2007; Wenz *et al.*, 2009), and MTERF4 with regulation of mitochondrial translation (Camara *et al.*, 2011).

1.8 Transcript processing and turnover

Full length polycistronic precursor RNAs are not commonly observed experimentally, which suggests processing may occur alongside transcription, or at least very shortly thereafter (Ojala *et al.*, 1981). The polycistronic transcripts are cleaved into

shorter transcription units and ultimately into the multiple mRNAs, tRNAs, and rRNAs by excision of tRNAs that flank the protein and rRNA coding regions. This produces individual discrete transcripts, and is known as the "tRNA Punctuation Model"(Ojala *et al.*, 1981). Current understanding indicates that the structure of the tRNAs at their 5' end creates a favorable target for the endoribonuclease activity of mitochondrial RNase P (Holzmann *et al.*, 2008). Cleavage at the 3' end of the tRNAs is carried out by the RNase Z like enzyme ELAC2 (Brzezniak *et al.*, 2011). The obvious problem with this model is that not all protein-coding genes in mtDNA are punctuated by tRNA genes, for example *MTATP6* and *MTCO3*. There also exist pairs of overlapping open reading frames that are maintained as bicistrons, namely *RNA14* encoding *MTATP6/8* and *RNA7* encoding *MTND4/4L*. Despite all the mt-RNA units being processed from a single polycistronic precursor transcript, the discrete RNAs that are generated as a result are not present in equal amounts at steady-state (Mercer *et al.*, 2011; Chujo *et al.*, 2012). This emphasizes the need to expand our current understanding of RNA transcript turnover, particularly its regulation, in mitochondria.

Post-cleaving of the polycistronic transcripts, modifications are made at the resulting 3' ends. The three types of 3' modifications that can occur are listed in Table 1.1, although there is dispute as to whether the mt-rRNAs are oligoadenylated (Temperley *et al.*, 2010b).

Table 1.1 3' termini modifications of mitochondrial RNAs

Mitochondrial RNA	3’ Modification
tRNAs	CCA Addition to the 3’ end
rRNAs	Short oligonucleotide extensions
mRNAs	Poly(A) Tail 40-60 nucleotides ND5 has 5-10nt ND6 poly(A)?

The CCA modification on tRNAs is carried out by an ATP(CTP):tRNA nucleotidyltransferase (Nagaike *et al.*, 2001). The mitochondrial poly(A) polymerase,

generates the poly(A) tails on mt-mRNAs (Gallerani *et al.*, 1976; Tomecki, 2004). The function of certain RNA modifications is clear. For 7 ORFs the addition of an (A) tail is required to complete the termination codons, and the CCA addition precedes charging tRNAs with their cognate amino acids. Whilst mt-rRNAs and –tRNAs do not vary in the 3’ modification, it has become clear that mt-mRNAs exhibit a variety in regards to poly(A) tail length, and whether polyadenylation contributes to the completion of termination codons (Temperley *et al.*, 2010b).

Another major aspect of RNA metabolism is degradation of transcripts. The total contingent of factors involved in this process is currently not known, but several significant players have been identified. There is hSuv3, a mitochondrial 3'-5' helicase (Dmochowska *et al.*, 1999). Removal of hSuv3, or inactivation of its enzymatic activity causes an accumulation of both RNA degradation intermediates, and the non-coding "mirror RNAs" from the non-template strand transcript (Khidr *et al.*, 2008; Szczesny *et al.*, 2010), implicating its role in mt-RNA turnover. The yeast homolog (Suv1p) operates in concert with a catalytic unit, Dss1p, which carries out the exoribonuclease action. A similar 3' exoribonuclease has not been identified in human mitochondria. Another enzyme engaged in RNA turnover is PNPase. It was initially speculated that it might be potentially either the mitochondrial 3' exoribonuclease or the poly(A) polymerase, due to the possession of both PAP and 3'5' exoribonuclease activities. It was later reported to be localized in the IMS, where it is involved with RNA import (Chen *et al.*, 2006). However, PNPase does co-purify with hSuv3 and vice versa, and they form a complex *in vitro* (D. D. Wang *et al.*, 2009; Szczesny *et al.*, 2010), which suggests that a smaller pool of PNPase does localize to the matrix. Depletion of PNPase causes accumulation of RNA degradation intermediates (particularly "mirror RNAs") and increases the half-life of transcripts, further implicating it in RNA turnover (Borowski *et al.*, 2013). The only mitochondrial enzyme shown to have explicit deadenylase activity is PDE12, poly(A)-specific 3' exoribonuclease. PDE12 has been shown to have deadenylase activity *in vitro* and *in vivo* (Rorbach *et al.*, 2011). Depletion of the PDE12 protein unlike depletion of hSuv3 or PNPase does not increase mt-mRNA half-life (Chujo *et al.*, 2012). Overexpression, however, has a profound effect on mt-mRNAs but this is not a uniform effect, as some transcripts are more stable, others less stable and others unaffected (Rorbach *et al.*, 2011). Finally, an oligoribonuclease, REXO2, has been reported to exist in mitochondria, and may be involved with degradation of small RNA oligomers (Bruni *et al.*, 2013). In total, these factors make up the current complement of enzymes known to be involved in RNA turnover.

1.9 Mitochondrial RNA binding proteins

In yeast, there exists a complement of translation activators, corresponding to specific mitochondrial mRNAs, which bind to the 5' UTRs and initiate translation by interacting with the ribosome (Towpik, 2005; Herrmann *et al.*, 2013). In human mitochondria, there is only one identified translational activator, specific to COXI, namely TACO1 (Weraarpachai *et al.*, 2009). The activator was identified through a patient harboring a mutation in the TACO1 gene displaying a substantial decrease exclusively in COX1 protein levels. Intriguingly *MTCO1* encodes COXI but does not have a 5' UTR for this activator to recognize leaving the molecular mechanism unexplained.

A well characterized family of RNA binding proteins are the pentatricopeptide repeat (PPR) proteins The PPRs are a large family of proteins first identified in terrestrial plants, and are involved in a range of essential post-transcriptional functions in mitochondria and chloroplasts (Small and Peeters, 2000; Schmitz-Linneweber and Small, 2008). There are seven known PPR proteins present in humans, all localized to mitochondria (Lightowlers and Chrzanowska-Lightowlers, 2013). These factors are leucine-rich PPR cassette (LRPPRC), the mitochondrial RNA polymerase (POLRMT), a mitochondrial ribosomal small subunit protein (MRPS27), three pentatrico- domain containing proteins (PTCD1, 2, and 3), and mitochondrial RNase P protein 3 (MRPP3).

LRPPRC was the first PPR protein to be found in man, discovered as causing a complex IV specific defect in the French Canadian Leigh Syndrome (Mootha *et al.*, 2003). Knock-down and knock-out experiments have shown that depletion of LRPPRC results in a general decrease of mt-mRNAs (although the reports of which specific transcripts show decreased levels are conflicting) (Gohil *et al.*, 2010), dysfunction in protein synthesis (Ruzzenente *et al.*, 2012; Xu *et al.*, 2012), and intriguingly, shortening of the mt-mRNA poly(A) tails (Ruzzenente *et al.*, 2012). LRPPRC has been reported to bind both nuclear and mt-mRNAs, although not in strictly sequence-specific manner (Mili and Pinol-Roma, 2003; Xu *et al.*, 2012). It does seem to have higher affinities for polypyrimidine tracts. LRPPRC has been confirmed to interact with another mitochondrial RNA binding protein, SLIRP (steroid receptor RNA activator stem-loop-interacting RNA-binding protein) (Sasarman *et al.*, 2010). First identified as a nuclear protein (Hatchell *et al.*, 2006), SLIRP was later shown to have the majority localize in

mitochondria (Baughman *et al.*, 2009). Beyond SLIRP, the number of other reported interactions with LRPPRC are many, and inconsistencies abound [reviewed in (Lightowlers and Chrzanowska-Lightowlers, 2013)]. While LRPPRC appears to be a critical factor in mitochondrial function, more work is required to fully understand its many potential roles.

POLRMT carries out the polycistronic transcript synthesis and primer generation for mtDNA replication, as described earlier in this chapter and is therefore clearly an essential protein for mitochondrial DNA maintenance and expression. MRPS27 depletion does not result in decreases of mt-mRNAs, rather an expected decrease in translation efficiency, although surprisingly this effect is exacerbated for COX1 and COX2. At present, it is difficult to know where in the mitoribosome MRPS27 would reside as there are no high resolution crystal or cryo-EM structures available. The three PTCD proteins have been reported to be involved in different ways with translation. PTCD1 has been shown to influence the levels of mt-tRNA^{LEU} and may play a role in polycistronic processing (Rackham *et al.*, 2009). PTCD2 disruption was reported to cause defects in complex III, through depletion of the mature *MTCYB* transcript (Xu *et al.*, 2008). It has also been identified as a potential biomarker in Alzheimer's disease (Nagele *et al.*, 2011). PTCD3 has also been shown to be an interactor with the mitoribosome, through association with the small subunit, although it does not appear to directly influence mt-RNA processing or stability (Davies *et al.*, 2009). The most recently discovered PPR protein in humans is MRPP3, which is a subunit of the RNase P complex (Holzmann *et al.*, 2008). Interestingly, disruption of certain PPR proteins in mitochondria has been shown to influence the levels of other PPR proteins (Xu *et al.*, 2012), perhaps suggesting functional connections between these factors in human mitochondria.

1.10 Translation in Mitochondria

The machinery of protein synthesis in mitochondria differs from its cytosolic counterparts in several significant ways. The composition of the mitoribosome differs noticeably [described in (Chrzanowska-Lightowlers *et al.*, 2011)]. The ratio in cytosolic 80S particles is 70% RNA to 30% protein, and this is reversed in the mammalian mitochondrial ribosome. This increase of protein content causes a change in the buoyancy and sedimentation of the mitoribosomal monosome, with the result that the mammalian mitoribosome is a 55S rather than an 80S particle as in the cytosol. Included in these changes is the loss of rRNA that corresponds to specific regions in the bacterial 70S

ribosome that would interact with "E" site tRNAs (Mears *et al.*, 2006). This indicates that the mitochondrial ribosomal structure does not possess what has been traditionally described as the "E" site, while the "P" and "A" sites remain more canonical in their structure (Sharma *et al.*, 2003). The emerging understanding is that recruitment of mRNA, tRNA interaction, and exiting of the newly synthesized polypeptide chains must differ markedly in the mammalian mitochondrial ribosome than its cytosolic counterpart.

Currently, aspects of the assembly of the mitoribosome are still being elucidated. The literature only contains few reports of ribosomal proteins (MRPS16, MRPS22, MRPL3 and MRPL12) mutated in patients, causing mitochondrial disorders (Miller *et al.*, 2004; Emdadul Haque *et al.*, 2008; Galmiche *et al.*, 2011; Serre *et al.*, 2013). Modifications must be made to mt-rRNA during the process of maturation. The 12S rRNA is dimethylated by TFB1M (Metodiev *et al.*, 2009), and the MTERF4-NSUN4 complex is critical for monosome assembly, although it is not known what/if methylation occurs via NSUN4 (Camara *et al.*, 2011). For small subunit assembly, there are two GTPases involved, EraL1 and NOA1 (Dennerlein *et al.*, 2010; Kolanczyk *et al.*, 2011). In the case of the large subunit, two other GTPases, Mtg1 and ObgH1, have been reported to be associated (Kotani *et al.*, 2013). The m-AAA protease is also required for proteolytic processing of the mitoribosomal subunit MRPL32, without which mitoribosome assembly is not completed (Nolden *et al.*, 2005). The only protein currently shown to act as a chaperone-like or stabilizing factor for protein insertion into the mitoribosome is C7orf30 (Rorbach *et al.*, 2012; Wanschers *et al.*, 2012), which interacts with the large subunit component MRPL14 (Fung *et al.*, 2013).

There are proteins necessary for initiation, elongation, and termination phases of mitochondrial protein synthesis. Initiation of translation is mediated by mitochondrial initiation factor 3 (mtIF3)(Koc and Spremulli, 2002). This is accomplished by binding of mtIF3 to the mtSSU, which inhibits assembly of the complete monosome, although it may take a more active role as well in disassembly of the monosome (Christian and Spremulli, 2009). The second initiation factor, mtIF2, while bound to GTP, promotes binding of the fmet-tRNA^{Met}, and generates a stable initiation complex with the mt-SSU and mRNA when the start codon is present (Ma and Spremulli, 1995). If the start codon is not present, the mt-SSU can dissociate (Christian and Spremulli, 2010). Once the initiation complex is formed with the mtSSU, the mtLSU can associate to form the complete monosome, then mtIF2 hydrolyzes GTP and the initiation factors release.

For the elongation action of protein synthesis in mitochondria, three factors are necessary: mtEFTu (Wells *et al.*, 1995; Ling *et al.*, 1997; Cai *et al.*, 2000), mtEFTs (Xin

et al., 1995), and mtEFG1(Hammarsund *et al.*, 2001). A second mtEFG exists, mtEFG2, but it has a role in ribosome recycling and lacks translocation activity (Tsuboi *et al.*, 2009). During elongation, mtEFTu (bound to GTP) delivers an aminoacylated-tRNA (aa-tRNA) to the A-site of the mitoribosome. Correctly-matched codon-anticodon interaction between the aa-tRNA and mRNA causes hydrolysis of the GTP, and drives the release of mtEFTu-GDP. mtEFTs acts as a guanine exchange factor, replacing the GDP with GTP on mtEFTu, ready to perform the cycle again (Cai *et al.*, 2000). Within the monosome, the peptidyl chain in the P site is transferred to the aa-tRNA bound in the A site via the catalytic action of the peptidyl-transferase center of the mtLSU, forming the new peptide bond. After this catalytic event, the extended peptidyl-tRNA is translocated from the A site to the P site, and the deacylated tRNA is released. This translocation reaction is driven by the hydrolysis of GTP bound to mtEFG1, via conformational changes in both mtEFG1 and the mitoribosome.

The final stage of mitochondrial protein synthesis is termination of translation. Once a stop codon reaches the A site, the mitochondrial release factor (mtRF1a) recognizes the codon, and via the GGQ domain localized to the peptidyl-transferase center of the ribosome, it catalyzes the release of the peptide chain (Soleimanpour-Lichaei *et al.*, 2007). There are also three other members assigned to the mitochondrial release factor family whose functions have not been fully characterized, these are mtRF1 (the initial candidate release factor), ICT1 and C12orf65. These all possess GGQ motifs, but only ICT1 exhibits release activity *in vitro*. Recycling of the mitoribosome is carried out by the mitochondrial recycling factor (mtRRF) (Rorbach *et al.*, 2008), in conjunction with mtEFG2 and mtIF3.

Notably, the codon usage in human mitochondria is altered from cytosolic, with AUA coding for methionine and the universal STOP codon UGA converted to coding for tryptophan. Until recently, it was thought that the human mitochondrial code also added two termination codons, AGA and AGG, which conventionally encode for arginine. However these two "termination codons" were shown to be involved in a frameshift mechanism in which the mitoribosome stalls on them due to a lack of corresponding tRNAs, and then shifts position -1 nucleotide upstream to create the UAG termination codon. This action enables utilization of just one release factor (mtRF1α) which recognizes the UAA and UAG codons, for translation termination and leaves the unique condition of AGA and AGG being unassigned codons in human mitochondria (Temperley *et al.*, 2010a).

1.11 Mitochondrial Disease

Disruptions in the processes and functions detailed here obviously have major impacts on human health. Due to the multifaceted roles played by mitochondria, there is a wide range of clinical pathologies where mitochondrial dysfunction plays a primary role. The prevalence of mtDNA-based disease in the population is 9.2/100,000 people (Schaefer *et al.*, 2008), with 1 in 200 people carrying potentially pathogenic mtDNA mutations (Elliott *et al.*, 2008). The majority of patients suffering from mitochondrial disease present with neuromuscular clinical pathologies, as neural and muscular tissues depend heavily on aerobic metabolism. Cells with high energy demands necessarily possess more mitochondrial mass. For example, a cardiomyocyte can be up to 35% mitochondria by volume (Barth *et al.*, 1992).

Current research has implicated mitochondrial dysfunction in many other diseases, such as cancer (Warburg, 1956), Alzheimer's (Swerdlow *et al.*, 2010) or Parkinson's (Schapira *et al.*, 1989). Although the symptoms associated with mtDNA disease can have a high degree of overlap there have been a number of specific syndromes resulting from mtDNA mutations (Goto *et al.*, 1990). Examples of these include MELAS (Pavlakis *et al.*, 1984), MERFF (Noer *et al.*, 1991), CPEO (Moraes *et al.*, 1989), and Kearns-Sayre syndrome (Bastiaensen *et al.*, 1982).

Until recently, relatively few nuclear encoded mutations that caused mitochondrial disease had been identified (Miller *et al.*, 2004), but with the advent of exome sequencing there is a rapidly expanding catalogue of nuclear-encoded mutations (Calvo *et al.*, 2010). This has facilitated identification of nuclear-encoded factors involved in mitochondrial function. Prior to the widespread adoption of exome sequencing technology, a more laborious and pedigree intensive approach, typically requiring arduous techniques such as linkage analysis, homozygosity mapping or positional cloning, was required to identify mitochondrial disease causing genes encoded in the nucleus. In this fashion a mutation in the gene encoding the mitochondrial poly(A) polymerase, was identified. Characterization of the consequences of the defect identified the first pathogenic mutation to affect mitochondrial mRNA maturation. At present, very little is understood about the fundamental physiological mechanisms and crucial role mt-mRNA maturation may play in human disease.

1.12 Mitochondrial polyadenylation and the mitochondrial poly(A) polymerase

Polyadenylation is a template-independent process whereby adenine nucleotides are added in succession to the 3' end of mRNA transcripts. The process serves differing roles across organisms and throughout cellular compartments. In bacteria (Xu and Cohen, 1995), plant mitochondria (Gagliardi and Leaver, 1999), and chloroplasts (Hayes *et al.*, 1999), polyadenylation serves as a signal for degradation of mRNA, aiding in the recruitment of exonucleases necessary for transcript turnover. Conversely, in the mammalian nucleus the poly(A) tail acts to stabilize the RNA transcripts (Bernstein *et al.*, 1989), bind poly(A)-binding protein PABP-N1 which protects from degradation (Keller *et al.*, 2000), and facilitate export into the cytosol. It this compartment it is bound by PABP-C1, which also protects the transcript from degradation and the poly(A) tail is subsequently involved in initiation of translation (Gallie, 1991; Huang and Carmichael, 1996). In yeast mitochondria, no poly(A) tail exists. Instead, transcripts have a DNA-encoded 3' dodecamer sequence which acts as an arbiter of stability (Osinga *et al.*, 1984). Trypanosome mitochondria use short poly(A) sequences to confer stability based on the editing status of the transcript itself (Etheridge *et al.*, 2008). These differing roles for polyadenylation are summarized in Table 1.2. In human mitochondria the complete function of polyadenylating mt-mRNAs is less clear.

Table 1.2. The Diverse Roles of Poly(A) Tails

Organism	Role of Poly(A) Tail
Bacteria	RNA Degradation
Plant mitochondria	RNA degradation (same in chloroplasts)
Yeast mitochondria	No poly(A) tail, 3' dodecamer sequence controls stability
Trypanosome mitochondria	Stabilization based on editing status of mRNAs
Humans (cytosol)	Confers mRNA stability, plays role in export from nucleus to cytoplasm
Humans (mitochondria)	Creates UAA stop codons in seven mt-mRNAs, role in stability unclear

Mammalian mitochondrial poly(A) polymerase (PAP) was first isolated in 1972 from rat liver mitochondria (Jacob and Schindler, 1972). Polyadenylation activity is necessary for creating the UAA stop codons in seven of the thirteen mitochondrial open reading frames. The terminal nucleotide in these seven transcripts is uridine 5'-monophosphate or a single adenosine 5'-monophosphate and the addition of a poly(A) tail creates the stop codon via further adenosine 5'-monophosphate additions. Some only require one "A" (*MTND1*, *MTATP6*), and the few transcripts that have 3' UTRs do not require polyadenylation at all for generation of their stop codons. This theme of heterogeneity continued as more became understood about the unique features of each mt-mRNA, with no two being exactly alike, as shown in table 1.3 (Temperley *et al.*, 2010b). The polyadenylation status of the *MTND6* transcript, in particular, is unclear (Lightowlers lab, unpublished data). Variation in poly(A) tail length exists between cell types, as well as between transcripts within the same cell. *MTND5* is consistently oligoadenylated, as opposed to polyadenylated, in most cell types (Temperley *et al.*, 2010b).

A cell line with a mtDNA microdeletion that removed the termination codon for the ATP8/6 bicistronic RNA unit (*RNA14*) indicated that deadenylation of the poly(A) tail on mitochondrial transcripts is translation-dependent (Temperley, 2003). The length of

poly(A) tails were observed using a novel assay, the mitochondrial poly(A) tail assay (MPAT). The deletion caused steady-state levels of *RNA14* to decrease, and while processing accuracy was not affected, and the polyadenylation profile visualized with the MPAT showed a prevalent truncated oligo(A) tail species of *RNA14* at steady-state. Thiamphenicol was used to inhibit translation, and over a course of time points the population of oligo(A) tails disappeared in the microdeletion cell line, with the population of poly(A) tails increasing. It was thought that this was evidence of the oligo(A) species being products of deadenylation. However, when subsequent experiments were performed with human cells depleted of mitochondrial poly(A) polymerase via RNAi, the oligo(A) tails were still present. If oligo(A) tails are products of deadenylated poly(A) tails, then it would be expected they would disappear when mtPAP activity is suppressed. These results suggested that oligoadenylation could be a separate process from polyadenylation, and may in fact be carried out by another enzyme.

The human mitochondrial poly(A) polymerase (mtPAP), encoded by the *PAPD1* gene, was identified by two groups shortly after (Tomecki, 2004; Nagaike, 2005). Tomecki *et al* showed via northern blotting that the expression level of mtPAP was highest in heart, brain, and skeletal muscle tissue. This pattern of expression is common in proteins localized to mitochondria. Further confirmation came from immunofluorescent imaging to identify the cellular localization of c-myc-tagged mtPAP.

Table 1.3. Characteristics of human mt-mRNAs

Gene	5' leader	ORF	3' trailer	initiation	termination	A's needed
MTND5	0	1811	568	AUA	UAA	0
MTCO1	3	1541	72	AUG	UAG	0
MTND4	296	1377	0	AUG	UAA	2
MTCYB	0	1140	0	AUG	UAA	2
MTND2	0	1041	0	AUU	UAA	2
MTND1	2	955	0	AUA	UAA	1
MTCO3	0	783	0	AUG	UAA	2
MTCO2	0	708	24	AUG	UAG	0
MTATP6	161	679	0	AUG	UAA	1
MTND6	0	524	no consensus	AUG	UAG	0
MTND3	0	345	0	AUA	UAA	2
MTND4L	0	296	1371	AUG	UAA	0
MTATP8	1	206	634	AUG	UAG	0

This was shown to overlay with mitotracker CMXRos in HeLa cells.

RNA interference was employed by both groups to deplete the mtPAP protein and observe the resulting effects. Knockdown of mtPAP caused changes in the population of poly- and oligo-adenylated transcripts, with a major shift towards oligoadenylation. Conflicting reports of the effect of depleting mtPAP, and thus presumably abrogating mt-polyadenylation, has led to differing interpretations of the role of poly(A) tails in mt-mRNA stability. Northern blotting has shown that certain transcripts are increased at steady-state, and others were decreased. It is unknown to what extent the unique features of each individual transcript play into the effects seen when the poly(A) tail is removed. There is one report of human mt-mRNA polyadenylation appearing to play a role in transcript turnover (Slomovic *et al.*, 2005). Truncated mt-mRNAs were found with poly(A) tails. However, this may merely indicate polyadenylation is a ubiquitous transcriptional maturation event being carried out in mitochondria, and degradation intermediates and misprocessed transcripts are still subject to addition of the poly(A) tail.

Other mitochondrial parameters have been shown to be affected by mtPAP knockdown, such as mitochondrial morphology, O_2 consumption, and mitochondrial membrane potential (Nagaike, 2005). siRNA depletion does not fully eliminate mtPAP from cells and so it is not surprising that there was some residual polyadenylation activity, as the population of full length poly(A) tails were decreased, but not completely gone. This is a problem with the siRNA method of mtPAP depletion, as residual polyadenylation activity exists and must be taken into account.

Work carried out concurrently on PNPase in mitochondria seemed to imply that it could potentially have a role in mt-polyadenylation, but siRNA depletion of PNPase has shown conflicting results on poly(A) tail lengths, and on steady-state levels of mitochondrial-encoded transcripts and proteins (Nagaike, 2005; Slomovic and Schuster, 2007). PNPase has also been localized to the intermembrane space of the mitochondria, and is implicated in import of RNA into mitochondria, which could indicate an indirect role in mt-RNA metabolism (Chen *et al.*, 2006). As mentioned earlier, despite the data indicating the majority of PNPase being localized to the IMS, purification of the matrix helicase hSuv3 revealed robust interactions with PNPase in the matrix (Szczesny *et al.*, 2010). Also in the report from Szczesny *et al* was data showing that overexpression of hSuv3p shortened mt-poly(A) tails, and expression of a dominant-negative mutant hSuv3caused lengthened poly(A) tails. The current understanding of hSuv3p and PNPase is that within the matrix, they form an mt-RNA degrading complex, termed the "degradosome". This interpretation is supported by data from multiple other groups, whose work details longer poly(A) tails in mitochondria via PNPase depletion (Nagaike,

2005; Slomovic and Schuster, 2007). So despite possessing some 5'-3' template-independent RNA polymerization capability, PNPase is much more strongly implicated in 3'-5' RNA degradation, and by extension, degradation of the mitochondrial poly(A) tails. The only other identified enzyme shown to participate in specific 3'-5' mt-RNA deadenylation is PDE12 (Rorbach *et al.*, 2011). Crucially though, depletion of PDE12 does not influence the turnover of mt-mRNAs (Chujo *et al.*, 2012). This leaves open the possibility that either more RNases are active in mitochondria, or the identified ones work in concert.

The use of siRNA suppression of mtPAP is not the only technique employed to probe mitochondrial polyadenylation. Perturbation of mt-mRNA turnover was attempted by targeting a cytosolic 3' poly(A) specific ribonuclease, mtPARN, to the mitochondria, as well as a cytosolic poly(A) binding protein, mtPABP1 (Wydro *et al.*, 2010). The results confirmed previous findings of variable effects on transcript stability. The poly(A) specific ribonuclease targeted to the mitochondria removed the poly(A) tails, and the effects on mt-mRNA stability showed that some transcripts were increased at steady state (*MTND1*, *MTND2*, *MTND5*) while others were decreased (*MTCO1*, *MTCO2*, *RNA14*). Mitochondrial protein synthesis was found to be decreased for all 13 mtDNA-encoded polypeptides. The targeting of mtPABP-C1 to the mitochondria exerted a significant negative effect on translation, but did not lead to increased transcript decay.

As detailed earlier, LRPPRC is a PPR protein that has been implicated in RNA metabolism. In 2012, Ruzzenente *et al* reported the results of LRPPRC knock-out in a mouse model (Ruzzenente *et al.*, 2012). One of the unexpected effects of LRPPRC removal was a noticeable truncation in mitochondrial poly(A) tails. This results had also been observed in *Drosophila melanogaster* mitochondria, when bicoid stability factor (BSF, the LRPPRC homolog) was knocked-down by RNAi (Bratic *et al.*, 2011). As LRPPRC is not thought to have RNase activity, this was a conspicuous consequence. The only other factors shown to have influence on mt-poly(A) length are PNPase, hSuv3p, and PDE12, all possessing 3' exoribonuclease activity. This suggested a positive role for LRPPRC in mitochondrial polyadenylation. This hypothesis was bolstered when *in vitro* experiments with LRPPRC and mtPAP were published in 2012 (Chujo *et al.*, 2012). The presence of LRPPRC was reported to allow extension of poly(A) tails, whereas the same paper reported data showing mtPAP had no activity on its own. While the observation of LRPPRC aiding the extension of poly(A) tails was novel, the notion that mtPAP is incapable or nearly incapable of poly(A) extension on its own runs counter to previously published results of *in vitro* polyadenylation (Nagaike, 2005; Bai *et al.*, 2011). In Chujo *et*

al., the addition of SLIRP to the *in vitro* polyadenylation reactions was also reported not to have an appreciable effect on poly(A) extension.

Currently, there is no confirmed mitochondrial poly(A) binding protein. However, the protein PABPC5 has recently been proposed as a candidate (He *et al.*, 2012). PABPC5 can co-immunoprecipitate both LRPPRC and mtPAP. This is particularly notable considering the previously published work with LRPPRC and mtPAP but more research is necessary to elucidate the exact role of PABPC5 in mitochondria.

In 2011, the crystal structure of mtPAP was reported (Bai *et al.*, 2011). Many notable characteristics of the polymerase were revealed by the crystal structure. A noncanonical poly(A) polymerase, mtPAP was shown to unexpectedly operate as a dimer, as opposed to the monomer status of canonical PAPs. An N-terminal region of the protein, C-terminal to the mitochondrial targeting sequence, contains a section similar to a RNP-type RNA binding domain (termed an RNA binding-like domain, or RL domain), which appears to aid in dimerization. Other than this region there is no obvious RNA binding domain. Structural similarities exist between mtPAP and canonical PAPs as it possesses palm and finger domains, with the active site located between the two. So while there is structural homology to canonical PAPs, there is very low polypeptide sequence homology (approximately 10-15%). mtPAP is able to utilize both ATP and UTP for polynucleotide extensions on RNA substrates.

The methods employed up to this point to disrupt mitochondrial polyadenylation all have their drawbacks. Artificial perturbations of a cellular system will always be an approximation of the actual physiological conditions of dysfunction. In a step towards establishing a better experimental model, an Old Order Amish family in Ohio was previously identified, in which four of five children are affected with an autosomal-recessive spastic ataxia with optic atrophy (Crosby *et al.*, 2010). A genome-wide microarray screen had been undertaken, and a mutation in the *PAPD1* gene was found to segregate with the disease phenotype. The variant was a 1432A>G mutation creating a

```
Human       ETLELLLKEFFEYFGNFAFDKNSINIRQGREQNKPDSSPLYIQNPFETSL 484
Chimpanzee  ETLELLLKEFFEYFGNFAFDKNSINIRQGREQNKPDSSPLYIQNPFETSL 484
Mouse       ETLELLIKEFFEYFGNFAFNKNSINIRQGREQNKPDSSPLYIQNPFETSL 487
Zebrafish   DTLEKLLQEFFEFYGNFPFNKASINIRKGKEQSKPEAAALHIQNPFEATL 481
Fly         SSLSELLLQFFEFYSQFDFHNRAISLNEGKPLSKPDHSAMYIVNPLEQLL 475
```

Figure 1.5. Sequence alignment of the mtPAP N478 motif in various species.
Regions of mtPAP from several species containing the highly conserved NPFE motif are shown, aligned with CLUSTALW software (Goujon *et al.*, 2010). The motif is highlighted in yellow. The numbers at the end of the sequences indicate the peptide position ending the shown sequence. Accession numbers: human (NP_060579.3), chimpanzee (XP_001136690.1), mouse (NP_080433.1), zebrafish (XP_692256.3), fly (NP_569904.1).

N478D polypeptide substitution. This substitution is in an N-P-F-E residue sequence, which is a highly conserved region of the mtPAP protein (Figure 1.5). Interestingly, the N478D mutation does not map to a region of the protein with a known function, according to the published crystal structure (Bai *et al.*, 2011). This makes the nature of its presumed deleterious effect much less obvious. Each affected child is homozygous for the mutation, while one sibling and the parents are heterozygous and do not display clinical pathology. The MPAT assay was used to assess the polyadenylation status of several mitochondrial transcripts in affected and unaffected members of the family. In the homozygous children, polyadenylation of mt-mRNAs is dramatically compromised, with an increase in the oligo(A) population of transcripts. This may be the primary pathological effect of the *PAPD1* mutation. The mutation presents a unique physiological environment in which polyadenylation is compromised to a greater degree than when using siRNA to knockdown mtPAP. Experiments utilizing cells that harbor the homozygous mutation would possibly avoid the potential residual polyadenylation activity seen in other methods acting to artificially disrupt the poly(A) tail, or other off-target effects.

1.13 Aims of this project

Over the last decade, much work has been done on mitochondrial poly(A) polymerase and mitochondrial polyadenylation. Unfortunately, little is understood about the process and the role it plays. While certain phenomena of steady-state transcript stabilities have been observed consistently, other results are conflicting. It is entirely possible, and even likely, that essential modulating factors remain to be identified. My project will use cell lines derived from the patients harboring the 1432A>G *PAPD1* mutation and is designed to provide crucial insights into the process and role of polyadenylation in mitochondria. The ablation of polyadenylation activity without an artificial depletion of the mtPAP enzyme or artificial disruption of mt-mRNA metabolism presents a physiological system ripe for exploration. Not only for elucidating the purpose of the poly(A) tail in mitochondria mRNA maturation, but for the understanding broader impacts of molecular pathologies due to mutations in nuclear genes encoding for essential mitochondrial functions.

The specific aims of these studies are as follows:

I.
To establish cell lines as a model to investigate the effects due to the 1432A>G mutation in the *PAPD1* gene. These will be generated using fibroblast samples from three siblings who possess the mutation, one of whom is heterozygous, the other two homozygous. The initial goal will be to "immortalize" the cells via retroviral transduction. A viral vector will integrate the HPV16-E6E7 region genes, allowing the cells to delay their transition into senescence, effectively doubling their lifespan. This immortalization of the cell lines will allow more in depth studying of the abrogated polyadenylation in mitochondria by reducing the cell division constraints commonly encountered when culturing primary cell lines. In addition one non-familial fibroblast line that does not harbor any form of the 1432A>G mutation will be immortalised as a control.

II.
Using immortalized 1432A>G mutant fibroblasts as a model, rescue of the dysfunctional cellular phenotype will be attempted by introducing a wild-type *PAPD1* gene. Expression of the wild-type protein will be introduced, and its compensating activity for the

endogenous mutant mtPAP will be assessed. This will generate evidence to establish whether the 1432A>G mutation in the *PAPD1* gene both caused the lack of polyadenylation activity in the endogenous protein, and caused the downstream biochemical defects which contributed to the clinical pathologies exhibited by the patients the samples were taken from.

III.

Recombinant expression and purification of the wild-type and N478 mtPAP proteins will be carried out. Generation of recombinant mtPAP will be necessary to study the characteristics of the wild-type and mutant enzyme *in vitro*. The protein will be expressed in a bacterial system, and conditions will need to be optimized for maximizing soluble product. Investigations will include polyadenylation activity, substrate preferences, and examination of the effect of the mutation on function.

IV.

Interactions of mtPAP with other factors will be examined, utilizing co-immunoprecipitation techniques, isokinetic sucrose gradient migration, and analysis by mass spectrometry.

Chapter 2

Materials and methods

2.1 Chemicals and Reagents

All tissue culture and basic chemicals were purchased from Sigma-Aldrich, unless otherwise specified.

2.2 Methods

2.2.1 Mammalian cell lines

Human dermal fibroblasts: The cell lines were derived from skin biopsies from individuals either heterozygous or homozygous for the 1432A>G mutation in the *PAPD1* gene and healthy controls. The *PAPD1* lines were established in culture by collaborators and sent to my host laboratory. Upon receiving these cells they were immortalized at passage number 14 by transgenic expression of the E6E7 early region from human papillomavirus type 16. Expression of the E6E7 can greatly extend the life span of primary cells (Lochmüller *et al.*, 1999).

Flp-In™ T-REx™ -293 cells: Human cell line derived from human embryonic kidney culture and transformed with sheared adenovirus 5 DNA. This commercial derivative of the HEK293 line constitutively expresses the Tet repressor (continuously selected for using Blastocidin^{S}) and has an integrated Flp recombination target (FRT) site for the purpose of generating stable expression of genes under the control of a tetracycline inducible system. For the rest of the text, this commercial cell line will simply be referred to as HEK293.

2.2.2 Tissue culture

All tissue culture manipulations took place in a Microflow Class II containment cabinet, under sterile conditions. All tissue culture plasticware was purchased from Corning. 6-well plates were purchased from TPP. Cells were routinely inspected on a Zeiss Axiovert 25 inverted transmitted light microscope.

2.2.2.1 Mammalian cell maintenance and storage

Human fibroblasts and HEK293 cells were grown as monolayers at 37°C in vented flasks in humidified, 5% CO_2. DMEM containing 4500mg/L glucose, 110mg/L sodium pyruvate, supplemented with 584mg/L L-glutamine, 10% fetal bovine serum, 50ug/ml Uridine, and 50U/ml Penicillin+50ug/ml Streptomycin (Gibco) was used for culture media. HEK293 cells had Blasticidin^S (Melford) added at a final concentration of 10ug/ml every 3rd replacement of media. During culturing, cells were routinely split at 80% confluency, and media was replaced every 2-3 days.

For harvesting fibroblasts, the cells were washed once with Dulbecco's A-PBS, then incubated for 2-5min in pre-warmed 1x Trypsin/EDTA (Gibco) diluted in Dulbecco's A-PBS at 37°C. They were then pipetted to make a single-cell suspension, and had media with 10% FBS added at a 1:1 ratio to quench the trypsin reaction. For seeding, the cells were then pelleted by centrifuging at 225*g* for 4 min, resuspended in fresh media, and seeded into new flasks at a 1:2 ratio. For HEK293 cells, the protocol was the same, except 1mM EDTA in Dulbecco's A-PBS was used in place of trypsin/EDTA.

2.2.2.2 Cell counting

Cells were counted using a Neubauer Hemocytometer. Cells were harvested, pelleted by centrifugation, then resuspended in media. 20ul of the cell suspension was pipetted under the glass slide on the hemocytometer, with 10ul per side. Cells were counted on two square grids on each side. The resulting numbers were averaged and multiplied by 10,000 to calculate the number of cells per 1ml.

2.2.2.3 Cell storage

For long term storage, cells were harvested, centrifuged to pellet the cells, then resuspended in 1ml 90% FBS/10% DMSO and transferred into cryotubes. The cryotubes were then moved into a Nalgene® Mr. Frosty container at -80°C, which enabled cooling at the rate of 1°/min, for 24-48hrs. After at least 24hr incubation, the cryotubes were moved into a liquid nitrogen storage tank, and housed in the vapor phase of the nitrogen within.

2.2.2.4 Mycoplasma testing

To test for the presence of mycoplasma, 1ml of media from growing cell culture flasks was removed, and centrifuged at 225*g* for 4min in order to remove unattached cells. Post-centrifugation media was then tested using the MycoAlert™ mycoplasma testing kit from Lonza. Contaminant mycoplasma in the media are lysed and the released enzymes react with the MycoAlert™ Substrate, catalyzing the conversion of ADP to ATP. The ATP then generates a luminescent signal via luciferase. By measuring the level of ATP in a sample both before (read A) and after the addition of the MycoAlert™ Substrate (read B), a ratio can be obtained that is indicative of the presence or absence of mycoplasma. Ratios of A:B of >1 indicate contamination. Contaminated cell lines were treated with plasmocin (Invivogen,) 25ug/ml for two weeks.

2.2.3 Bacterial culturing

2.2.3.1 Bacterial strains

Bacterial Strain	Genotype	Application	Antibiotic Resistance
α-Select Bronze Efficiency (Bioline)	F^- *deo*R *end*A1 *rec*A1 *rel*A1 *gyr*A96 *hsd*R17(r_k^-, m_k^+) *sup*E44 *thi*-1 *pho*A Δ(*lac*ZYA-*arg*F)U169 Φ80*lac*ZΔM15 λ^-	Propagation of plasmids	None
Rosetta (DE3) (Novagen)	F^-*ompT hsdS*$_B$(r_B^- m_B^-) *gal dcm*(DE3) pRARE (Cam^R)	Expression of recombinant eukaryotic proteins with rare E. coli codons,	Chloramphenicol 34ug/ml
Rosetta-gami B (DE3)pLysS (Novagen)	F^-*ompT hsdS*$_B$ (r_B^- m_B^-) *gal dcm lacY1 ahpC* (DE3) *gor522*::Tn*10 trxB* pLysSRARE (Cam^R, Kan^R, Tet^R)	Combines features of Rosetta and Origami strains, enhanced disulfide bond formation	Chloramphenicol 34ug/ml, Kanamycin 15ug/ml, Tetracycline 12.5ug/ml
Tuner (Novagen)	F– ompT hsdSB (r_B– m_B–) gal dcm lacY1	Induction by IPTG can be titrated	None

2.2.3.2 DNA vectors:

Name	Application	Restriction Sites Used
pcDNA5/FRT/TO	Tetracycline-inducible vector for use with the Flp-In™ T-REx™ system. Contains a hybrid CMV/TetO2 promoter for high-level expression.	BamH1, NotI

	Also contains a hygromycin resistance gene which is only completed by proper Flp-recombinase mediated integration of target gene. Encodes ampicillin resistance.	
pGEX-6P-1	Generates a glutathione-S-transferase fusion protein, for increased soluble eukaryotic protein expression in *E. coli.* Encodes ampicillin resistance.	BamH1, NotI
pOG44	Expresses the Flp recombinase to mediate integration of genes cloned into the pcDNA5/FRT/TO vector into FRT site.	n/a
pET28a	The pET-28a vector carries an N-terminal His•Tag®/thrombin/T7•Tag® configuration plus an optional C-terminal His•Tag sequence. Encodes Kanamycin resistance.	NdeI, NotI

2.2.3.3 Bacterial media recipes

LB Medium (1L)	**LB-agar (1L)**	**SOC Medium (1L)**
10g Bacto tryptone	10g Bacto tryptone	20g Bacto tryptone
5g Bacto yeast extract	5g Bacto yeast extract	5g Bacto yeast extract
10g NaCl	10g NaCl	0.5g NaCl
	20g Bacto agar	20ml glucose (1M)
		5ml $MgCl_2$ (2M)

All Bacto products were purchased from BD. The solutions all had the pH adjusted to 7.2.

2.2.3.4 Bacterial maintenance

E. coli were grown on LB-agar plates and in liquid LB medium. For LB liquid media cells were grown in varying volumes in glass tubes or baffled flasks, shaking, at 37°C overnight (for plasmid-expression) or 20°C overnight (for protein expression). For selection on LB-agar plates, antibiotics (50ug/ml ampicillin, and strain specific antibiotic concentrations, see 2.2.3.1) were added prior to the LB-agar solidifying, and the LB-agar poured into plastic petri dishes. Bacteria were then spread on the plates and incubated inverted overnight at 37°C.

2.2.3.5 Bacterial storage

For short term storage, LB-agar plates with bacteria were kept at 4°C for no more than 2 weeks. For long term storage of bacterial strains, cells were grown on LB-agar plates with appropriate antibiotics, and incubated inverted overnight at 37°C. The following day LB media with 18% glycerol was pipetted onto the plates, and the bacteria suspended in solution. This bacterial suspension was transferred into a microtube and stored at -80°C.

2.2.3.6 Transformation of chemically competent cells

Frozen 40ul aliquots of competent bacterial cells were thawed on ice, and gently resuspended by flicking the tube. DNA (10ng) was added to the cell mixture, and incubated on ice for 30min. The cells were then subjected to a 30sec heat shock at 42°C, then incubated on ice for 2min. 1ml of SOC media pre-warmed at 37°C was then added, and incubated for maximum 1 hour at 37°C, shaking. The cell mixture was then centrifuged at 2000rpm on a Micro Centaur centrifuge (MSE) for 5min to pellet the bacteria. This pellet was resuspended in fresh 100ul pre-warmed SOC media, and spread on LB-agar plates supplemented with the appropriate antibiotics. The plates were incubated inverted at 37°C overnight.

2.2.4 DNA handling and manipulations

2.2.4.1 DNA isolation from human cells

Human cultured cells were harvested from 25cm^2 flasks and pelleted by centrifugation, then resuspended in 400ul low TE buffer (10mM Tris pH 8, 1mM EDTA). 50ul of 10% SDS and 50ul of proteinase K (20mg/ml stock) were added to give final concentrations of 1% and 2mg/ml respectively, and the samples incubated at 37°C with gentle shaking overnight. If the sample was clear following overnight incubation, phenol/chloroform extraction and ethanol precipitation was carried out (see 2.2.4.4), if not then further proteinase k was added and the incubation extended.

2.2.4.2 Plasmid DNA isolation from bacteria

Antibiotic-resistant colonies were used to inoculate 5ml LB media cultures that were incubated at 37°C overnight, shaking. The plasmid DNA was then extracted using the GeneJet plasmid prep kit (Thermo), according to manufacturer's protocol. Purified plasmid DNA was then stored in deionized water at -20°C.

2.2.4.3 Amplification of DNA by polymerase chain reaction (PCR)

To amplify DNA regions of interest, polymerase chain reactions using various primers and polymerases were used. Reactions were performed in thick-walled 0.5ml tubes, in a final volume of 50ul. PCR products were purified via phenol/chloroform extraction and ethanol precipitated. KOD Hot Start Polymerase 10x Buffer contains $MgCl_2$. KOD polymerase was utilized for cloning PCRs, as it is a proofreading enzyme. For non-cloning PCRs, the DreamTaq (Thermo) polymerase was used. For DreamTaq PCRs, the MgSO4 was omitted due to its presence in the corresponding 10x buffer

Standard proofreading PCR reaction mix:

Component	Final Concentration in PCR Reaction
10X Buffer for KOD Hot Start Polymerase	1X
25mM $MgSO_4$	1.5mM
2mM dNTPs	0.2mM
Forward Primer (10uM)	0.6uM
Reverse Primer (10uM)	0.6uM
Template DNA	10ng Total
KOD Hot Start Polymerase (1 U/ul)	0.02U/ul
Nanopure H_2O	Made up to 50ul

Standard KOD polymerase PCR Profile:

Step	Reaction Profile	Reaction Step
1	95°C - 4 minutes	Initial Denaturation
2	95°C - 1 minute	Denaturing
3	T_m-4°C - 1 minute	Annealing
4	70°C - 2 minutes, 30 seconds	Extension
5	*Back to Step 2, 35 cycles*	# of cycles
6	70°C - 7 minutes	Final Extension
7	4°C - Indefinitely	Hold

Example DreamTaq polymerase PCR Profile:

Step	Reaction Profile	Reaction Step
1	95°C - 1 minute	Initial Denaturation
2	95°C - 30 seconds	Denaturing
3	T_m-4°C - 30 seconds	Annealing
4	72°C - 1 minute/kb	Extension
5	*Back to Step 2, 35 cycles*	# of cycles
6	72°C - 5 minutes	Final Extension
7	4°C - Indefinitely	Hold

2.2.4.4 Primers used in this investigation

Primer Name	Primer Sequence	T_m
mtPAPF	5’ CACACGGATCCTTAGCAATGGCGGTTCC 3’	52ºC
mtPAPFLAGR	5’CAC ACG CGG CCG CTA CTT ATC GTC GTC ATC CTT GTA ATC TGT TCT CTT CCC ACT GG 3’	52ºC
mtPAP6PF	5' CACACAGGATCCAGTTGCCCAGGAACTGTG 3’	52ºC
Mut-mtPAPF	5' CTC TGT ACA TTC AGG ATC CAT TTG AAA CTT C 3'	54ºC
Mut-mtPAPR	5' GAA GTT TCA AAT GGA TCC TGA ATG TAC AGA G 3'	54ºC
mtPAPR2	5' CAC AGC GGC CGT CAT GTC TGA GTA CTA ATT GTT CTC TTC CCA CTG G 3’	54ºC
MPAT: DNA Linker	5' P-ATGTGAGATCATGCACAGTCATA-NH_2 3'	52ºC
MPAT: Anti-LIGN	5' GAC TGT GCA TGA TCT CAC 3'	54ºC
MPAT: *RNA14*	5' GTG ATT ATA GGC TTT CGC 3'	50ºC
MPAT: *RNA14* Nested	5' AGT AAG CCT CTA CCT GCA CG 3'	54ºC
MPAT: *MTND3*	5' CCG CCC GCG TCC CTT TC 3'	54ºC
MPAT: *MTND3* Nested	5' GAC TAC AAA AAG GAT TAG ACT-3'	54ºC
MPAT: *MTCO1*	5' CAT ATT CAT CGG CGT AAA TC 3'	54ºC
MPAT: *MTCO1* Nested	5' CAA CCC CAT GGC CTC CA 3'	54ºC
MPAT: *MTCO3*	5' TC TGC TTC ATC CGC CAA CTA 3'	54ºC
MPAT: *MTCO3* nested	5' TGT ATG TCT CCA TCT ATT GAT 3'	54ºC
ND3PAP-F	5' ATT TAG GTG ACA CTA TAG AAC TAC CAC AAC TCA ACG G 3'	54ºC
ND3PAP-R	5' ATT CGG TTC AGT CTA ATC C 3'	54ºC
ND3Rev-A8	5' TTTTTTTT ATT CGG TTC AGT CTA ATC C 3'	54ºC
A6PAP-F	5' ATT TAG GTG ACA CTA TAG AGA AAC CAT CAG CCT ACT C 3'	54ºC
A6PAP-R	5' TAT GTG TTG TCG TGC AGG 3'	54ºC
ATP6Rev-A8	5' TTTTTTTT TAT GTG TTG TCG TGC AGG 3'	54ºC
pGEX-mtPAPΔN Sequencing ORF 5'	5' TAC GAC AGC ATA GAG ACC 3'	54ºC
pGEX-mtPAPΔN Sequencing ORF 3'	5' GGA AGG GAG CAA AAC AAA CC 3'	58ºC
pcDNA5-mtPAPFLAG Sequencing ORF 5' (CMV Forward)	5'CGC AAA TGG GCG GTA GGC GTG 3'	60ºC
pcDNA5-mtPAPFLAG Sequencing ORF 3' (BGH Reverse)	5' TAG AAG GCA CAG TCG AGG 3'	50ºC
MTND4 qPCR F	*5' CCA TTC TCC TCC TAT CCC TCA AC 3'*	59ºC
MTND4 qPCR R	5' CAC AAT CTGATG TTT TGG TTA AAC TAT ATT T 3'	59ºC
18S qPCR F	5' GTA ACC CGT TGA ACC CCA TT 3'	59ºC
18S qPCR R	5' CCA TCC AAT CGG TAG TAG CG 3'	59ºC

2.2.4.5 Phenol/chloroform extraction and ethanol precipitation of DNA

DNA samples were made up to at least 100ul dH_2O, then an equal volume of phenol (Sigma) was added. The mix was vortexed for 30 seconds, then centrifuged for 3 minutes, 13,000rpm, at room temperature in a Micro Centaur (MSE) centrifuge. The aqueous phase was transferred to a fresh microtube, and mixed with an equal volume of 50% phenol and 50% CIAA (CIAA = 24:1 chloroform: isoamylalcohol). The mixture was vortexed for 30 seconds, then centrifuged as before. The aqueous phase was again moved to a fresh microtube, and an equal volume of CIAA added. Vortexing and centrifuging were done again as before. The aqueous phase was transferred to a fresh microtube, and 1ul of linear acrylamide, 1/10th volume of 3M NaOAC pH 5.2, and 2 volumes of 100% ethanol were added. This mixture was then incubated at -20°C overnight. The next day, the mixture was centrifuged at 20,800*g*, for 30 minutes at 4°C in an Eppendorf 5417R centrifuge. The supernatant was discarded, and the DNA pellet washed once with 75% ethanol and once after that with 100% ethanol. The DNA pellet was then re-suspended in 20-40ul dH_2O.

2.2.4.6 DNA electrophoresis and gel excision

For analysis of DNA size, 100ng DNA in dH_2O was mixed 1:1 with a 50% glycerol/dH_2O mixture, and loaded onto a 0.7% agarose gel (0.35g agarose (NBS Biologicals), 50ml 1x TAE buffer (40mM Tris, 20mM acetic acid, 1mM EDTA, pH 8.4), and 0.2ug/ml ethidium bromide). For gel purification the conditions were the same but the agarose gel consisted of 1% low melting temperature agarose (Lonza), and the entire DNA sample was loaded for electrophoresis. In both types of agarose gels, the DNA was electrophoresed at 70V for approximately 1 hour in 1x TAE buffer. DNA was visualized by UV transillumination. For gel excision, specific base pair sizes were cut out of the agarose gel using sterile scalpel blades, reserved in a fresh microtube and then phenol/chloroform extracted, followed by ethanol precipitation.

2.2.4.7 Restriction digests

Restriction endonucleases used were BamH1 (NEB), Not1 (NEB), and FspI (NEB). Reaction conditions for BamH1, Not1, or BamH1/Not1 double digests were 2ug DNA, 1x NEB buffer 3, 100ug/ml BSA, 20 Units each restriction enzyme, incubated for 3 hours at 37°C. FspI digest conditions were 20ug DNA, 1x NEB buffer 4, 25 Units enzyme, incubated overnight at 16°C. Post-digestion, DNA was phenol/chloroform extracted and EtOH precipitated. At points in the project, High-Fidelity (HF™) versions of BamH1 and Not1 (NEB) were used. Reaction conditions were the same as before, except both are 100% active in Buffer 4 (NEB), and incubations were carried out at 37°C for 1 hour. Restriction digests were used for generating sticky ends of PCR fragments as well as linearizing plasmid DNA.

2.2.4.8 Dephosphorylation of plasmid DNA

Post-restriction digest, 1ul calf intestinal alkaline phosphatase (Boehringer Mannheim), 1ul 10% SDS, and 3.5ul 1M Tris pH 9 was added to the 20ul plasmid digest. This was incubated at 37˚C for 30 mins, then 0.5ul of 0.5M EDTA was added to terminate the reaction. The dephosphorylated plasmid DNA was purified by phenol/chloroform extraction and ethanol precipitation prior to use in ligation reactions.

2.2.4.9 Ligation of DNA

Ligation reactions were carried out in 10ul volumes, using the T4 ligase (Fermentas). The molar ratio of restriction digested PCR fragment to vector was 3:1. The amount of insert DNA required in nanograms was determined with the following equation:

$$\frac{(ng\ vector) \times (kb\ size\ of\ insert)}{(kb\ size\ of\ vector)} \times (Ratio\ of\ insert\ to\ vector) = ng\ insert$$

The appropriate amount of both fragment and vector had 1ul 10x ligation buffer and 1ul T4 ligase added to a final volume of 10ul, and were incubated overnight at 16°C. After overnight incubation, the reaction was incubated at 65°C for 15min to inactivate the T4 ligase.

2.2.4.10 Quantification of nucleic acids

Quantifying the concentration of nucleic acids in samples was performed with a NanoDrop® ND-1000 (Thermo) UV-Vis Spectrophotometer at a wavelength of 260nm, using 1ul of sample. At 260 nm, the average extinction coefficients are 40mM for RNA, 50mM for dsDNA and 25mM for ssDNA.

2.2.4.11 DNA sequencing

Sequencing was carried out using a 3130*xl* Genetic Analyzer (Applied Biosystems), according to the manufacturer's instructions. The sequencing reactions were kindly carried out by Ms. Charlotte Alston. Primers for sequencing are listed in 2.2.4.4. Samples were prepared by mixing 500ng DNA with 1.5ul 5x sequencing buffer v3.1, 1 ul primer (stock 3.2uM), and 3ul BigDyes® Terminator v3.1. Reactions were made up to 20ul, and cycle sequenced according to the following parameters:

Step	Reaction Profile	Reaction Step
1	95°C - 5 minutes	Initial Denaturation
2	95°C - 30 seconds	Denaturing
3	50°C - 10 seconds	Annealing
4	60°C - 4 minutes	Extension
5	*Back to Step 2, 30 cycles*	# of cycles
6	4°C - Indefinitely	Hold

The PCR products were then precipitated in a 96-well plate, and 10ul of Hi-Di added, followed by incubation at 95°C for 2 min. Samples were then loaded onto the 3130*xl* genetic analyzer. Sequencing data was analyzed using SeqScape® v2.6 software (Applied Biosystems).

2.2.5 RNA handling and manipulations

2.2.5.1 RNA isolation from human cells

RNA was isolated from cultured human cells using Trizol (Invitrogen) following the manufacturer's instructions. Cells were harvested and pelleted by centrifugation. The cell pellet was thoroughly homogenized by pipetting in 1ml of Trizol reagent (Invitrogen). The suspension was incubated 5min at RT. 0.2ml chloroform per 1ml Trizol was added, and the tube was shaken vigorously by hand for 15sec, then incubated for 2-3min at RT. The sample was centrifuged at 12,000*g* for 15min at 4^{0}C. The aqueous RNA phase was transferred into a fresh tube and 0.5ml of isopropyl alcohol per 1ml of Trizol added. This was mixed and incubated at RT for 10min, then centrifuged at 12,000*g* for 10min at 4^{0}C. The supernatant was removed, and the RNA pellet washed once with 70% ethanol in DEPC treated H_2O, and once with 100% ethanol. Then the pellet was resuspended in 20-40ul DEPC treated H_2O. The RNA was then quantified by Nanodrop® analysis.

2.2.5.2 *In vitro* transcription of RNA

Generation of RNA species via *in vitro* transcription was accomplished using the Ampliscribe Sp6 kit (Epicentre® Biotechnologies), following the manufacturer's instructions. DNA templates for *in vitro* transcription were PCR products with an SP6 promoter incorporated on to the 5' end. Briefly, the transcription reaction mix was assembled in the following order:

Amount (ul)	Component
To final vol of 20	Nuclease-free H_2O
1	50mM ATP solution
1	50mM CTP solution
1	50mM GTP solution
1	50mM UTP solution
2	10x reaction buffer
0.1-1	DNA template
2	100mM DTT
2	SP6 enzyme mix

Once assembled, the reaction mix was mixed thoroughly and incubated for 2 hours at 37°C. Then 1ul of TURBO DNase I (2U) was added and incubated at 37°C for a further 15min to remove the DNA template. RNA was recovered by phenol/chloroform

extraction and ethanol precipitation. The RNA pellet was washed once with 75% ethanol in DEPC H_2O, and once in 100% ethanol, then resuspended in 20-40ul DEPC treated H_2O. The RNA concentration was determined via Nanodrop®, then finally SUPERase-In™ (Ambion), an RNase inhibitor, was added to a final concentration of 1U/ul to prevent degradation of the RNA samples.

2.2.5.3 Denaturing RNA electrophoresis

Total RNA (5-10ug) was mixed in sample buffer consisting of 1x MOPS (40mM MOPS acid, 10mM NaOAc, 1mM EDTA pH 7.2), 15% formaldehyde, 35% formamide, 0.1mg/ml ethidium bromide, bromophenol blue and xylene cyanol), heat denatured for 15min at 55°C, then electrophoresed through a 1% agarose-formaldehyde denaturing gel (0.75g agarose, 1.5ml formaldehyde, 6ml 10x MOPS, 52.5ml dH_2O) in 1x MOPS buffer at 50V for 2-3 hrs. Integrity and migration of RNA was visualized with a UV transilluminator after electrophoresis. For *in vitro* transcribed RNA, 6% polyacrylamide/8M Urea/1x TBE (100mM Tris, 90mM boric acid, 1mM EDTA) gels were used for electrophoresis. The sample buffer was 90% formamide/1x TBE. These gels were pre-run at constant 150V for 30-60min prior to loading RNA. Electrophoresis was performed at constant 150V for 1.5-2 hours.

2.2.5.4 Reverse transcription

For generating complementary DNA (cDNA) the Superscript II Reverse Transcription kit (Invitrogen) was used. RNA (5-10ug) was mixed with 1ul oligo δT primer (stock 100uM), made up to 12ul with DEPC-treated H_2O, and incubated at 70°C for 10min, then moved directly to ice for 1min. On ice, 4ul of 5x First-Strand Reaction Buffer, 2ul of 0.1M DTT, and 1ul of 10mM dNTPs were added to the reaction mix. The reaction was then incubated at 42°C for 5min. Superscript II reverse transcriptase was then added (1ul, 200U), the solution gently mixed, then incubation at 42°C was continued for 59min. The reverse transcriptase was inactivated by heating at 70°C for 15min. The resulting cDNA was stored at -80°C.

2.2.5.5 Northern blotting

RNA was electrophoresed through agarose as described above. Gels were imaged to confirm RNA migration and quality, then transferred to Genescreen Plus membrane (Perkin Elmer) by overnight capillary transfer in 10x SSPE (3.6M NaCl, 200mM phosphate buffer pH 7, 20mM EDTA) any gel fragments were removed, the blot washed with 2x SSPE and baked at 80°C for 2 hrs in vacuum dryer. The membrane was then blocked with pre-hybridization solution containing 50% formamide, 5x SSPE, 1% SDS, 1x Denhardts solution, rotating 2 hrs at 42°C. ^{32}P-labeled DNA probes against RNA targets were generated using DNA templates synthesized by PCR amplification. These random hexamer labelling reactions (15ul) consisted of 50ng DNA template, 3ul random hexamer mix, 1ul (5U) DNA polymerase I (Klenow fragment, Promega), 2ul ^{32}P α-dCTP (10-20uCi, Perkin Elmer NEG513H), and incubated at 37°C for 1 hour. Free nucleotides were removed by use of an Illustra G-25 column (GE Healthcare), according to manufacturer's protocol. The activity of the labeled probes was estimated using a Cerenkov counter. The probes averaged 5000cpm/ul, and 10ul of probe was added to the pre-hybridization solution following blocking, and membranes were incubated overnight at 42°C with rotating. Following hybridization, membranes were washed twice with 20ml of 2x SSPE for 15min at RT, then once with 20ml pre-warmed 2x SSPE/2% SDS for 15min at 65°C. The membrane was wrapped in SARAN wrap and exposed to Phosphor-Imager screens, the signal was then visualized with a Typhoon FLA 9500 imaging system and ImageQuant software (GE Healthcare).

2.2.6 Protein handling and manipulations

2.2.6.1 Protein isolation from human cells

Cell lysates were prepared from cultured primary and immortalized human fibroblasts, and HEK293 cells. Cells with confluency of approximately 80% had culture media refreshed the night before harvesting. Cells were detached and pelleted as described previously, washed once in Dulbecco's A-PBS, pelleted again, and stored on ice until protein extracted. Cell pellets were suspended in chilled lysate buffer (50mM Tris pH 7.5, 130mM NaCl, 2mM $MgCl_2$, 1mM PMSF, 1% NP-40, with 1x EDTA-free protease inhibitor cocktail (Pierce)) by adding 80ul lysate buffer (per 5,000,000 cells) to cell pellets, and pipetting to lyse. The lysate was incubated on ice for 15min, with occasional mixing. The nuclear fraction of the lysate was then removed by centrifuging at 560g at

4°C for 2 minutes in an Eppendorf 5415R centrifuge. The supernatant, comprising the cytoplasmic fraction, was transferred to a fresh chilled tube. The protein concentration was then quantified via Bradford assay.

2.2.6.2 Isolation of crude mitochondria from human cells

Cultured human cells grown in 225cm^2 flasks were detached and pelleted as described above. These cells were then suspended in 2ml of homogenization buffer (0.6M mannitol, 10mM Tris pH 7.4, 1mM EGTA, 1mM PMSF, 0.1% BSA). This suspension of cells was subjected to 15 passes of homogenization in a 2 ml glass-teflon homogenizer (Glas-Col), followed by centrifugation at 400*g*, 4°C, for 10min in an Eppendorf 5415 R centrifuge. The supernatant containing the crude mitochondria was retained on ice, while the pelleted material was resuspended in fresh 2ml of homogenization buffer, and homogenization and centrifugation were repeated. The supernatant fractions were collected and centrifuged at 400*g*, 4°C, for 5min to further clear non-mitochondrial material. All cleared supernatant fractions were then centrifuged at 11,000*g*, 4°C, for 10min to pellet the mitochondria. The mitochondrial pellets were washed in a minimum of 300ul each of homogenization buffer without BSA, and combined into one tube. This combined mitochondrial fraction was centrifuged again at 11,000*g*, 4°C, for 5min to generate a single pellet of crude mitochondria. Pellets were flash-frozen in liquid nitrogen and stored at -80°C.

2.2.6.3 SDS polyacrylamide gel electrophoresis

Cell and mitochondrial lysates were analyzed by SDS polyacrylamide gel electrophoresis using either Hoefer Mighty Small™ system or Bio-Rad Mini-Protean® tetra cell. Stacking and resolving gels were prepared according to table below.

Component composition of SDS polyacrylamide gels

Reagent	3.75% Stacking Gel	12% Resolving Gel
30% polyacrylamide (29:1 acrylamide/bis-acrylamide)	0.625ml	1.998ml
3.75M Tris-HCl pH 8.5	n/a	0.5ml
0.5M Tris-HCl pH 6.8	1.25ml	n/a
10% SDS	50ul	50ul
10% Ammonium Persulfate	50ul	50ul
TEMED	5ul	5ul
dH_2O	Up to 5ml	Up to 5ml

Prior to loading on to gels, samples were diluted with 5x Laemmli buffer (10% SDS, 250mM Tris-HCl pH 6.8, 500mM DTT, 50% glycerol, and bromophenol blue). Especially viscous samples were incubated with 25U benzonase (Novagen) to digest any cellular DNA present. The samples were electrophoresed at a constant voltage of 100V for the Hoefer system, or 200V for the Bio-Rad system, in a running buffer consisting of 25mM Tris, 192mM glycine, and 0.1% [w:v] SDS. The Spectra^{TM} Multicolor Broad Range Protein Ladder (Thermo Scientific) was loaded for protein size comparison.

2.2.6.4 Coomassie blue staining

Total protein content separated by electrophoresis through polyacrylamide gels was visualized by staining gels with Coomassie Brilliant Blue. After electrophoresis, gels were immersed in staining solution containing 30% methanol, 10% acetic acid, and 0.1% Coomassie Brilliant Blue R250 for 1 hour. The background was then removed with destaining solution containing 30% methanol and 10% acetic acid for at least 1 hour or more as necessary. Stained gels were imaged using the ChemiDoc^{TM} MP system (Bio-Rad).

2.2.6.5 Silver staining

Silver staining is a more sensitive method for visualizing protein content compared to Coomassie staining. After electrophoresis of samples, polyacrylamide gels were fixed overnight at RT in 50% methanol with gentle rocking. The following day the gel was incubated in freshly made silver staining solution (0.1% $AgNO_3$, 10mM NH_4OH, 0.36% NaOH) for 15min, then washed three times for 5min in dH_2O. Developer solution (0.04% formaldehyde, 0.05% citric acid) was then added, and the gel incubated until desired intensity of protein signal was observed. The reaction was terminated by washing gel with 5% acetic acid. Stained gels were imaged using the ChemiDoc™ MP system (Bio-Rad).

2.2.6.6 Immunoblotting

Typically 40ug of total cell lysate was separated by SDS-PAGE as described above. Prior to transfer, PVDF membranes (Immobilon-P, Millipore) were activated by immersion in methanol for 20sec, and rinsed in dH_2O before equilibrating in transfer buffer (25mM Tris, 192mM glycine, 0.02% SDS, and 15% methanol). The polyacrylamide gel and membrane were assembled between two pieces of Whatman 3MM filter on each side. Proteins were then transferred using Mini Trans-blot™ module (Bio-Rad) at a constant 100V, for 1 hr at 4°C in transfer buffer. Membranes were blocked in 5% milk/TBS-Tween at for 1 hr at RT. Antibodies used for blotting are listed in 2.2.6.8. Primary antibody incubations were performed in 1% milk-TBST for 3 hrs at RT or overnight at 4°C, and secondary antibody incubations were performed in 1% milk/TBST for 1 hr at RT. Blots were developed using ECL Prime (GE Healthcare), and imaged using a ChemiDoc™ MP system (Bio-Rad).

2.2.6.7 Antibodies used for immunoblotting

Primary Antibody	**Species**	**Clonality**	**Dilution**
M2 Flag (Sigma F1804)	Mouse	Monoclonal	1:1000
Cytochrome *c* Oxidase Subunit 1 (Mitosciences MS404)	Mouse	Monoclonal	1:1000
Cytochrome *c* Oxidase Subunit 2 (Mitosciences MS405)	Mouse	Monoclonal	1:1000
Cytochrome *c* Oxidase Subunit 3 (Mitosciences MS406)	Mouse	Monoclonal	1:1000
Cytochrome *c* Oxidase Subunit 4 (Mitosciences MS407)	Mouse	Monoclonal	1:1000
Succinate Dehydrogenase Subunit A (Mitosciences MS204)	Mouse	Monoclonal	1:5000
Porin (Mitosciences MSA03)	Mouse	Monoclonal	1:10,000
TOM20 (Santa Cruz sc-17764)	Rabbit	Polyclonal	1:750
mtPAP (GeneTex GTX70156)	Mouse	Monoclonal	1:1000
mtPAP (Epitomics S3295)	Rabbit	Polyclonal	1:500
MRPL3 (Abcam ab39268)	Goat	Polyclonal	1:2000
DAP3 (Abcam ab11928)	Mouse	Monoclonal	1:1000
NDUFA9 (Mitosciences MS111)	Mouse	Monoclonal	1:1000
NDUFB8 (Mitosciences MS105)	Mouse	Monoclonal	1:1000
Complex V α-subunit (Mitosciences MS502)	Mouse	Monoclonal	1:1000
Complex III core 2 (Mitosciences MS304)	Mouse	Monoclonal	1:1000
ATP8 (Santa Cruz sc-84231)	Rabbit	Polyclonal	1:200
LRPPRC (Santa Cruz sc-66844)	Rabbit	Polyclonal	1:200
ND1 (gift from A. Lombes)	Rabbit	Polyclonal	1:1000
ND1 (Gift from Dr A Spinazzola)	Chicken	Polyclonal	1:10,000
ATAD3 (Gift from I. Holt)	Rabbit	Polyclonal	1:50,000
Secondary Antibodies	**Species**	**Clonality**	**Dilution**
Anti-Mouse, HRP-conjugated (Dako P0260)	Rabbit	Polyclonal	1:2000
Anti-Rabbit, HRP-conjugated (Dako P0399)	Swine	Polyclonal	1:3000
Anti-Goat, HRP-conjugated (Dako P0449)	Rabbit	Polyclonal	1:2000

Chapter 3

Modification of the mitochondrial poly(A) tail assay to a fluorescent platform

3.1 Introduction

Since the discovery of polyadenylation activity in thymus nuclei extracts over 50 years ago (Edmonds and Abrams, 1960), analyzing the properties and functions of poly(A) tails has been a major focus of research. Characterization of nuclear and cytosolic polyadenylation, both in terms of molecular mechanics and functional purposes has come a long way. The major characteristic of polyadenylation that can confer function, is the chain of adenosine monophosphates added to mRNAs. Initial characterization of polyadenylating enzymes was primarily focused on *in vitro* studies, as it was difficult to isolate intact poly(A)+ mRNA from cells for analysis of tail lengths. These *in vitro* systems were extremely useful and much of our modern understanding of polyadenylation mechanics stems from those experiments.

There are multiple techniques that have been utilized to assess the length of poly(A) tails. These include RNase protection assays, northern blots, using PCR to amplify 3' regions of transcripts for comparison on denaturing gels, and direct sequencing of cDNA generated from RNA. Another common approach to assess poly(A) tail length is circularizing the mRNAs to capture the full tail, then reverse transcribing and PCR amplifying the region of interest. The amplicons can then be cloned into plasmids, and sequenced. This was the method undertaken in the first published description of the human mitochondrial poly(A) polymerase (Tomecki, 2004). As an alternative to direct sequencing of the PCR products, the amplicons can be radioactively labeled and separated by polyacrylamide-urea gel electrophoresis (Slomovic and Schuster, 2007).

There are benefits and drawbacks to each technique. One of the primary benefits of sequencing is the lack of ambiguous results of the nucleotide sequences. A major drawback is that many sequencing platforms have difficulty with homopolymeric tracts, causing distorted sequence readouts. The existence of populations of different poly(A) length poses a problem for sequencing based methods as well. Following PCR that will preferentially expand the shortest template will be of the most prevalent and will not allow for a broad view of differing poly(A) lengths. When using separation via electrophoresis to analyze tail lengths, these benefits and drawbacks are largely reversed. Populations of differing lengths can be observed relatively easily on the gels, but careful

design of size markers and clarity of detection methods are paramount for correct interpretation of results.

In 2003, our lab published a paper describing the functional consequences of a pathological microdeletion in the *MTATP6* gene in a patient (Temperley, 2003). To determine poly(A) tail length this reported a modification of a technique used for cytosolic transcripts, and was the first published protocol for the mitochondrial poly(A) tail assay (MPAT). The assay allowed analysis of the lengths of poly(A) tails on mitochondrial mRNAs with the single nucleotide resolution. Data using this technique was also reported in an article on characteristics of human mitochondrial mRNAs and their polyadenylation status (Temperley *et al.*, 2010b) and an investigation into the effects of mitochondrial poly(A) tail removal and blockage by mitochondrially-targeting the cytosolic deadenylase PARN and the poly(A) binding protein PABPC1 respectively (Wydro *et al.*, 2010). In each of these investigations, the MPAT provided critical data on the poly(A) tail lengths of mt-mRNA, both the absolute tail length and the distribution of oligo- and polyadenylated populations present in cells.

The most recent use of the MPAT was in the assessment of a family harboring a mutation in the *PAPD1* gene, which encodes the mitochondrial poly(A) polymerase, mtPAP (Crosby *et al.*, 2010). Individuals homozygous for the 1432A>G mutation showed a short oligo(A) tail on mt-mRNAs. Heterozygous carriers did not show such a severe truncation, essentially reflecting the ratio of oligo- and polyadenylation observed in control cells. This was the extent of the characterization of this novel mutation in the research article. The initial impetus for this thesis work was to further our understanding of the function of the mitochondrial poly(A) tail in gene expression and to analysis the effect of the PAPD1 mutation, both in terms of downstream biochemical effects. The MPAT would thus be a valuable tool to employ in this research.

The MPAT assay was designed using standard 5'- radiolabeling of PCR primers in order to visualize nucleotide lengths once products had been separated by denaturing polyacrylamide/urea gel electrophoresis. In light of the increase in sensitivity of fluorescent moieties, the decision was made to convert the MPAT assay from a radiation-based platform to a fluorescence-based one. This would have several benefits over the previous employments of the assay. First and foremost the ^{32}P-radiolabelled primers have a short half life and need to be remade frequently to prevent loss of sensitivity. This contrasts with fluorescently tagged primers that once synthesized, retain their sensitivities indefinitely if corrected stored. With radiolabeled PCR products, post electrophoresis the gel needs to be immobilized on Whatman paper, dried for several hours, then exposed to

phosphorscreens for several hours up to multiple days. Fluorescent labeling again has an advantage as it allows immediate imaging of the gel itself, removing all the drying and exposure steps of autoradiography. Using radiolabeled primers means that for maximum sensitivity experiments must be completed within the window dictated by the isotope decay rate. Fluorescent-labeling of probes allows for highly sensitive, permanently available probes. Finally, fluorescence allows users to avoid exposure to ionizing radiation, while ideally maintaining or exceeding the sensitivity of radiation-based methods. In total, there was much to be gained by developing a fluorescent MPAT assay.

In this chapter, the results show that after the initial phase of optimization, I was able to establish the fluorescent MPAT with comparable sensitivity to the radiation-based MPAT results. This allowed it to be used in replacement of the radioactive assay for the poly(A) analysis of the *PAPD1* 1432A>G mutant fibroblasts.

3.2 Methods

3.2.1 Radioactive mitochondrial poly(A) tail assay

This technique was performed essentially as described in (Temperley, 2003).

RNA Ligation: RNA (2.5ug) isolated from cultured human cells was ligated to 20pmol of a universal DNA 5' phospho oligonucleotide linker (see 2.2.4.4) blocked with an NH_2 group at the 3' end. First, 10x T4 RNA Ligase buffer (NEB) was thawed and pre-warmed at 37°C and vortexed to assure it was all in solution. RNA and linker were chilled on ice, in a thick-walled 0.5ml microtube. This mix was then preheated at 90°C for 2 min, then transferred onto ice for a minimum of 1 min. PEG 1000 (50% stock in DEPC-treated H_2O) (final conc. 12.5% v:v) was added whilst still on ice, and then 1ul of pre-warmed 10x T4 RNA Ligase buffer was added. This mixture was pulsed down and 20 units T4 RNA Ligase (NEB) added. The ligation was performed for 3 hrs at 37°C. After incubation, the reaction products were made up to 100ul with DEPC H_2O, and phenol (at pH 6.7)/chloroform extracted and precipitated using 1/10th volume 3M sodium acetate pH 5.2 (made up in DEPC-treated H_2O) and 2 volumes 100% ethanol.

Reverse Transcription and PCR Amplification: Once the RNA was precipitated, it was re-suspended in 11ul DEPC H_2O. 5.5ul of re-suspended product was mixed with 10pmol of Anti-LIGN primer (appendix A). The RNA and Anti-LIGN primer were heated at 70°C for 10 min, then transferred on to ice, where a master mix of 2ul of 5x Superscript buffer, 1ul of 100mM DTT and 0.5ul 10mM dNTPs were added. This mixture was pre-heated at 42°C for 5 min, then 0.5ul (100U) Superscript II enzyme (Gibco) was added. Reverse transcription was performed at 42°C for 59min, followed by 70°C for 15min. The resulting cDNA (1ul) was used as a template in a 50ul reaction mix for a 35 cycle PCR reaction. This is termed the "cold PCR" reaction. The reaction mix consisted of 34.5ul dH_2O, 2.5ul 20uM Anti-LIGN primer, 2.5ul 20uM *RNA14* primer (see 2.2.4.4), 3ul 25mM $MgCl_2$, 1ul 10mM dNTPs, 5ul 10x PCR buffer (Thermo), and finally 0.5ul (2.5U) Taq polymerase (Thermo) was added once the reaction mix was heated to 94°C. The PCR profile is detailed in 3.2.3. The PCR reaction products (5ul) were analyzed by agarose gel electrophoresis to confirm presence of correct sized product prior to precipitating. PCR reaction products were then ammonium acetate/ethanol precipitated by adding 1 ul linear acrylamide, ½ volume of 7.5M NH_4OAC, and 2 volumes EtOH. This was incubated for 2 hours at -80°C. The product was pelleted by centrifuging as detailed for normal EtOH precipitation, not washed with EtOH, but re-suspended in 10-12.5ul dH_2O.

Radiolabeling PCR and Sequencing Gel: Re-suspended "Cold PCR" products (2.5ul) were used in a 2nd PCR reaction (termed the 'hot PCR') programmed with 1 Unit Taq polymerase (Thermo) 1x PCR buffer (Thermo), 1.5mM $MgCl_2$, 0.2mM dNTPs, 0.3uM nested radiolabelled forward primer internal to the target gene and 0.3uM Anti-LIGN reverse primer, in a final reaction volume of 10ul, with 30ul of mineral oil overlaid. The 'hot PCR' profile is shown in 3.2.3, and underwent 5 cycles of amplification. The forward primers (5 pmol) were all 5' end-labeled by T4 polynucleotide kinase (NEB) with [γ-^{32}P] dATP (3000 Ci/mmol, Perkins-Elmer), in 1x PNK buffer (NEB), for 30min at 37°C, and free radioactive nucleotides removed by overnight dialysis. The amount of radiolabeled primer needed per hot PCR was calculated by dividing the desired input of moles (0.3pmol) by the amount initially radiolabeled (5pmol) and multiplied by the recovered dialysis volume (ul). This gave the number of ul of labeled primer stock needed per reaction. As an alternative to purification by dialysis, illustra Microspin G-25 columns were used for removal of radioactive nucleotides from labeling reactions, according to manufacturers protocol. Following the PCR, 3ul aliquots of the labeled products, mixed

with 8ul loading buffer (1x TBE buffer, 90% [v:v] formamide, bromophenol blue, xylene cyanol) were separated on a pre-electrophoresed (for 30 min) 10% polyacrylamide (29:1 ratio of bis/acrylamide), 8.2 M urea denaturing gel in 1x TBE buffer at 50W for 2-3 hours. Bromophenol blue and xylene cyanol were used to monitor sample migration during electrophoresis. The gel was then transferred to Whatman paper and vacuum dried at 80°C for 2 hours. Finally the gel was exposed to a PhosphorImager cassette (Molecular Dynamics) and visualized by a Storm PhosphorImager.

3.2.2 Fluorescent mitochondrial poly(A) tail assay

The fluorescent assay follows the same procedures as the radiolabeled assay to generate the 'cold' PCR products. The remaining sections were modified and described below.

Fluorescent PCR and Sequencing Gel: 2.5ul of re-suspended "Cold PCR" products were used in a 2nd PCR reaction (now termed the 'fluoro-PCR') programmed with 1 Unit Taq polymerase (Thermo) 1x PCR buffer (Thermo), 1.5mM $MgCl_2$, 0.2mM dNTPs, 3uM nested Alexafluor-647 labeled forward primer internal to the target gene and 0.3uM Anti-LIGN reverse primer, in a final reaction volume of 10ul. The "fluoro-PCR" profiles are shown in 3.2.3, and these reactions underwent 15 cycles of amplification. The forward primers used in the PCR reaction were commercially synthesized as 5' labeled with the Alexafluor® 647 dye (Eurogentec). Aliquots (4ul) of the labeled products, mixed with 5ul loading buffer (1x TBE buffer, 90% [v:v] formamide) were separated on a pre-electrophoresed (for 30 min) 10% polyacrylamide (29:1 ratio of bis/acrylamide), 8.2 M urea denaturing gel at 50W for 2-3 hours. Bromophenol blue and xylene cyanol were used to monitor sample migration during electrophoresis. The dyes were loaded in a lane towards the edge of the gel, and as far from the fluorescent product lanes as feasible, due to their intrinsic fluorescence which interfered with sample detection. The gel was then transferred to acetate plastic sheets for direct imaging on a Typhoon FLA 9500 instrument.

3.2.3 MPAT PCR profiles

Radioactive MPAT

Step	Reaction Profile "Cold PCR"	Reaction Profile "Hot PCR"	Reaction Step
1	94ºC - 4 minutes	94ºC - 4 minutes	Initial Denaturation
2	94ºC - 1 minute	94ºC - 1 minute	Denaturing
3	54ºC - 1 minute	54ºC - 1 minute	Annealing
4	72ºC - 1 minute	72ºC - 1 minute	Extension
5	*Back to Step 2, 35 cycles*	*Back to Step 2, 5 cycles*	# of cycles
6	72ºC - 7 minutes	72ºC - 7 minutes	Final Extension
7	4ºC - Indefinitely	4ºC - Indefinitely	Hold

Fluorescent MPAT

Step	Reaction Profile "Cold PCR"	Reaction Profile "Fluoro-PCR"	Reaction Step
1	94ºC - 4 minutes	94ºC - 4 minutes	Initial Denaturation
2	94ºC - 1 minute	94ºC - 1 minute	Denaturing
3	54ºC - 1 minute	54ºC - 1 minute	Annealing
4	72ºC - 1 minute	72ºC - 1 minute	Extension
5	*Back to Step 2, 35 cycles*	*Back to Step 2, 15 cycles*	# of cycles
6	72ºC - 7 minutes	72ºC - 7 minutes	Final Extension
7	4ºC - Indefinitely	4ºC - Indefinitely	Hold

3.3 Results

3.3.1 Optimizing the fluorescent MPAT platform

There were two main issues to resolve with developing a fluorescent MPAT, namely, sensitivity and efficacy of detection of the fluorophore to be used. For maximum sensitivity, the Alexafluor® 647 dye was chosen, as it possessed the highest extinction coefficient, and thus emits most intensely with minimal crossover interference into the near-infrared range. At the moment, Life technologies has improved the sensitivity of many fluorescent moieties used in biological systems and this includes relabeling the Alexafluor® 647 dye as near-infrared as opposed to far-red. Although the Anti-LIGN reverse primer is used for all reactions, the radioactive assay radiolabels each gene-specific nested forward primer for use in the final PCR reaction, as products did not resolve well if the reverse primer was labeled. However, the Anti-LIGN reverse primer being a universal primer also made it ideal to label with a fluorophore, as it would require a single labeled universal primer, for all reactions versus buying primers for each mt-mRNA transcript individually.

The Anti-LIGN primer (see 2.2.4.4) labeled with the Alexa Fluor® 647 dye was commercially synthesized, and range of primer quantities (10 pmol to 0.01 fmol)

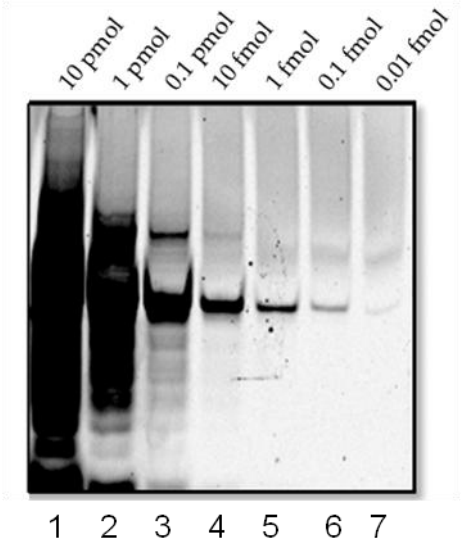

Figure 3.1. Titration of Alexa Fluor® 647-labeled Primer
To assess detection limits, a 1:10 serial dilution series of the fluorescent primer was electrophoresed through a 10% polyacrylamide, 8.2M urea, 1x TBE gel, and imaged on a Typhoon FLA 9500 imager. Lanes are labeled with total amount of primer loaded. The purity of the primer was also assessed by this method.

electrophoresed through a 10% denaturing polyacrylamide gel (figure 3.1). The goal was

to determine detection limits with the expectation that 0.01 fmol would be a viable sensitivity for the assay. Even if signal was only visible at 0.1 fmol, it would likely be sensitive enough for MPAT usage. Fortunately, fluorescent product was visualized down to 0.01 fmol, although the signal was fairly weak at that amount (far right lane). This level of detection was well within the necessary range of sensitivity. I was, therefore, confident that I could incorporate the fluorescent primer into the MPAT assay in replacement of the radiolabeled primers.

The first attempt at replacing radiolabeled primers with fluorescent-labeled followed the radioactive MPAT protocol exactly. The only divergence from that protocol was fluorophore was conjugated to the reverse primer of the fluoro-PCR, versus radiolabeling the nested gene-specific forward primer. The RNA samples used in the assay were isolated from three patient cell lines, two of which harbored a homoplasmic 1432A>G mutation in the *PAPD1* gene. This mutation causes a characteristically short mitochondrial (A) tail. The third cell line came from a relative heterozygous for the 1432A>G mutation, who is clinically unaffected and does not show a mitochondrial oligo(A) tail. These three samples would act as an experimental control as the recognizable pattern of the (A) tails had already been determined using the radioactivity based MPAT. The latter demonstrated that the homoplasmic samples had short and the heteroplasmic samples had wild-type poly(A) lengths. Thus, 'Cold PCR' samples from these cell lines were used as templates for the second PCR. This second round of PCR was carried out using a nested primer for *RNA14* and the Alexa Fluor® 647 labeled Anti-LIGN primer. The reaction products were then electrophoresed through a large sequencing-type 10%

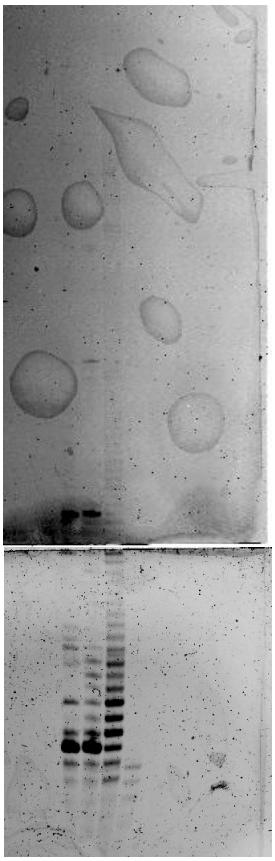

Figure 3.2. Fluorescent MPAT on Large Gel

Fluorescently-labeled samples from two homozygous *PAPD1* mutant RNA samples (lanes 1-2), one heterozygote (lane 3) carrying the 1432A>G *PAPD1* mutation, and a PCR control (lane 4) were separated on a 10% polyacrylamide/8.2M urea denaturing gel. Visualized on Storm PhosphorImager.

polyacrylamide 8.2M Urea denaturing gel, and visualized directly on a Storm PhosphorImager. The plastic acetate sheets the gel was transferred to in order to read it on the Storm Imager were not large enough to hold the entire gel, making part of the difficulty of visualizing the gels determining where to cut them so they fit on the plastic sheet. This is a step that is technically more difficult compared to transferring gels to Whatman paper. The gel does not adhere to plastic acetate sheets as well as the Whatman paper, so the user must be extremely careful when transferring the very thin, but large, gel onto plastic sheets for imaging. The results of this large fluorescent gel are shown in Figure 3.2.

The gel image is shown in two pieces due to the necessity of cutting the gel to fit onto the plastic sheets. In this initial experiment, I had not yet determined the proper areas to cut the gel while preserving the integrity of the fluorescent signal in the lanes. Two major conclusions were reached when considering this gel: the first was that when using fluorescence, the quality of the electrophoresis run and that of the gel itself would be paramount to generating clean results. That is, imperfections on the gel such as bubbles, fingerprints, and even dust would readily be visible. In Figure 3.2, bubbles formed when transferring the gel to plastic sheets are clearly visible, and issues like this would need to be resolved in order to produce high quality images. The second conclusion is that the previously observed patterns of the poly(A) tails for these patients published in (Crosby *et al.*, 2010), using the radioactive MPAT, are not present. Having robustly established the radioactive MPAT protocol and results in the past, we knew these patterns should be present if the assay is operating correctly. With the fluorescently-labeled Anti-LIGN primer, the assay did not appear to be functioning correctly. After repeating this fluorescent assay protocol multiple times, and still not generating the expected results, the next step was to return to the radioactive-based MPAT protocol and make sure the assay was working correctly in my hands.

While switching back to the radiation-based MPAT, I accomplished two goals. The first was to make sure I could perform the assay correctly. The second, was to establish that the poly(A) phenotype observed in the *PAPD1* mutant patients was present in RNA isolated from dermal fibroblasts. The previous published work had used RNA extracted from blood. My thesis project was to be largely based on work from patient fibroblasts, so confirming the oligo(A) phenotype was paramount. Towards this end, I isolated RNA from the patient fibroblast cultures, two homozygous and one heterozygous for the *PAPD1* mutation, one from a healthy unrelated control fibroblast line, and

performed all stages of the MPAT assay. A gene-specific nested forward primer for *RNA14* was radiolabeled, and used for the final hot PCR as shown in Figure 3.3.

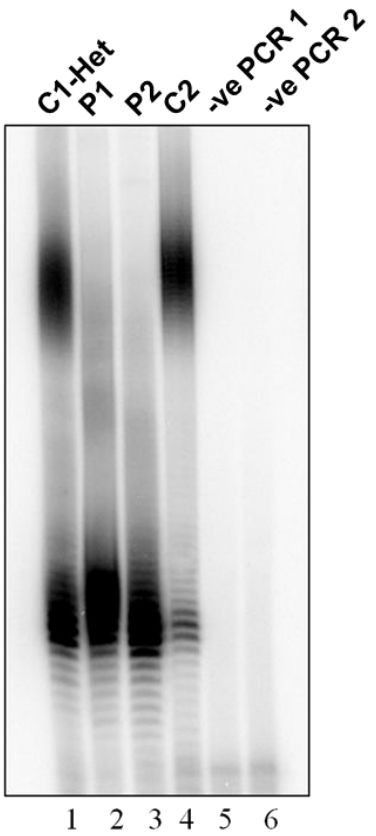

Figure 3.3. Radiolabeled *RNA14* MPAT Analysis of Patient Fibroblasts

RNA isolated from fibroblasts was processed for the MPAT using radiolabeled primers. The individuals were heterozygous (lane 1) or homozygous (lanes 2, 3) for a *PAPD1* 1432A>G mutation or control (lane 4). Controls were performed for the 1st (lane 5) and 2nd (lane 6) rounds of PCR. The signals were visualised via autoradiography on a Storm PhosphorImager and ImageQuant software.

In this gel, the characteristic oligo vs full length poly(A) tails in the mutant and wild-type cells, respectively, was present. This was evidence of correct handling of the MPAT protocol in my hands. For the needs of the thesis research, the radioactive MPAT assay could serve as a viable tool to analyze mitochondrial poly(A) tails, and this was enough to do the necessary experiments with the fibroblasts. So the drive to switch the assay to a fluorescent platform was lessened at this point. However, the idea of having the Anti-LIGN reverse primer be the labeled primer was still appealing, as it provide a universal primer that permanently retained maximal sensitivity. As the standard MPAT was now working in my hands and could be used for my thesis work, I concurrently attempted to repeat my results with the radiolabeled Anti-LIGN primer.

The result of switching the position of the radiolabeled primer was unexpected. In theory, either of the primers in the pair should be able to be labeled, and the same result should be observed. When the Anti-LIGN primer was labeled, and used with the same four cell line samples used in Figure 3.3, the characteristic poly(A) pattern was not observed. In fact, there did not appear to be a discernible pattern at all, as shown in Figure 3.4. This result was similar to that of the fluorescently-labeled Anti-LIGN primer in the MPAT (figure 3.2). These outcomes from both the radioactive and fluorescent Anti-LIGN primer procedures provoked rethinking of labeling the reverse primer in the final PCR of the MPAT protocol. Instead, gene-specific nested primers conjugated to the Alexa Fluor® 647 dye were synthesized to test in the fluorescent MPAT.

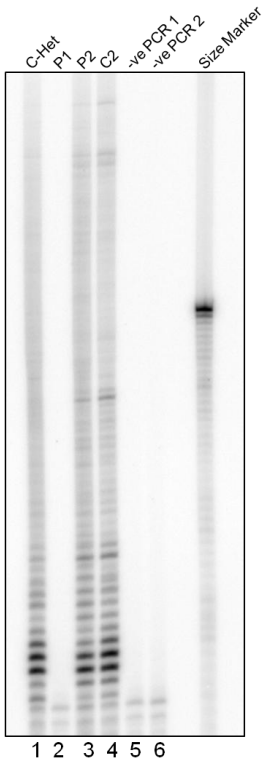

Figure 3.4. MPAT using radiolabeled Anti-LIGN primer
RNA isolated from fibroblasts was processed for use in the MPAT using radiolabeled Anti-LIGN primer. Samples were heterozygous (lane 1) or homozygous (lanes 2, 3) for the *PAPD1* 1432A>G mutation or control (lane 4). Controls were performed for the 1st (lane 5) and 2nd (lane 6) rounds of PCR. The signals were visualised via autoradiography on a Storm PhosphorImager and ImageQuant software

The next attempt at the fluorescent MPAT was with an *RNA14*-specific nested primer conjugated to the Alexa Fluor® 647 dye, and it also included several other modifications. The standard radiolabeled protocol was followed with a parallel reaction performed with both an increase in the final concentration of the fluorescent primer (from 0.3uM to 3uM), and an increase in PCR cycles (from 5 to 15 cycles).

With the use of a fluorescently-labeled forward primer, I finally saw the established pattern of polyadenylation from the PAPD1 mutant and control cells. Adhering to the previously used primer concentrations and cycle numbers did not produce as intense a signal as the higher primer concentrations and cycle numbers (Figure 3.5, panel A vs B). The increased primer concentration and cycle numbers produced a pattern that recapitulated previously observed results, and furthermore lacked much of the smeary signal seen with radiolabeled nucleic acids on my gels. The fluorescent MPAT was repeated to confirm consistency of the observed poly(A) patterns. The results also show that the single-nucleotide resolution obtained using the radiation-based MPAT experiments was maintained with the fluorescent primer. With the adjusted protocol and fluorescent primers, the updated MPAT appeared to have all the sensitivity and accuracy of the radiation based assay while adding the benefits of the long-lived primer status of fluorescence primer. Thus, it was adopted for use in this thesis research for analyzing poly(A) tails in patient fibroblasts.

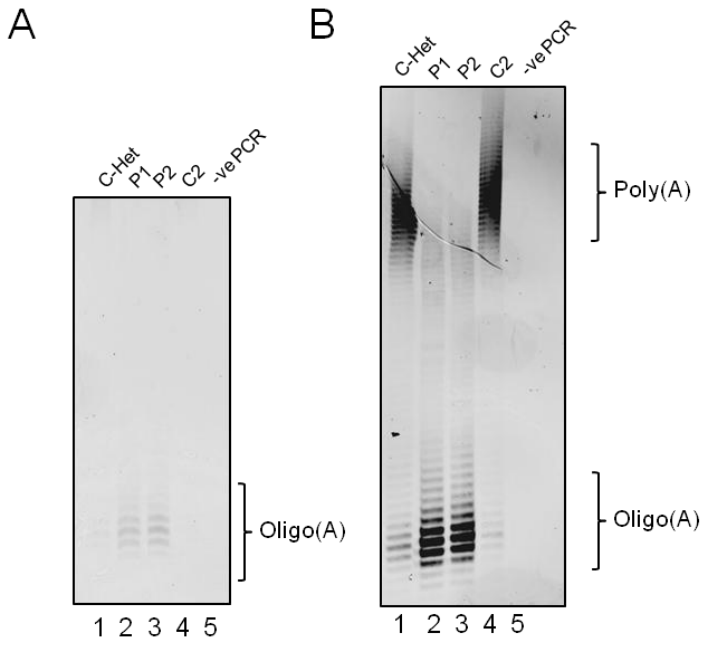

Figure 3.5. Assessing various PCR conditions for the fluorescent MPAT.
A. Fluorescent MPAT of *RNA14* products using 5 cycles for the final PCR separated on a 10% denaturing gel. **B**. Modified protocol for *RNA14* MPAT using 15 cycles and 3uM primer concentration in final PCR. Lanes are labeled with cell lines used and PCR controls.

While this thesis work was being carried out, a research group at the University of Tokyo published a paper investigating the role of LRPPRC, SLIRP, and PNPase in mitochondrial RNA metabolism and polyadenylation (Chujo *et al.*, 2012). They employed a modified version of the MPAT assay, with the primary adjustment being electrophoresing through shorter polyacrylamide gels and visualizing the separated PCR products via staining with SYBR Gold (Molecular Probes). Our version of the fluorescent MPAT (with all the steps detailed in Figure 3.6) provides higher resolution data, as the Tokyo results lack single-nucleotide resolution of the poly(A) tails. Their protocol allows for missed observations of subtle poly(A) tail effects that may occur. For example, the oligoadenylation observed in *PAPD1* 1432A>G homozygous mutant fibroblasts, mtPAP siRNA knockdowns, or LRPPRC knock-outs is much more difficult to distinguish from naked 3' ends using their short acrylamide gels. Our MPAT allows for a more detailed analysis of the lengths and perturbations of poly(A) tails, and presents a superior method for investigations such as these.

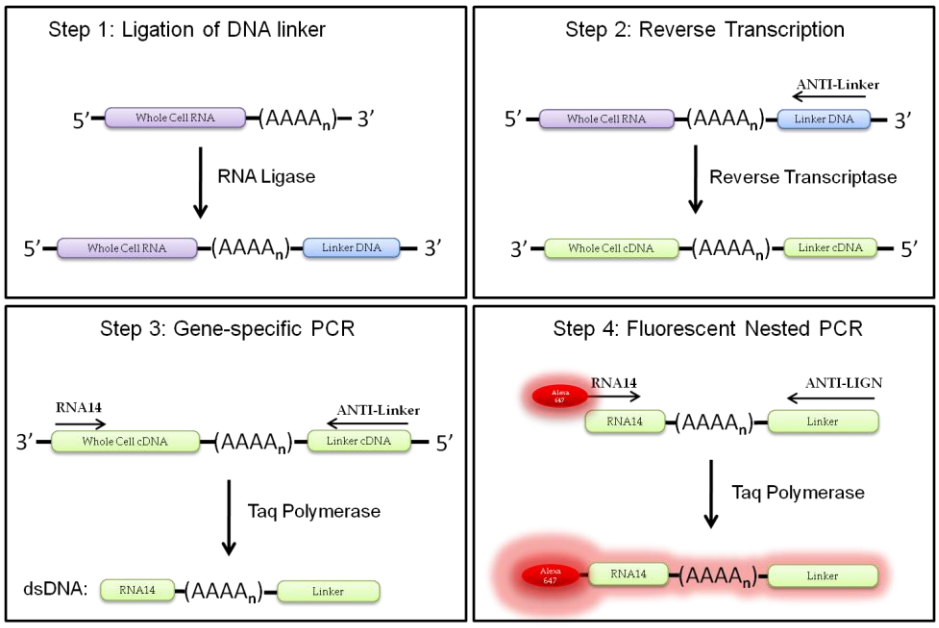

Figure 3.6. Steps of the fluorescent MPAT

A cartoon depicting the steps of the fluorescent MPAT procedure. **Step 1**: The isolated whole cell RNA is ligated at the 3' end to a DNA linker oligonucleotide. **Step 2**: The ligated RNA-linker is used with anti-LIGN primer to prime a reverse transcription reaction, generating cDNA incorporating the linker, and capturing the poly(A) tail. **Step 3**: The cDNA is used as a template in a gene-specific PCR to amplify the gene of interest. **Step 4**: The gene-specific amplicon is used as a template for a nested PCR, using forward primers conjugated to the AlexaFluor® 647 dye with the Anti-LIGN primer, to generate a fluorescently-labeled PCR products that reflect the population of poly(A) tails. This known size is used for calculating where the 3' end of the amplicon is located upon separation via polyacrylamide/urea gel electrophoresis.

Chapter 4

Characterization of the effect of the *PAPD1* 1432A>G mutation on mitochondrial gene expression

4.1 Introduction

Polyadenylation fulfills a critical role in gene expression and RNA metabolism. As detailed in Chapter 1, it is a 3' RNA modification that is performed in the nucleus, cytosol and mitochondria in mammalian cells, with nuclear and cytosolic polyadenylation being particularly well-characterized (Kuhn *et al.*, 2009). Mammalian mitochondrial polyadenylation, in contrast, is much less well understood. The modification defies superficial comparison of functionality with other organisms, as the role that polyadenylation carries out can differ drastically. In the mammalian nucleus, polyadenylation acts to facilitate transport of RNA into the cytosol (Huang and Carmichael, 1996), protect the 3' end of mRNAs (Bernstein *et al.*, 1989), and aid initiation of translation (Gallie, 1991). In bacteria, the poly(A) tail acts as a signal for degradation, initiating RNA turnover (Xu and Cohen, 1995). Plant chloroplasts utilize poly(A) tails for degradation, like bacteria (Hayes *et al.*, 1999).

The trend of the poly(A) tail being able to fulfill different roles is observed in mitochondria from different species. Plant mitochondria use the poly(A) tail to stimulate mRNA degradation (Gagliardi and Leaver, 1999). In yeast mitochondria, there is no polyadenylation (Osinga *et al.*, 1984). Instead, a conserved 3' dodecamer sequence acts as a stabilizing modification (Butow *et al.*, 1989). The mitochondrial mRNAs of trypanosomes feature short poly(A) sequences to confer stability based on the editing status of the transcript itself (Etheridge *et al.*, 2008). These diverse roles fulfilled by poly(A) tails in mitochondria of various species emphasize the difficulty of predicting the poly(A) function in human mitochondria. As a mutation identified in the *PAPD1* gene has been linked to human disease (Crosby *et al.*, 2010), it is critical to elucidate the exact role of the poly(A) tail in human mitochondria.

While it has long been known that mammalian mitochondria possess their own poly(A) polymerase activity (Jacob and Schindler, 1972), the human mitochondrial poly(A) polymerase, mtPAP, was only identified in 2003 (Tomecki, 2004). It is a 66kDa protein, and is a noncanonical poly(A) polymerase. It is operational as a dimer, as opposed to the canonical monomer (G. Martin *et al.*, 2000). The human mitochondrial poly(A) tails have an average length of 50 adenine nucleotides, in contrast to the nuclear-

encoded mRNA poly(A) tail lengths of 250 nucleotides (Kuhn *et al.*, 2009). At the start of my project, the only convincing function of mitochondrial mRNA polyadenylation was completion of the stop codon for seven of the thirteen open reading frames coded by mtDNA (Ojala *et al.*, 1981). Beyond this, the role of the poly(A) tail on human mt-mRNAs is unclear.

Several groups have attempted to elucidate the function of the poly(A) tail in human mitochondria, utilizing a variety of methods. The current state of understanding is complicated by potentially conflicting data. In the initial paper identifying mtPAP, RNAi was used to deplete the protein levels of mtPAP, and the authors found that as a consequence steady-state levels of the *MTND3* and *RNA14* transcripts were increased (Tomecki, 2004). The authors speculated therefore that the poly(A) tail may not act as a stabilizing modification. In parallel, a group from the University of Tokyo published conflicting results, reporting that siRNA depletion of mtPAP caused reduction of steady-state transcript and protein levels of mtDNA encoded gene products (Nagaike, 2005). Another report found that depletion of mtPAP caused a non-uniform effect on mt-mRNA, with some species being depleted and others increased at steady-state (Piechota *et al.*, 2006). The decrease in transcript levels of *RNA14* was consistent with the report from Nagaike *et al*, but the increased *MTND3* transcript levels were consistent with the results of Tomecki *et al.* Targeting of the cytosolic poly(A)-specific 3'-5' exoribonuclease PARN to mitochondria to remove the mitochondrial poly(A) tails also showed this variation of effects on mt-mRNA stabilities (Wydro *et al.*, 2010). The transcripts for mtDNA-encoded subunits of complex I showed increased levels, while transcripts for mtDNA-encoded subunits of complex IV were decreased, as was the *RNA14* transcript. This is consistent with the results of Piechota *et al*. In that same report from Wydro *et al.*, the cytosolic enzyme PABPC1 was targeted to mitochondria, coating the mt-mRNA poly(A) tails. This caused a severe oxidative phosphorylation defect, a decrease in respiratory chain complex steady-state levels, and inhibition of mtDNA-encoded polypeptide translation. The mt-mRNAs were not destabilized, however.

Another method for elucidating poly(A) tail function is the targeted depletion, knock-out, or overexpression of factors that have modulating effects on mitochondrial mRNA polyadenylation. These modulators include LRPPRC and SLIRP, proteins that have been shown to bind mt-mRNAs; PNPase and PDE12, which function in mt-mRNA exoribonuclease/deadenylase activity. There are advantages and limitations to all these approaches. RNAi can cause significant off-target effects, but is relatively cheap and convenient. Targeting modulating factors can aid in elucidating regulatory pathways, but

the results can be difficult to dissect into individual factor contributions. Overexpression can induce artifacts due to abnormally high levels of a given gene product. Generating knock-out animal models can be expensive and time-consuming, but robust tissue specific and organism specific effects can be observed. Consistently, many of these reports, utilizing these various methods have observed oligoadenylated mt-mRNAs in the knock-downs and knock-out experiments.

In 2010, my host lab published a paper in collaboration with Professor Andrew Crosby of St. George's University London, identifying an Old Order Amish family harboring a novel 1432A>G mutation in the *PAPD1* gene (Crosby *et al.*, 2010). Their investigation was initiated as multiple children of the family exhibited a slowly progressive autosomal-recessive neuromuscular condition. The clinical features were a combination that was suggestive of a novel condition. These included cerebellar ataxia, optic atrophy, dysarthria, and learning difficulties. Using DNA extracted from blood, a genome-wide microarray screen was undertaken. The screen identified the nonsynonymous 1432A>G base change in the *PAPD1* gene. The clinically affected children were homozygous for the mutation, while the unaffected parents and sibling were heterozygous. The base change was predicted to substitute an asparagine residue at position 478 for an aspartate. This amino acid lies within a small protein motif that is part of one of the most conserved regions of the mtPAP enzyme. Using RNA extracted from blood samples taken from multiple family members, both heterozygous and homozygous, the poly(A) tails on the mt-mRNAs *MTCO1* and *RNA14* were analyzed using the MPAT assay. In the patients homozygous for the mutation, the mt-mRNA adenylate tails were found to be only oligo(A) tails, with lengths of ≤10nt, rather than the normal 40-50nt range. Combined with the genetic data, this profound defect was predicted to underlie the neurodegenerative condition of the homozygous patients. However, as it was only possible to isolate nucleic acid from patient samples at this time, there was no confirmation that the lack of polyadenylation really caused a defect in mitochondrial gene expression in this initial description of the mutation. More recently, with the invaluable support of the affected family, colleagues in the United States were able to establish cell lines from several members

The initial goal of this thesis work was therefore to thoroughly characterize the downstream effects of the 1432A>G PAPD1 mutation. Through this, insights into the functions of mitochondrial polyadenylation would be elucidated. At the time this project was undertaken, the only known effect of this mutation was the dramatic shortening of the mitochondrial poly(A) tail on mt-mRNAs. In this chapter, I will detail the propagation

of dermal fibroblast cultures derived from several of these patients, their immortalization, and the subsequent analysis of the effect the mutation has on multiple levels of mitochondrial gene expression and overall mitochondrial function.

4.2 Materials and methods

4.2.1 Culturing primary and immortalized PAPD1 1432A>G fibroblasts

Human fibroblasts were obtained from patient skin biopsies, and grown in a humidified atmosphere at 37°C in 5% CO_2 in DMEM (Sigma) containing 4500mg/L glucose, 110mg/L sodium pyruvate, 584mg/L L-glutamine, 1x NEAA, 10% (v:v) fetal bovine serum (Sigma), 50ug/ml Uridine (Sigma), and 50U/ml Penicillin+50ug/ml Streptomycin (Gibco). During normal culturing, cells were routinely split at 80% confluency. For immortalized fibroblasts, every 3rd passage had geneticin added at a concentration of 200ug/ml. Splitting of cells was previously described (*c.f.* 2.2.2.1).

4.2.2 Geneticin titration

For the Geneticin (G418, Gibco) titration in killing curves, heterozygous 1432A>G *PAPD1* human fibroblasts were seeded at 50,000 cells/well in 6-well plates, and allowed to incubate overnight. The next day, the culture media was replaced with media containing geneticin. The concentration range for Geneticin killing curves were 200-600ug/ml. Cells were grown in the presence of geneticin for 7 days, then trypsinized and counted on a hemocytometer. The geneticin was purchased as a powder, and a 50mg/ml stock solution made in H_2O to be stored at -20°C. This stock solution was diluted in culture media as described above, and then added to cells at specified concentrations.

4.2.3 Fibroblast immortalization

The immortalization procedure was carried out by Morten Ritso (Institute of Genetic Medicine, Newcastle University) and myself. Retroviral constructs, carrying the E6E7 gene region of human papillomavirus type 16, were transfected into packaging cells. These packaging cells (PA317) were grown to near confluence in DMEM containing 10% FBS; 24 h later the medium containing retroviral particles was harvested and filtered through a 0.4-mm filter. Retroviral titers were determined by infecting NIH/3T3 cells. Human fibroblasts (non-familial control line, heterozygous and two homozygous lines for *PAPD1* 1432A>G mutation) were seeded in 6-well plates in supplemented DMEM at

50,000 cells/well. After allowing cells to adhere overnight, cell culture media was removed and 1ml viral stock (retroviral vector containing E6E7 genes) mixed with 3 ml serum-free media and 4ug/ml polybrene was added to wells. Cells were then incubated at 37°C for 2 hrs, then 5ml more serum-free media containing polybrene was added. Cells were incubated for a further 5 hrs after which the viral mixture was removed. The cells were washed once with fresh supplemented media and then fed with another aliquot of fresh media. Cells were cultured for two days prior to Geneticin (G418) addition at 400ug/ml. Once selection with G418 was under way, media containing G418 was refreshed every other day. Selective media was used for 10 days, after which the G418-resistant population of cells were isolated and subsequently expanded. DNA was isolated from immortalized fibroblasts for sequencing of the *PAPD1* gene by Professor Andrew Crosby's lab to confirm presence of the 1432A>G mutation.

4.2.4 Cell proliferation measurements

Human fibroblasts were harvested and seeded 25,000 cells/well in triplicate for each time point in 24-well plates. For standard growth curves in media containing glucose, cells were harvested and counted every two days of the time course. For growth measurement in conditions forcing oxidative respiration, after seeding and incubating overnight, the standard culture media was replaced with DMEM medium lacking glucose (Sigma) supplemented with 10% (v:v) dialyzed FCS, 0.9 mg/ml galactose, 0.11 mg/ml sodium pyruvate, 1x non-essential amino acids, 50U/ml Penicillin+50ug/ml Streptomycin, and 50ug/ml uridine. Cells were then harvested and counted every two days.

4.2.5 Blue native PAGE

Blue native PAGE analyses were performed by Dr. Hue Tran Hornig-Do, as described in (Hornig-Do *et al.*, 2012). Briefly, crude mitochondria isolated from human fibroblasts (*c.f.* 2.2.6.2) were solubilized using *n*-Dodecyl β-D-maltoside at 2 g/g protein, then incubated for 20 min on ice. After 20 min centrifugation at 25 000*g* at 4°C, the supernatant was collected and mixed with Blue Native sample buffer (750mM aminocaproic acid, 50mM Bis-Tris/HCl pH 7.0, 0.5mM EDTA, 5% Coomassie brilliant blue G250). To resolve individual complexes DDM-treated mitochondrial proteins (25ug) were separated on 4.5–16% gradient gels at 4°C. After electrophoresis, the proteins were

transferred to PVDF membrane and sequentially probed with antibodies for respiratory chain complexes, and ATP synthase (*c.f.* 2.2.6.7).

4.2.6 [^{35}S]-cysteine/methionine metabolic labeling of mitochondrial proteins

[^{35}S]-labeling was performed by Dr. Francesco Bruni and myself. All cell incubations were performed at 37°C. Fibroblasts were grown in T25 flasks until 60-70% confluence. The medium was then replaced with 2ml pre-warmed methionine/cysteine-free DMEM (Sigma) medium, and cells were incubated for 10min. This was repeated once. Then medium was replaced with methionine/cysteine-free medium containing 10% dialyzed FCS (10,000 MWCO) and 100ug/ml emetine dihydrochloride (20mg/ml in Dulbecco's A-PBS). Cells were incubated in this medium for 1 hour. At this point, 0.5ml of the medium was discarded, and 20ul of [^{35}S]-methionine/cysteine mix (Perkins-Elmer Easy-Tag express protein labeling mix, NEG-772) was added directly to the flask. The cells were incubated in this medium for 2 hours, with agitation of the flasks every 30min. In the case of pulse-chase experiments, cells were then washed with chilled standard growth medium supplemented with 7.5ug/ml methionine, allowed to incubate for an hour, and then washed again. The non-radioactive medium incubation times were extended for specific pulse-chase experiments. Cells were harvested with 1ml chilled 1mM EDTA in PBS, and pelleted by centrifugation at 250*g* for 4min. After washing the cell pellets 3 times with chilled PBS, the cells were resuspended in 30-100ul chilled PBS, containing EDTA-free Protease Inhibitor cocktail (Roche) and 1mM PMSF. Samples were stored at -80°C.
For electrophoresis, 50ug of whole cell lysate was electrophoresed through a 15-20% SDS-polyacrylamide gel at 100V, the gel was then fixed over night in 3% glycerol, 10% acetic acid, 30% methanol. The fixed gel was vacuum-dried for 4 hours at 60°C, covered in cling film, then exposed to a PhosphorImage screen for 2 days. Results were visualized with a Typhoon FLA 9500 system (GE/FujiFilm).

4.2.7 PicoGreen and TMRM staining

Immortalized patient fibroblasts were seeded 25,000 cells/well in 1ml complete medium in glass bottomed dishes (WilCo) during the evening of the day prior to imaging. One hour prior to imaging, 3ul of PicoGreen working solution (Invitrogen) was added per ml

of culture medium, and cells incubated for 45min at 37°C, shielded from light. Next, 1ul TMRM (from 5uM stock in methanol) was added (final conc. 5nM), and light shielded incubation continued for 10min. The cells were then washed twice with KBr buffer (135mM NaCl, 5mM KCl, 0.4mM KH_2PO_4, 1mM $MgSO_4$, 20mM HEPES, pH 7.4) supplemented with 5.5mM glucose, 1.3mM CaCl and 5nM TMRM. The supplements for the KBr buffer were added fresh for each experiment. For imaging, the cells were then left in supplemented KBr buffer. Image acquisition was performed with an inverted fluorescence microscope (Axiovert 200 M, Carl Zeiss). The microscope settings used were GFP channel for Pico Green, 75ms exposure time, and Texas Red channel for TMRM, with 250ms exposure time. Transmission light brightfield images were taken with 400ms exposure time. The 63X objective with oil was used, and z-stack settings were 10 layers 0.4μM apart.

4.2.8 Quantitative PCR

DNA was isolated from immortalized patient fibroblasts, as detailed in General Methods. This DNA was used for measuring mtDNA copy number, via quantitative PCR in the presence of SYBR Green I. The target gene was mtDNA-encoded *MTND4* and the reference gene was nuclear-encoded ribosomal *18S* DNA. Forward and reverse primers for each gene are listed in 2.2.4.4. For each qPCR reaction, 5ul of DNA template (50ng total) was pipetted in triplicate into polypropylene qPCR microtube strips. 1ul each of the appropriate forward and reverse primers were added, for a final reaction concentration of 0.5uM. Nanopure H_2O was added to bring reaction volume to 10ul. Finally, 10ul of FastStart Essential DNA Green Master (Roche) was added to each reaction. The contents of the microtubes were pulsed down to ensure mixing of all reagents. All qPCR reactions were performed in a Lightcycler® Nano instrument. The reactions parameters were as follows:

Step	Reaction Profile	Reaction Step
1	95°C - 10 minutes	Initial Denaturation
2	95°C - 10 seconds (ramp 5°C/s)	Denaturing
3	59°C - 10 seconds (ramp 4°C/s)	Annealing
4	72°C - 10 seconds (ramp 5°C/s)	Extension
5	*Back to Step 2, 45 cycles*	# of cycles
6	95°C - 5 minutes	Final Extension
7	60°C to 95°C at 0.1°C/s	Melting Curve

The Cq value (equivalent to C_T) was determined using the Lightcycler® Nano software. For analysis of quantitative PCR results, the $2^{-\Delta\Delta Cq}$ (Livak) method was used (Livak and Schmittgen, 2001). This method assumes that both the target and reference genes have an amplification efficiency of approximately 100%, and are within 5% of each other. The Cq of the target gene is normalized to the Cq of the reference gene for both the test sample and the calibrator sample:

$$\Delta Cq_{(test)} = Cq_{(target,\ test)} - Cq_{(reference,\ test)}$$

$$\Delta Cq_{(calibrator)} = Cq_{(target,\ calibrator)} - Cq_{(reference,\ calibrator)}$$

Next, the ΔCq of the test sample is normalized to the ΔCq of the calibrator:

$$\Delta\Delta Cq = \Delta Cq_{(test)} - \Delta Cq_{(calibrator)}$$

Finally, the expression ratio is calculated:

$2^{-\Delta\Delta Cq}$ = normalized expression ratio

For this analysis, the test samples were the heterozygous and homozygous PAPD1 1432A>G cells, while the calibrator sample was the control fibroblast line.

4.2.9 Complex I and IV activity measurements

Measurements were performed by Dr. Hue Tran Hornig-Do, as described in (Kirby *et al.*, 2007).

4.2.10 In-gel activity assay

Assay was performed by Dr. Hue Tran Hornig-Do, as described in (Hornig-Do *et al.*, 2012) and (Calvaruso *et al.*, 2008).

4.3 Results

4.3.1 Confirmation of pathological phenotype in patient fibroblasts

In order to undertake investigation of the PAPD1 1432A>G mutation, a cell culture model was necessary. Previous work had utilized blood samples from the affected parents and children for experimental material. However, for this more involved project, a readily available source of patient material was needed. Through collaboration with Professor Andrew Crosby, we were able to obtain dermal fibroblast cell lines established from tissue biopsies from three of the family's children, one heterozygous for the mutation, and two that were homozygous.

The fibroblast lines were labeled:

Heterozygous control (C1-Het): Heterozygous for 1432A>G mutation in *PAPD1* gene, unaffected by clinical pathology, utilized in this work as a familial control.

Patient 1 (P1): Homozygous for 1432A>G mutation in *PAPD1* gene, exhibits clinical pathology.

Patient 2 (P2): Homozygous for 1432A>G mutation in *PAPD1* gene, exhibits clinical pathology.

Control (C2) - Unrelated fibroblast line, exhibits no clinical pathology. Served as a non-familial control line.

Upon receiving the patient cell lines seeded in T25 flasks, their condition was thoroughly inspected. The C-Het line showed minimal levels of cell death, as evidenced by detached cells, with a lack of fibroblast granularity and debris in the medium. The homozygous lines, however, were in quite poor condition. Much of the cell population had perished, accompanied by large stretches of deteriorated cell remnants. It was difficult to identify by light microscopy healthy cells. Due to the difficulty in obtaining these samples from the Amish family in Ohio, it was of the utmost importance that these cells be successfully cultured. In order to maximize their recovery, and trusting that there were viable cells present, even if not obvious under the microscope, fresh extra-enriched

DMEM media was used for growing the cells. Fetal calf serum was increased to 20%, and 50ug/ml uridine, 1x non-essential amino acids supplemented, 100U/ml Penicillin and 100ug/ml Streptomycin were added.

The viable homozygous cells did proliferate. After enough cells were frozen at early passage stocks, the immediate priority was confirming the pathological phenotype in these lines and subsequent immortalization of the cell lines. Fibroblasts have been reported as not recapitulating the biochemical defects arising from mitochondrial defects (Rodenburg, 2011). In these cases, alternative tissue is often required, for example skeletal muscle cultures. Thus, prior to immortalization of the fibroblast lines, preliminary examination for the presence of the defect was assessed by immunoblotting.

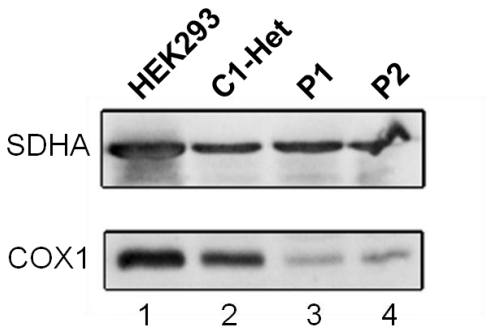

Figure 4.1. Steady-state COX1 levels in patient fibroblasts
Whole cell lysate (40ug) from patient fibroblasts and HEK293 cells was separated by 12% SDS-PAGE and transferred to PVDF membrane. Respiratory chain complex subunits COX1 and SDHA were then immunoblotted. Lanes are HEK293 (lane H), heterozygous line (C1-Het, lane 1), homozygous lines (P1 and P2, lanes 2 and 3, respectively).

As nuclear and cytosolic poly(A) tails have major impacts on translation, a similar impact on mitochondrial translation would be predicted. As a proxy for the predicted mitochondrial dysfunction from shortened poly(A) tails, immunoblotting of cytochrome *c* oxidase subunit 1 (COX1) was performed, as shown in Figure 4.1. The nuclear-encoded complex II subunit SDHA was utilized as loading control. A depletion of COX1 at steady-state was observed in the homozygous fibroblast lines (lanes 3 and 4), as compared to the heterozygous fibroblasts (lane 2) and HEK293 cells (lane 1). Levels of SDHA did not differ between fibroblast lines, as expected. This gave the necessary confidence in the recapitulation in the fibroblast lines of the pathological phenotype observed in the patients. The cells were therefore suitable as models to analyze the downstream effects of the *PAPD1* mutation. The advantages of this cellular system is that it is more physiological and is free from artificial perturbation as a result of gene knock-out or RNAi . These lines provided a pure genetic background in which to study the impact of lack of the full-length mitochondrial poly(A) tail. Analysis of the downstream effects would hopefully help elucidate the function of polyadenylation of transcripts in mitochondria.

4.3.2 Immortalization of 1432A>G and Control Fibroblasts

Once the patient fibroblasts were established in culture and expanded into stocks, immortalization of the cells was a priority. The primary goal was to significantly extend the lifespan of the fibroblasts, allowing a range of experiments to be performed. The

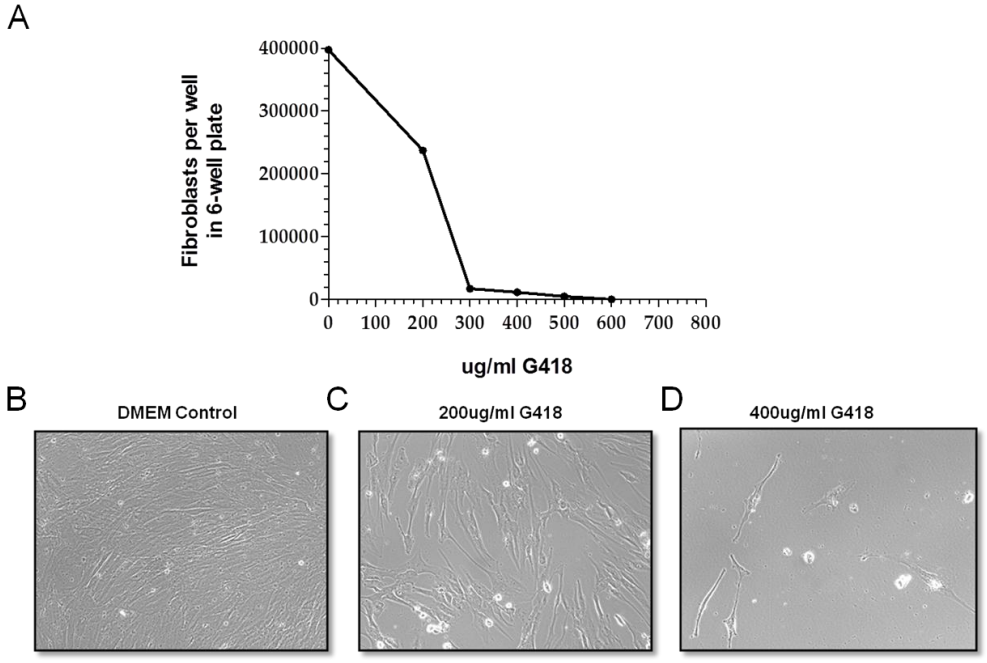

Figure 4.2. Determination of Geneticin Kill curve on Patient Fibroblasts
Heterozygous *PAPD1* mutant fibroblasts (C1-Het) were seeded 50,000 cells/well. The cells were then cultured in the presence of increasing concentrations of geneticin (G418) and counted after 7 days. Representative images are shown for no G418 (B), 200ug/ml (C), and 400ug/ml G418 (D).

vehicle for immortalization was a retroviral vector encoding the E6E7 early region gene from HPV. The particular immortalization procedure was carried in Professor Hanns Lochmuller's laboratory and uses Geneticin as a selection agent. It was important to generate a killing curve to determine the optimal concentration to use during the selection process. As shown in Figure 4.2, 400ug/ml Geneticin exhibited sufficient cytotoxicity in the 7-day time frame to be certain non-immortalized cells would die, but not so toxic that immortalized cells would have difficulty surviving.

Once the optimal geneticin concentration was established, all three fibroblast lines carrying the *PAPD1* mutation (homo or heterozygote) were seeded 50,000 cells/well in a 6-well plate. Included in the immortalization cohort of cell lines was non-familial control fibroblast line. The control fibroblast line would be utilized as a more appropriate

comparison for differences observed in the mutant cells, as the HEK293 cells differ significantly from fibroblasts.

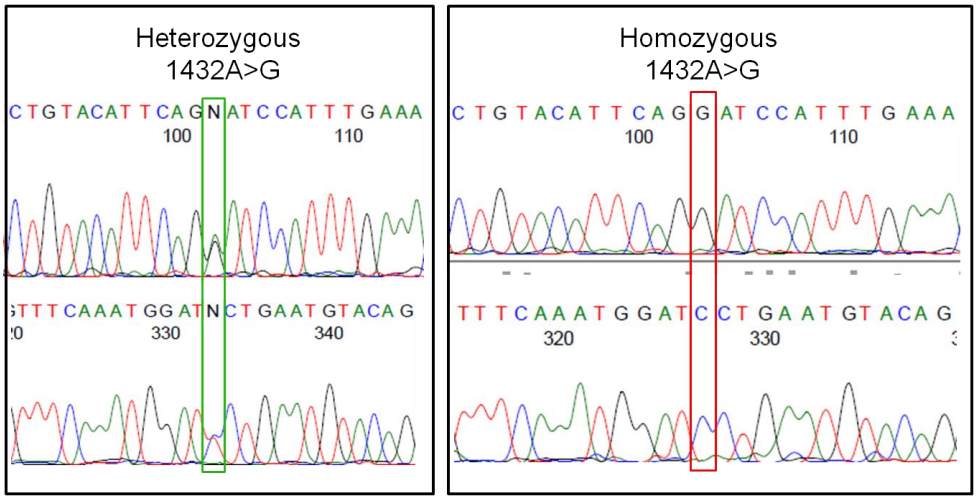

Figure 4.3. Sequencing confirms persistence of *PAPD1* 1432A>G mutation post-immortalization.
DNA from both homozygous mutant fibroblast lines and the heterozygous line was isolated as detailed in chapter 2 and subjected to sequence analysis. Electropherograms covering the region of the mutation are presented for the heterozygous mutant line, and one representative homozygous mutant line.

After treatment with the retrovirus, cells were put under geneticin selection, and monitored for resistant colonies. A high number of cells in each fibroblast line became geneticin-resistant, and were then expanded and continued to be cultured under selecting conditions. The only marker of "immortalization" was the continued geneticin resistance observed with the fibroblasts, so geneticin was kept in culture media at 200ug/ml every 3rd feed for maintenance. Sequencing of the *PAPD1* gene (Figure 4.3) was performed to confirm the persistence of the 1432A>G mutation post-immortalization.

Immunoblotting was carried out on cell lysates pre- and post-immortalization to assess mitochondrial protein levels. It was crucial to confirm that any defect seen in the primary lines was maintained, and was present to the same extent after immortalization. The levels of mitochondrial mtDNA and nDNA-encoded proteins would be analyzed and the observations compared pre- and posts-immortalization.

Included in the immunoblotting was the steady-state levels of mtPAP. This could indicate any changes from wild-type, and would identify if these changes were maintained in the immortalized lines. Based on the published crystal structure (Bai *et al.*, 2011), N478 does not appear to reside in a region of the protein that has a catalytic, dimerizing, or RNA binding role. It should be noted that the published crystal structure was not able to visualize the specific region where the mutation occurs (residue 478), leaving open the possibility that there is a function to this domain that has not yet been assigned. The N478D mutation in mtPAP could have potentially affected the stability of

the enzyme, and if so, it would be depleted at steady-state. The steady-state levels of mtPAP in the homozygous mutant fibroblasts were not decreased in comparison to the either the heterozygous fibroblasts or the non-familial fibroblasts (Figure 4.4A lanes 2,3 and 6,7 cf. lanes 1,4 and 5,8). No difference was observed between primary and immortalized cells. TOM20, a mitochondrial OMM protein, served as a loading control for the blot.

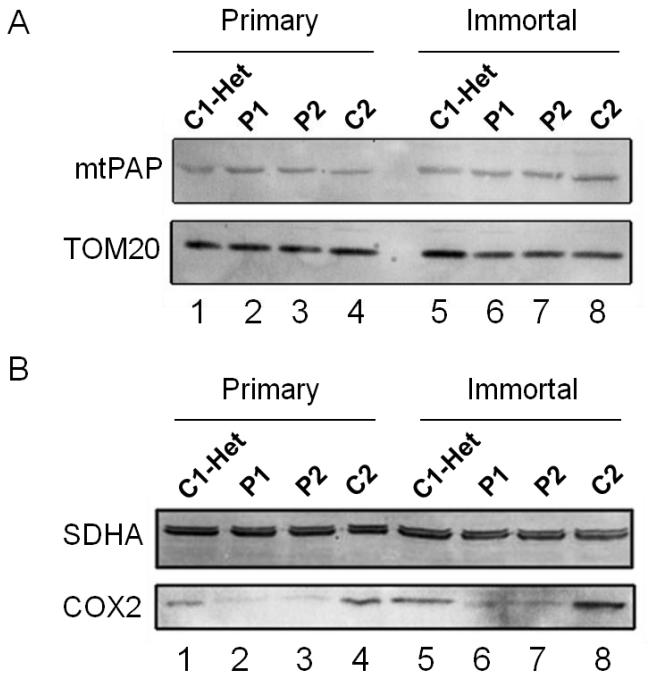

Figure 4.4. Steady-state mtPAP levels pre- and post-immortalization.
Whole cell lysate (40ug) from primary and immortalized fibroblasts were separated via 12% SDS-PAGE and following transfer the membrane was immunoblotted with **A.** anti-mtPAP, TOM20, and **B.** SDHA, and COX2 antibodies. TOM20 and SDHA were used as loading controls.

A second immunoblot was carried out to probe for SDHA and COX2. The purpose of this blot was to ensure that mitochondrial defects exhibited by the mutant fibroblasts would not be affected by the immortalization process. As shown in Figure 4.4B, COX2 is significantly depleted in the homozygous fibroblast lines (lanes 2,3 and 6,7 cf.1,4 and 5,8)). The heterozygous line appears to possess COX2 levels comparable to the control line. At least for steady-state levels of protein, the heterozygote does not appear to possess an intermediate phenotype between pathological and wild-type. Treatment with the retroviral vector did not alter the phenotypes of the patient fibroblasts, which provided confidence about continuing with the immortalized cells as the ongoing model of dysfunctional mitochondrial polyadenylation.

From this point onwards, any references to the patient or control fibroblasts refers to the immortalized versions of the cells.

4.3.3 Analysis of fibroblast mitochondrial mRNA 3' termini by MPAT

I had optimized the MPAT assay for detection via fluorescence in replacement of radiation (as detailed in chapter 3), and it was ready to be implemented in mt-mRNA 3' end analysis. C-Het, P1, P2, and C2 fibroblasts were harvested, and RNA was isolated from each line. Four mt-mRNAs were chosen, two of which, *MTCO1* and *RNA14*, matched the transcripts analyzed previously in these patients (Crosby *et al.*, 2010). The other two transcripts analyzed were *MTND3* and *MTCO3*. Mitochondrial tRNAs and rRNA transcripts were not analyzed as these have been shown to not be polyadenylated (Temperley *et al.*, 2010b).

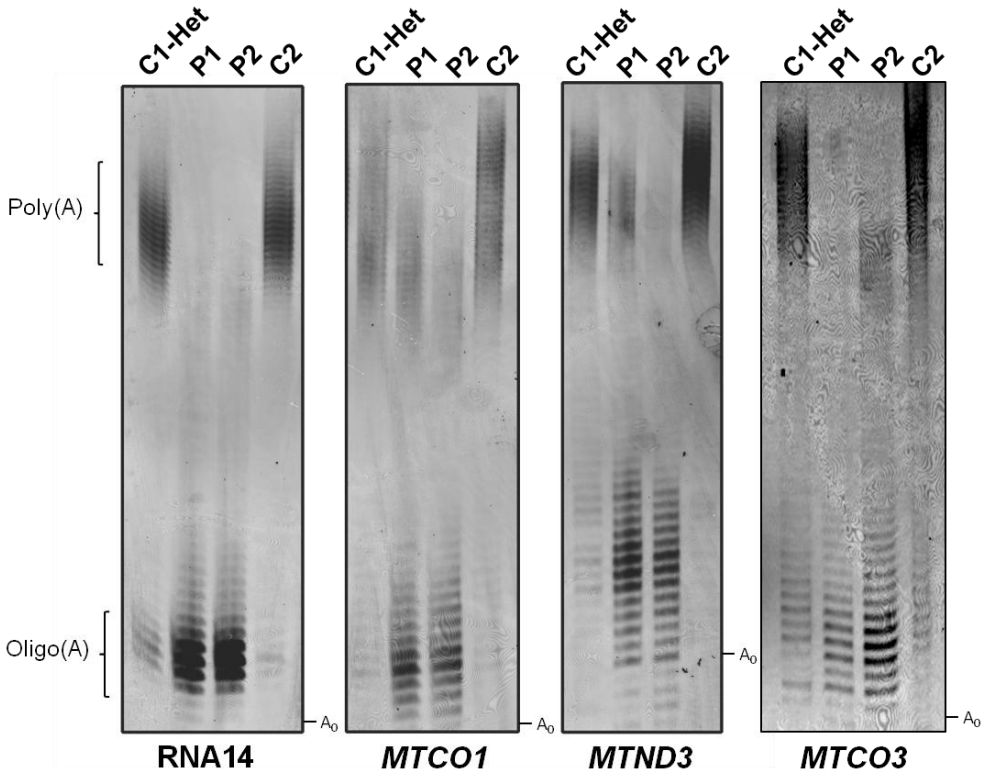

Figure 4.5. Polyadenylation profiles of PAPD1 mutant and control fibroblasts.
Selected mitochondrial mRNAs were analyzed using the MPAT assay, as described in chapter 3. RNA was isolated from heterozygous mutant (C1-Het), homozygous mutant (P1 and P2), and control (MB-I) fibroblasts. The fluorescently labeled reaction products were separated on a 10% polyacrylamide/urea gel, and imaged on a Typhoon FLA 9500 (GE/Fuji). Oligo- and polyadenylated populations were determined by using free primer size as a reference, and the start of the poly(A) tail is marked with A_0.

As illustrated in Figure 4.5, the adenylation profiles for each transcript in the mutant cell lines match the characteristic oligo(A) lengths observed previously for the homozygous *PAPD1* mutation. In the homozygous mutant fibroblasts, the adenylate tail

of the analysed mt-RNA species is significantly shorter, as compared to the heterozygous and control fibroblasts. The majority of the transcript population exhibits a 3' terminal extension in the range of 4-10 adenines, versus the 40-50 adenine extensions of the heterozygote and control. The "full-length" poly(A) tails observed in my controls match previous reports of average mt-mRNA polyadenylation length for these transcripts (Temperley, 2003; Nagaike, 2005; Slomovic and Schuster, 2007; Wydro *et al.*, 2010).

All four mRNAs examined exhibited short oligo(A) tails in the homozygous mutant fibroblasts, and this is consistent with the results from MPAT assays conducted using RNA extracted from patient blood samples (Crosby *et al.*, 2010). The heterozygous cell line shows a mild intermediate phenotype with regards to polyadenylation status. The presence of a small proportion of oligoadenylated mt-mRNA transcripts has been reported as a normal occurrence (Temperley, 2003; Crosby *et al.*, 2010; Wydro *et al.*, 2010). Consistent with this observation, a faint signal in the MPAT gel showing a minimal level of oligoadenylation for each transcript can be seen in the non-familial control line. The heterozygous mutant line shows a mild increase in this amount of oligoadenylation, which likely corresponds to the mixed *PAPD1* genotype that the cells harbor. This slight change in ratio of adenylation lengths may not be sufficient to cause negative impacts downstream.

In summary, these results served as confirmation of the presence of the primary defect of shortened adenylate tails in the homozygous mutant fibroblasts. In addition, the diminished levels of mtDNA-encoded subunits of complex IV present evidence of downstream effects as a result of the *PAPD1* mutation.

4.3.4 Effect of *PAPD1* 1432A>G mutation on cell proliferation

With the oligo(A) tail defect established in the mutant fibroblasts, the planned experiments were concerned with characterizing in greater depth the downstream effects resulting from the mutation. On a gross cell level, this consisted of examining the differences in fibroblast growth rates in normal glucose-rich media, versus glucose-free media, substituting galactose as the only carbon source. This forces cells to rely heavily on oxidative respiration. A compromised growth rate in the homozygous mutant cells would indicate that the mutation causes oxidative respiration to be negatively affected. The panel of fibroblast lines utilized in this experiment were the heterozygous mutant line, both homozygous mutant lines, and the non-familial control line.

Cells were seeded 25,000 per well in 24-well plates, and harvested in triplicate every other day for either eight or ten days. The results are shown in Figure 4.6. There are not large differences in growth rates between the four cell lines when cultured in glucose-

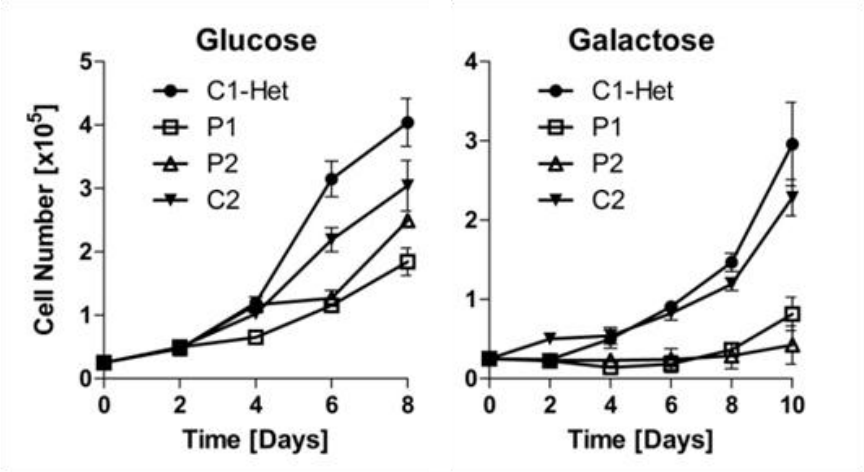

Figure 4.6. Growth curves of *PAPD1* 1432A>G fibroblasts propagated in glucose or galactose media.
Heterozygous mutant (C1-Het), homozygous mutant (P1 and P2), and control (C2) fibroblast lines were seeded at 25,000 cells/well in glucose or galactose-containing culture media. Cells were seeded in triplicate and counted every two days. *Left*: Growth curves from the four fibroblast lines in standard glucose-based media. *Right*: Growth curves from all four fibroblast lines cultured in galactose-based media. Error bars represent S.D. from three replicates.

based media, although the homozygous mutant fibroblast lines (P1 and P2) do grow the slowest. The heterozygous line proliferates at a similar rate to the control line. When cultured in galactose, a more pronounced difference in growth rate between patient and control lines is observed. Forcing the cells to rely on oxidative metabolism has an impact on the growth rate for all the fibroblast lines, but the homozygous mutant cells are preferentially suppressed in their growth. This presents supporting evidence that the mtPAP mutation causes an impairment of oxidative respiration. When able to utilize glycolysis, the homozygous mutants can maintain growth rates relatively close to the heterozygous mutant and control line, although the rate is still slightly depressed. It is clear that in cells missing full length poly(A) tails, the capacity of oxidative respiration is diminished, which is in agreement with previous reports (Nagaike, 2005; Wydro *et al.*, 2010; Rorbach *et al.*, 2011) each utilizing differing methods of poly(A) tail removal.

4.3.5 Steady-state levels of mitochondrial mRNAs in mutant fibroblasts

To address the question of what direct effect polyadenylation has on mRNA stability, we analyzed steady-state levels of mitochondrial RNAs. Previous reports have generated conflicting results in terms of mRNA stability when mtPAP is knocked-out/down, or the poly(A) tail itself is artificially removed. So the results from these cells free from artificial perturbation could provide clarification in a physiological environment. RNA was isolated from the four fibroblast panel and then analyzed via northern blotting. The panel of mt-mRNAs analyzed included *RNA14, MTCO1 MTCO3* and *MTND3,* which had been examined with the MPAT assay, and *MTND1*. *MTRNR2* and *MTRNR1*. rRNAs were included as mitochondrial-encoded loading controls, and nuclear-encoded *18S* rRNA as an additional loading control. As the mt-tRNAs are not oligo/polyadenylated, none were included in this set of genes to analyze.

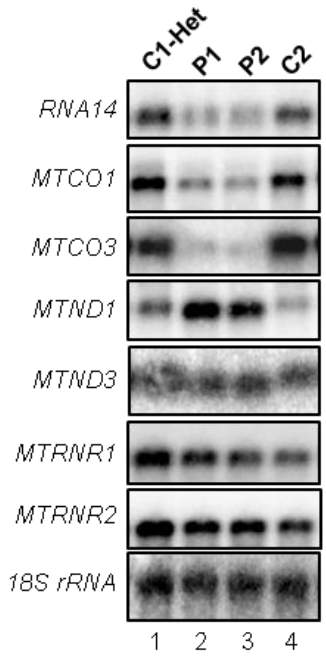

Figure 4.7. Assessment of mt-mRNA steady-state levels in patient fibroblasts

Northern blot analysis was performed using total RNA (4ug) extracted from heterozygous mutant (C1-Het), homozygous mutant (P1 and P2), and control (C2) fibroblast lines. RNA was separated by formamide/agarose gel electrophoresis and transferred to a nylon membrane. Membranes were hybridized with radiolabeled DNA probes corresponding to the listed RNA transcripts, and visualized by autoradiography.

A non-uniform pattern was observed upon visualizing the mRNA steady-state levels in the fibroblast mitochondria. As shown in Figure 4.7, the mRNAs are differentially affected by shortening of the poly(A) tail. Three outcomes are observed for the mt-mRNAs: depletion, increase, or no effect. The bicistronic *RNA14* transcript appears depleted at steady-state in the homozygous mutant cells.

The *RNA14*, *MTCO1,* and *MTCO3* transcripts in the homozygous mutant cells are depleted. Conversely, the steady-state levels of *MTND1* appear to be increased in the homozygous mutant lines. For *MTND3,* there does not appear to be any significant difference in steady-state levels, with or without the shortened poly(A) tail. The faster migration of the *MTND3* transcript allows easy visualization on the northern blot of the size difference that occurs as a result of polyadenylation loss. The transcript in the homozygous mutant cells clearly migrated further through the gel, consistent with a reduction in size due to a shorter adenylate tail. This is much less obvious for the larger

mRNA transcripts. In the case of the mt-rRNAs, no changes in migration or steady-state levels were observed. The mt-rRNAs are not polyadenylated in HeLa cells, only having been reported experimentally to possess 3-4 adenine extensions (Temperley *et al.*, 2010b), so this was expected. The northern blots show non-uniform changes to steady-state levels for the mt-mRNAs. There are no obvious characteristics of the mRNAs that might correlate with the changes in stability, such as 5' or 3' UTRs, or size of the open reading frames.

4.3.6 Steady-State levels of mitochondrial proteins in mutant fibroblasts

A more extensive analysis of OXPHOS complex components was performed by western blot. Of particular importance were the steady-state levels of mtDNA encoded proteins, as these transcripts are the direct substrates of mtPAP, and would be potentially affected by alterations in its activity. The mtDNA-encoded proteins analyzed included ND1, and COX1-3. There are two antibodies to subunits of complex I which are nuclear encoded, NDUFB8 and NDUFA9. NDUFB8 provides information pertaining to the assembly of the complex and levels are believed to reflect proper complex assembly, as it is rapidly degraded if not correctly integrated. Other nuclear-encoded mitochondrial proteins blotted include TOM20, complex II subunit A, and mtPAP.

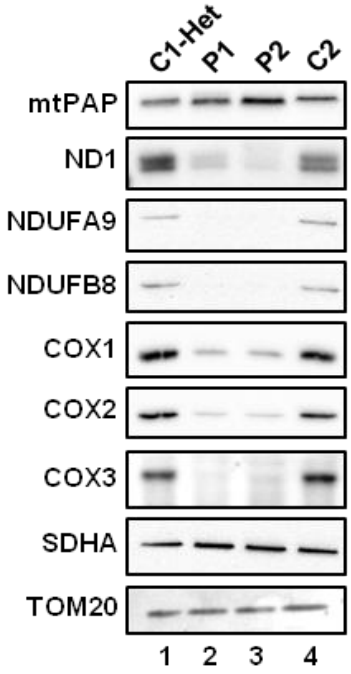

Figure 4.8. Steady-state Levels of Mitochondrial Proteins in *PAPD1* Mutant Fibroblasts
Immunoblot analysis was performed using whole cell lysate (40ug) from fibroblast lines. Cell lysates were separated by 12% SDS-PAGE, and transferred to PVDF membranes for blotting. Membranes were probed with antibodies against mtDNA and nDNA-encoded proteins, and visualized with ECL Prime (GE).

As shown in Figure 4.8, a more consistent pattern is

exhibited, compared to changes in mt-mRNA steady-state levels. Rather than the non-uniform changes in levels of the mt-mRNA transcripts, the mtDNA-encoded respiratory chain complex subunits appear to be uniformly decreased at steady-state. The nuclear-encoded complex I subunits, NDUFB8 and NDUFA9, both show decreased signal on immunoblotting as well. NDUFB8 is recognized as an indicator of levels of complex I. With ND1 and NDUFB8 depleted on immunoblotting, this may indicate decreased levels of fully assembled complex I. Notably, *MT-ND1* mRNA is increased at steady-state in the homozygous mutant fibroblasts. More transcript is present, but the protein is markedly depleted compared to controls. The nuclear-encoded complex II subunit, SDHA, was not affected by the mtPAP mutation. As previously observed, mtPAP does not appear to differ significantly between the cell lines. Both SDHA and TOM20 act as loading controls for the immunoblotting.

4.3.7 Mitochondrial protein synthesis and turnover in *PAPD1* mutant fibroblasts

Having observed depletion at steady-state levels for mtDNA-encoded proteins, it was not immediately apparent whether the cause was reduced expression, or increased turnover. It was therefore important to characterize any changes in *de novo* protein synthesis as a result of the *PAPD1* mutation. Unlike in the nucleus or cytosol, the role of the poly(A) tail in mitochondria in potentially facilitating translation is unclear. As a consequence, it was appropriate to identify if the loss of the poly(A) tail had a direct effect on translation in mitochondria.

There is currently no *in vitro* system to address questions such as these pertaining to mitochondrial translation. Hence, Dr. Francesco Bruni and I employed a well-established technique for analysis of *de novo* synthesis of mitochondrial proteins (Ching and Attardi, 1982; Chomyn, 1996; Fernandez-Silva *et al.*, 2007; Sasarman and Shoubridge, 2012). This technique utilizes [^{35}S]-labeled methionine/cysteine to radiolabel newly synthesized mitochondrial polypeptides. This is performed in the presence of a cytosolic translational inhibitor, emetine, which allows only the mitochondrial-encoded proteins being synthesised to incorporate the radiolabeled amino acids. Once incubation with the radiolabeled amino acids was complete, a second incubation with unlabeled culture medium supplemented with methionine, referred to as the "chase", was

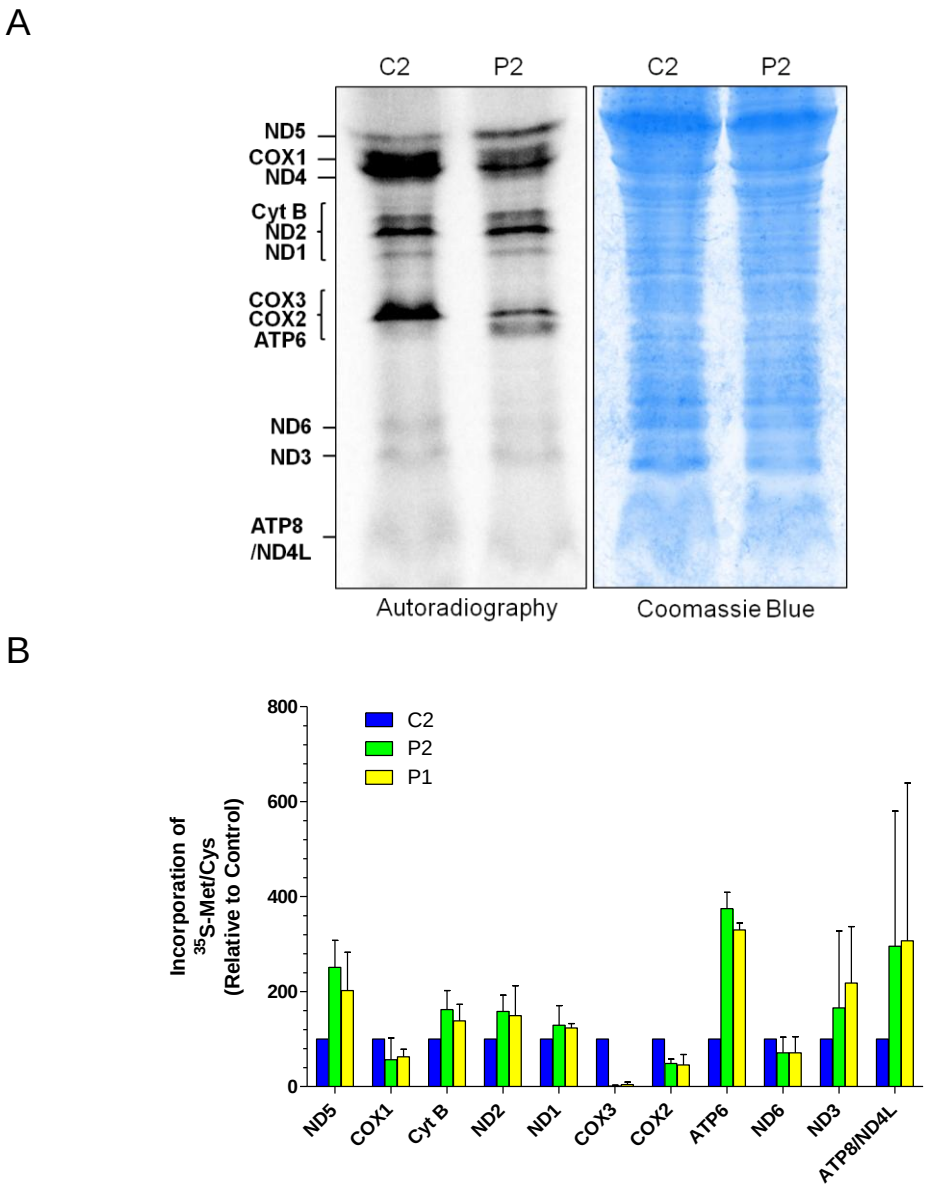

Figure 4.9. *De novo* synthesis of mitochondrial translation products in *PAPD1* mutant fibroblasts.

To assess mitochondrial translation products, whole cell lysate (50ug) harvested from fibroblasts labeled with [^{35}S]-methionine/cysteine was separated on a 15-20% SDS polyacrylamide gel. **A.** A representative image of the control and homozygous mutant *de novo* synthesis of mtDNA-encoded proteins. Protein identities are indicated to the left of the image. Comassie blue staining was used protein loading comparison. **B.** Quantification of [^{35}S]-labeling for both homozygous mutants and control fibroblast lines (n=3 for C2 and P2 lines, n=2 for the P1 line). Translation product intensities were quantified by densitometry using Image J. Only clearly discrete products were analyzed. Results were normalized to the control values. Error bars represent S.D. Images analyzed include the image in A, lanes 1,2, and 5 in Figure 4.10, and a third independent labeling experiment (data not shown).

performed. The cells were then lysed and the radiolabeled mitochondrial translation products were separated by gel electrophoresis and visualized by autoradiography.

The initial experiments using this technique were to visualize differences in translation of each mtDNA-encoded polypeptide between the control fibroblast line and the homozygous mutant fibroblast lines. These products are identified according to their predicted identities based on previous reports (Chomyn, 1996). Staining of the gel with Comassie blue was performed for assessing any differences in protein loading. Again,

there is a non-uniform pattern in the homozygous mutant cell lines compared to the non-familial control line. The results from multiple labeling experiments are shown graphically in Figure 4.9B, with a representative image shown in Figure 4.9A. The labeling shows increases, decreases, or no change, depending on the polypeptide. The major translation decreases are observed for COX1, COX2, COX3 in the mutant, while ND5 and ATP6 appear to be increased. The rest of the labeled translation products do not appear to show significant changes in the mutant cells, as the levels are comparable to control. As with the mRNA transcripts, there are no obvious characteristics that could explain the changes. The ND1 and ATP6 data stand out, as their mRNA species are increased and decreased, respectively, but their translational products do not reflect this. Levels of translation of *MTND1* are similar between mutant and control cells, however immunoblot analysis shows that the protein is severely depleted at steady-state. The *RNA14* steady-state mRNA levels are significantly lower in the mutant cells, but its translation product is increased. At the time of the labeling experiments, there were not antibodies available for analyzing the steady-state levels of ATP6 or ATP8. A commercial antibody did become available for ATP8, and this result is shown and discussed in Chapter 5. The gel patterns of multiple independent labeling experiments were quantified by densitometry, and graphed for comparison (Figure 4.9B).

Having visualized the state of mitochondrial protein synthesis in the control and homozygous mutant fibroblasts, mtDNA-encoded protein turnover was examined. Changes in turnover rates could potentially explain the lower steady-state levels for respiratory chain subunits in the homozygous mutants that did not appear to have decreased synthesis. This pulse-chase experiment, performed by Dr. Bruni, was carried out over several time points in order to observe the rate of degradation of the radiolabeled polypeptides. As the experiment used emetine for inhibition of cytosolic translation, the time points only extend to eight hours. A longer time course would result in cytotoxicity from the emetine. Eight hours was shown to be sufficient to observe any gross changes in mitochondrial protein turnover in the homozygous mutant fibroblast line, compared to the control line. The C2 (control) and P2 (patient 2) lines were chased for multiple time points, while the P1 (patient 1) line was labeled for only one time point. This inclusion was for comparison at time zero for all three fibroblast cultures.

The pulse chase experiment results are shown in Figure 4.10. Time point zero for all three cell lines recapitulates the patterns observed in the pulse labeling experiment.

Two mitochondrial polypeptides show an increased rate of turnover in the homozygous mutant line, these are complex I subunits ND2 and ND5. COX1 also

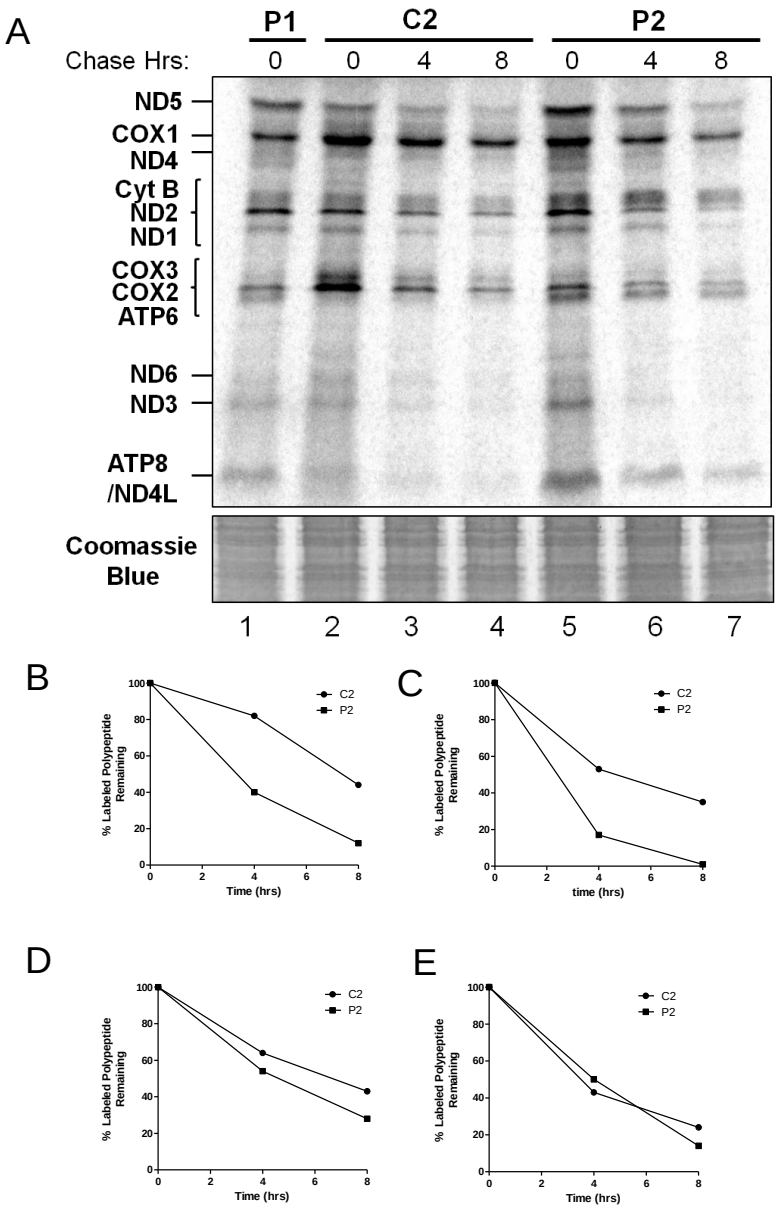

Figure 4.10. Pulse-chase labeling of *de novo* protein synthesis in *PAPD1* mutant fibroblasts.

A. Autoradiography image of mitochondrial translation products labeled with [^{35}S]methionine/cysteine and chased for 0, 4, and 8 hours post-labeling. The control (C2) and homozygous mutant (P2) were labeled and chased as indicated, while the other homozygous mutant (P1) was labeled for a single time point. Predicted translation product identities are listed on the left side of the gel image. Coomassie blue staining of the gel is included for comparison of loading in each lane. **B-E**. Analysis by densitometry using Image J was performed on the gel image in A, and the resulting values for translation products were normalized to the 0hr time point value to graph the percent reduction in value for the 4hr and 8hr time points. The graphs shown are for ND5 (**B**), ND2 (**C**), COX1 (**D**), and ND1 (**E**).

appears to show an increased rate of turnover in the mutant line, but to a much lesser extent than the aforementioned complex I subunits (Figure 4.10B-E). The majority of the mitochondrial polypeptides in the homozygous mutant lines did not appear to be

markedly affected in their turnover time, when compared to the control fibroblasts (data not shown).

4.3.8 Assembly of complexes I-V in mutant *PAPD1* fibroblasts

After observing major decreases of steady-state levels for mtDNA-encoded complex I and IV subunits, as well as alterations in mRNA levels and their translation, it was important to confirm potential disruptions to the assembly of the respiratory complexes. This was accomplished by isolating mitochondria from control and homozygous mutant fibroblasts, and analyzing by blue native polyacrylamide gel electrophoresis (BN-PAGE). The BN-PAGE and subsequent blotting was carried out by Dr. Hue-Tran Hornig-Do. This method preserves assembled complex integrity during isolation. *n*-dodecyl β-D-maltoside (DDM) was used for solubilization and Coomassie blue G-250 was added to the supernatant. This binds to proteins and introduces a shift in charge for the protein complexes

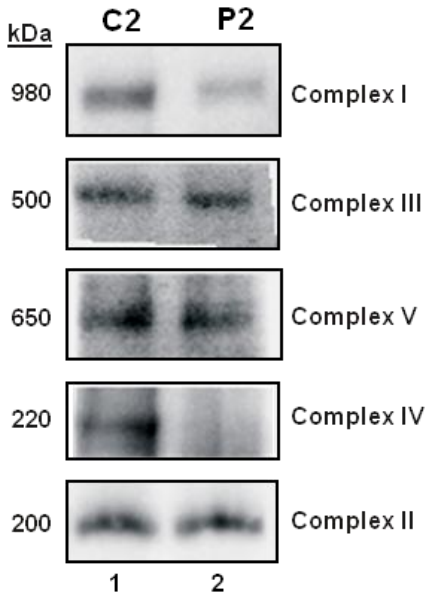

Figure 4.11. Analysis of OXPHOS complexes assembly.
Control (C2) and homozygous mutant (P2) mitochondria (40ug) were solubilized and separated by 4.5-16% blue native PAGE. Separated complexes were transferred to a PVDF membrane and immunoblotted for each of the five OXPHOS complexes. Sizes of the detected complexes are indicated to the left of panels, and the complex identities are shown on the right. Primary antibody targets were NDUFA9 (CI), Core 2 subunit (CIII), alpha subunit (CV), the holoenzyme (CIV), and SDHA (CII).

As shown in Figure 4.11, the assembly of all five OXPHOS complexes was investigated. A clear reduction in the amount of complexes I and IV in the homozygous mutant is observed, compared to control. Complexes II and III appear to be unaffected by the *PAPD1* mutation, as their levels are equivalent between the homozygous mutant and control cell lines. Despite the decrease in steady-state levels of the *RNA14* transcript, the amount of complex V present in the homozygous mutant cells does not differ markedly from the control cells. Complex II is also used here as a loading

control, as its subunits are entirely nuclear-encoded and thus assembly should be not be affected. The specific reduction of Complexes I and IV in the homozygous mutant is consistent with the depletion at steady-state of mtDNA-encoded subunits. With multiple missing subunits, the respiratory chain complexes may not be able to fully assemble, and complexes I and IV seem most vulnerable to this effect. This outcome would likely significantly compromise the enzymatic capabilities of these two complexes. As complex IV is the terminal electron acceptor of the respiratory chain, the ATP production capacity of the mitochondria may be compromised. This is consistent with the cell proliferation data from culturing the homozygous mutant cells in galactose-based media.

4.3.9 Complex I and IV activity in *PAPD1* homozygous mutant fibroblasts

To complement blue native data, the direct enzymatic activity of complexes I and IV were measured. While decreased levels of respiratory subunits is a pathological feature of mitochondrial dysfunction, it was important to establish the actual impairment in complex activity. This was performed by Dr. Hue-Tran Hornig-Do on mitochondria I isolated via the standard procedure. The complex activities of mitochondria from one homozygous mutant fibroblast line (P2) and one control line (C2) were assayed spectrophotometrically. The activity for complexes I and IV in the homozygous mutant line compared to the control line was 49.2% and 36.2%, respectively, compared to control values, as shown in Figure 4.12. These measurements represent a significant activity decrease in the mutant cells. This is

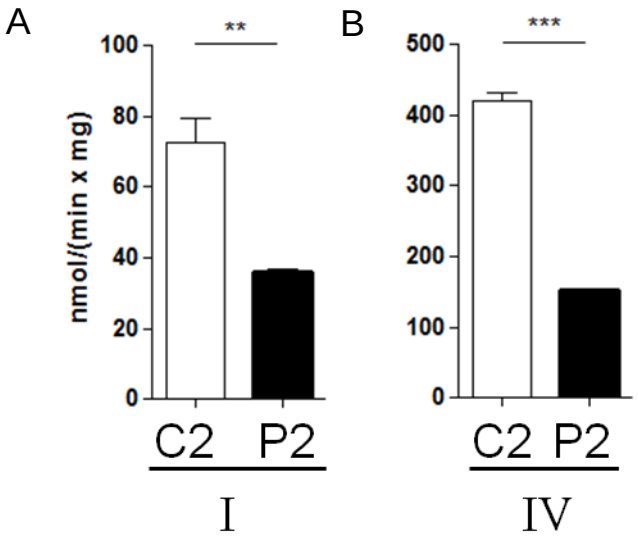

Figure 4.12. Measurement of complex I and IV activity in *PAPD1* mutant fibroblast mitochondria. Isolated mitochondria from control (C2) and homozygous mutant (P2) fibroblasts were assayed for complex I and IV activity. **A)** Measurement of complex I activity for the control and mutant samples. Activities are expressed as nmol rotenone sensitive NADH oxidized per min per mg mitochondrial protein. **B)** Measurement of complex IV activity for control and mutant samples. Activities are expressed as nmol reduced cytochrome *c* oxidized per min per mg mitochondrial protein For both complexes, n=2. Error bars represent S.D. ** P<0.01, ***P<0.001, Students *t*-test.

consistent with depletion of respiratory chain complex subunits and the reduced levels of assembled complex. These results also provide evidence that the major pathology in the homozygous mutant patients is that of an oxidative deficit resulting from a compromised electron transport chain.

4.3.10 Examination of mitochondrial morphology in *PAPD1* mutant fibroblasts

One of the critical parameters for proper mitochondrial function is finely regulated fission and fusion events. This allows for exchanges of mitochondrial material, organelle turnover, and mobility within the cell. I sought to examine whether the *PAPD1* homozygous mutant fibroblasts exhibited changes in mitochondrial morphology, as this could be indicative of perturbed fission and fusion.

For imaging the fibroblast mitochondria, TMRM was used, and for staining dsDNA in the cells PicoGreen was used. The images were acquired using an inverted fluorescence microscope. The PicoGreen dye stained both the nuclear DNA, and the mtDNA-containing nucleoids within the mitochondria. The dye is capable of binding both linear and supercoiled DNA, but has a lower fluorescence yield when bound to supercoiled DNA. TMRM is a cationic fluorescent dye that emits orange fluorescence as it accumulates in polarized mitochondria, and its lipophilic structure allows the dye to traverse cell and mitochondrial membranes. This membrane potential-driven accumulation in mitochondria allows for examination of membrane potential collapse or flux in cells. Assuming the membrane potential is not compromised, the fluorescence emitted by the accumulated TMRM allows for clear visualization of the mitochondrial reticular network in cells.

For this imaging experiment, I did not set a constant value for the exposure times, they were calibrated by the microscope software for each image taken, resulting in differing exposure times. The mitochondrial morphology is easily observed. However, the ability to compare subtle differences in the fluorescent intensities potentially resulting from disruptions in the membrane potential is compromised. The clarity of the mitochondrial networks observed in all the imaged cell lines suggests that major depolarization of the mitochondrial membrane potential has not taken place.

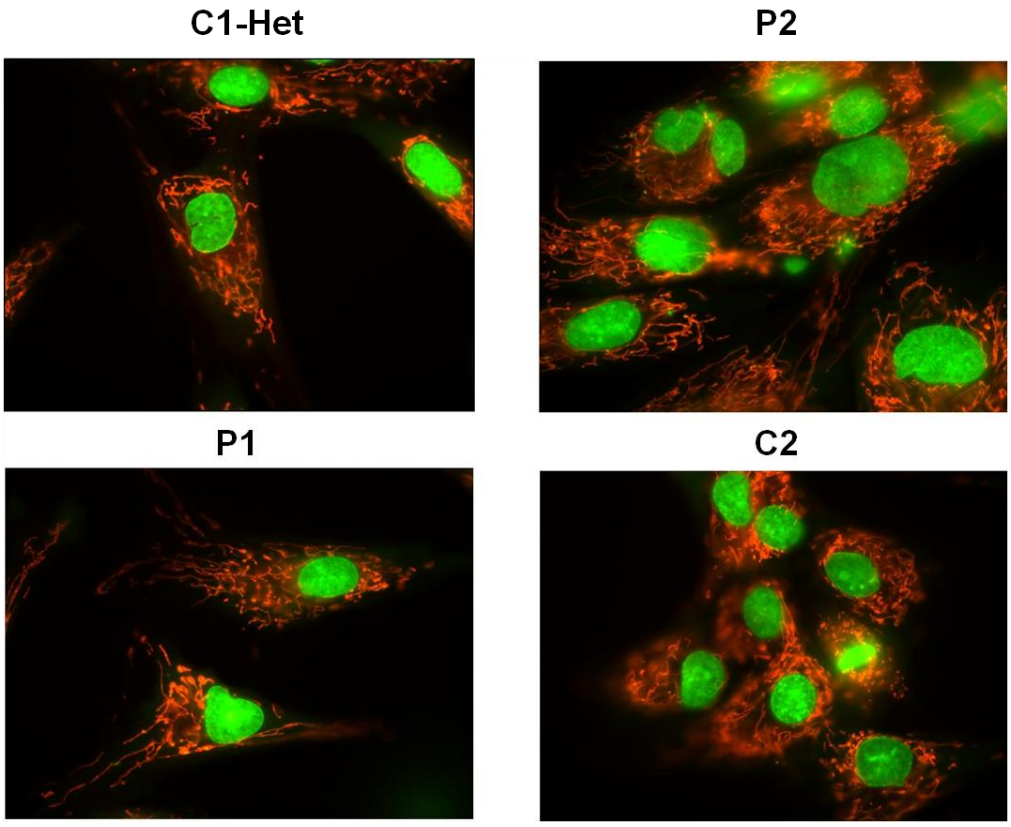

Figure 4.13. Examination of mitochondrial morphology via TMRM staining.
The complete panel of fibroblast lines, control (C2), patient 1 (P1), patient 2 (P2) and heterozygous mutant (C1-Het) were stained with TMRM and PicoGreen fluorescent dyes. TMRM staining was viewed with the Texas Red channel, and PicoGreen staining was viewed with the GFP channel. The mitochondrial networks are stained with TMRM, and nuclear and mtDNA stained with PicoGreen. The images shown here are the two channels merged for a single image per fibroblast line.

As shown in Figure 4.13, gross morphological analysis does not reveal any discernible differences but to be certain proper quantification of networks would need to be measured. The nucleoid staining for the four cell lines does not appear on observation to differ significantly. These results imply that aspects of mitochondrial function not related to oxidative phosphorylation are not dramatically impaired in the homozygous *PAPD1* mutant cells. As only respiratory chain complex subunit mRNAs are polyadenylated by mtPAP, this is expected.

4.3.11 Assessment of mitochondrial membrane potential in *PAPD1* mutant fibroblasts

In order to assess mitochondrial membrane potential in the homozygous mutant *PAPD1* fibroblasts, one homozygous mutant cell line and the control line were stained with JC-1 dye, and imaged via fluorescent microscopy. JC-1 is a widely used dye that fluoresces in the green or red spectrum based on its aggregation status. As a lipophilic cationic dye, it accumulates in mitochondria in a membrane potential-dependent fashion, forming oligomers. The transition from monomer to oligomer shifts its fluorescent emission from green (529nm) to red (590nm). Changes in the ratio of red to green fluorescence can be used as an indicator of compromised membrane potential.

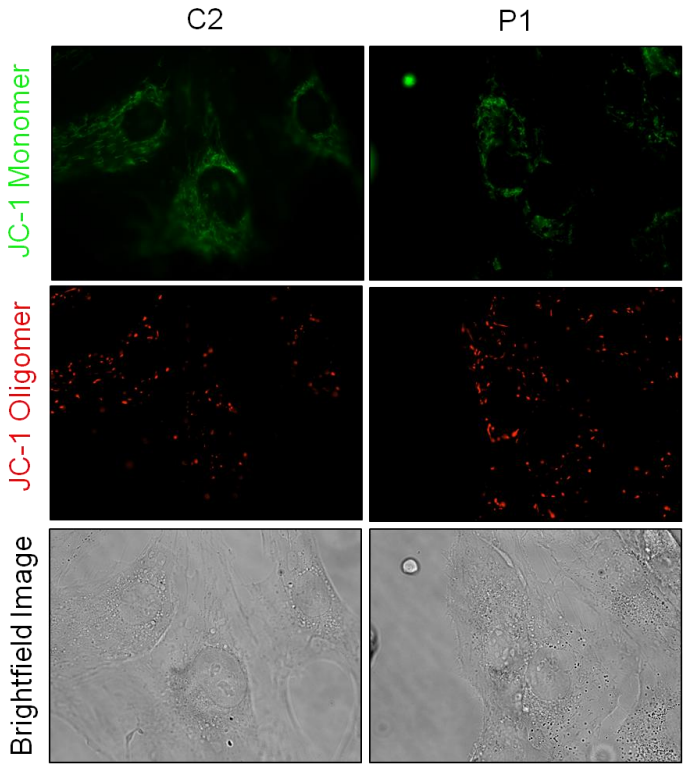

Figure 4.14. Membrane potential assessment via fluorescent microscopy.
Control (C2) and patient 1 (P1) fibroblasts were stained with JC-1 cationic dye. The monomer fluorescence was viewed with the GFP channel, and the oligomer fluorescence was viewed with the Texas Red channel. The left column of images corresponds to the control fibroblasts, and the column to the right the homozygous mutant fibroblasts. Brightfield images are provided for orientation of the cells in the viewing field.

Figure 4.14 shows the results of the JC-1 staining. As with the mitochondrial morphology, there did not appear to be gross differences in JC-1 oligomer red fluorescence as detected by staining between the control and homozygous mutant cell lines. There was a small difference between the two lines from the JC-1 monomer green. As the red fluorescent signal is driven by accumulation in the mitochondria, and does not change in a dramatic fashion in the mutant cells, this seemed to indicate that the *PAPD1*

mutation did not cause significant disruption to mitochondrial membrane potential. However, as with the TMRM/PicoGreen staining, quantitative assessment is necessary in order to clarify any subtle changes that are not obvious upon gross observation.

4.3.12 mtDNA levels in *PAPD1* mutant fibroblasts

A common pathologic feature of mitochondrial disorders is a change in the steady-state levels of mtDNA copy number. While polyadenylation of mt-mRNAs does not have a known direct connection to mtDNA metabolism and regulation, the possibility exists that shortening of the mt-mRNA poly(A) tails would produce some indirect perturbation of mtDNA levels. The mtDNA copy numbers were assessed in the mutant *PAPD1* fibroblasts as compared to control fibroblasts to confirm that the molecular pathologies stemming from the mutation occur outside the context of mtDNA metabolism. Using quantitative PCR, the levels of mtDNA were analyzed by measuring the amplification of a mtDNA encoded gene relative to a nuclear gene. Previously validated primer pairs for the *MTND4* and *18S* genes were employed for this analysis. DNA was isolated from the four fibroblast cultures.

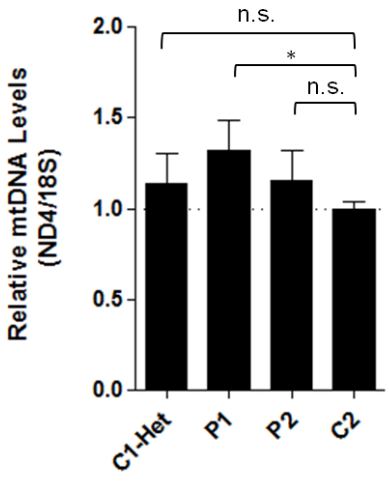

Figure 4.15. mtDNA copy number in *PAPD1* mutant and control fibroblasts.
Total DNA (50ng) isolated from all four fibroblast lines and quantitative PCR was performed, amplifying a mitochondrial gene (*MTND4*) and a nuclear gene (*18S*). The heterozygous line (C1-Het), homozygous mutant lines (P1 and P2) and control line (C2) are all shown on the graph. The ratio of *MTND4* amplification to 18S amplification was calculated, then normalized to the average ratio of the control line. Error bars refer to S.D.; n=3, *P>0.05, Student's *t*-test.

Figure 4.15 shows the results of the qPCR analysis of mtDNA levels. The only significant difference in mtDNA levels is between patient 1 and the control line, an average 25% increase of mtDNA levels. The mtDNA levels in the heterozygous mutant line and second patient line did not differ significantly from the control line (Figure 4.15, C1-Het cf. C2). This confirms that there is no depletion of mtDNA in the *PAPD1* mutant lines and that such a depletion is not the cause of downstream depleted and misregulated respiratory chain complex subunit levels. These results do not rule out the

possibility of mtDNA deletions or alterations outside of the*MTND4* gene. Major common deletions normally include *MTND4*, and these can be rules out based on these results.

4.4 Discussion

4.4.1 Oligo(A) tails are present in *PAPD1* patient fibroblasts

The aim of characterizing the *PAPD1* mutant fibroblasts was to understand the molecular mechanisms underlying the patient pathology, and leverage those observations to gain insights into the natural role of the poly(A) tail in mitochondria. In the case of the latter, the patient fibroblast cultures benefit from the lack of an artificial intervention to knock down or knock out mtPAP. The sole primary molecular pathology is a specific shortening of the poly(A) tail on mt-mRNAs. This presented a unique model for this study.

The immortalized fibroblasts were analyzed using the MPAT assay, focusing on a representative panel of mt-mRNAs, *MTCO1 MTCO3, RNA14* and *MTND3*. These three transcripts represented the varying degrees of polyadenylation necessary for stop codon completion: no adenines, one adenine, or two adenines. Each transcript recapitulated the characteristic oligo(A) tail described previously in (Crosby *et al.*, 2010), when the RNA was extracted from blood.

The homozygous mutants exhibited near-complete reduction of full length poly(A) tails. In contrast to the homozygous cells, the heterozygous mutant fibroblasts exhibited a mild intermediate phenotype. The population of full length poly(A) tails appears comparable to wild-type levels, but the oligo(A) population of transcripts seems to be increased slightly compared to the non-familial control line. Some oligoadenylation of mt-mRNAs is consistently observed (Crosby *et al.*, 2010; Temperley *et al.*, 2010b), and increases of this population may not be pathogenic. Rather, the loss of the full length poly(A) tails underlies the molecular pathology. By being able to generate wild-type amounts of full length poly(A) tails, this is probably how the heterozygous patients are able to avoid the clinical pathologies exhibited by the homozygous patients.

4.4.2 Oligo(A) tails cause non-uniform misregulation of mitochondrial gene expression products

The immediate impact of changes to poly(A) tail length would be expected to be on the mt-mRNA transcripts themselves. I examined the steady-state levels of several mt-mRNAs by northern blotting, which allowed me to observe alterations in size and quality

in addition to observing differences in the amount of transcripts present in each cell line. The results showed non-uniform changes to the steady-state levels of the transcripts analyzed. *MTCO1, MTCO3* and the *RNA14* bicistronic transcript were decreased, while *MTND1* was elevated. *MTND3* appeared unaffected by the abrogated poly(A) tail. The mt-rRNAs were unaffected as well, but as these are not subject to polyadenylation, no changes were expected.

The qPCR analysis of mtDNA levels ruled out the possibility of mtDNA depletions causing downstream decreases in transcripts, although such a decrease in mtDNA would not have explained the increased levels of *MTND1*. There appeared to be a small but significant (for patient 1) increase in mtDNA levels in homozygous mutant cells. Patient 2 and the heterozygous mutant line were not significantly different from control. There is no obvious evidence that mtDNA is involved in the pathological phenotype of the mutant cells.

There are no obvious characteristics of the transcripts that can account for their discrepant behaviors when oligoadenylated. No consistent pattern emerges, such as related open reading frame lengths, or the presence of 5' leader or 3' trailer transcript regions. The mechanisms that allow certain mRNAs to be elevated, while others are decreased at steady state, remain to be elucidated. *MTND2* was not analyzed by northern blot in this work, but other reports show it to be another extra-stable mt-mRNA, alongside *MTND1 (Piechota et al., 2006; Wydro et al., 2010; Rorbach et al., 2011).* According to these previous reports, the other mtDNA-encoded complex I subunits are not stabilized to the same extent as *MTND1* and *MTND2.* The location of the two mRNAs within the polycistronic RNA molecule may have some impact on their subsequent cleavage and polyadenylation, and may influence regulation by yet unknown factors. My experiments, and others reported in the literature, have not shown other mt-mRNAs besides *MTND1* and *MTND2* to be stabilized by shortening or removal of their poly(A) tails. There appear to be factors unique to these two transcripts that cause this difference. As mentioned, these factors are not clear at present.

In my experiments, *MTCO1, MTCO3* and *RNA14* were decreased at steady-state. This agrees with most reports in the literature for *MTCO1* (Nagaike, 2005; Wydro *et al.*, 2010; Rorbach *et al.*, 2011). The same results exist for *RNA14* in these reports, however the overexpression of PDE12, a putative mitochondrial deadenylase, in HEK293 cells showed no effect on *RNA14* steady-state levels while otherwise matching the results for other transcripts (Rorbach *et al.*, 2011). *MTCO2* and *MTCO3* have been shown in several of these reports to be decreased as well. This is consistent with the status of *MTCO3* that I

observed in the homozygous mutant cells. As with the complex I subunit-encoding mRNAs, there is no obvious pattern to explain why the complex IV subunit-encoding mRNAs are specifically depleted. *MTCO3* does appear to be decreased to a much more marked degree than *MTCO1* or *MTCO2*. This difference could in part be explained by *MTCO3* being the only mtDNA-encoded complex IV transcript that requires adenylation in order to complete its stop codon, as it possesses no 3' UTR. However, even in the homozygous mutant lines the transcript is oligoadenylated, thus completing the stop codon. Thus, the stop codon necessity of adenylation does not completely explain the transcript decrease. The remainder of the mt-mRNAs appear to have their steady-state levels unaffected when only oligoadenylated. My northern blotting analysis of *MTND3*, showed no changes in steady-state levels as a consequence of oligoadenylation.

These results suggest, that unlike other organisms and cellular compartments where polyadenylation has a primary positive or negative effect on mRNA stability, polyadenylation may have a more complex role in mammalian mitochondrial mRNA metabolism. There is no single pattern of degradation, as in bacteria, or stabilization, as in the human cytosol. Whether this observed complexity is a product of unknown levels of regulation, or mid-evolutionary transition of mt-mRNA poly(A) tail necessity, is yet to be elucidated.

4.4.3 Translation of oligo(A) mt-mRNAs

While the variable effects on mt-mRNA stability are not easily explained, it was possible that the downstream effects would align in a more coherent manner. Thus, I sought to investigate the translation status of the oligoadenylated mt-mRNAs. Analysis of *de novo* protein synthesis presented yet another complex set of results. There were once again increases, decreases, and lack of change on mitochondrial mRNA translation. Interestingly, not all of the trends observed at the mRNA level were recapitulated at the translational level. For example, *RNA14* is clearly depleted, yet synthesis of the ATP6 polypeptide appears to be increased. Whilst, for *MTCO1*, and *MTCO3*, there appears to be a relationship as both the transcript and protein synthesis are decreased. *MTND1*, one of the several curiously extra-stabilized mt-mRNAs, does not show significant changes in *de novo* protein synthesis in the homozygous mutants, compared to control.

There are several possible explanations for the discrepancies observed here. The discovery of TACO1, a human mitochondrial translational activator for COX1, suggests that there may be more translational activation factors for the other mt-mRNAs, such as

exist in yeast (Weraarpachai *et al.*, 2009; Herrmann *et al.*, 2013). These activators could be responding to the same stimuli (short oligo(A) tails) in differential manners, thus producing variable translation changes. As mentioned in context of the mt-mRNA stability differences, the mitochondrial genes could be in varying phases of losing the necessity of a poly(A) tail for optimal protein synthesis. However, we know that yeast translational activators interact with UTRs. In human mt-mRNA only a subset of transcripts have sequences that correspond to a UTR. MTCO1, for example, has a sequence that is not cleaved off that represents the antisense of tRNA serine at the 3' end.

Despite this variation at the protein synthesis level, steady-state respiratory subunit analysis showed a consistent trend towards depletion. I immunoblotted against multiple mtDNA-encoded gene products: COX1, COX2, COX3, ND1, and ATP8 (data shown in Chapter 4, as the ATP8 antibody was not available when this characterization work was being carried out. Subsequent availability allowed for expansion of analysis during characterization of the lentiviral-treated fibroblasts). All of these subunits were decreased in the homozygous mutant fibroblasts. So in a functional sense, the endpoint of the poly(A) truncation is loss of various mtDNA-encoded OXPHOS subunits. The mechanisms underlying this effect are not clear in the case of complex I. For complex IV, there is a logical sequence of dysfunction, with the transcripts decreased at steady-state, then reduced protein synthesis which causes reduced levels of steady-state proteins, which causes a decrease of the assembled complex. The pulse-chase experiment was performed in order to assess the rates of mitochondrial translation product turnover, and investigate whether changes in turnover rates were contributing to depleted steady-state subunit levels. Small differences were observed in OXPHOS protein turnover, with the most affected proteins being ND5 and ND2, and COX1 to a much lesser extent, but the rest of the translation products did not show major turnover differences between the homozygous mutant and control fibroblasts.

Interestingly, other approaches for removal of the poly(A) tail have all shown a uniform decrease in protein synthesis for all mitochondrial polypeptides. This includes overexpression of the PDE12 deadenylase, and mitochondrial targeting of either cytosolic PARN or PABPC1. Consistent with the results presented here, both LRPPRC knockout mice and human patients harboring mutations in LRPPRC show a similar non-uniform translation pattern (Sasarman *et al.*, 2010; Ruzzenente *et al.*, 2012). Important to note, however, is the translation products that are increased/decreased do not all match with the *PAPD1* homozygous mutant patterns. The fact that LRPPRC has been shown to be involved with mt-mRNA metabolism and pro-polyadenylation strengthens the idea that

some underlying process may be disrupted when the protein's function is impinged upon. Perhaps *cis*-regulatory elements exist in the transcripts that require the poly(A) tail for functioning in the context of translation, and LRPPRC interacts with these elements.

Another important point is the lack of mtPAP depletion as a result of the N478D mutation. In other experimental systems of mtPAP suppression, such as the knock-downs, the enzyme is not physically present. This could cause assembly defects of a potential larger protein complex that mtPAP may associate with. The loss of the protein could have other unpredicted effects as well. The homozygous N478D mutant mtPAP fibroblasts provide a system where the enzyme is physically present, with only activity impaired. This is an ideal situation for analysis of poly(A) activity defects only, without the possibility of other confounding physiological perturbations, unless the mutation affects interactions with LRPPRC or other *trans*-acting factors. This possibility is investigated in chapters 6 and 7.

4.4.4 The *PAPD1* 1432A>G mutation causes an oxidative defect

The cumulative result of the transcription and translation changes stemming from the homozygous *PAPD1* mutation is a significant oxidative metabolism defect. Blue native PAGE was performed to confirm if any assembly disruption of complexes I-V had occurred. Specifically, complexes I and IV showed the lowest levels of fully assembled complex. There was not any evidence of partially assembled subcomplexes for I or IV. This logically follows from depletion of mtDNA-encoded subunits for each complex. Subsequent analysis of the activity from the complexes in isolated mitochondria confirmed an impairment of enzymatic activity. Considering complexes I and IV have the largest number of mtDNA-encoded subunits, their preferential disruption in the presence of the homozygous *PAPD1* mutation can be rationalized. While mitochondrial morphology and membrane potential did not appear substantially disrupted, cell growth defects in galactose-based media revealed the extent of the oxidative impairment. The growth curves for the homozygous mutant cells mildly lags compared to the heterozygous and control lines in standard glucose media. Once cultured in media that forces heavier reliance on oxidative metabolism, the impairment of cellular proliferation is considerably more evident. Time permitting, it would informative to measure the levels of ATP present in the homozygous mutant cells and their synthesis rate.

Taken together, these experimental results indicate that the respiratory defect acts as the source of clinical pathology in the affected patients. The decrease in COX1-3 proteins due to transcript decreases would have a major impact on complex IV assembly. As complex IV is the terminal respiratory complex, disruption of its assembly and activity would directly cause an OXPHOS defect. Importantly, complex I is the most commonly involved respiratory complex in mitochondrial disease, and thus its involvement in the patient pathology is likely substantial.

Mitochondrial disorders defined by nuclear gene mutations causing mitochondrial translation defects are a currently expanding category. The symptoms of the homozygous *PAPD1* 1432A>G patients overlap those observed in nuclear mutation-based mitochondrial disease: these include autosomal-recessive ataxia, optic atrophy, neurological deficits. The clinical presentation of these disorders can be quite varied, but neurological involvement is common. The lack of mtDNA involvement only underscores the similarity to other nuclear mutations, which cause disorders of mitochondrial translation. The molecular and clinical data from these *PAPD1* follow in a logical manner from the disruption of the respiratory chain function causing oxidative metabolism defects, to a neurodegenerative pathology, with ataxia as the principle component. This rational relationship between clinical pathology and molecular dysfunction in the *PAPD1* patients is in contrast to certain other nuclear-encoded mitochondrial factor-driven disorders. For example, mutations in the mitochondrial aminoacyl-tRNA synthetases, which would be expected to affect mitochondrial protein synthesis in all tissues, in fact present with highly variable phenotypes and remarkable tissue specificity depending on which of the synthetases is mutated (Konovalova and Tyynismaa, 2013).

Analyses of steady-state levels of mt-mRNAs and respiratory subunits showed the heterozygote to be essentially indistinguishable from control cells. The cell growth curve for heterozygous cells matched control in galactose media, and even exceeded the control in glucose media, implying the lack of an oxidative metabolism defect. There does not appear to be an obvious reason why the heterozygous fibroblasts would proliferate at a greater rate than control cells, as none of our analyses showed any gains on the molecular level. The cell growth results more likely fall within the normal range of rates exhibited by wild-type fibroblasts, and would be more apparent with the inclusion of more control fibroblast lines. At the time of this work, only the one immortalized non-familial control line I immortalized was available.

It is still unclear whether the mtPAP N478D monomer can heterodimerize with wild-type mtPAP monomer, or if they can only homodimerize. Regardless of which

situation occurs in the heterozygous background, there exists enough poly(A) activity to overcome the mutation. This is important when considering complementation experiments, as the expressed transgene must be able to exert an effect on the phenotype. Had the heterozygous cells shown the deficiencies observed in the homozygous cells, a rescue experiment might not be feasible if the wild-type transgene expression ratio was 1:1 with mutant expression. Fortunately, the mutation is recessive, thus expression of wild-type mtPAP in the homozygous mutants to suppress the defect was a reasonable hypothesis.

4.4.5 What is the role of the poly(A) tail?

As stated, the aim of this section of research was two-fold: to characterize the downstream effects of truncated poly(A) tails on mt-mRNAs by analyzing the molecular phenotype of the mutant fibroblasts and then to use these results to gain insight into what specific role the poly(A) tail plays in mitochondria. While I have completed an investigation of the molecular phenotype of the mutant fibroblasts, and generated some informative data, progress in understanding the role of mitochondrial polyadenylation has been complicated. The differential effects observed resulting in differing levels of gene expression do not clearly illustrate a single fundamental mechanism across all mtDNA-encoded OXPHOS subunits. The effects observed on complex IV follow a trend of stabilization of the mRNA transcripts conferred by the poly(A) tail, but the transcripts encoding other OXPHOS proteins do not adhere to this paradigm. Unlike the generally uniform degradation or protective role found in other organisms and cellular compartments, human mitochondria may utilize the poly(A) tail for more than a single function. The specific endogenous components of the translation machinery interacting with the tail are not known, and whether they interact in differing manners depending on the mt-mRNA is also not known. In a broad fashion, without full length poly(A) tails, respiratory chain defects result. This interpretation is complicated in part by the lack of quality antibodies to examine steady-state levels of all mtDNA-encoded polypeptides. The closest available alternative is the information derived from labeling of *de novo* mitochondrial protein synthesis. From that experiment, there are translation products that appear unaffected by oligoadenylated status of their coding transcript. If they are indeed unaffected, what is the mechanism of differentiation between transcripts? These questions are difficult to answer at present. The exact degree of poly(A) tail truncation necessary to cause these effects is also unclear, as in the homozygous mutant fibroblasts, the

shortening of the tail is quite dramatic. Future work may explore whether there is a threshold length of poly(A) tail required for optimal mtDNA gene expression, or if the shortened lengths are proportional to the downstream dysfunction incurred.

These cell biology and biochemistry based investigations presented here have not uncovered a full understanding of the precise nature of the N478D mutation. As the enzyme domain within which the mutation is located does not currently have an exact function attributed, more work is needed to understand the structural or enzymatic dysfunction. This was the impetus for the *in vitro* investigations using recombinant proteins detailed in chapter 6.

In summary, this study of the heterozygous and homozygous *PAPD1* 1432A>G mutant fibroblasts has yielded valuable, if complex, insights as to the effect of oligoadenylated mt-mRNA transcripts. The mutation results in a shortening of the adenylate tail on mt-mRNAs, leading eventually to activity deficits in complexes I and IV, which presumably underlie the neurodegenerative condition afflicting the patients harboring the homozygous genotype. While their condition is tragic, it underscores the notion that impairment of polyadenylation is not an embryonic lethal condition and that cells can somewhat tolerate the mitochondrial dysfunction. The cells survive and proliferate, although in a hampered fashion. The use of these patient fibroblasts has been a critical tool, and beyond the insights gathered by my investigations, they will continue to serve as a valuable resource for research into mitochondrial polyadenylation.

Chapter 5

Rescue of mt-mRNA oligoadenylation by lentiviral-based wild-type mtPAP expression

5.1 Introduction

In parallel to the characterization studies of the *PAPD1* 1432A>G fibroblasts, it was imperative to be confirm that the 1432A>G mutation was the sole effecter of the pathological cellular phenotype observed. The most straightforward method for confirming this is ectopic expression of the wild-type gene in the afflicted cells, and monitoring for recovery of the dysfunction. The aim of this study was therefore ameliorating the biochemical defects in the *PAPD1* mutant fibroblasts by rescuing the mutant phenotype. With the data for the heterozygous mutant line, I knew that introduction of a similar amount of wild-type mtPAP to N478D mtPAP would be sufficient to recover dysfunction.

There are multiple techniques for introducing an exogenous transgene into cultured cells. These include cationic lipid based methods for delivery of DNA. Electroporation is another common method, harnessing an electrical discharge through solution that causes temporary pores to open in cell membranes through which DNA can move. A particularly effective approach for gene delivery is the use of viral vectors. Lentivirus-based transduction, specifically, has a host of benefits over other methods, as a high percentage of cells are transduced, a broad variety of cell types can be infected, and the ability to infect both non-dividing and dividing cells.

While the use of viral vectors was considered from the outset, the initial transduction strategy for this rescue experiment used lipid-based transfection methods with a DNA plasmid (pcDNA5/FRT/TO) typically used for HEK293 Flp-In™ T-REx™ transfections to generate stable transfections in the immortalized *PAPD1* mutant cells. The pcDNA/FRT/TO plasmid possesses a tetracycline-inducible promoter for expressing the gene of interest. The pcDNA6/TR plasmid, which encoded the Tet repressor, is co-transfected into target cells in parallel with pcDNA5/FRT/TO in order to generate tetracycline-inducible cellular expression of the gene of interest. This strategy had the added benefit of producing a DNA construct that would also be suited for transfection into the HEK293 cells for other experiments. Unfortunately this approach proved unsuccessful for use in immortalized fibroblasts. I attempted to generate stable transfectants with the same DNA plasmids using electroporation, but this also failed.

A lentiviral vector was therefore designed to deliver a wild-type FLAG-tagged *PAPD1* gene into both the wild-type and mutant cells. In this chapter, I will describe the generation of the *PAPD1* DNA construct, the initial attempts at transfection, then the implementation and results of the wild-type *PAPD1* lentiviral transduction on the mutant fibroblasts.

5.2 Materials and Methods

5.2.1 Generation of the pcDNA5/FRT/TO-mtPAPFLAG construct

Full length coding region of mtPAP was PCR amplified using single stranded cDNA prepared from human fibroblasts via Oligo dT as template. The forward and reverse primers used in the PCR reaction were mtPAPF and mtPAPFLAGR (2.2.4.4). This generated a C-terminal FLAG-tagged mtPAP amplicon with BamH1 and Not1 restriction sites at the 5' and 3' ends, respectively. The PCR reaction products were then separated through a 1% low melting temperature agarose gel, and the DNA band of the correct size was excised and purified. The purified mtPAPFLAG PCR product was then digested with BamH1 and Not1 to create sticky ends, followed by phenol/chloroform extraction and EtOH precipitation. The expression vector pcDNA5/FRT/TO (Invitrogen) was also digested with BamH1 and Not1, and the linear products phenol/chloroform extracted and EtOH precipitated, then dephosphorylated using calf intestine alkaline phosphatase (NEB). The mtPAPFLAG fragment was ligated into pcDNA5/FRT/TO, and then used to transform Bioline α-select bacterial cells (Novagen). Transformed colonies were selected for ampicillin resistance (100ug/ml) on LB-agar plates. Confirmed colonies harboring the pcDNA5-mtPAPFLAG construct were expanded into 5ml cultures and incubated at 37°C overnight shaking. The construct was then purified with GeneJet plasmid prep kit (Fermentas), according to manufacturers protocol. The purified construct was then sequenced with a 3130*xl* Genetic Analyzer (Applied Biosystems) to confirm correct ligation, orientation, and full sequence. See section 2.2.4.4 for primers, and 2.2.4.3 for PCR profiles and reaction mixes.

5.2.2 Blasticidin^{S} titration

Immortalized heterozygous *PAPD1* 1432A>G mutant fibroblasts (C-HET) were seeded 50,000 cells/well in 6-well plates (Corning) in standard DMEM and incubated overnight. The following day, Blasticidin^{S} was added to the media in five wells at the following concentrations: 0, 1, 2, 5, 7, and 10ug/ml. The cells were cultured in the presence of Blasticidin^{S} for six days, with one media replacement at day 3. After six days, cells were trypsinized and counted using a Neubauer hemocytometer.

5.2.3 Lipid-based transfection of fibroblasts

The pcDNA5/FRT/TO-mtPAPFLAG construct and pcDNA6/TR plasmid were linearized by FspI digestion. Digest reactions were then phenol/chloroform extracted, EtOH precipitated, and the DNA re-suspended in 20ul sterile dH_2O. The immortalized human fibroblast cell lines were split into 6-well plate wells to achieve 30-60% confluency by the day of transfection. Immediately prior to transfection, linearized construct and plasmid were mixed in a 9:1 ratio to give a total DNA amount of 2ug (1.8ug pcDNA5-mtPAPFLAG and 0.2ug pcDNA6/TR). This DNA mix was made up to 100ul with DMEM lacking serum, antibiotics, and supplements, and combined with 10ul Superfect (Qiagen). The solution was *gently* mixed by pipetting and allowed to incubate 10min at RT. While Superfect/DNA mixture incubated, the medium was removed and cells were washed twice with PBS. After 10min 1200ul of complete supplemented medium was added to DNA/superfect mixture, gently mixed and then transferred on to washed cells. The cells were incubated in for 2.5-3hrs, then transfection mix was removed, and cells washed twice with PBS. A second round of transfection, performed as detailed above, was then completed. Following the second round of transfection, cells were fed with normal growth medium until two days later when selection with Blasticidin^S at 2ug/ml began.

5.2.4 Transfection by electroporation

Immortalized fibroblasts were washed once with Dulbecco's A-PBS, then trypsinized, pelleted, and each cell pellet suspended at 800,000 cells in 25ul of Resuspension buffer R. The plasmids to be used for transfection were mixed in a 9:1 ratio, pcDNA5/FRT/TO-mtPAPFLAG to pcDNA6/TR, in sterile TE buffer. 4ug of this 9:1 DNA mix was added to the 25ul cell suspension. 10ul of the suspension (~400,000 cells) was electroporated with a pulse voltage of 1500V, pulse width of 10, and pulse number of 3. The cells were then transferred to 2ml of complete DMEM without antibiotics in a 6-well plate. This was repeated with a second 10ul of the cell suspension, and these cells seeded in a second 6-well plate well. Then both steps were repeated for each individual cell line. After incubation for 48 hours, selection with Blasticidin^S was initiated.

5.2.5 Transduction of fibroblasts using a lentiviral vector

A custom lentiviral vector encoding C-terminal FLAG-tagged mtPAP, and a puromycin resistance gene for selection, was purchased from Genecopoeia (Cat #: LP-W1687-Lv121, Lot #: GC10312K1105). The virus particles were provided as 200ul, with a viral titre of $9.4x10^9$ copies/ml. Immortalized heterozygous (C-HET) and homozygous (P1 and P2) *PAPD1* 1432A>G fibroblasts and control fibroblasts (MB-I) were seeded at 200,000 cells in T25 flasks in standard DMEM. The following day, in a BSL-2 certified laboratory space, 100ul (4×10^{10} viral particles) of custom lentivirus encoding mtPAP-FLAG was added to 16ml of complete supplemented DMEM + 10ug/ml polybrene. The media was removed from the fibroblast seeded flasks, and replaced with 4ml/flask of virus-containing media, then incubated overnight. The following day virus-containing media was removed, and replaced with complete DMEM. Cells were incubated overnight. On the third day, puromycin was introduced to the cultures at a final concentration of 2ug/ml. Transduced cells were cultured in the presence of puromycin until only resistant cells were present, approximately seven days. The lentiviral vector map is shown in Appendix B.

5.3 Results

5.3.1 Initial attempts at transfection using pcDNA5/FRT/TO-mtPAPFLAG construct

This initial transfection strategy utilized an already established system in our lab, the HEK293 Flp-In™ T-REx™ cell line and associated plasmids. This HEK293 line has an integrated stable FRT site in the genome used for targeted insertion of a gene of choice cloned into the Flp-In™ vector. The cell line also has pcDNA6/TR stably integrated, for constitutive expression of the Tet repressor, creating an inducible system for exogenous gene expression. While there was value in generating HEK293 cells that could express tagged mtPAP, in the early stages of the project the goal was stable transfection with FLAG-tagged mtPAP into the mutant fibroblasts, with co-transfection using the pcDNA6/TR vector for Tet repressor expression. This was designed to create an inducible, tagged mtPAP rescue of the mutant phenotype. The pcDNA5/FRT/TO plasmid is typically used in our lab for the HEK293 transfections, and would be used for cloning of the FLAG-tagged mtPAP. The fibroblasts do not have a stable FRT site in their genome like the HEK293 cells, so integration into the fibroblast genomes would be a random in location.

Generation of the mtPAPFLAG amplicon was successful (Figure 1A), using 10ng fibroblast cDNA as a template in a PCR with the mtPAPF and mtPAPFLAGR primers (See appendix A). The mtPAPFLAG primer inserted a FLAG-tag at the 1731nt position in the C-terminus of mtPAP amplicon, replacing the terminal five residues.

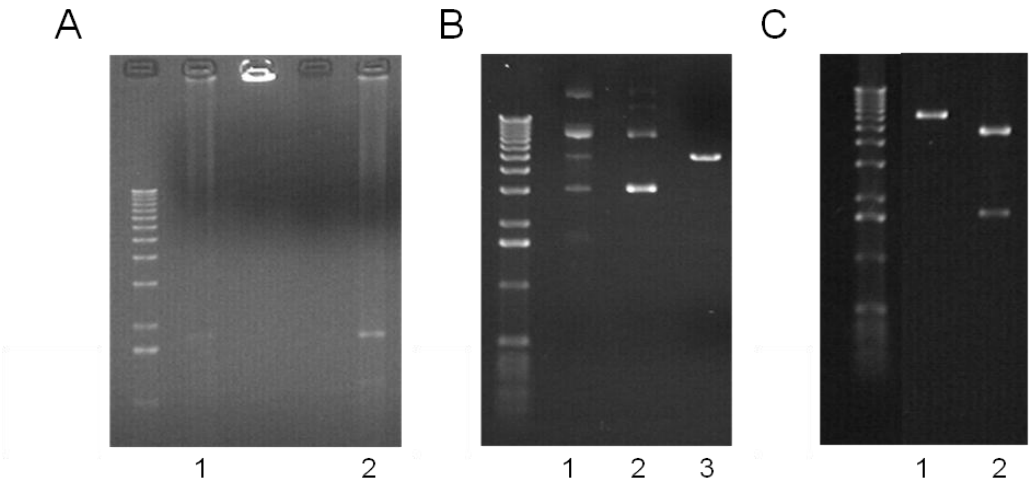

Figure 5.1. Amplification, digestion, and confirmation of the pcDNA5-mtPAPFLAG construct.
A. Result of mtPAPFLAG PCR (lane 2). **B.** Result of BamH1+Not1 digest on pcDNA5/FRT/TO. The uncut plasmid (lanes 1-2) and the digested plasmid (lane 3). **C.** Confirmation of the insertion in the plasmid. Single digest with BamH1 of pcDNA5-mtPAPFLAG construct (lane 1), digest of construct with BamH1 and Not1 (lane 2). All gels are 1% agarose and DNA visualized by UV transillumination. Size markers are the same on all gels.

In parallel, the pcDNA5/FRT/TO plasmid, a tetracycline-regulated, CMV/TetO_2 promoter driven expression vector, was harvested and purified from bacterial stocks. Digestion with BamH1 and Not1 (Figure 5.1B, lane 3), then dephosphorylation, was performed to prepare the vector for ligation with the mtPAPFLAG insert. The ligation reaction was used to transform Bioline α-select bacteria. However only one resistant colony harbored the correctly assembled construct, as confirmed by BamH1 and Not1 digestion (Figure 5.1C). Sequencing confirmed the correct orientation and fidelity of the mtPAPFLAG amplicon in the construct, which will be referred to as "pcDNA5-mtPAPFLAG".

While the work cloning mtPAPFLAG into the vector was ongoing, heterozygous *PAPD1* mutant fibroblasts were seeded for generating a 1-10ug/ml titration curve for Blasticidin^S (Figure 5.2). A concentration of 2ug/ml Blasticidin^S was chosen as the optimal concentration for the transfections, as this concentration exerted the desired killing effect while using minimal antibiotic.

The pcDNA5-mtPAPFLAG vector contains a promoter that is bound by the Tet repressor, encoded on the pcDNA6/TR vector. Both vectors must be used in co-transfection of cells to allow for inducible expression of mtPAPFLAG with tetracycline. Only pcDNA6/TR encodes for resistance to Blasticidin^S, so its presence is the only one selected for. To increase the chances of resistant cells harboring both constructs, rather

than only pcDNA6/TR, the ratio of pcDNA5-mtPAPFLAG to pcDNA6/TR used to transfect the cells is 9:1. The total amount of DNA used in the transfections was 2ug.

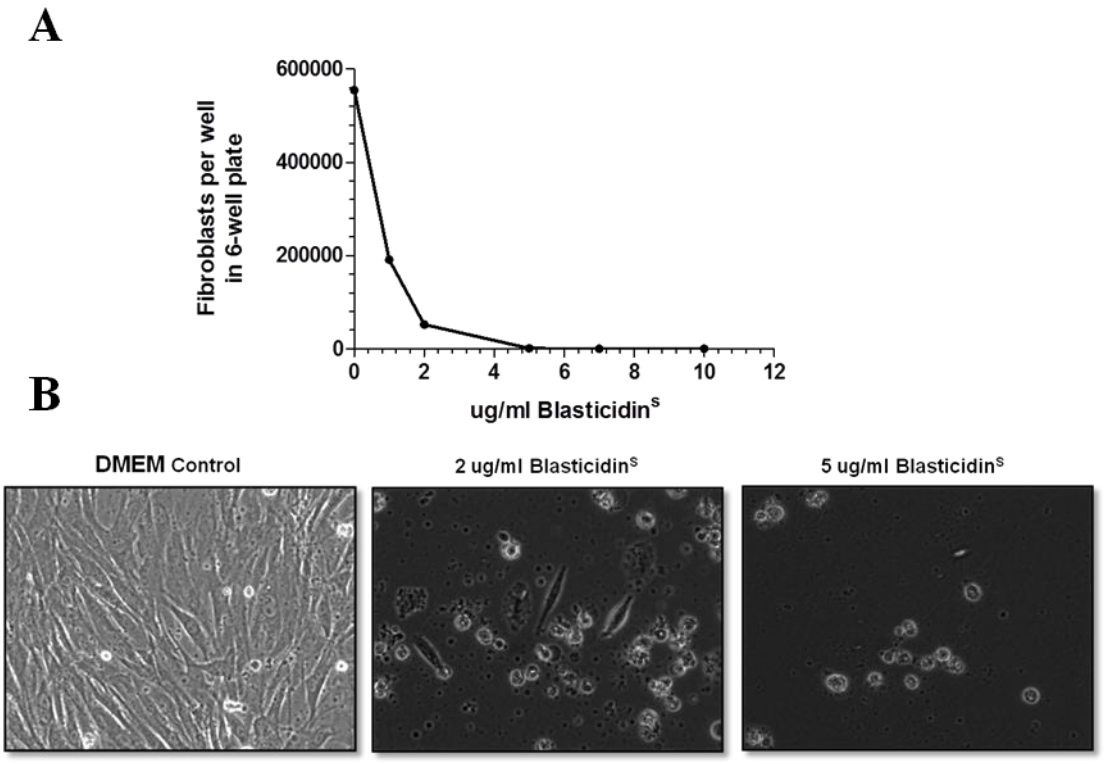

Figure 5.2. Titration of Blasticidin^S to generate a kill curve.
A. Fibroblasts heterozygous for the *PAPD1* 1432A>G mutation were seeded 50,000 cells/well in 6-well plates. After 7 days treatment with Blasticidin^S the cell growth was assessed by cell counting. **B.** Representative brightfield images of three concentrations of Blasticidin^S after 7 days. 2ug/ml was chosen as the optimal selection concentration.

Multiple attempts to transfect the immortalized fibroblasts with the pcDNA5-mtPAPFLAG and pcDNA6/TR plasmids using Superfect were unsuccessful. While small numbers of cells survived the first few days of selection, these did not divide and slowly died off. After repeated transfections not producing Blasticidin^S resistant cells, it became apparent a more effective transfection method would be necessary.

Electroporation was the second method attempted for transfection of the immortalized fibroblasts. Using the Neon^{TM} transfection system (Invitrogen), electrical pulses replaced the cationic lipid-based reagents in the reaction. The same constructs and plasmids, pcDNA5-mtPAPFLAG and pcDNA6/TR, were used. As with the earlier transfections, once selection by Blasticidin^S began most cells died off quickly, with only few remaining. These surviving cells did not proliferate, and eventually died.

5.3.2 Lentiviral transduction of *PAPD1* mutant fibroblasts

The varying methods of transfection were unsuccessful, underscoring the requirement for a more robust gene delivery method. Viral vectors are routinely employed for difficult to transfect cell lines, and so one was designed for this experiment. A custom replication-incompetent lentivirus was designed and purchased from

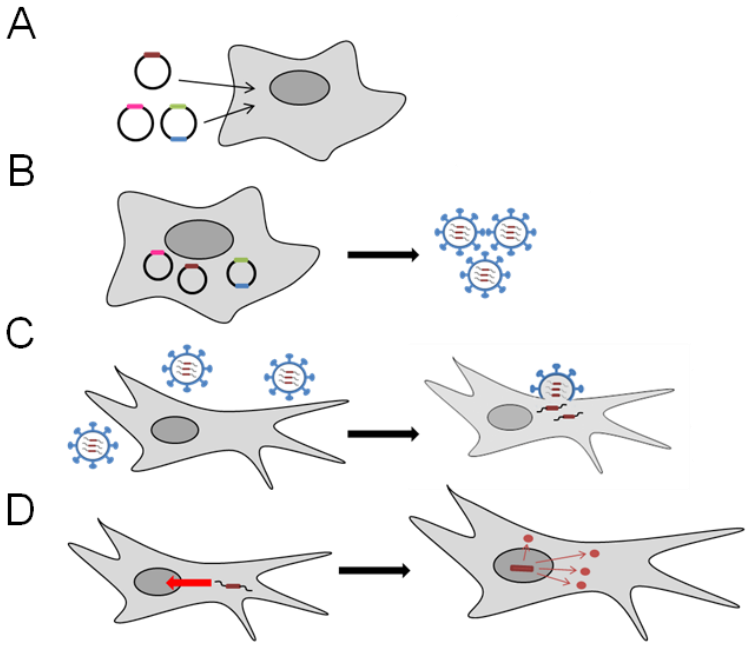

Figure 5.3. Cellular transduction using lentiviral vectors
Cartoon representation of the process of producing and employing a lentivirus for cellular transduction of a gene of interest. **A**. The plasmids encoding viral packaging factors as well as the gene of interest are transfected into HEK293 cells. **B**. The packaging cells produce replication-deficient viral particles over a span of time, these viral particles are collected and titer assessed. **C**. The target cell line is exposed to the lentiviral particles, which infect/transduce the cell with gene of interest. **D**. The gene of interest is stably integrated into the genome of the target cell line, and expresses the desired gene product.

Genecopoeia. The custom virus encoded a FLAG-tagged wild-type version of mtPAP, driven by the CMV promoter and paired with a puromycin resistance gene for selection purposes (the lentiviral vector is referred to as LVPAPD1 in this text).

An excessively high multiplicity of infection was chosen, in order to ensure high levels of transduction. Under BSL-2 conditions, each of the fibroblast cells lines, C-Het, P1, P2, and C2 were exposed to virus-containing medium in the presence of polybrene and incubated overnight. The next day the virus-containing medium was removed, and replaced with fresh media. On day 3 puromycin at 2ug/ml final concentration was introduced to the cultures to begin selection of transductants. Previously, a 0.5-10ug/ml kill curve had demonstrated that 0.5ug/ml puromycin was sufficient to kill off non-resistant fibroblast cells (data not shown). The concentration was increased to 2ug/ml on the recommendation of Dr. Chris Morris (Newcastle University), to select for high transgene expression. The non-transduced immortalized fibroblasts died off quickly, with

a relatively high rate of transduction observed from the percentage of surviving cells (estimated 50% survival). The cells resistant to puromycin quickly proliferated and once cryogenic stocks had been stored, molecular analysis of the effects of the wild-type mtPAP expression was undertaken.

5.3.3 Transgenic expression of wild-type *PAPD1* restores poly(A) length in homozygous *PAPD1* 1432A>G mutant fibroblasts

With the necessary amounts of transduced fibroblasts grown in culture, the cells were harvested and RNA and protein isolated as detailed in chapter 2. The three initial parameters to be analyzed were polyadenylation status, steady-state levels of mitochondrial mRNAs, and steady-state levels of respiratory chain proteins, particularly the mtDNA encoded subunits. The initial analysis was via immunoblot. To establish whether the transduction was successful, increased levels of mtPAP was probed and any recovery of depleted respiratory chain proteins was investigated. One of the homozygous fibroblast lines (P1) was not included in the initial analysis, as the culture was not ready at the time. The other three transduced lines were probed for the SDHA, COX1, COX2, and TOM20.

When mtPAP levels were probed on the membrane, an increased amount of the protein was present, evidence of elevated expression due to presence of the transgene. Upon probing for COX1 and COX2 levels, a recovery of the depletion for both subunits was observed. This was the first indication that the pathological phenotype had been rescued with exogenous expression of WT mtPAP.

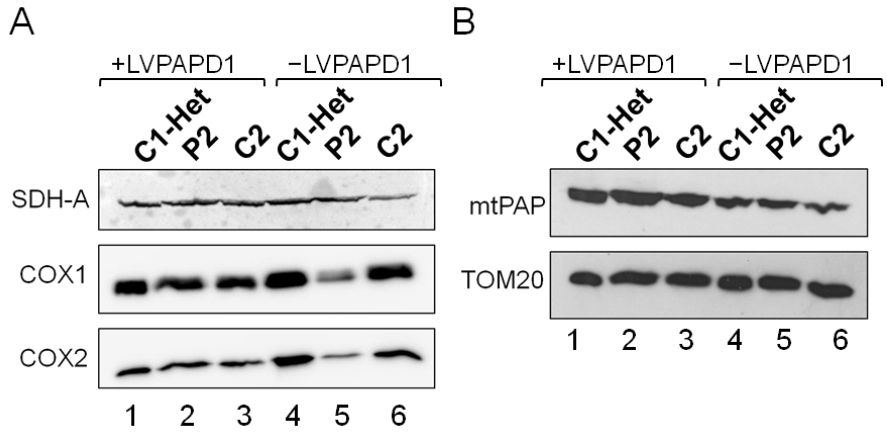

Figure 5.4. Immunoblot evaluation of transduction of wild-type mtPAP
Whole cell lysate (40ug) from pre- and post-LVPAPD1 transduced fibroblast lines was separated by SDS-PAGE and transferred to PVDF membranes. **A**. Antibodies against COX1and COX2 were used to assess steady-state levels of the proteins, with SDHA as a loading control. **B**. Antibodies against mtPAP were used to assess steady-state levels of the proteins, with TOM20 as a loading control.

Following preliminary evidence that transduction of the fibroblasts with the WT *PAPD1* transgene was successful via immunoblotting, I isolated whole cell RNA from all four transduced fibroblast lines to perform the fluorescent MPAT assay. The *RNA14*, *MTND3* and *MTCO1* transcripts were analyzed for changes in polyadenylation profiles. The effect of the mtPAP transgene expression was clear. As shown in Figure 5.5, there is a complete rescue of the short oligo(A) population of the transcripts. All four cell lines show a uniform population of polyadenylated transcript sizes, with increases in the median lengths. The range of poly(A) tail sizes has also expanded in the transduced cell lines, extending to longer lengths than observed with the non-transduced transcripts. These changes are consistent for both mutant and control fibroblasts. The rescued homozygous mutant fibroblasts still show small amounts of oligoadenylation, which matches the comparative amounts detected in the non-transduced cells. Both the *RNA14* and *MTND3* transcripts conformed to this pattern.

The *MTCO1* polyadenylation in the transduced homozygous mutant cells showed smeared results in the corresponding lanes on the gel (data not shown). Both the heterozygous and control transduced cell lines exhibited the same pattern observed for the other two analyzed transcripts, uniform poly(A) tails with increased median length and range of lengths. For reasons unclear, after multiple repeats of the MPAT assay, clear detection of *MTCO1* poly(A) status with the transduced homozygous mutant cells was unobtainable. However, recovery of the COX1 and COX2 depletions on immunoblotting strongly suggests that the *MTCO1* truncated poly(A) tail has been restored to some degree in the transduced homozygous mutant fibroblasts.

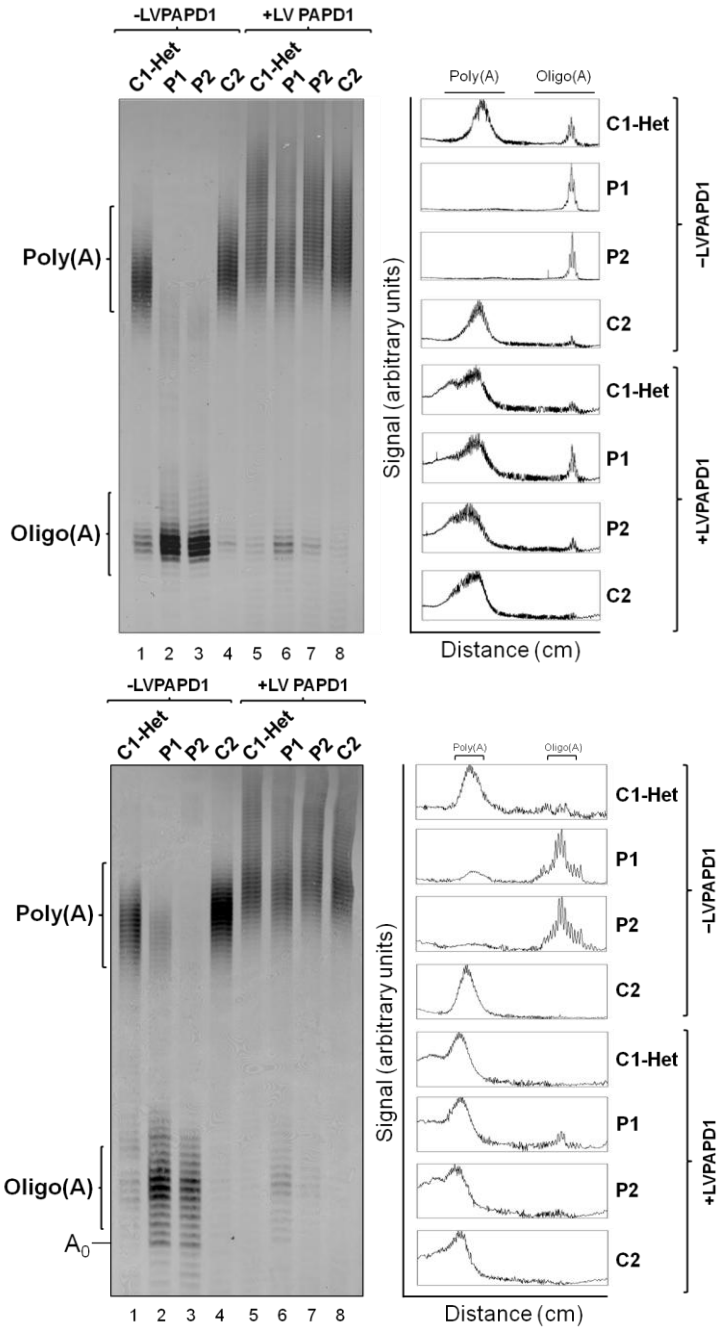

Figure 5.5. Wild-type *PAPD1* transgene expression restores poly(A) tails on mt-mRNAs

Whole cell RNA was isolated from pre- and post-transduced fibroblasts and 5ug used for performing the fluorescent MPAT assay. *RNA14*(**A**) and *MTND3* (**B**) polyadenylation statuses was analyzed. The positions of poly(A) and oligo(A) populations are labeled on the left side of the gel images. To the right of the gel images are lane plot profiles of signals.

5.3.4 Transgenic WT *PAPD1* expression restores steady-state levels of mt-mRNAs

Once the polyadenylation recovery status was confirmed in the +LVPAPD1 fibroblasts, the steady-state levels of the mt-mRNAs were analyzed by northern blot to establish whether changes had occurred as a consequence of transduction. The panel of transcripts shows a significant recovery of wild-type steady-state levels in the transduced cells, as shown in Figure 5.6. For *MTCO1*, *MTCO3* and *RNA14*, the depletions are largely reversed, bringing transcript levels back up to comparable levels with the control cell line. In the case of *MTND1*, the extra-stabilization of the transcript associated with the

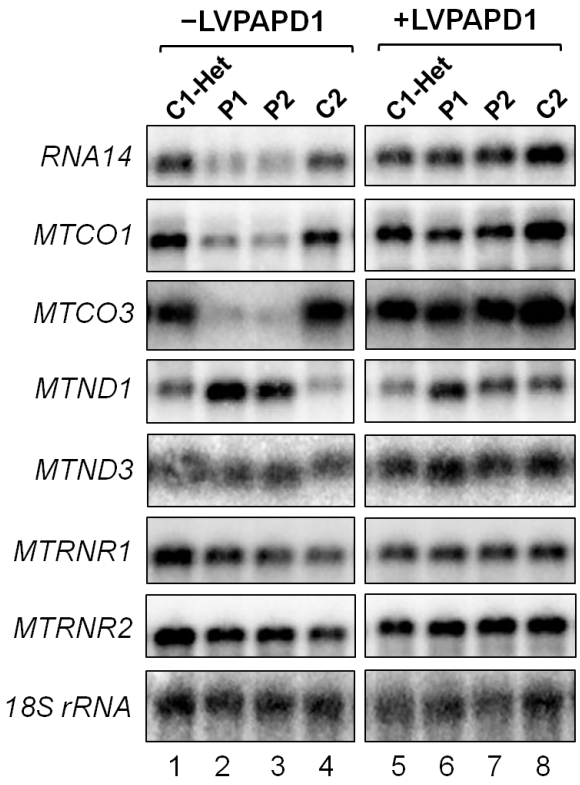

Figure 5.6. Expression of wild-type *PAPD1* transgene restores steady-state levels of mt-mRNAs

Whole cell RNA (4ug) isolated from pre- and post-transduced fibroblast lines was separated by formamide/agarose gel electrophoresis and transferred to a nylon membrane. Steady-state levels of mitochondrial mRNAs were assessed by hybridization with [^{32}P] radiolabeled probes corresponding to target mRNAs and rRNAs. 18S rRNA was used as a loading control. Blots were developed by autoradiography, and imaged by a Typhoon FLA 9500 imager. Note: Pre-transduced blot images are the same shown in Figure 4.7.

homozygous mutants is reduced to closer to wild-type levels, but still moderately elevated compared to the transduced heterozygous mutant and control lines. *MTND3*, which was unaffected in both the heterozygous and homozygous *PAPD1* mutants, shows no changes as a result of transgene expression. The mt-rRNAs that are not polyadenylated, are not included here and they do not show significant changes resulting from LVPAPD1 treatment. *18S* rRNA was probed as a loading control for the blot.

5.3.5 Transgenic *PAPD1* expression restores steady-state levels of mtDNA-encoded OXPHOS proteins

The depletion of respiratory complex subunits stands as the most likely cause of the complex assembly defects and activity disruption that underlies the neuromuscular disorder the patients are afflicted with. Thus, it was imperative to observe whether the

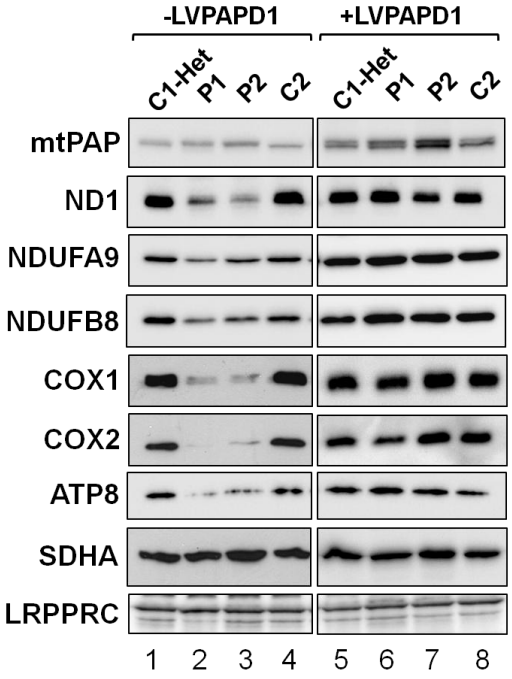

Figure 5.7. Expression of wild-type *PAPD1* transgene reverses depletion of mtDNA-encoded respiratory subunits.
Whole cell lysate (40ug) harvested from the fibroblast panel pre- and post-treatment with LVPAPD1 was separated by 12% SDS-PAGE and transferred to PVDF membranes. The membranes were then probed with antibodies against mitochondrial mtDNA and nDNA-encoded respiratory subunits. SDHA was included to serve as a loading control. Blot were developed using ECL+ (GE) and imaged using the Chemidoc MP imaging system (Bio-Rad).

recovery of full length poly(A) tails and mt-mRNA stabilities translated to restoration of steady-state levels of mtDNA-encoded polypeptides. This was assessed by immunoblotting for respiratory chain subunits. As shown in Figure 5.7, the major decreases in steady-state levels for mtDNA-encoded proteins appear to be substantially replenished and closer to wild-type levels (lanes 2-3 vs 6-7). Four mtDNA-encoded respiratory subunits were probed on the immunoblots: COX1, COX2, ND1, and ATP8. Two nuclear-encoded complex I subunits, NDUFB8 and NDUFA9, were probed as well. As mentioned in Chapter 4, while not mtDNA-encoded, the NDUFB8 signal on immunoblots can act as an indicator of complex I assembly. In the homozygous mutant fibroblasts, these subunits show decreased signal. In the transduced lines, the signals are

significantly recovered. This likely indicates an amelioration of the complex I assembly defect due to the reversal of complex I subunit depletion. It would also be predicted that the complex IV assembly defects would be rescued from the reestablished levels of subunits. LRPPRC was probed to assess any changes pre- and post-transduction, as it is a putative regulator of mitochondrial polyadenylation. No changes LRPPRC steady-state levels were observed pre- or post-LVPAPD1 treatment.

When mtPAP was probed as part of the immunoblot panel, a doublet was observed in the transduced cells. The second mtPAP species served as confirmation of transgene expression. As the FLAG-tag changes the charge of the enzyme enough to alter the migration through the SDS polyacrylamide gel during separation, this could cause the doublet effect.

5.4 Discussion

5.4.1 Stable integration of wild-type *PAPD1* transgene via lentiviral vector

Primary fibroblasts are classically considered a difficult to transfect cell line, and indeed the initial attempts to transfect the cells were unsuccessful. Using two plasmids in the same transfection reaction, only one of which could be selected for, likely made the situation more complicated and difficult than it needed to be. The use of cationic lipid reagents and electroporation was unsuccessful, for reasons that are unclear. This is a common problem with fibroblast transfection, at least in the creation of stable transfectants. Transient transfection also presents a problem, potentially, via the heterogeneous levels of transgene expression in the cell culture population. The effects resulting from restored wild-type expression may not be as clear in such a system. Thus, a priority was put on generating stable transfectants.

Viral vectors presented a much more efficient method of delivering the *PAPD1* transgene. The drawback with viral vectors is largely the necessity of dedicated handling facilities. As my host lab did not have permission for viral production, custom designed and preprepared virus particles were purchased commercially. Handling of the virus was facilitated by access to BSL-2 certified culture hoods in Dr. Chris Morris's lab in a neighboring institute.

The custom lentivirus carrying a wild-type *PAPD1* gene, termed here "LVPAPD1", was employed to successfully transduce a significant percentage of the fibroblast populations exposed to virus-containing medium, as initially assessed by resistance to puromycin. Experimental evidence indicated that the transduction was successful, and rescued the pathological phenotype in the homozygous mutant fibroblasts.

5.4.2 Transgenic expression of wild-type *PAPD1* restores full length poly(A) tails on mt-mRNAs

The primary defect of the N478D mtPAP mutation is a reduced ability to generate full-length poly(A) tails on mt-mRNAs. The aim of this complementation experiment was a rescue of this specific deficiency. All the downstream molecular pathologies that were observed logically could be a consequence of the shortened mitochondrial poly(A) tails.

The analysis of polyadenylation status of several mitochondrial mRNAs using the MPAT demonstrated that full length poly(A) tails were recovered in the transduced homozygous mutant fibroblasts. The majority of poly(A) tail lengths were of the average control length or modestly longer. Additionally, both control and patient transduced lines showed an increase in the range of lengths for polyadenylation. This may be due to the existence of an equilibrium of activities between the poly(A) polymerase and deadenylation factors. Rather than poly(A) tail length solely reflecting the poly(A) polymerase's processivity, with deadenylation acting as a degradation event independently at a later point, precise regulation of poly(A) tail length could be a balancing act of these activities. These factors could be the PNPase/hSuv3 "degradosome" complex, PDE12, or yet undiscovered exoribonucleases. Evidence supporting this include mild poly(A) length increases when depleting PNPase via siRNA (Slomovic and Schuster, 2007), or overexpression of PDE12 causing shortening of poly(A) tails in mitochondria (Rorbach *et al.*, 2011). The increase in average poly(A) length and range of poly(A) lengths in the transduced fibroblasts may be a result of increased steady-state levels of mtPAP, shifting the ratio of adenylation to deadenylation events towards polyadenylation.

Both *RNA14* and *MTND3* exhibited similar oligo(A) patterns and recovery of full length poly(A) tails in transduced cells. *MTCO1* was analyzed via MPAT, however the transduced homozygous mutant cells demonstrated aberrant signal on the polyacrylamide/urea gel. Rather than discrete poly(A) tails lengths produced, there was

smearing of signal. This result was obtained on multiple independent repeats. Analysis of the gene-specific PCR products from the homozygous mutant cell lines by agarose gel electrophoresis, prior to the fluorescent-labeling PCR, showed no discernible size difference between heterozygous mutant and control cell line's PCR products (Appendix C). In the non-transduced homozygous mutant cell lines, the size differences of the PCR products due to poly(A) truncation are clearly observable. This indicates the full length poly(A) tail has been recovered for *MTCO1* transcripts in the homozygous mutant cell lines. The reason *MTCO1* is the only one to show these results is unclear, but may be a technical artifact of the MPAT assay. The recovery of COX1 and protein supports re-establishment of the wild-type poly(A) tail length on the *MTCO1* mt-mRNA.

5.4.3 Transgenic expression of wild-type *PAPD1* reverses altered stability of mt-mRNAs and depletions of OXPHOS proteins

Analysis of the heterozygous mutant fibroblasts had provided some insight into the nature of the mutation. As the heterozygous cells demonstrated an essentially wild-type phenotype, it could be inferred that the N478D substitution was not a dominant loss of function mutation. At a minimum, expression of wild-type mtPAP equal to that of the heterozygous mutant would be predicted to bring the homozygous mutant phenotype closer to normal functioning.

Once the rescue of the oligo(A) tails was confirmed via the MPAT assay, it was necessary to investigate whether there was also correction of the downstream defects. This was accomplished by northern blotting and immunoblotting. Steady-state levels of mt-mRNAs and respiratory chain subunits were compared pre- and post-LVPAPD1 treatment. As predicted, both mt-mRNA and polypeptides demonstrated considerable recovery towards control levels of gene expression products. The reasons for such variable changes in mt-mRNA stabilities in homozygous mutant cells is still unclear, but the effect is reversed upon expression of transgenic wild-type mtPAP. The levels of *MTND1* are still mildly elevated compared to control and heterozygote levels, however this may be due to the heterogeneous mtPAP population present in the transduced cells. The N478D mtPAP may still be generating oligo(A) tails, that are not further adenylated by the transgenic wild-type mtPAP. It may be these persisting transcripts with oligo(A) tails are responsible for the increased transcript levels observed. This gain of stability may

be more difficult to reverse than recovery of decreased steady-state levels. Despite the persistence of extra-stable *MTND1* transcripts, the depletion of protein levels observed at steady-state is rescued. The immunoblots of the OXPHOS subunits all show decreased levels at steady-state in the homozygous mutant fibroblasts, and in the transduced cells this effect is abolished. The causative pathogenicity of the N478D mutation was convincingly confirmed by the analysis of poly(A) status, and mt-mRNA/mtDNA-encoded protein steady-state levels. By rescuing the fundamental defect of polyadenylation, the broader mitochondrial dysfunction was ameliorated.

There are many characteristics of the N478D mtPAP still unknown. These include whether N478D mtPAP can homodimerize, or heterodimerize with wild-type monomers. In the heterozygous, and rescued transduced fibroblasts, either heterodimers possess enough poly(A) activity to generate enough full length poly(A) tails, or the amount of wild-type homodimers is sufficient for functional polyadenylation. In addition, it is unknown if the N478D mtPAP generates the oligo(A) tails on mt-mRNA transcripts, or if another polymerase is responsible. In order to answer some of these questions, a more thorough investigation of the wild-type and N478D mtPAP enzymes was carried out using recombinant versions of the proteins, as detailed in the next chapter.

Chapter 6

In vitro analysis of recombinant wild-type and N478D mtPAP polyadenylation activity

6.1 Introduction

The data presented thus far have shown that the poly(A) tail generated by mtPAP by has an important role in mitochondrial gene expression dynamics. However, these biochemical characterizations of the *PAPD1* 1432A>G mutant and control fibroblasts have not offered insights as to the exact mechanism by which the N478D mutation disrupts polyadenylation activity. Furthermore, there are many aspects of the wild-type polymerase that are still ill-defined. As stated earlier, and shown here in Figure 6.1, the N478D mutation is located in a region of the enzyme that was not resolved in the published crystal structure reported in Bai *et al.* 2011. As a result, there is not a defined domain assigned to the region. The nature of this region's function is obscured by this lack of structural data. This makes it hard to predict what the loss of functionality caused by the mutation may be. The motif falls within a section of the fingers domain. As the N-P-F-E polypeptide motif in particular is highly conserved across species, and is within a conserved region of approximately 40 amino acids, this may be evidence of its importance to enzyme integrity. There is not an obvious involvement in catalytic activity, RNA binding, dimerization, or protein-protein interactions. Particularly catalytic activity, as the mutation is far removed from the active site of the enzyme.

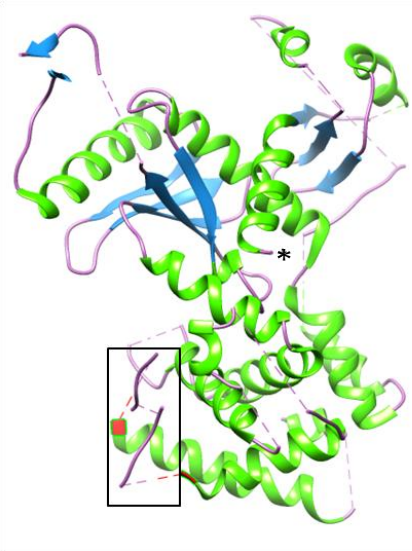

Figure 6.1. The location of the mtPAP N478D mutation
Structural model of the recombinant mtPAP monomer, indicating the location of the N478D mutation. Color is by secondary structure: alpha-helix (green), beta-sheets (blue), unstructured regions (magenta). The section of the peptide harboring the N478D mutation is highlighted by red residues at the beginning and end of the region (boxed). The N-terminus end of the recombinant protein is indicated by an asterisk(*). The structure is available from the Protein Data Bank, PDB: 3QP1, reported by Bai *et al*., 2011. This image was generated using the Chimera 1.8.0 software, available from UCSF.

This lack of insight from the fibroblast studies necessitated investigating the wild-type and N478D mtPAP enzymes in an isolated fashion. This was best accomplished by

generating recombinant proteins and constructing an *in vitro* experimental system. An in-depth report on the structural and activity characteristics of mtPAP was provided in Bai *et al*. 2011. This was the first report of the crystal structure of mtPAP, although the first report of mtPAP *in vitro* activity came from Nagaike *et al*. 2004. The initial strategy for generating recombinant enzyme was generating GST-tagged proteins, but this approach lacked high protein yields. Subsequently, a formal collaboration between my host lab and Professor Liang Tong's lab at Columbia University was established. This provided me with their His-tagged recombinant mtPAP construct, from which I generated constructs to express the mutant mtPAP protein. Professor Tong's group then assisted in generating and purifying the necessary recombinant proteins.

There are conflicting reports and conclusions regarding *in vitro* studies of mtPAP. Several groups have reported that the enzyme is independently capable of generating poly(A) tails (Nagaike, 2005; Bai *et al.*, 2011), while another has reported the necessity of LRPPRC being present for optimal activity (Chujo *et al.*, 2012). Resolving this conflict was one of the priority aims of this *in vitro* work. There are multiple other questions these investigations aim to address:

Which factors, if any, does mtPAP need to polyadenylate RNA?

What is the exact contribution of LRPPRC on poly(A) activity?

Does the N478D mutation compromise catalytic activity itself, or disrupt critical interactions? What is the effect of LRPPRC on mutant poly(A) activity?

Is mtPAP active only on specific RNA substrates, or is its specificity more broad?

Is SLIRP necessary for poly(A) activity, with or without LRPPRC?

Does the mutant mtPAP generate the oligo(A) tails observed *in vivo*?

Do oligoadenylated RNAs present as a more optimal substrate for mtPAP?

These are the questions that a well designed *in vitro* system would be equipped to answer. Towards that end, in addition to the collaboration with Liang Tong's lab, we also established a collaboration with Professor Nils-Goran Larsson's lab (Dr. Henrik Spahr), to acquire recombinant LRPPRC, SLIRP, and LRPPRC/SLIRP complexed together. This allowed for an array of experiments utilizing mtPAP, LRPPRC, SLIRP, and varying RNA substrates to be examined individually and in concert for their impact on polyadenylation activity.

6.2 Materials and methods

6.2.1 Generation of the mtPAPΔN-GST fusion construct

A PCR product coding for the first 30 amino acids of the N-terminus of mtPAP removed was generated using the primers mtPAP6PF and mtPAPR2 (2.2.4.4). The pcDNA5-mtPAPFLAG construct was used as a template, although mtPAPΔN was designed to regenerate the normal C-terminus with its stop codon, rather than a FLAG-tag. Deletion of the first 30 amino acids removed the predicted mitochondrial targeting sequence, which would be cleaved off upon import into mitochondria. This generated an amplicon that would encode an N-terminal truncated mtPAP with BamH1 and Not1 restriction sites at the 5' and 3' ends, respectively. The PCR reaction was then separated through a 1% low melting temperature agarose gel, and the DNA band corresponding to the correct size was excised and purified. The purified mtPAP6P PCR product was then digested with BamH1 and Not1, followed by phenol/chloroform extraction and EtOH precipitation. The expression vector pGEX-6P-1 was digested with BamH1 and Not1, dephosphorylated, and the linear products phenol/chloroform extracted and EtOH precipitated. The PCR fragment was then cloned into the BamH1 and Not1 sites of pGEX-6P-1 expression vector. The pGEX-mtPAPΔN construct was used to transform Bioline α-select bronze bacterial cells (Novagen). Transformed colonies were selected with ampicillin (100ug/ml) on LB-Agar plates. Colonies confirmed by PCR analysis harboring the pGEX-mtPAPΔN construct were expanded into 5ml cultures and incubated at 37°C overnight shaking. The construct was then purified from cultures with GeneJet plasmid prep kit (Fermentas), according to manufacturers protocol, and sequenced (as detailed earlier) to confirm accuracy of the construct. See 2.2.4.4 for primers, PCR profiles, and reaction mixes. Bacterial propagation of other constructs was carried out in the same manner described here, with varying antibiotics for selection based on the vectors.

6.2.2 Generation of 1432A>G mutant pET28a-mtPAP by site-directed mutagenesis

The pET28a-mtPAP construct was a generous gift from Liang Tong's lab. For generating the 1432A>G substitution within the construct, the Quikchange® II Site-Directed Mutagenesis Kit (Stratagene) was used, according to manufacturer's instructions. The

pET28a-mtPAP construct was used as the template for the mutagenesis reaction. The primers Mut-mtPAPF and Mut-mtPAPR (2.2.4.4) were used for generating the point mutation. The mutant strand synthesis reaction was assembled as below:

Component	Final Concentration in PCR Reaction
10X Reaction Buffer	1X
dNTP Mix	1ul
mtPAPmutF (10uM)	125ng
mtPAPmutR (10uM)	125ng
pET28a-mtPAP DNA	50ng Total
PfuTurbo Polymerase (2.5 U/ul)	2.5U
ddH_2O	Made up to 50ul

The PCR profile for the mutagenesis reaction:

Step	Reaction Profile	Reaction Step
1	95°C - 30 seconds	Initial Denaturation
2	95°C - 30 seconds	Denaturing
3	55°C - 1 minute	Annealing
4	68°C - 6 minutes	Extension
5	*Back to Step 2, 12 cycles*	# of cycles
7	4°C - Indefinitely	Hold

Once thermal cycling was complete, 1ul (10U) of Drp I was added directly, the reaction mixed, then incubated at 37°C for 1 hour. The completed reaction was then used for transforming XL1-Blue supercompetent bacterial cells. The cells were thawed on ice, as a 50ul aliquot, and then had 1ul of the Drp I-treated mutagenesis reaction added. This was incubated on ice for 30 minutes, followed by a heat pulse at 42°C for 45 seconds, then moved back to ice. 0.5ml of SOC media was added to the cell mixture, moved to 37°C, shaking, for 1 hour. From there, the cells were spread on kanamycin and chloramphenicol agar plates and incubated overnight at 37°C. Resistant colonies were screened for correct construct transformation.

6.2.3 Recombinant expression of mtPAPΔN-GST

Chemically competent *Escherichia coli* strains Rosetta (DE3) (Novagen) were transformed according to manufacturer's protocol with pGEX-mtPAPΔN construct. Tuner strain (Novagen) was also transformed by adding 10ng construct DNA to 50ul aliquot of bacteria, incubating on ice 30min, heat shocking at 42°C for 2 min, then incubating on ice 2 min. Selection was performed by 100ug/ml ampicillin (Rosetta and Tuner) and 34ug/ml chloramphenicol (Rosetta) on antibiotic supplemented LB-agar plates. Resistant colonies were expanded to 5ml cultures supplemented with 100ug/ml ampicillin (Rosetta and Tuner) and 34ug/ml chloramphenicol (Rosetta). Once cultures reached an OD_{600} of 0.5 they were induced with 1mM isopropyl β-D-thiogalactopyranoside (IPTG) either overnight at 16°C or for 3 hrs at 37°C. Various induction conditions included an initial cold shock of 5min on ice prior to the addition of IPTG for Rosetta strain, as well as titrating induction with 0.05mM, 0.1mM, and 0.2mM IPTG for the Tuner strain. Samples were taken from the uninduced and induced cultures, and lysed. The remaining culture volume was split into soluble and insoluble fractions via pelleting bacterial cells at 5000*g* for 5min at 4°C, then re-suspending in CelLytic B (Sigma). Mixture was then centrifuged at 15,000*g* for 8min at RT. The supernatant was collected, and this constituted the "soluble" fraction, and the remaining pellet was re-suspended in PBS, which constituted the "insoluble" fraction. Samples of bacterial cell lysate were prepared and separated via 12% SDS-PAGE as detailed for western blotting, and then visualized by Coomassie blue staining. Confirmation of recombinant mtPAPΔN-GST fusion protein expression was shown via immunoblotting the bacterial lysate samples using anti-mtPAP antibodies, as detailed in western blot methods. For removal of the GST-tag, the soluble fraction of bacterial lysate was transferred to a gravity flow chromatography column (Bio-Rad) containing 0.6ml glutathione-Sepharose beads (GE Healthcare), which were pre-washed with dH_2O and then PBS. The lysate and beads were incubated overnight in the column at 4°C on a rocker. The next day the beads were washed with 5 column volumes of PBS, with 1mM PMSF and protease inhibitors (Roche). Then washed with 5 column volumes of PBS alone. Elution of the tag-free protein was accomplished with adding 48U PreScission Protease (GE Healthcare) to 0.75ml PBS, 1mM DTT, 1mM EDTA, and incubated overnight at 4°C on a rocker. The cleaved protein was collected by gravity flow the next day in a chilled 1.5ml tube.

6.2.4 Recombinant expression and purification of His-mtPAP

Chemically competent *Escherichia coli* Rosetta DE3 strain (Novagen) were transformed according to manufacturer's protocol with pET28a-PAPD1 construct. Selection was performed on 50ug/ml kanamycin and 37ug/ml chloramphenicol supplemented LB-agar plates. Resistant colonies were expanded to 1L cultures supplemented with 50ug/ml kanamycin and 34ug/ml chloramphenicol. Once cultures reached an OD_{600} of 0.5 recombinant protein production was induced with 1mM isopropyl β-D-thiogalactopyranoside (IPTG) overnight at 20°C. After the overnight incubation the cultures were pelleted by centrifugation in a Sorvall RC5 centrifuge (GSA rotor), set at 5000rpm, at 4°C, for 15 minutes. These pellets were either frozen at -80°C for use within two weeks, or directly processed. The pellet was resuspended in 10ml 50mM Tris pH 8.5, 0.3M NaCl, 1mM PMSF and 1 tab protease inhibitors (Roche) and kept on ice. The bacterial cells in suspension were then disrupted on ice using a Sonopuls ultrasonic homogenizer (Bandelin), set at 4 minutes for 5 cycles, at 50% power. The insoluble fraction of the homogenized suspension was pelleted by centrifugation in the Sorvall RC5 centrifuge (SS-34 rotor), set at 15,900rpm, at 4°C, for 30 minutes. The soluble fraction was collected, then syringe filtered using a 0.45um filter (Anachem). During centrifugation, a gravity flow chromatography column with 0.5ml of HIS-Select® Ni-NTA affinity gel (Sigma) was prepared by washing the resin with 2 column volumes of dH_2O, then 3 column volumes of 50mM Tris pH 8.5, 0.3M NaCl. The filtered soluble fractions were added to the column, mixed with the nickel resin, and incubated at 4°C for 1 hour, rotating. The column was then emptied by gravity flow, and washed with 5 column volumes of 50mM Tris pH 8.5, 0.3M NaCl, 20mM imidazole. Elution of his-tagged mtPAP was performed with 2ml 50mM Tris pH 8.5, 0.3M NaCl, 250mM imidazole. The elution was injected onto a HiLoad 16/60 Superdex 200 prep grade size exclusion chromatography column (GE Healthcare), connected to an AKTA platform (GE Healthcare). The column buffer was 50mM Tris pH 8.5, 0.3M NaCl, flow rate was 0.1ml/minute, with a column pressure of 0.5 MPa. Fractions were monitored by UV absorbance and collected every 2ml. Eluted fractions corresponding to UV absorbance peaks were analyzed by 12% SDS-PAGE and staining with Coomassie brilliant blue. The fractions harboring correct sized protein were pooled, and concentrated using 30,000 MWCO Amicon Ultra centrifugal filters (Millipore). Glycerol was added to a final concentration of 5%, and the protein aliquoted, flash frozen, and stored at -80°C.

For recombinant proteins sent from collaborators (wild-type and N478D His-mtPAP, LRPPRC, SLIRP, LRPPRC/SLIRP complex), the primary stocks were stored at -80°C upon arrival. When aliquoting, the frozen stocks were thawed by hand, and quickly aliquoted in 0.5ml tubes pre-chilled on ice, then immediately flash frozen. The flash frozen aliquots were stored at -80°C for future use in polyadenylation assays.

6.2.5 *In vitro* transcription and radiolabeling of RNA

Templates for *in vitro* transcription were prepared by PCR amplification. Amplicons corresponding to the 3' 277nt of *MTND3* and 3' 248nt of *MTATP6*, with and without oligo(A) tails were generated using the primers ND3PAP-F, ND3PAP-R, A6PAP-F, A6PAP-R, ATP6RevA8, and ND3RevA8 (*c.f.* 2.2.4.4). PCR amplicons were purified using StrataPrep® PCR purification columns (Agilent Technologies). The template DNA was then used in transcription reactions using the Ampliscribe Sp6 transcription kit (Epicentre Biosciences). The reaction was assembled as follows:

Component	Volume (ul)
Template DNA	250ng
10x Sp6 Reaction Buffer	2
100mM ATP	1.5
100mM GTP	1.5
100mM CTP	1.5
100mM UTP	1.5
100mM DTT	2
SUPERase-In	0.5
Ampliscribe Sp6 Enzyme Solution	2
DEPC-treated H_2O	Up to 20

For radiolabeling RNA transcripts, 5ul of [α-^{32}P]-UTP at 3000 Ci/mmol (Perkins-Elmer) was added to the reaction, with corresponding decreases in H_2O volume. The transcription reaction was incubated for 2 hours at 37°C, then had 1ul DNase I (1U) added, and continued incubating for 15min. RNA was purified by phenol/chloroform extraction and ethanol precipitation, then resuspended in DEPC-treated H_2O. For non-radiolabeled RNA, concentration was determined by UV spectrophotometry. For radiolabled transcripts, concentration was measure by scintillation.

For higher resolution analysis of *in vitro* polyadenylation, custom ordered RNA 40nt and 48nt transcripts from Dharmacon were used as polyadenylation substrates. These transcripts corresponded to the 3' 40 nucleotides of *MTATP6*, with or without an 8nt oligo(A) tail.

6.2.6 Polyadenylation Assay

A 10x poly(A) reaction buffer was made up, RNase-free, consisting of 500mM Tris pH 8, 400mM KCl, 5mM $MgCl_2$, 1mM $MnCl_2$. A typical poly(A) activity reaction was assembled as follows:

Component	**Volume**
10x poly(A) buffer	1ul
100mM DTT	0.15ul (1.5x concentration)
100mM ATP	1.5ul (1.5x concentration
SUPERase-In™ (20U/ul)	0.5ul
0.5M $MgCl_2$	0.3ul (1.5x concentration)
RNA	50ng
DEPC-treated H_2O	Up to 10ul
LRPPRC/SLIRP, LRPPRC, or SLIRP (diluted in 1x poly(A) reaction buffer)	0.5uM final
His-mtPAP enzyme (diluted in 1x poly(A) reaction buffer)	0.55uM final

Reactions were assembled as master mixes without mtPAP, starting with the DEPC H_2O, then adding 10x poly(A) buffer, DTT, ATP, SUPERase-In™, and $MgCl_2$. Recombinant wild-type or N478D mtPAP, LRPPRC, SLIRP, or LRPPRC/SLIRP complex were the final reaction components, added after the master mixes were assembled and aliquoted. The proteins were removed from -80°C, and thawed by hand, then diluted in 1x poly(A) buffer. They were then immediately added to the *in vitro* polyadenylation reactions, which were placed at 37°C for variable time lengths. Any remaining volume of the non-diluted protein stock was flash frozen, and returned to -80°C. Once the polyadenylation reaction time was complete, the reactions were quenched by adding 25ul 90% formamide/1x TBE/xylene cyanol buffer. The terminated reactions were either stored at -20°C, or directly analyzed. To observe the polyadenylation results, the terminated

reactions were either loaded on low-resolution (6%) or high-resolution (15%) polyacrylamide/8M urea gels. Low-resolution gels were used for analyzing the 248/277nt RNA transcripts, and high-resolution gels were used for analyzing the 40nt RNA transcripts. The RNA was electrophoresed at 100V in 1x TBE buffer, for 2-4 hours at room temperature. Once electrophoresis was complete, the gels were stained with 1x SYBR Gold (Invitrogen) in 1x TBE buffer for 15-40min. The gels were scanned using a Typhoon FLA 9500 imager (GE Healthcare), with settings for "SYBR Gold": Long Pass Blue filter, 473nm laser, 450V PMT. For analysis of poly(A) extensions, approximate lengths were calculated using the log of the molecular weight of the ssRNA standards, along with the standard's migration distance through the gel. These values were graphed using GraphPad Prism and a best fit line was determined for the ssRNA standards. The slope and y-intercept of the line was used to determine the sizes of the poly(A) extensions, then nucleotide lengths were calculated from the size determinations.

6.2.7 Electrophoretic Mobility Shift Assay (EMSA)

The EMSA binding reactions were performed in a similar manner to the polyadenylation assays, but lacking ATP and the addition of 10% glycerol. The binding reactions were assembled as follows, typically as a master mix:

Component	**Volume**
10x poly(A) buffer	1ul
100mM DTT	0.15ul (1.5x concentration)
SUPERase-In (20U/ul)	0.5ul
0.5M $MgCl_2$	0.3ul (1.5x concentration)
RNA	50ng
Glycerol	0.75ul (5% final)
DEPC-treated H_2O	Up to 10ul
Protein (diluted in 1x poly(A) reaction buffer)	Varying amounts in 5ul, for a total reaction volume of 15ul

Once proteins were added to the reaction, samples were incubated at 37°C for 20min. The whole samples were then loaded onto 6% polyacrylamide/0.5x TBE gels. Running buffer for the gel electrophoresis was pre-chilled 0.5x TBE buffer. The bound and unbound RNA/protein complexes were separated by electrophoresis at 100V, at 4°C, for 60-80 minutes. Once separation was complete, the gels were stained with 1x SYBR gold in 0.5x

TBE buffer for 20 minutes. Visualization of the RNA/protein complexes was performed with a Typhoon FLA 9500, using the "SYBR gold" setting: long pass blue filter, 473nm laser, 450V PMT.

6.2.8 Far-UV Circular Dichroism Spectroscopy

This analysis was performed in Professor Alastair Hawkins' lab. Briefly, the wild-type His-tagged mtPAP protein was diluted to 0.22mg/ml (3.75uM), and the recombinant His-tagged N478D protein diluted to 0.21mg/ml (3.58uM) in a buffer consisting of 50mM Tris HCl pH 8.5, 0.3M NaCl, and 5% (v/v) glycerol. The instrument used was a Jasco J-810, with a 0.01cm pathlength. The wavelength scanned was 260nm to 195nm. 5 cumulative scans were carried out each sample and this was repeated with buffer. The buffer baseline was subtracted from the experimental trace, the data adjusted for concentration, and presented as molecular CD units.

6.2.9 Analysis of mtPAP dimerization by size-exclusion chromatography

Calibration standards (GE Healthcare) prepared according to manufacturer's instructions and injected onto a Superdex 200 HR 10/30 analytical grade size exclusion chromatography column (GE Healthcare), connected to an AKTA platform (GE Healthcare). The column was equilibrated overnight with buffer consisting of 50mM Tris pH 8.5, 0.3M NaCl, flow rate was 0.1ml/minute, with a column pressure of 0.5 MPa. The elution of proteins was monitored by UV absorbance. After elution of the calibration standards, wild-type and N478D recombinant mtPAP proteins were diluted to 0.45mg/ml in 200ul of the equilibration buffer, and 100ul of each injected onto the column separately. The elution fractions of the mtPAP proteins was compared to the elution fractions of the calibration standards to ascertain dimerization status.

6.3 Results

6.3.1 Generation of wild-type and 1432A>G pGEX-mtPAPΔN construct

For developing a recombinant mtPAP protein with a fusion tag, initially the pGEX-6P-1 vector was used for expression, as the system is well established in our lab. The pGEX-6P-1 plasmid is a chemically-inducible, tac promoter driven vector for

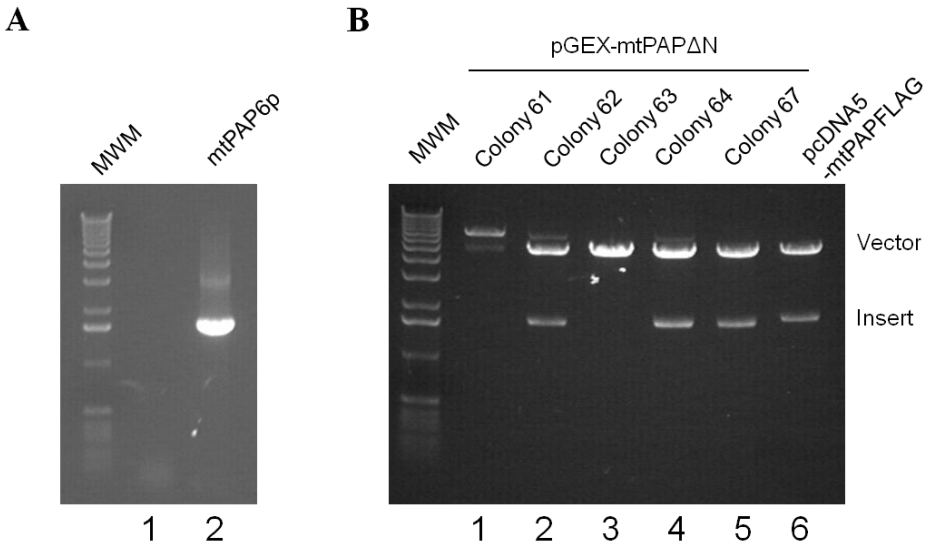

Figure 6.2. Amplification, digestion, and confirmation of the pGEX-mtPAPΔN construct
A. PCR control (lane 1) and mtPAPΔN PCR reaction (lane 2). **B**. Confirmation of correct construct by excision of the insert with BamH1 and Not1 digests. Plasmids were harvested from multiple colonies, with several showing correct size inserts (lanes 2, 4-5). The plasmid from lane 4 was used for further recombinant work.

expression of GST-tagged recombinant proteins in *E. coli*. The protein product produced from this vector is fused at the N-terminus to a glutathione S-transferase (GST) tag. This promotes solubility, and also serves as a means of purification. Initially, the solubility of recombinant mtPAP enzyme was unknown, thus a pro-solubility tag seemed optimal. The GST tag binds to glutathione-Sepharose beads, and can be enzymatically cleaved by a commercial protease (PreScission Protease), allowing for elution of GST-free recombinant protein. The mtPAP amplicon generated for recombinant expression had the sequence encoding the first 30 amino acids removed. This region is predicted to be the mitochondrial targeting sequence. These sequences are generally hydrophobic, and therefore can have an impact on solubility. The targeting sequence is also cleaved off when the protein is transported into mitochondria, and the recombinant mtPAP

(designated mtPAPΔN) was designed to reflect this mature form. The primers mtPAP6PF and mtPAPR2 (*c.f.* 2.2.4.4) were used in the PCR reaction, and the DNA template was the pcDNA5-mtPAPFLAG construct. The region of the gene being cloned for recombinant expression was internal to the coding region in the pcDNA5-mtPAPFLAG construct. The mtPAPR2 primer was designed to replace the FLAG tag with the five C-terminal peptides and stop codon of the protein coding sequence. This PCR reaction was successful, generating a product of 1.6 kb (Figure 6.2A). The amplicon was termed mtPAP6p. The pGEX-6P-1 vector was BamH1 and Not1 digested, then dephosphorylated to prepare for ligation with the mtPAPΔN amplicon. The ligation reaction products were successfully transformed into Bioline α-select bacteria, generating many ampicillin-resistant colonies. Several were picked for plasmid harvesting, and the resultant plasmids subjected to BamH1/Not1 double digestion to confirm the mtPAPΔN insert. As shown in Figure 6.1B, multiple colonies harbored the correct pGEX-mtPAPΔN construct. Specifically, colony 64, as shown in Figure 6.2B, was used for isolating plasmid to transform Rosetta (DE3) cells, after it was sequenced to confirm lack of mutations introduced by PCR and accuracy of the construct.

For generating the 1432A>G point mutation within the pGEX-mtPAPΔN construct, the Quikchange® II Site-Directed Mutagenesis kit was employed. The

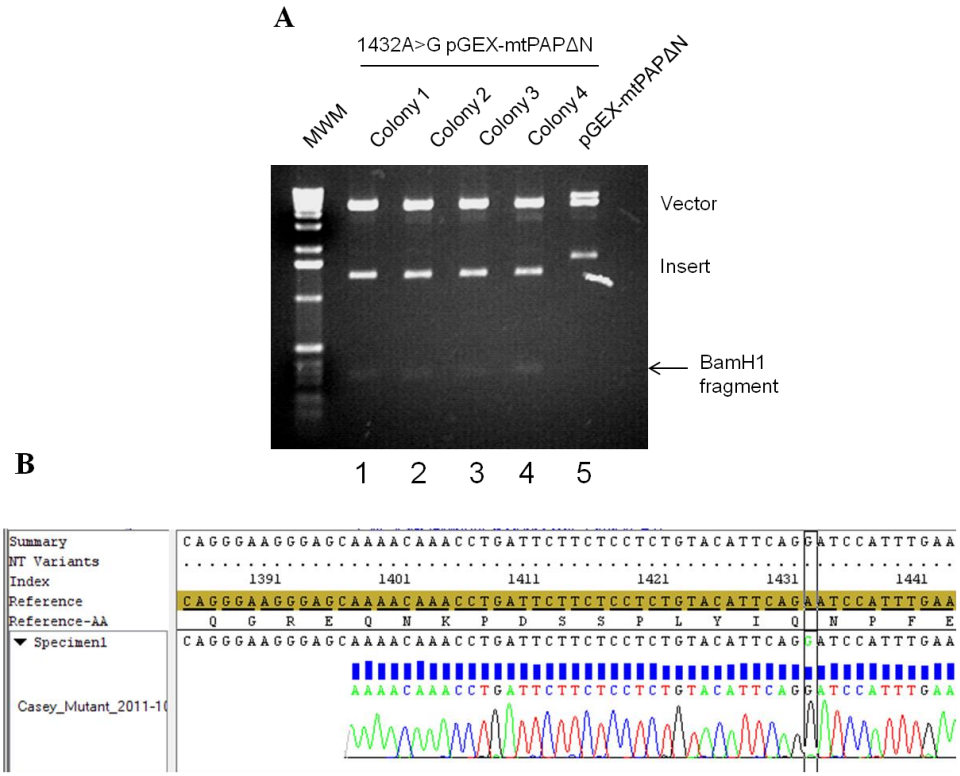

Figure 6.3. Confirmation of the 1432A>G mutation in the pGEX-mtPAPΔN construct

A. The presence of the 1432A>G mutation in pGEX-mtPAPΔN was confirmed using restriction digest analysis, as the mutation creates a BamH1 site. The size change and resulting smaller fragment excision are visible via separation by 1% agarose gel electrophoresis. **B**. Sequencing was undertaken to confirm the mutation's presence, as well as the fidelity of the insert and insertion into the vector.

mutagenesis reaction was used to transform bacterial cells for propagation of the mutant plasmid. The bacteria were analyzed by restriction digest to confirm presence of the mutated construct, then sequenced to verify the correct placement of the point mutation. These analyses are shown in Figure 6.3. The 1432A>G mutation creates a BamH1 restriction digest site within the *PAPD1* gene. As a BamH1 restriction site was used for cloning the *PAPD1* gene into the pGEX-6P-1 vector, digestion with BamH1 creates three fragments visible on agarose gel electrophoresis: the vector backbone, the excised mtPAP6p insert, and a fragment of the insert corresponding to the length of nucleotides between the 5' BamH1 restriction site used for cloning and the BamH1 site generated as a result of the point mutation. Figure 6.3A shows this characteristic three fragment pattern from BamH1 restriction digestion of the mutant plasmid.

6.3.2 Expression of wild-type and N478D recombinant mtPAPΔN-GST

With the integrity of the wild-type and 1432A>G pGEX-mtPAPΔN constructs verified, the next step was to express the fusion proteins in *E. coli* cells. Expression of the wild-type fusion protein was undertaken first, with the goal of optimizing the process before expression and purification of the mutant protein commenced. The first bacterial strain used for expressing mtPAPΔN-GST was Rosetta (DE3) cells. The bacterial cells

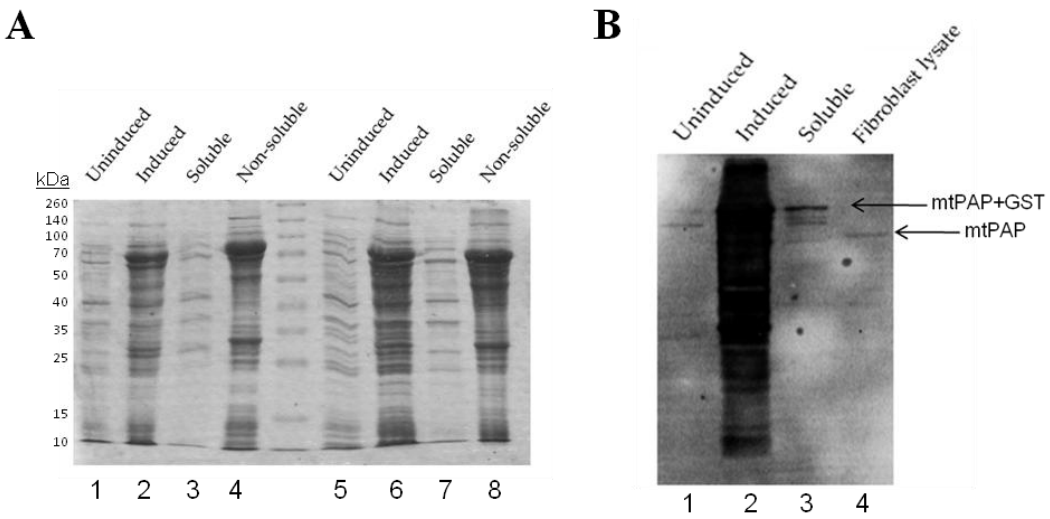

Figure 6.4. Expression of recombinant mtPAPΔN-GST fusion protein
A. Coomassie stain showing two incubation conditions of Rosetta cells, with separate fractions. The expected size of mtPAP is approximately 92 kDa. **B**. Fractions from 3 hours at 37°C were separated with SDS-PAGE, then immunoblotted using an antibody against mtPAP. The soluble fraction showed mtPAP at an increased size, as expected with the GST fusion product. Fibroblast whole cell lysate (20ug) was loaded to act as a size comparison for mtPAP and mtPAPΔN-GST.

were induced under two different conditions to test which produced more soluble protein. Cultures were either incubated at 37°C for 3 hours, or at 16°C overnight. The uninduced, induced, soluble, and insoluble fractions were then analyzed by 12% SDS-PAGE and Coomassie staining. As shown in Figure 6.4A, it was immediately apparent that the vast majority of protein being produced was insoluble, regardless of the incubation conditions. There appeared to be small amounts of the fusion protein present in the soluble fraction of both conditions, so arbitrarily the 37°C incubation fractions were analyzed further. These samples were used for immunoblotting with the anti-mtPAP antibody (Figure 6.4B), in order to confirm the identity of the protein size assumed to be mtPAPΔN-GST on the comassie stained gel. The product visualized on the immunoblot appeared at the weight

expected for the mtPAPΔN protein with the GST tag, an increase in size of approximately 26 kDa, from 60kDa to 86kDa.

In an attempt to improve upon the expression profiles observed in the Rosetta

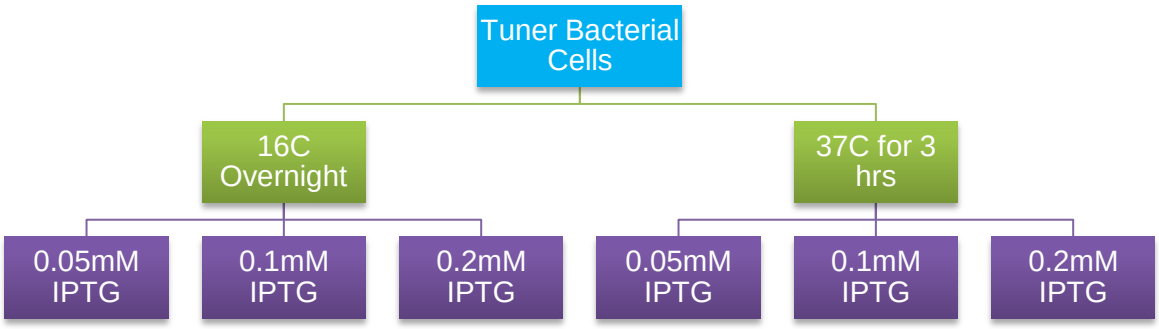

Figure 6.5. The Incubation Conditions and IPTG Concentrations used for Tuner Strain mtPAPΔN-GST Expression
Schematic of the assorted conditions tested for mtPAPΔN-GST expression using the Tuner strain of bacteria.

cells, the Tuner strain of bacteria was transformed with the pGEX-mtPAPΔN construct. Tuner cells can be induced in a concentration-dependent manner with IPTG. Six cultures were generated from a transformed colony to be induced with three separate concentrations of IPTG and incubated either overnight at 4°C or 3 hours at 37°C, as outlined in Figure 6.5. None of these conditions in the Tuner strain produced more soluble fusion protein than the original conditions described earlier (data not shown). As use of the Rosetta (DE3) cells was well established, further work with the Tuner cells was suspended and Rosetta cells were returned to as the expression vehicle of choice. Based on the reports from Naigaike *et al.* and Bai *et al.* there was not an expectation of needing large amounts of recombinant protein for *in vitro* studies. Thus, the amount of soluble mtPAPΔN-GST expressed in the Rosetta cells seemed sufficient to attempt scaling up the culture size, as the small amounts of protein recoverable would be enough for experimental needs.

The expression of N478D mtPAPΔN-GST was the next priority. The mutation is not predicted to massively alter the conformation of the enzyme, so major changes in solubility of the mutant recombinant fusion protein were not expected. The Rosetta (DE3) cells were transformed with the mutated pGEX-mtPAPΔN plasmid, and induced in the same manner as the wild-type expression. As shown in Figure 6.6, the expression and solubility profile of the mutant recombinant protein is essentially identical to the wild-

type. Once again there is a very small percentage of the total expressed protein present in the soluble fractions. As with the wild-type, this small percentage would potentially still be sufficient with larger cultures prepared, considering the small amounts of enzyme used in *in vitro* assays reported in previous research articles.

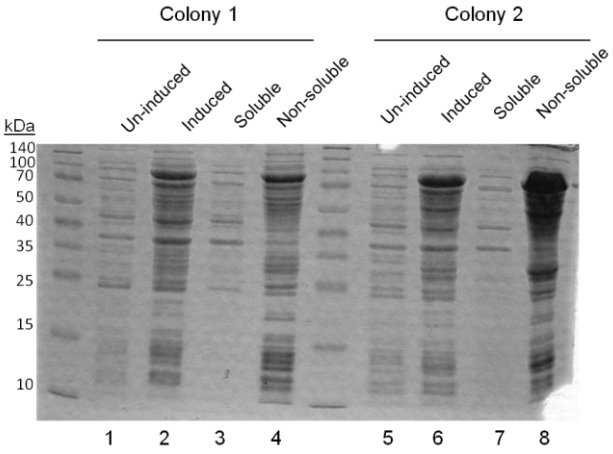

Figure 6.6. Expression and solubility of N478D mtPAPΔN-GST
Comassie stained gel showing two colonies of Rosetta cells expressing N478D mtPAPΔN-GST. The expected size of the mutant mtPAP is approximately 92 kDa, unchanged from the wild-type. The majority of the expressed protein was still in the non-soluble fractions.

6.3.3 Analysis of mtPAPΔN behavior in solution

Large 500ml cultures were prepared for both wild-type and N478D mtPAPΔN expression. The final overnight incubation is with the Prescission Protease at 4°C, after which the cleaved recombinant protein is eluted. The proteins were eluted in PBS, with 0.5mM ATP and 2mM $MgCl_2$. In order to assess aggregation or precipitation of the cleaved protein, I examined the protein in solution at three separate storage temperatures, with or without 50% glycerol added. The purpose of which was to determine optimal storage conditions for the cleaved enzyme. The aggregation of the protein was assessed using dynamic light scattering (Figure 6.7). Ideally, the particle of interest will be a size between 10nm and 100nm, with all 5 traces virtually superimposable. The condition that led to the optimal particle size readings was primarily lack of glycerol added to the solution. Although it is possible that 50% glycerol was too high a concentration. All three temperatures of storage produced similar readings, although -20°C storage appeared to be the most favorable condition, as can be seen by the consistent DLS readings and size of the particle (approximately 20nm).

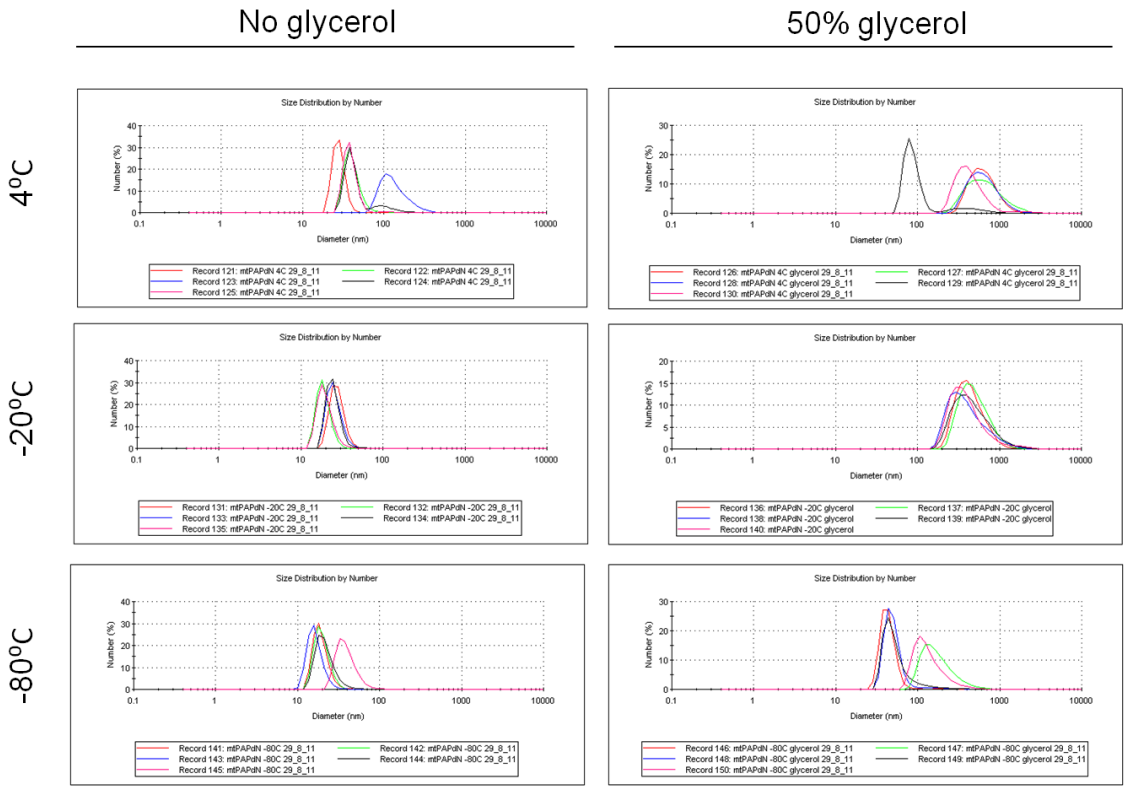

Figure 6.7. Analysis of mtPAPΔN in solution by dynamic light scattering.
Purified mtPAPΔN was stored at three separate temperatures, with or without 50% glycerol added to the buffer, for 24 hours. The next day samples of 20ul were taken from the stored aliquots and analyzed by DLS. Monodispersed protein is represented by a uniform peak between 10 and 100nm. Larger peaks may indicate aggregation of protein. Each graph represents a series of five measurements. No glycerol and storage at -20°C gave the best results.

The *in vitro* polyadenylation assay was based on the method detailed in Bai *et al.* The buffer composition from their procedure was used, as was the reaction temperature and gel electrophoresis conditions. The RNA substrate, however, differed. Rather than using pre-cleaved mRNA from the pG3SVL-A plasmid, my experiments used RNA transcripts corresponding to regions of mitochondrial mRNAs. I generated [^{32}P] radiolabeled transcripts corresponding to the final 248nt of the *MTATP6* transcript, and the final 277nt of the *MTND3* transcript. Approximately 50-200ng of the wild-type and N478D mtPAPΔN proteins were incubated at 30°C for 30min with radiolabeled transcripts (approximately 1000cpm) in 1x reaction buffer with ATP, DTT, and RNase inhibitor.

Over the course of several polyadenylation assays, each analyzed by separation on a 6% polyacrylamide/8M urea gel and developed by autoradiography, the results failed to show poly(A) extensions on the radiolabeled transcripts. This was true for both the wild-type and mutant mtPAPΔN. The concentration of recombinant protein in the reactions was difficult to increase due to the minute amounts of soluble protein being generated.

After the failed polyadenylation assays were analyzed, the decision was made to contact the authors of Bai *et al.* and request the plasmid reported in the paper for use in this work's recombinant mtPAP expression. This would benefit from following a protocol optimized for generating soluble mtPAP, and allow the project to move forward with a validated expression construct.

6.3.4 His-mtPAP expression and generation of the 1432A>G substitution in the pET28a-PAPD1 construct

The construct, designed and assembled in Liang Tong's lab at Columbia University, is a 44-538 residue fragment of mtPAP cloned into the pET28a(+) vector using the NotI and NdeI restriction sites. This generates an N-terminal 6xHis-tagged version of mtPAP, allowing for affinity purification using nickel-charged resin. The cloning, propagation, expression and purification of the plasmid and its product is detailed in Bai *et al*. These methods were largely adopted here. I transformed α-select cells for propagating the plasmid, and Rosetta (DE3) cells for expressing the recombinant protein. The initial expression results were encouraging. An initial half liter of transformed Rosetta culture was lysed, using new buffer for resuspension of the pelleted cells and subsequent sonication, based on Bai *et al*'s methods (50mM Tris pH 8.5, 0.3M NaCl, 1 tab protease inhibitors, 1mM PMSF, 1ul Benzonase). The sonicated suspension was separated into soluble and non-soluble fractions by centrifugation, then the soluble supernatant was placed into a gravity flow chromatography column loaded with Ni-NTA

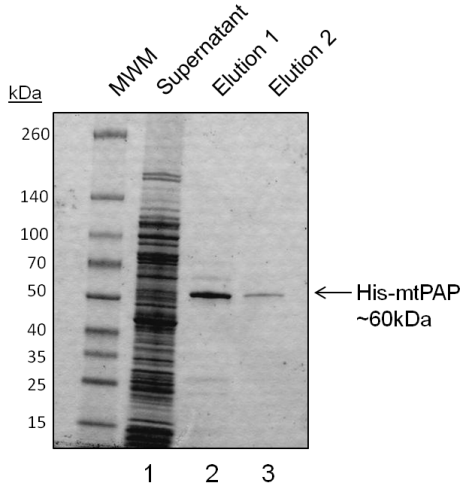

Figure 6.8. Initial expression and affinity purification of 6xHis-tagged mtPAP
His-mtPAP was expressed in Rosetta (DE3) cells overnight with 1mM IPTG at 20°C. The recombinant enzyme was then purified from lysed bacteria using nickel affinity chromatography. The gel lanes are induced bacterial lysate soluble fraction (lane 1), an initial 1ml of elution buffer passed through the column (lane 2), and a second 1ml of elution buffer passed through the column (lane 3). These samples were separated by 12% SDS-PAGE and the gel stained with Coomassie Brilliant Blue, dried, and imaged.

resin. Once the supernatant had flowed through, and the resin was washed with buffer, the bound His-mtPAP was eluted using a high concentration of imidazole (0.25M). The results of the elution are shown in Figure 6.8. The expected recombinant product was observed, migrating at approximately the mature 60kDa size, a decrease from the 66kDa full-length enzyme. The yield of soluble protein bound to the nickel resin was significantly greater than observed with the mtPAPΔN-GST recombinant protein. As shown in Figure 6.8 (lanes 2-3 compared to lane 1), the amount of soluble His-mtPAP is not dramatically higher than other soluble proteins present in the bacterial supernatant. Most of the expressed protein is likely still in the non-soluble fraction. The yield that is available in the soluble form, however, was enough of an increase over mtPAPΔN-GST expression levels to justify further use of the His-mtPAP system.

As a result of using imidazole to elute the His-tagged protein from the nickel resin, removal of the imidazole (present at 250mM in the elution buffer) is necessary. This can be accomplished in a variety of ways. Dialysis with buffer that does not contain

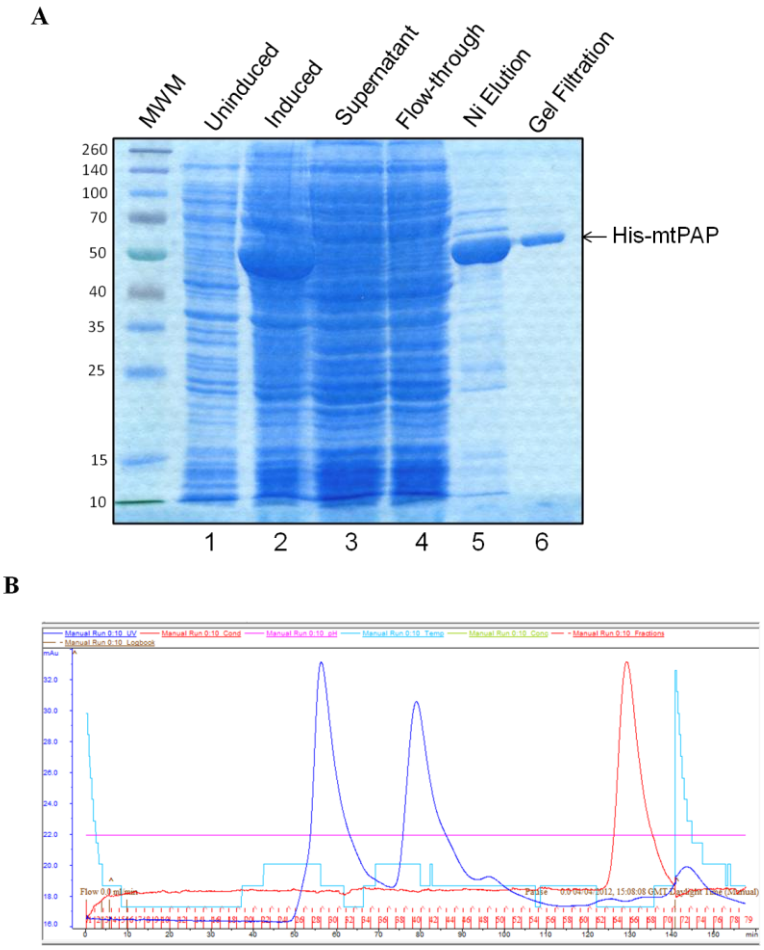

Figure 6.9. Purification of His-mtPAP via size exclusion chromatography
A. His-mtPAP recombinant protein was purified using nickel affinity chromatography, followed by size-exclusion chromatography. Samples taken from each step of purification were separated by 12% SDS-PAGE, and the gel stained with Coomassie Brilliant Blue. **B**. Chromatogram produced by the AKTA platform used for performing the size-exclusion chromatography. The characteristic dual peaks are present, represented by the dark blue line.

imidazole is one solution, another is size-exclusion chromatography, which has the added benefit of further purifying the extract from the nickel resin. Size-exclusion chromatography was chosen as the second purification step as it was the method of choice in Bai *et al.* A HiLoad 16/60 Superdex 200 prep grade size exclusion chromatography column was used for the gel filtration. The purity of the fractions eluted from the chromatography column were a marked improvement from the affinity purification step, as shown in Figure 6.9A (lane 6). The chromatogram from the AKTA showed a characteristic two peak profile during the column run (Figure 6.9B). Only the second peak corresponded to the His-mtPAP protein. Figure 6.9A (lane 5) shows, to a better

extent, the increase in yield of soluble recombinant protein that the pET-PAPD1 construct provided. This was coupled with information gained from consulting members of Professor Tong's lab, specifically Dr. Jeong Ho Chang, specifically regarding expression of His-mtPAP. Their recommendation was performing much larger bacterial preparations and purifications in order to generate enough protein to pool into stocks with high His-mtPAP concentrations. With the expression data from our lab for His-mtPAP, as well as recommendations for larger purifications, I then moved on to generating a mutant version of His-mtPAP.

The process for producing the 1432A>G substitution in the pET28a-PAPD1 construct followed in exactly the same manner as mutating the pGEX-mtPAPΔN construct. The Quikchange II Site-Directed Mutagenesis kit was again employed, with the same set of primers used to create the mutation. Figure 6.10A shows confirmation of the

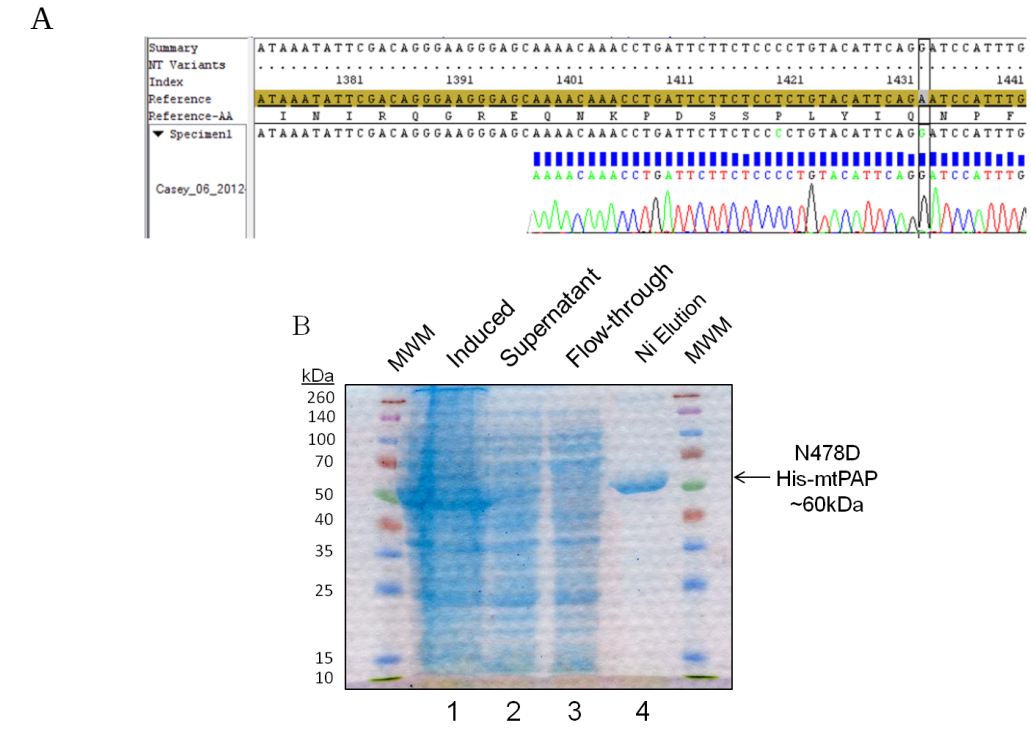

Figure 6.10. Production of the N478D His-mtPAP
A. Electropherogram of mutant pET28a-PAPD sequencing, to confirm the presence of the 1432A>G point mutation. **B**. Coomassie stained gel of mutant His-mtPAP purification by nickel affinity chromatography.

1432A>G substitution in the plasmid, which will alter the asparagine residue to an aspartate. The mutated plasmid was then used to transform α-select and Rosetta (DE3) bacterial strains, for plasmid propagation and protein expression, respectively. As illustrated in Figure 6.10B, the N478D His-mtPAP appeared to express at a similar level to the wild-type His-mtPAP protein. At this point, with both wild-type and mutant protein generated, the next priority was assessing their *in vitro* polyadenylation activity.

6.3.5 Initial His-mtPAP poly(A) assay results

The initial attempts at observing *in vitro* polyadenylation activity using the His-mtPAP enzyme were based partly on the methodology from Bai *et al.* RNA transcripts corresponding to the 3' 248nt of the *MTATP6* mt-mRNA were radiolabeled, incubated with His-mtPAP, separated on a 6% polyacrylamide/8M urea gel, then visualized with autoradiography. Changes in substrate length due to polyadenylation were actually visible, and corresponded to increases in protein concentration in the assay reactions. As shown in Figure 6.11, the signal for the naked 3' end ATP6 substrate RNA diminishes as the concentration of wild-type His-mtPAP increases (lanes 4-5). There also appears to be

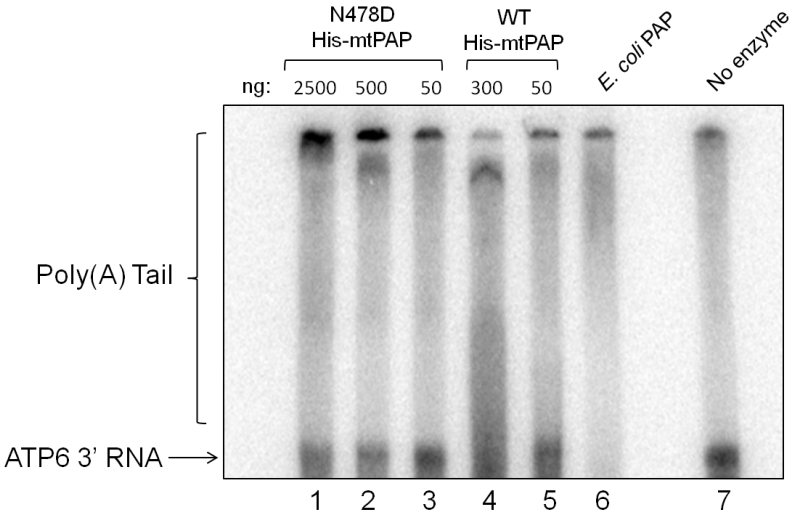

Figure 6.11. Early stage *in vitro* polyadenylation reactions.
Wild-type (lanes 4-5) and N478D His-mtPAP (lanes 1-3) produced in our laboratory used in polyadenylation reactions. *E. coli* PAP included as positive control (lane 6). RNA substrate was radiolabeled with [α-^{32}P] UTP. The poly(A) reactions were separated by polyacrylamide/urea gel electrophoresis, then the gel dried and visualized by autoradiography.

an increase in signal above the substrate, which may be polyadenylated RNA. *E. coli* poly(A) polymerase (PAP) was included as a positive control for the assay (lane 6), and all substrate appears shifted to larger species. While the results were encouraging, particularly compared to the assays using mtPAPΔN-GST, the resolution and interpretation of the results were not particularly clear. This was the first evidence however, in our lab, that mtPAP was capable of adenylation without other factors needing to be present.

The wild-type and N478D mutation His-mtPAP enzymes poly(A) activity were compared, to assess potential differences in polyadenylation. Figure 6.11 shows several amounts of wild-type (lanes 4 – 5) and N478D (lanes 1 – 3) His-mtPAP poly(A) activity compared. It is suggestive that there is more activity in the wild-type reactions than in the mutant reactions. Whether the mutant His-mtPAP is generating the oligo(A) tails observed *in vivo* is unclear from this gel. The most clear change is the decrease in RNA substrate signal that likely amount to size changes resulting from polyadenylation. The actual signals from polyadenylated transcripts are less clear, and more difficult to interpret. Despite these hurdles, this assay suggested the N478D mutation may directly affect poly(A) activity of the enzyme. The results also provide potential evidence that the mutant does retain some amount of enzymatic activity, albeit significantly less than the wild-type. This is shown by decrease in the non-adenylated substrate signal compared to the no enzyme lanes.

While these poly(A) assay gels provided some preliminary insight as to the polyadenylation capabilities of the recombinant protein, and to differences between the

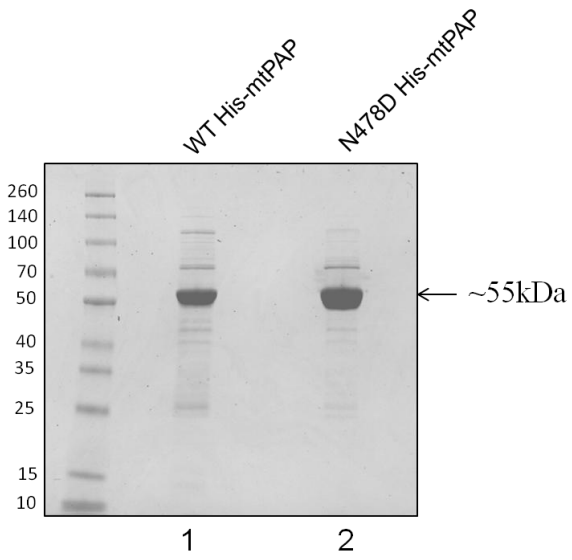

Figure 6.12. Coomassie staining of wild-type and N478D His-mtPAP from the Tong lab.
Wild-type (lane 1) and N478D His-mtPAP (lane 2) stocks (1ul) were separated by 12% SDS-PAGE and stained with Coomassie Brilliant Blue. The stocks were estimated at 6mg/ml and 9mg/ml for the wild-type and mutant protein, respectively.

wild-type and mutant enzymes, the aesthetic quality and clarity of the results were poor. There were multiple issues with the recombinant protein stocks as well. The concentration of the protein eluting from the nickel affinity gel was high, but the background proteins carried over was unsatisfactory, and the high amount of imidazole present was problematic. Both of these issues were solved by implementing gel filtration

as a second purification step. However, further problems were encountered when it came to concentrating the fractions eluting off the gel filtration column. Both wild-type and mutant His-mtPAP appeared very prone to sticking to the membranes of concentrator columns. This was a major issue, as higher concentrations are required in order to dilute out the storage buffer for use in the polyadenylation assays. This in turn made measurements for use in activity assays difficult, affecting replication and interpretation of results. These problems were largely technical in nature, and with time, would likely have been able to be resolved. Professor Liang Tong and a postdoctoral researcher in his lab, Dr. Jeong Ho Chang had already provided consultation about the recombinant expression of the His-mtPAP protein, as we were using their pET28a-PAPD1 expression construct. Rather than allow the momentum of the research to be slowed by the potentially extensive troubleshooting of the purification/concentrating, the decision was made to establish a formal collaboration with Professor Tong's lab. Dr. Chang at Columbia University was sent the mutant plasmid, and they provided high concentration stocks of the wild-type and mutant His-mtPAP protein. This allowed the experiments on *in vitro* activity to continue, while the difficulties with the purification of the recombinant enzymes in our lab could be resolved. Figure 6.12 shows the comparison of the protein concentrations of the enzyme stocks. The wild-type protein stock was 6mg/ml, and the N478D mutant was 9mg/ml. The following experiments in this chapter were performed using the recombinant wild-type and N478D His-mtPAP that was sent to our lab from Professor Tong.

6.3.6 Analysis of secondary structure for wild-type and N478D His-mtPAP

In order to assess possible structural impacts from the N478D mutation, both wild-type and mutant recombinant His-mtPAP protein were examined using far-UV circular dichroism spectroscopy. This method is able to estimate secondary structure of proteins. By comparing the wild-type spectroscopic signature to that of the mutant, inferences as to changes in the secondary structure as a result of the mutation can be made. Figure 6.13 shows the spectra of the two enzymes. The signatures are virtually superimposable. The spectra are also consistent with that of well-folded proteins. The intensity of the signal from the mutant protein is greater than that for the wild type

protein, and this would typically imply greater secondary structure. However it is unlikely that a mutation would increase rather than decrease secondary structure. The difference in intensity likely stems from minor imprecision in measurement of protein concentrations, as the Nanodrop spectrophotometer has limited sensitivity. The spectroscopic data suggest that the N478D mutation does not cause major disruption to the enzyme structure.

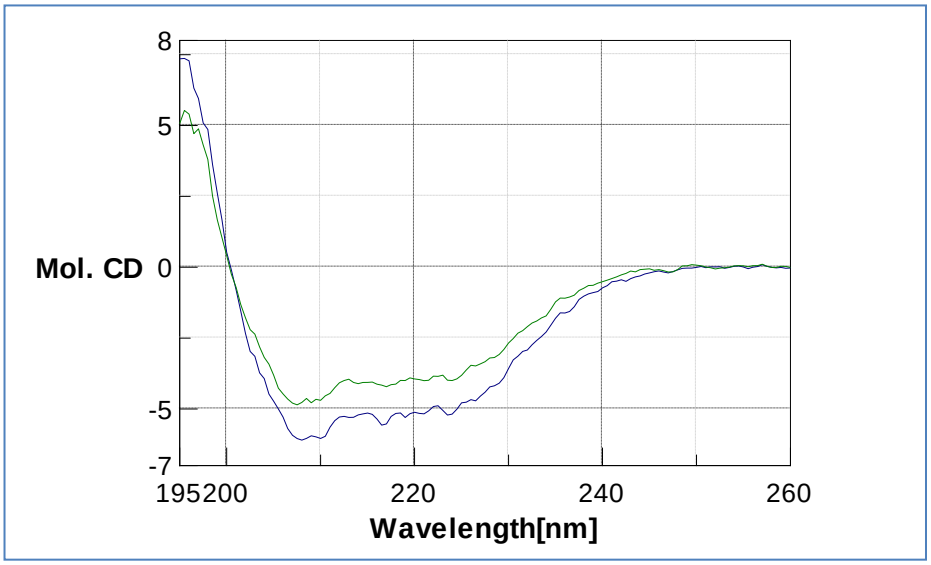

Figure 6.13. Analysis of wild-type and N478D recombinant His-mtPAP by far-UV circular dichroism spectroscopy.
Wild-type (blue line) and N478D (green line) His-mtPAP were analyzed in a solution of 50mM Tris HCl pH 8.5, 0.3M NaCl, 5% (v/v) glycerol buffer. Both spectra results are consistent with well-folded proteins, and virtually overlap. The measurements were carried out with a Jasco J-810 instrument, with a cuvette pathlength of 0.01cm.

6.3.7 Analysis of wild-type and N478D His-mtPAP dimerization

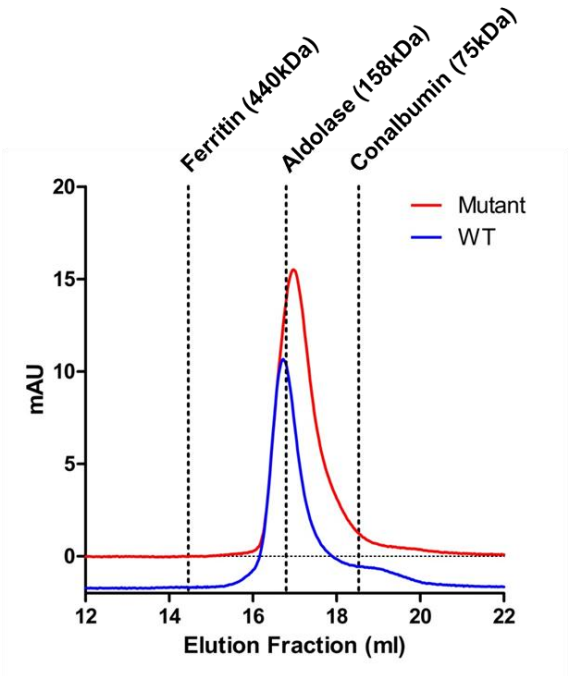

Figure 6.14. Analysis of wild-type and N478D His-mtPAP multimerization.
Wild-type and N478D His-mtPAP (4.5ug) were assessed by analytical grade size exclusion chromatography. Elution fractions for ferritin (440KDa), aldolase (158kDa) and conalbumin (45kDa) are indicated.

One potential effect of the mutation was disruption of dimerization. According to Bai *et al.* 2011, dimerization is necessary for enzymatic activity. As the mutant had shown reduced activity in the preliminary assays, its potential monomer status had to be investigated. To accomplish this, both the wild-type and N478D recombinant His-mtPAP were injected on to an analytical grade size exclusion chromatography column, used for high resolution separation of proteins. The elution fractions of the His-mtPAP proteins were compared to calibration standards of known and varying size. As showin in Figure 6.14, the peaks for wild-type and N478D His-mtPAP were both located very close to the elution peak of aldolase, a 158kDa protein. As neither protein was eluted after conalbumin, a 75KDa protein, it did appeared that neither wild-type nor N478D His-mtPAP enzyme adopts a monomeric form in solution. This effectively ruled out the mutation causing a disruption of the dimeric state previously reported to be the only active form of mtPAP.

6.3.8 Optimization of the fluorescent poly(A) activity assay

With high-concentration stocks of the recombinant His-mtPAP enzymes, I was able to convert the poly(A) activity assay to a fluorescent, rather than radiolabeled, platform. The major change from previous experiments was not radiolabeling the RNA substrates used in the poly(A) reactions, but staining the gels on which the products had been separated with SYBR gold, a fluorescent nucleic acid-binding dye. The dye can be

visualized by scanning the gel itself with the 473nm laser on a Typhoon imager. This approach provided much cleaner data, with a quicker turnaround time, as no long exposure times associated with autoradiography were necessary.

The initial experiments utilizing this fluorescent approach, and employing the Tong lab-produced recombinant His-mtPAP examined the amount of poly(A) activity relative to the protein levels in the reactions. The oligoadenylated *MTND3* RNA substrate was used in the initial assays. An RNA concentration of 0.25uM was employed for these

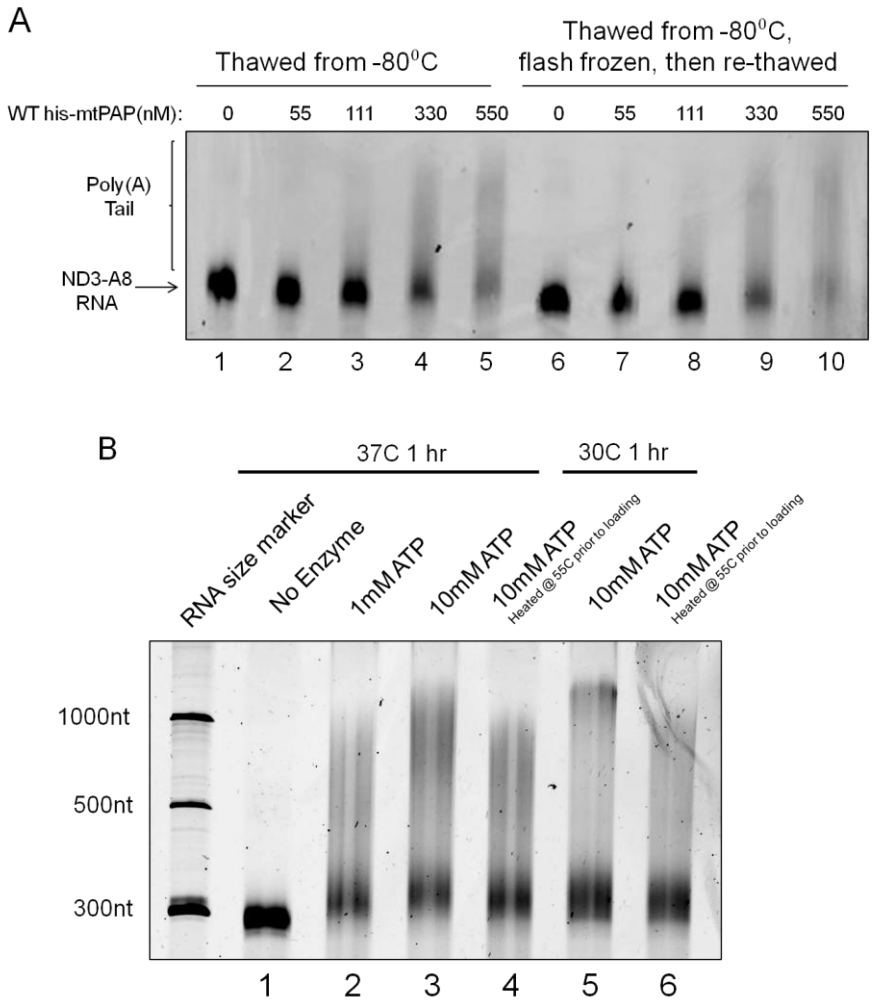

Figure 6.15. Optimizing conditions for the fluorescent poly(A) activity assay.
A. Varying amount of one or two freeze-thaw cycled wild-type His-mtPAP (0.55uM) were incubated with RNA substrate (0.25uM) for 1hr at 37°C. Reactions were quenched with 90% formamide/1x TBE, separated through a 6% polyacrylamide/8.3M urea gel, then stained with SYBR gold. Stained products were visualized by scanning with a Typhoon FLA 9500 instrument. **B**. The effect of different incubation temperatures for the poly(A) assay was investigated, then analyzed in the same manner as A. The RNA substrate in A and B was a 278nt oligo(A) 3' fragment of *MTND3.*

assays, as it was easily visualized using SYBR Gold. As Figure 6.15A demonstrates, the degree of size change as a result of polyadenylation increases with the amount of His-mtPAP input into the reaction. The other condition tested in the experiment was whether the activity changes as a result of a single round of freeze-thawing, provided the thawed

protein is quickly flash frozen once the necessary amount is removed. This provided an approximate understanding of whether stocks of protein could be used again in assays if thawed once before. Figure 6.15A demonstrates that the polyadenylation activity from a single thawing cycle versus two does not appear to differ significantly.

Another assay condition investigated was the optimal incubation temperature of the polyadenylation reaction. Other reports detailing *in vitro* polyadenylation reactions have incubated reactions at 30°C. The poly(A) assay was carried out at this temperature, as well as 37°C to observe any differences in enzymatic activity. In parallel, I tested whether heating the reactions to 55°C after the addition of formamide prior to loading on to the gels aided in electrophoresis results. It was imperative that the lengths of the poly(A) tails being generated in the *in vitro* reactions were able to be measured. Towards this end, a ssRNA ladder was included in the gels analyzing the poly(A) results.

Figure 6.15B illustrates the results of the conditions tested on polyadenylation activity, as well as the inclusion of the ssRNA size markers. An obvious aspect of the reactions is the length of poly(A) tail being generated. While the majority of the lengths appear to be within the physiological 40-60nt range, there is a significant amount of product even extending up to approximately 1000nt. Poly(A) tails extended to such a degree have not been observed in mitochondria. Incubating the polyadenylation reactions at 30°C versus 37°C seemed to affect the distribution of larger poly(A) length, tighter at 30°C, more disperse at 37°C. There did appear to be less remaining non-adenylated RNA substrate at 37°C, compared to 30°C, although the difference is not great. For this reason, 37°C continued to be the incubation temperature utilized in these *in vitro* assays.

Heating the reactions in formamide prior to loading had a negative effect on poly(A) length on gel separation. Whether this is due to degradation of the RNA or is a gel migration issue, is unclear. The reactions were no longer heated prior to loading on gels for future assay analysis.

6.3.9 Wild-type and mutant His-mtPAP nucleotide affinities

A potential explanation for the reduced polyadenylation observed with the N478D mutant mtPAP could be alterations to its affinity for ATP. Thus, I sought to examine the

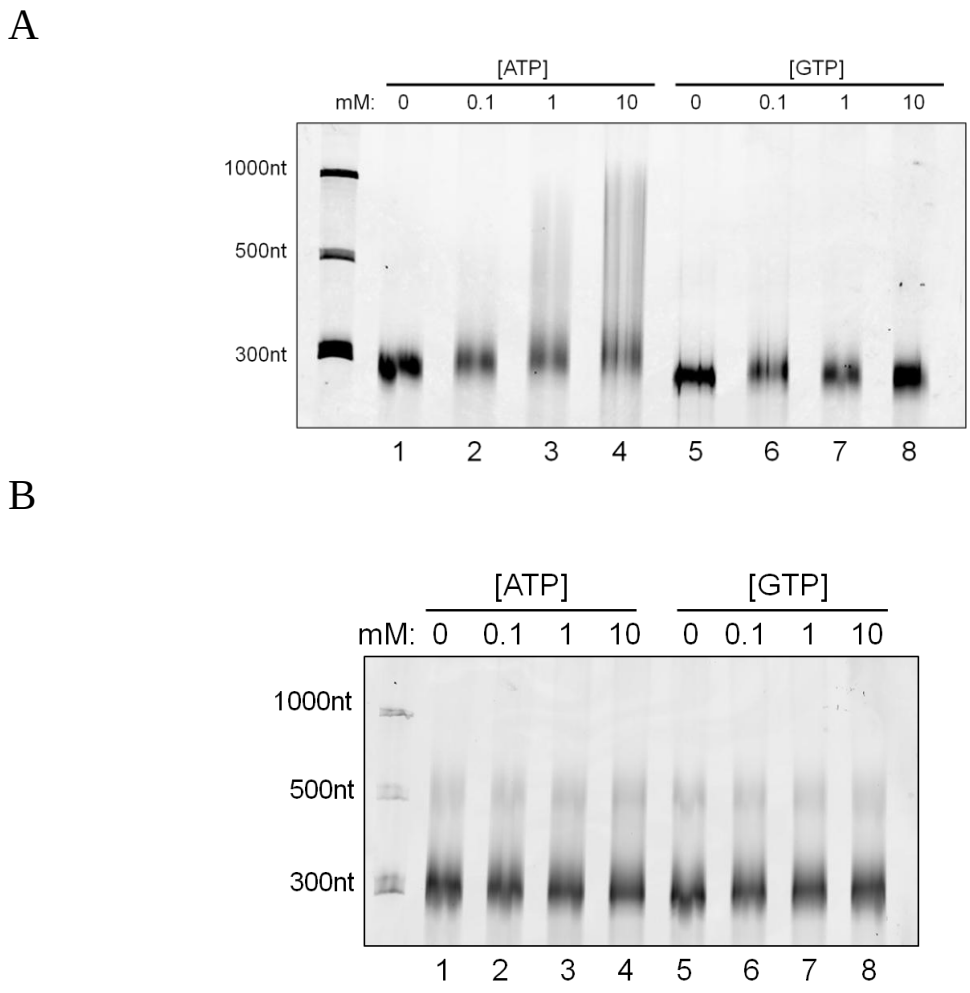

Figure 6.16. Nucleotide affinities for wild-type and N478D His-mtPAP
A Wild-type His-mtPAP (0.55uM) activity with titrations of ATP and GTP. **B** N478D His-mtPAP (0.55uM) activity in the presence of ATP and GTP titrations. A gel artifact is present at 500nt. The RNA substrate in A and B were different preparations of the 277nt 3' fragment of *MTND3* (0.25uM). Reactions were quenched with 90% formamide/1x TBE, separated through a 6% polyacrylamide/8.3M urea gel, then stained with SYBR gold. Stained products were visualized by scanning with a Typhoon FLA 9500 instrument.

polyadenylation activities of the wild-type and mutant enzymes in the presence of several concentrations of ATP. Discussions with structural biologist and crystallographer Professor Rick Lewis (Newcastle University) yielded the hypothesis that the N478D mutation could potentially have shifted the affinity of the active site from ATP towards GTP as a substrate. So in addition to poly(A) reactions with a titration of ATP, I performed the same reactions in the presence of different concentrations of GTP. The results are shown in Figure 6.16. The wild-type enzyme exhibited an affinity for ATP, with major activity between 0.1mM and 1mM ATP concentrations. It is difficult to determine if there is any activity for the N478D His-mtPAP in the presence of ATP, or if the extensions are too short to be resolved clearly on the gel. On the 6% polyacrylamide

gels, the resolution within the physiological poly(A) length range is poor. Only the larger sizes are able to be clearly measured in these gels. Neither protein can utilize GTP to any significant degree. Again, assessment of polyadenylation in the physiological length range is difficult here. Certainly, the hypothesis of the N478D mutation conferring GTP nucleotide preference is refuted by these results, at least to the extent that GTP would confer any activity comparable to ATP.

6.3.10 Comparison of oligoadenylated vs non-oligoadenylated transcripts as substrates for poly(A) extensions

The presence of oligo(A) tails on mt-mRNAs in systems where mtPAP is knocked down (Slomovic and Schuster, 2007), as well as LRPPRC knock-outs (Ruzzenente *et al.*, 2012), raises the possibility that oligoadenylation is a step that precedes polyadenylation. It is possible that the oligoadenylated 3' termini present a more optimal substrate for mtPAP, rather than a naked 3' end. In order to test this possibility, both oligoadenylated (with 8 adenines) and naked 3' end transcripts (prepared as detailed in 6.2.5) were incubated with wild-type His-mtPAP enzyme. The results are shown in Figure 6.17. Wild-type His-mtPAP does not appear to utilize the +/− oligo(A) substrates differently. The characteristic two populations of polyadenylated transcripts are present, the

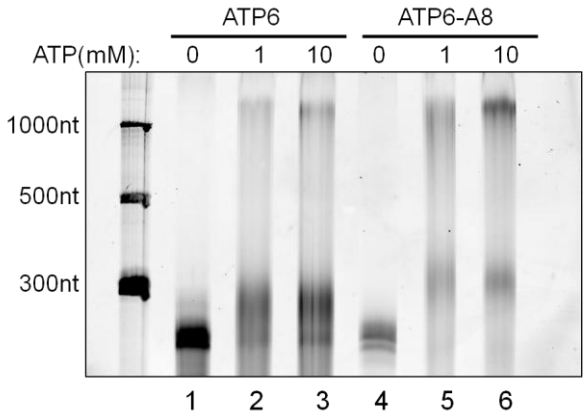

Figure 6.17. Polyadenylation of oligoadenylated and naked 3' end transcripts
Wild-type His-mtPAP (0.55uM) was incubated with oligo(A8) and naked 3' end ATP6 RNA 248nt transcripts (0.25uM) in the presence of increasing concentrations of ATP. RNA loading between oligoadenylated and non-oligoadenylated RNA is unequal (lane 1 vs 4) but consistent within each transcript panel (1-3 or 4-6). Reactions were incubated at 37°C for 1 hour, then quenched with 90% formamide/1x TBE, separated through a 6% polyacrylamide/8.3M urea gel, then stained with SYBR gold. Stained products were visualized by scanning with a Typhoon FLA 9500 instrument.

physiological poly(A) lengths and the super-adenylated lengths. In the case of the ATP6-A8 RNA, more of the starting substrate is extended by adenylation, however this may be

due to the relative amounts of RNA in the reactions. The signal from each substrate alone are not equal, indicating a difference in the amount of transcript used in each reaction. However, the amount added was but consistent within each transcript panel. Thus, the complete shift of substrate transcript into the adenylated form in the ATP6-A8 reactions may be due to less RNA being present to be adenylated.

6.3.11 Polyadenylation in the presence of LRPPRC and LRPPRC/SLIRP complex

Chujo *et al.* claimed that LRPPRC was a requirement for optimal mtPAP polyadenylation (Chujo *et al.*, 2012). Their data reported showed no mtPAP activity in the absence of LRPPRC. At this point, however, multiple experiments in my study had shown polyadenylation activity from His-mtPAP alone, without putative associated factors. In addition, various other reports of *in vitro* mtPAP activity exist (Nagaike, 2005; Bai *et al.*, 2011). Still, these results did not rule out some sort of effect as a product of LRPPRC interaction. To investigate this possibility, our lab established the second major collaboration for this study, with Professor Nils-Goran Larsson and Dr. Henrik Spahr. In

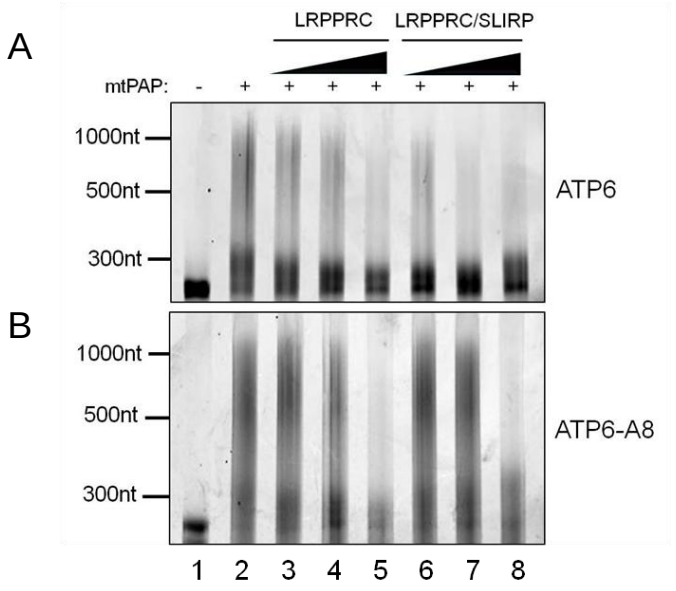

Figure 6.18. The effect of LRPPRC and LRPPRC/SLIRP complex on polyadenylation
A. Wild-type His-mtPAP (0.55uM) was incubated either alone, or with 5nM, 50nM, or 500nM of LRPPRC or LRPPRC/SLIRP complex. The RNA substrate (0.25uM) was the 3' 248nt ATP6 transcript. **B**. Same reaction conditions as in A, but the RNA substrate was oligoadenylated. Reactions were incubated for 1 hour at 37°C. Reactions were then quenched with 90% formamide/1x TBE, separated through a 6% polyacrylamide/8.3M urea gel, and stained with SYBR gold. Stained products were visualized by scanning with a Typhoon FLA 9500 instrument.

their lab they have generated recombinant LRPPRC, as well as co-expressed recombinant

LRPPRC complexed with SLIRP. As anecdotal reports of the difficulty of expressing recombinant LRPPRC, and indeed any other PPR protein, (Professor Lightowlers, personal communication) persist, the decision was made to collaborate with a group that had navigated the process successfully. Their lab sent high concentration stocks of the recombinant proteins, and I proceeded to carry out experiments designed to dissect the relationship of LRPPRC, SLIRP, and mtPAP in our *in vitro* system.

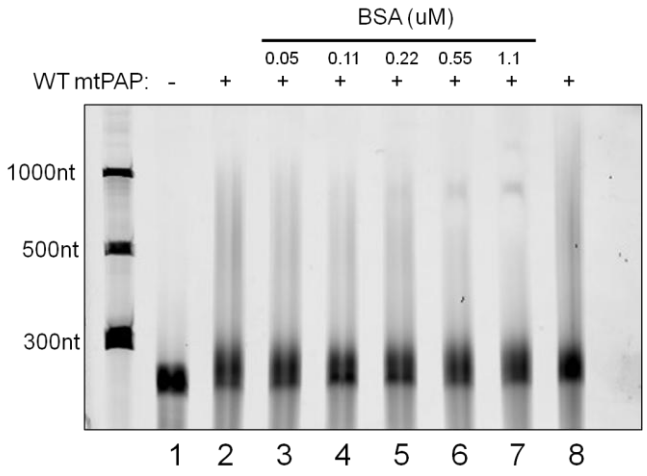

Figure 6.19. The effect of BSA on *in vitro* polyadenylation activity.
Poly(A) reactions consisting of wild-type His-mtPAP (0.55uM) were incubated in the presence of increasing amounts of BSA to control for protein-concentration specific effects on poly(A) activity. BSA was titrated from 0.05-1.1uM. Reactions were incubated for 1 hour at 37°C. Reactions were then quenched with 90% formamide/1x TBE, separated through a 6% polyacrylamide/8.3M urea gel, and stained with SYBR gold. Stained products were visualized by scanning with a Typhoon FLA 9500 instrument.

The first experiments carried out were examining the effect of LRPPRC and the LRPPRC/SLIRP complex on polyadenylation of oligo(A) and non-oligo(A) transcripts in the presence of the wild-type His-mtPAP. The results, shown in Figure 6.18, were contrary to the claims of Chujo *et al*. As the amount of LRPPRC increased in reactions with His-mtPAP, the amount of super-adenylated transcript appeared to decrease. The same pattern was exhibited with the LRPPRC/SLIRP complex. There did not appear to be an obvious increase in poly(A) activity. The physiological range of lengths did not seem to differ significantly, or consistently, with either LRPPRC or LRPPRC/SLIRP. Again, the resolution on the 6% polyacrylamide gels is not optimal for analysis of those poly(A) lengths. The LRPPRC/SLIRP complex had a greater inhibitory effect on super-adenylated extensions with non-oligo(A) RNA as the substrate.

To examine whether the inhibitory effect observed on these gels was a result of LRPPRC or LRPPRC/SLIRP directly, or a product of increased general protein concentration in the reactions, BSA was titrated into poly(A) reactions with wild-type

His-mtPAP. As shown in Figure 6.19, there are similarities between the LRPPRC, LRPPRC/SLIRP, and BSA effects. There is mild inhibition of the super-adenylated extensions, starting at equimolar (0.55uM) concentrations of BSA to His-mtPAP. However, the inhibition of super-adenylated lengths is not exactly identical to those seen with LRPPRC or LRPPRC/SLIRP. This leaves open the possibility that the inhibitory effects on super-adenylation by LRPPRC and LRPPRC/SLIRP are comprised of a mix of direct interaction and inhibition of enzymatic activity from higher protein concentrations in the reactions.

6.3.12 Analysis of N478D mutant activity by high-resolution poly(A) assay

As the results from the *in vitro* poly(A) assay (using 248/277nt RNA transcripts and separating the products by 6% polyacylamide/8M urea gel electrophoresis) were examined, it became increasingly clear that the ability to measure polyadenylation products within the physiological range of lengths was critical to interpreting the data. This ability was not properly developed in the assay. While differences between the wild-type and mutant His-mtPAP enzymes, and with/without LRPPRC or LRPPRC/SLIRP were apparent in the "super-adenylated" populations of transcripts, the relevance of those extension lengths *in vivo* was not clear. It was essential the physiological range of poly(A) lengths be examined in greater detail, and the *in vitro* poly(A) assay needed to be modified to address this crucial point.

To produce a higher resolution analysis of recombinant polyadenylation activity, several changes were made to the assay. New RNA substrates were employed, these were commercially generated 40 and 48 nucleotide RNA oligomers from Dharmacon, corresponding to the terminal 3' 40 nucleotides of the *MTATP6* transcript, with or without an eight adenine oligo(A) tail. Usage of these RNA oligomers overcame a consistent problem from using *in vitro* transcribed RNA substrates, namely, the high levels of nucleotides necessary for the transcription reactions often carried over to the purified RNA. This caused quantitation difficulties, as the primary method of quantifying the RNA was via Nanodrop UV absorbance analysis. The extraneous nucleotides distorted the readings and often caused overestimation of RNA concentrations. This made for inconsistent inputs of RNA into poly(A) reactions, which complicated interpretation of

results at times. This problem was solved with the new oligomers, and more precise measurement of the RNA quantities input to poly(A) reactions was obtained.

The second change to the *in vitro* assay was increasing the polyacrylamide percentage in the gels used for separating the reaction products. The gels were increased from 6% polyacrylamide to 15% polyacrylamide. This allowed for a greater degree of separation for the smaller RNA molecules, and would hopefully impart the level of resolution necessary to examine poly(A) tails in the physiological range of lengths.

For the first experiment with the high-resolution approach, wild-type and mutant His-mtPAP activity on oligo(A) and non-oligo(A) RNA was analyzed. As Figure 6.20 details, the poly(A) extension generated by the wild-type His-mtPAP is approximately

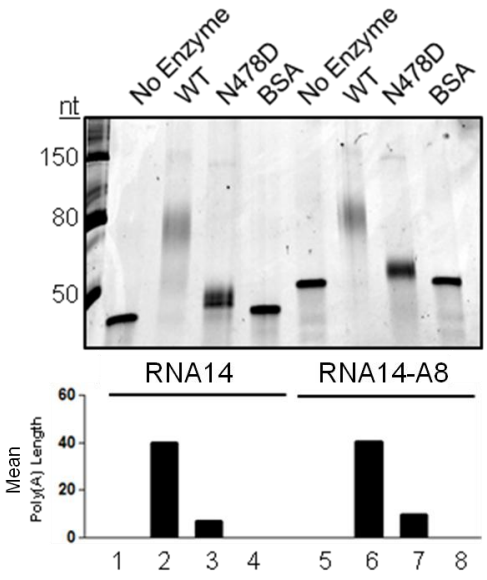

Figure 6.20. High-resolution poly(A) analysis of wild-type and mutant polyadenylation of oligo(A) and non-oligo(A) RNA substrates.
Wild-type (0.55uM, lanes 2, 6) or N478D His-mtPAP (0.5uM, lanes 3,7) was incubated with oligo(A) and non-oligo(A) 40nt RNA substrates (0.25uM) corresponding to 3' end of *MTATP6*. BSA (0.55uM, lanes 4,8) was included as a control for protein concentration. Incubations were for 1 hour at 37°C. Reactions were then quenched with 90% formamide/1x TBE, separated through a 15% polyacrylamide/8.3M urea gel, and stained with SYBR gold. Stained products were visualized by scanning with a Typhoon FLA 9500 instrument. Gel lanes were analyzed by densitometry using Image J. Distance of RNA migration through the gel was used for calculating mean lengths of the poly(A) extensions.

30-40nt long. This measurement is much more accurately confirmed with this high-resolution gel approach. The extensions generated by the mutant enzyme are able to be visualized with much greater detail, and surprisingly, appear to match the oligo(A) tails observed with the MPAT in the homozygous 1432A>G *PAPD1* fibroblasts. These short adenine tails are approximately 5-10nt long. When the oligoadenylated 40-mer (RNA14-A8) is utilized as the substrate, no subsequent increase in adenylate tail length results. Equimolar amounts of BSA to His-mtPAP were incubated with the RNA substrates

(without His-mtPAP present) to control for non-enzymatic protein effects on RNA integrity and migration. Confident in the technique, the subsequent series of experiments continued usage of the modified procedure for poly(A) analysis.

6.3.13 High-resolution analysis of the effect of LRPPRC and LRPPRC/SLIRP complex on polyadenylation

Low-resolution analysis of the *in vitro* polyadenylation products had not shown dramatic differences between LRPPRC and the LRPPRC/SLIRP complex in terms of their pro- or anti-poly(A) effects. To determine whether the effects were too subtle to be detected by the more cumbersome "low resolution" poly(A) assay, and to more thoroughly investigate poly(A) lengths within the likely more relevant physiological length range, the "high resolution" analysis was employed. Similar to the previous poly(A) reactions, wild-type His-mtPAP was incubated with equimolar amounts of LRPPRC, LRPPRC/SLIRP, and BSA. The RNA substrate was the non-oligo(A) 40-mer. A reaction with an increased amount of LRPPRC (1.25uM) was included, as this was the concentration shown in Chujo *et al.* to impart the highest poly(A) extension increase in their assays.

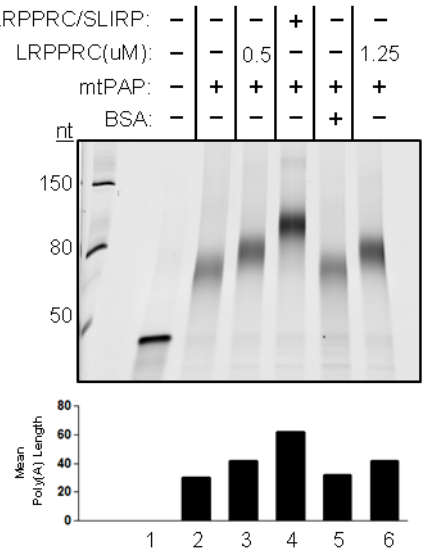

Figure 6.21. High-resolution analysis of LRPPRC and LRPPRC/SLIRP complex effects on polyadenylation.
Wild-type His-mtPAP (0.55uM) was incubated with 40nt RNA substrate (0.25uM), either alone (lane 2) or with 0.5uM LRPPRC (lane 3), 0.5uM LRPPRC/SLIRP complex (lane 4), 0.5uM BSA (lane 5), or 1.25uM LRPPRC (lane 6). Incubations took place for 1 hour at 37°C. Reactions were then quenched with 90% formamide/1x TBE, separated through a 15% polyacrylamide/8.3M urea gel, and stained with SYBR gold. Stained products were visualized by scanning with a Typhoon FLA 9500 instrument. Gel lanes were analyzed by densitometry using Image J. Distance of RNA migration through the gel was used for calculating mean lengths of the poly(A) extensions.

As shown in Figure 6.21, with more precise insight into the physiological range of poly(A) lengths, effects on polyadenylation were seen with LRPPRC and LRPPRC/SLIRP present. An increase in poly(A) extension lengths was observed in the

presence of LRPPRC, with the effect magnified in the presence of LRPPRC/SLIRP. The BSA control reaction showed no difference from the reaction with His-mtPAP alone, indicating the extension increases are solely the result of LRPPRC and LRPPRC/SLIRP activity or interactions. More than doubling the amount of LRPPRC incubated with His-mtPAP did not produce further increases in poly(A) length, suggesting the effect on poly(A) extension is saturated at 0.5uM. The range of lengths remained the same with both 0.5uM and 1.25uM concentrations, which were both shorter than 0.5uM LRPPRC/SLIRP. The presence of SLIRP complexed to LRPPRC appears to produce a synergistic effect on stimulating poly(A) activity.

6.3.14 High-resolution analysis of the effect of LRPPRC and LRPPRC/SLIRP complex on wild-type versus N478D His-mtPAP activity

Continuing the analysis of the effects of LRPPRC/SLIRP on *in vitro* polyadenylation, the reactions examining mutant His-mtPAP activity were performed again, now with the high resolution assay. The purpose of this experiment was to investigate the effect the LRPPRC/SLIRP complex may have on mutant poly(A) activity, specifically within the physiological range of poly(A) lengths, as this was poorly resolved on previous assays. LRPPRC/SLIRP was used, rather than LRPPRC alone, because the complex appeared to be the optimal vehicle for extending polyadenylation length, compared to the less potent effect from LRPPRC alone. Further, there is significant evidence that LRPPRC and SLIRP are complexed *in vivo*, use of the complex in the recombinant reactions was presumed to impart more physiologically relevant data.

Figure 6.22 shows the results of these reactions. The poly(A) extensions generated by the wild-type His-mtPAP enzyme with and without LRPPRC/SLIRP replicate the results from Figure 6.21. For the mutant His-mtPAP alone, the oligo(A) extension is observed, again matching the lengths seen on the MPAT analysis of mutant fibroblasts.

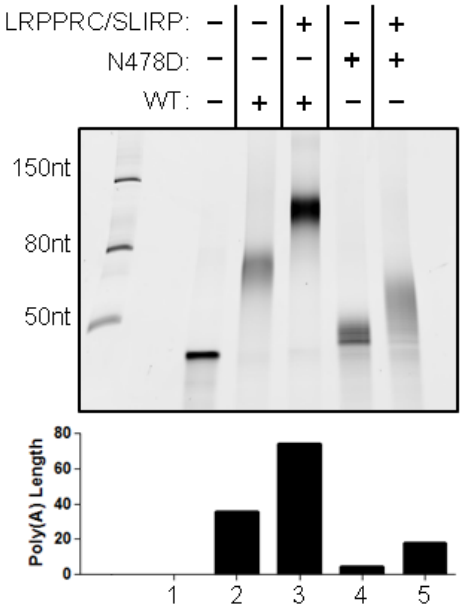

Figure 6.22. The effect of LRPPRC/SLIRP complex on N478D His-mtPAP activity
Wild-type (0.55uM, lanes 2,3) or N478D (0.55uM, lanes 4, 5) His-mtPAP was incubated with (lanes 3, 5) and without (lanes 2, 4) LRPPRC/SLIRP complex (0.48uM). RNA substrate was included at 0.25uM. Incubations took place for 1 hour at 37°C. Reactions were then quenched with 90% formamide/1x TBE, separated through a 15% polyacrylamide/8.3M urea gel, and stained with SYBR gold. Stained products were visualized by scanning with a Typhoon FLA 9500 instrument. Gel lanes were analyzed by densitometry using Image J. Distance of RNA migration through the gel was used for calculating mean lengths of the poly(A) extensions.

Interestingly, the addition of the LRPPRC/SLIRP complex to the mutant polymerase reaction still facilitates an increase in poly(A) length over mutant polymerase alone.

6.3.15 Doubling reaction time does not significantly increase the LRPPRC/SLIRP pro-polyadenylation effect

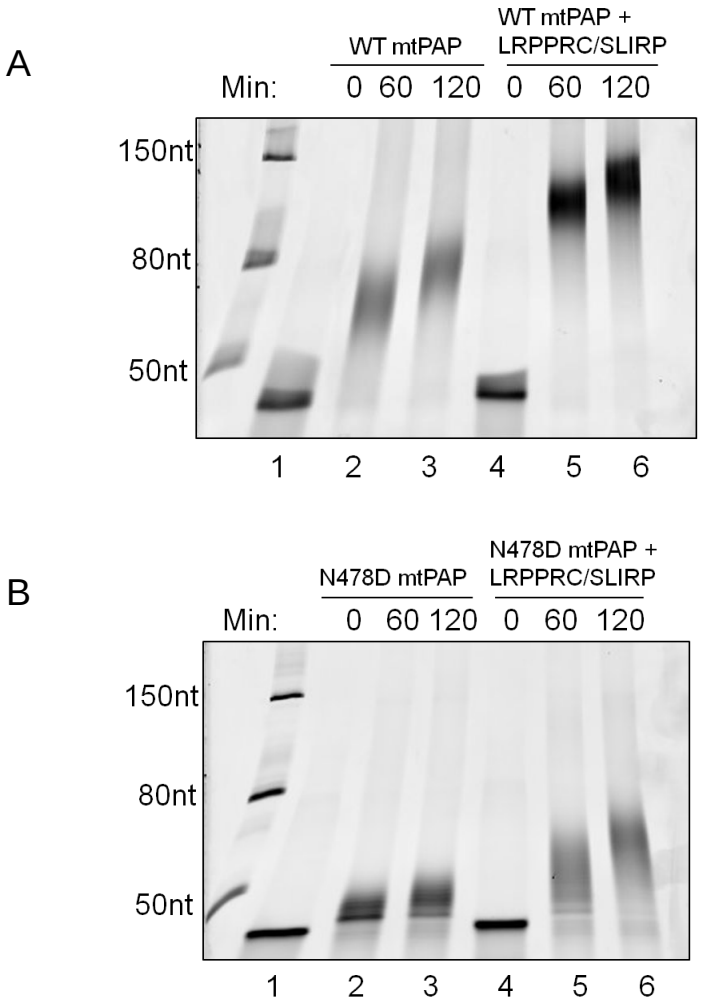

Figure 6.23. Doubling reaction time from 1 hour to 2 hours imparts small gains in poly(A) extension.

A. Wild-type (0.55uM) or **B**. N478D (0.55uM) were incubated with (lanes 5,6) and without (lanes 2,3) LRPPRC/SLIRP complex (0.48uM) present. The incubation times were in sets of 0min, 60min, and 120min. The RNA substrate was 40nt *MTATP6* 3' end fragment (0.25uM). Reactions were quenched with 90% formamide/1x TBE, separated through a 15% polyacrylamide/8.3M urea gel, and stained with SYBR gold. Stained products were visualized by scanning with a Typhoon FLA 9500 instrument.

The standard incubation time for the polyadenylation reactions was one hour at 37ºC. To assess whether wild-type mtPAP on its own could generate poly(A) tails of similar lengths observed in the presence of LRPPRC/SLIRP with extended reaction time, the poly(A) assay was performed over a 2 hour period. Reactions were performed with wild-type and mutant His-mtPAP alone, and in the presence of LRPPRC/SLIRP. As illustrated in Figure 6.23, doubling the incubation times of the polyadenylation reactions produced only small gains in poly(A) extension lengths, indicating that the standard reaction times of one hour were already near maximal extension. These reactions also provide further replication of the pro-poly(A) extension effect exhibited by LRPPRC/SLIRP in the presence of both both wild-type and N478D polymerases.

6.3.16 LRPPRC/SLIRP-mediated pro-poly(A) activity is not specific to mt-mRNA 3' termini

In an effort to elucidate determinants of the poly(A) length increase exerted by LRPPRC/SLIRP, the *in vitro* poly(A) assay was performed using an RNA substrate that

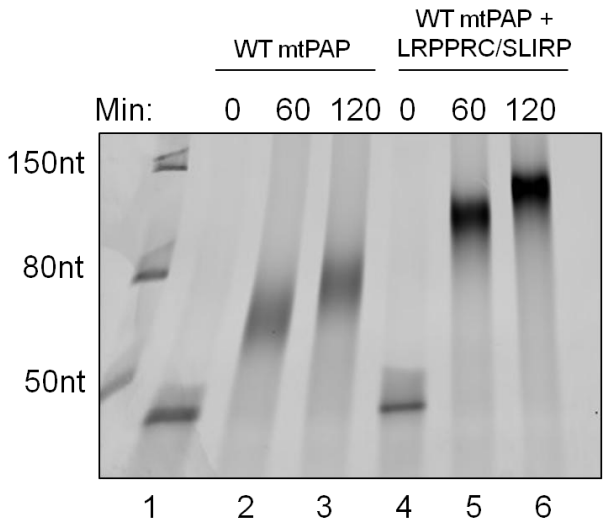

Figure 6.24. Pro-poly(A) activity exerted by LRPPRC/SLIRP is sequence independent.
Wild-type His-mtPAP (0.55uM) was incubated with (lanes 5,6) and without (lanes 2,3) LRPPRC/SLIRP complex (0.48uM). The RNA substrate (0.25uM) was a 40nt upstream segment corresponding to the *MTND3* transcript. The incubation times were in sets of 0min, 60min, and 120min at 37°C. Reactions were then quenched with 90% formamide/1x TBE, separated through a 15% polyacrylamide/8.3M urea gel, and stained with SYBR gold. Stained products were visualized by scanning with a Typhoon FLA 9500 instrument.

was a 40nt upstream segment of the *MTND3* transcript. This as opposed to the standard RNA substrate in the assay corresponding to the terminal 40nt of *MTATP6*. The aim of the experiment was to test if the pro-poly(A) effect is specific for polyadenylation of 3' sequences of mt-mRNAs. Or alternatively, if the effect is general for exposed RNA 3' ends.

In Figure 6.24, polyadenylation of the ND3 40-mer is extended with the addition of LRPPRC/SLIRP to the reaction, and thus the effect is not specific to 3' ends of mt-mRNAs acting as the polymerase substrate. In addition, this represents the first result within this study demonstrating that His-mtPAP can polyadenylate non-mitochondrial mRNA 3' ends. Other reports have shown similar capability for recombinant mtPAP (Nagaike *et al.*, 2008; Bai *et al.*, 2011; Chujo *et al.*, 2012), however up to this point this ability had not been confirmed with experiments as part of this study.

6.3.17 Time courses of *in vitro* polyadenylation reactions

In order to observe the rate of *in vitro* polyadenylation, and how this rate changes depending on the factors present with His-mtPAP, poly(A) reactions were assembled and incubated at 37°C for a variety of time points. The maximum time point was two hours, as this had previously been observed to demonstrate the a plateau in extension. The initial conditions compared were the time courses of wild-type His-mtPAP alone, and then with the addition of the LRPPRC/SLIRP complex. The results of these time courses are shown in Figure 6.25A. The poly(A) tails are longer at each time point when LRPPRC/SLIRP is present, as opposed to His-mtPAP alone. The His-mtPAP used in all the *in vitro* polyadenylation reactions shown on the two gels in Figure 6.25A was taken at the same time from the same thawed aliquot and added to all the reactions at once. This was done to enable comparison between the two gels. The differences in polyadenylation are clear. The results are represented graphically in Figure 6.25B, where the mean of poly(A) lengths at each time point was quantified via densitometry. For these time course experiments, the addition of LRPPRC/SLIRP averages a 40nt extension increase over the maximal extension achieved by mtPAP alone.

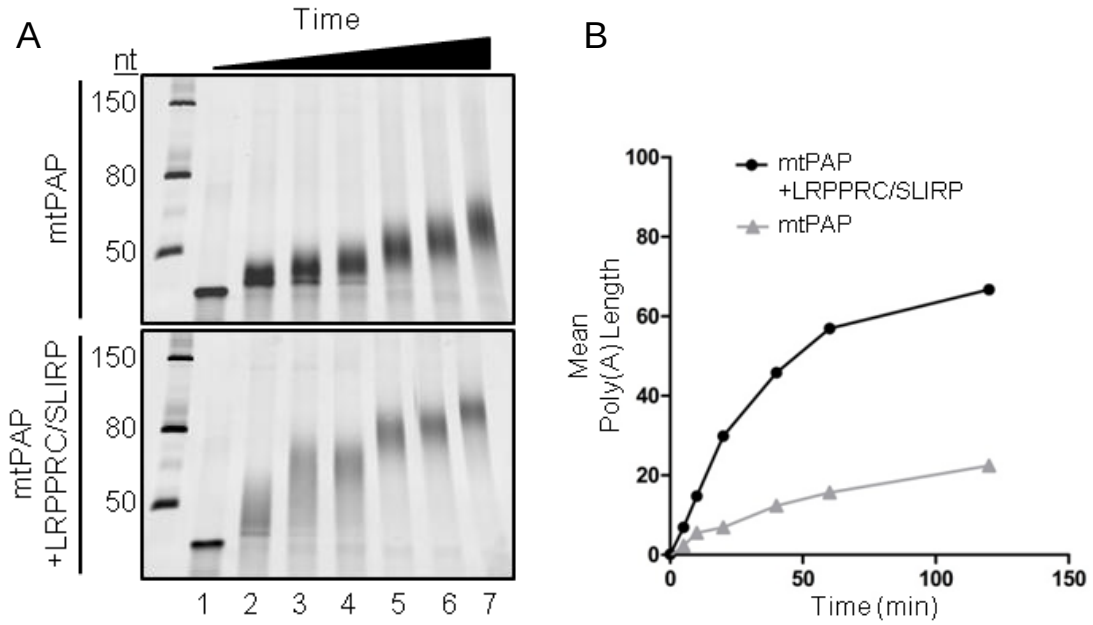

Figure 6.25. Polyadenylation time courses with LRPPRC/SLIRP.
A. Wild-type His-mtPAP (0.55uM) was incubated for multiple time points with and without LRPPRC/SLIRP complex (0.48uM) present. RNA substrate was present at 0.25uM. Incubations took place at 37°C. At each time point, reactions were quenched with 90% formamide/1x TBE, and stored at -20°C. Samples were later thawed, then separated through a 15% polyacrylamide/8.3M urea gel, and stained with SYBR gold. Stained products were visualized by scanning with a Typhoon FLA 9500 instrument. **B**. The log(molecular weight) of ssRNA size standards from the gels in A were graphed against migration through the polyacrylamide/urea gels. A line of best fit was generated, and the slope and y-intercept of the line used to calculate the mean poly(A) length ranges observed.

As the recombinant protein had been stored at -80°C for several months at this point, a reduction of enzymatic activity over that time had to be considered. Two more sets of *in vitro* activity experiments, however, were performed after this point in time. One set consisted of the same time course conditions as in Figure 6.25, only utilizing the oligoadenylated 48nt RNA transcript as a substrate, in order to assess if using an oligoadenylated substrate gave a different pattern of poly(A) synthesis either rate or maximal extension. The other set consisted of two 120min time courses, one which only had SLIRP added to the reaction with His-mtPAP, and the other only having LRPPRC added along with His-mtPAP, in order to dissect out the individual contributions of LRPPRC and SLIRP to the pattern of poly(A) extension. These results are shown in Appendix A. They are not included here, because the poly(A) lengths produced were shorter than previously observed, although increases in poly(A) lengths over those derived from mtPAP alone were still observed with LRPPRC/SLIRP and LRPPRC present. As very little amount of His-mtPAP protein remained, and time had not permitted production of a new batch of recombinant protein, the results have not been replicated as of this time, but need to be repeated to evaluate the effects of each protein independently.

6.3.18 RNA binding capability of LRPPRC/SLIRP and mtPAP

The LRPPRC/SLIRP complex has been reported to interact directly with mitochondrial mRNA (Sasarman *et al.*, 2010; Ruzzenente *et al.*, 2012). In light of the previously described *in vitro* data, it was important to confirm that the recombinant LRPPRC/SLIRP complex was interacting with the RNA substrates and investigate whether the presence of mtPAP affects that RNA binding capacity. The RNA binding capacities of the recombinant proteins were assessed by electrophoretic mobility shift assays (EMSAs). LRPPRC/SLIRP complex was titrated into reactions containing a constant amount of RNA 40-mer substrate, with and without His-mtPAP present.

As presented in Figure 6.26, increasing the amounts of LRPPRC/SLIRP in the binding reactions caused increasing shifts in the migration of the RNA substrate,

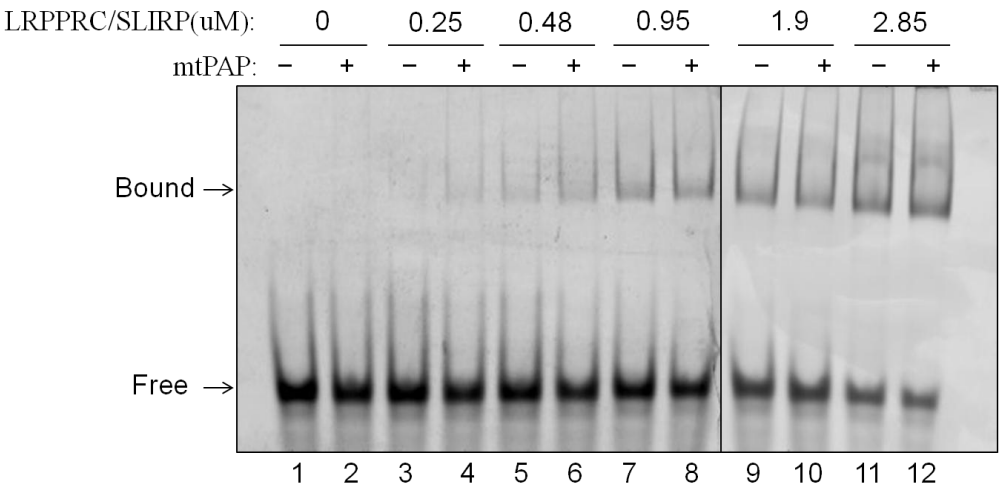

Figure 6.26. LRPPRC/SLIRP RNA binding capacity with and without mtPAP present

RNA substrate (0.25uM) was incubated with increasing amounts of LRPPRC/SLIRP in modified poly(A) buffer (see 6.2.7). Each reaction was performed with and without wild-type His-mtPAP (0.55uM) present. These reactions were electrophoresed through native 6% polyacrylamide/0.5x TBE gels at 4°C in 0.5x TBE buffer. Gels were then stained with 1x SYBR gold and imaged with a Typhoon FLA 9500.

indicating direct binding by the complex. The addition of mtPAP in addition to any of the reactions containing different amounts of LRPPRC/SLIRP did not appear to make any impact on the affinity of the complex for the RNA substrate. Binding reactions using His-mtPAP alone did not cause any shift in migration of the RNA substrate (data not shown). Unpublished data shared by Dr. Henrik Spahr indicated that while LRPPRC alone seems to bind RNA substrates in the EMSA, SLIRP does not appear to do so. Similar to the pro-

poly(A) effect, LRPPRC seems to be the dominant contributor within the complex to RNA binding *in vitro*.

6.4 Discussion

6.4.1 The N478D mutation causes a disruption of polyadenylation activity

One of the primary aims of the *in vitro* analysis of polyadenylation was to dissect the impact of the N478D mutation on mtPAP. Due to its location in an unresolved portion of the crystal structure (Bai *et al.*, 2011), assignment of a change in function is elusive. The initial hypothesis was that the mutation potentially disrupted a critical protein-protein interaction necessary for optimal polyadenylation of mitochondrial mRNA transcripts by mtPAP. This arose from the fact that the mutated residue is far from the active site of the enzyme, as well as the putative dimerization domain or RNA binding-like (RNL) domain. In the context of the mtPAP dimer, the unresolved regions within the "fingers" domains are asymmetrically distal to the dimerization interface shared by the bound monomers. This placement could potentially make the residues available for interacting with other factors, and is represented with a cartoon in Figure 6.27 for clarity. The analysis with far-

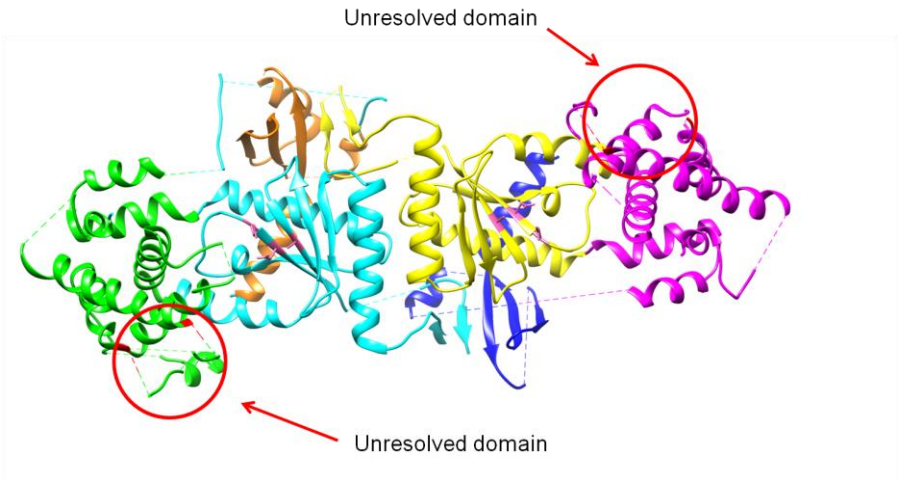

Figure 6.27. Locations of unresolved regions containing the N478D mutation in mtPAP dimer
Cartoon image of mtPAP dimer. Each monomer has the major domains labeled with different colors. For the monomer on the left, the domains are Palm (cyan), RNL (orange), and Fingers (green). For the monomer on the right, the domains are Palm (yellow), RNL (blue), and Fingers (purple). The catalytic residues are labeled pink, towards the center of the monomers. The unresolved domains, which contain the asparagine 478 residue, are circled on the image. The structure is available from the Protein Data Bank, PDB: 3QP1, reported by Bai *et all*., 2011. This image was generated using the Chimera 1.8.0 software, available from UCSF.

UV CD spectroscopy was consistent with this hypothesis, as the mutation did not appear to disrupt the secondary structure of the enzyme.

If this hypothesis was correct, the activity of the wild-type enzyme *in vitro* would be predicted to be less than optimal in adding poly(A) tails on to RNA substrates, as the necessary interacting-factor would not be present. The mutant would exhibit the same behavior, as the enzyme activity itself would not be disrupted. Only the interacting residues, presumably including the N478D residue, would be disrupted, but with the interacting factor not being present in the reaction in the first place, this change would not be observed. However, as clearly demonstrated in Figure 6.20, as well as many others, the His-mtPAP enzyme alone can generate poly(A) tails that are close to the range of lengths observed *in vivo*. The mutant polymerase only generates a short oligo(A) tail, indicating that the mutation effects protein-intrinsic properties governing its polyadenylation activity. One could postulate that LRPPRC, or the LRPPRC/SLIRP complex, is the missing interacting factor, due to the effect of longer poly(A) tails being generated in their presence, but this increase in extension is still exerted on the mutant mtPAP. This argues against the mtPAP-LRPPRC/SLIRP protein-protein interaction explanation of the N478D mutation's impact. Clear differences are seen between the wild-type and mutant protein activities, and these differences are similar to the MPAT data of endogenous transcripts. However, the many differences between an *in vitro* assay and *in vivo* results must be kept in mind. There may be residues required for potential interactions with mtPAP, but the data presented thus far does not support asparagine 478 of mtPAP being one of them.

As demonstrated in Figures 6.20 and 6.22, the mutant His-mtPAP generates significantly shorter poly(A) tails, even in the presence of LRPPRC/SLIRP. One potential explanation for this diminished polyadenylation capability is a defect in processivity. Precise confirmation of a processivity defect is reported as being difficult to establish, and the ability to distinguish discrete substrate binding events in this experimental system is not possible. In this scenario, the mutation may affect the ability of the polymerase to interact with substrates, be it the RNA polymer or ATP. If binding of the RNA is the root problem, this could take the form of disruption of interactions necessary for translocation (if this occurs) along the extending RNA polymer as mtPAP adds adenine ribonucleotides, or by disrupting the ability of the enzyme to associate initially with the 3' end. Similarly, a decreased affinity for ATP could lead to shorter adenylate tails, even if the RNA binding/association capabilities were intact. As EMSA results with wild-type His-mtPAP and RNA substrate did not show conclusive binding, it is difficult to make comparisons between wild-type and mutant RNA binding affinities.

Alternative possibilities are defects in catalytic activity, arising from a number of sources. Bai *et al.* predicted that the structure of mtPAP, while existing in a more closed conformation than canonical poly(A) polymerases in the absence of substrate, may yet adopt a more closed architecture upon substrate binding (Bai *et al.*, 2011). It is possible that the N478D mutation decreases the ability of the polypeptide to perform this conformational change. At this juncture we cannot distinguish the difference between a decrease in processivity or catalytic rate. Both states could produce the shorter oligo(A) tails observed. So while this study increased our understanding of the N478D mtPAP mutant, the precise impact of the substitution is still elusive.

6.4.2 The LRPPRC/SLIRP complex increases polyadenylation extension length

Chujo *et al.* reported that LRPPRC was a critical requirement for mtPAP to efficiently polyadenylate RNA substrates, with only oligoadenylation (length not specified) occurring in its absence. The results from my study presented here are in contrast to that claim, and are consistent with other reports in the literature (Nagaike, 2005; Bai *et al.*, 2011). In our assay, mtPAP is capable of independently generating 20-30nt poly(A) tails, significantly longer than the oligo(A) tails observed with LRPPRC knock downs. The addition of LRPPRC or LRPPRC/SLIRP caused further extension of the tail, potentially through an increase the processivity of mtPAP. Chujo *et al.* report that this effect is dose-dependent for LRPPRC, with increases observed up to 1.25uM LRPPRC. The results of my study partially contrast with this observation. The longer poly(A) tails in the presence of LRPPRC was the same at concentrations of either 0.5uM and 1.25uM, indicating that beyond quantities equimolar with mtPAP (0.55uM) the effect is likely saturated. For concentrations of LRPPRC less than equimolar with mtPAP, a dose-dependent effect may be observable. Our results are consistent with LRPPRC being the dominant effecter of the poly(A) extension within the LRPPRC/SLIRP complex. In my preliminary data, when His-mtPAP was paired with SLIRP alone, the further extension of poly(A) tails beyond that generated by mtPAP alone was not observed. However, the effect from the combined LRPPRC/SLIRP complex is greater than LRPPRC only paired with His-mtPAP. As Chujo *et al.* do not show their data on the

effect of SLIRP alone, it is difficult to know how consistent my results are compared to theirs.

The critical question is, how does LRPPRC and LRPPRC/SLIRP affect polyadenylation activity? A hypothesis posed by Chujo *et al.* is that LRPPRC acts to prevent mRNA 3'-end secondary or tertiary structure forming, presenting mtPAP with an optimal substrate. The 40nt RNA substrates used in the high-resolution poly(A) assays are not predicted to be highly structured at the 3'-end, nor predicted to adopt any complex structure in general. LRPPRC and LRPPRC/SLIRP were both able to exert their effects on poly(A) tails when presented with the RNA 40-mers. While LRPPRC may be involved with 3' unwinding *in vivo*, it does not appear a property required *in vitro* for promotion of polyadenylation. These results from our laboratory are particularly relevant, as the RNA substrates both 40nt oligomers and 248/277nt larger RNA fragments actually correspond to the 3' sequences from *MTATP6* and *MTND3*, rather than "mimicking the 3' terminal

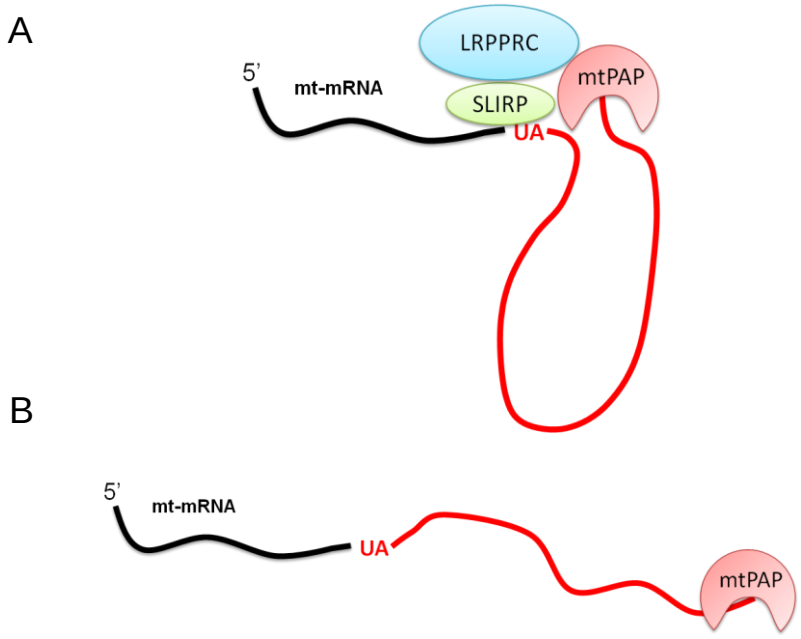

Figure 6.28. Hypothetical mechanism of LRPPRC/SLIRP and mtPAP interaction

A. In a manner potentially similar to the nuclear mechanism of PAP, PAPBN1 and CPSF, mtPAP, LRPPRC and SLIRP may constitute a complex assembling on the 3' ends of mt-mRNAs. The complex would coordinate the extension of poly(A) tails, facilitating a processive elongation of the tail to a certain length, which then forces disassembly of the complex and dissociation of mtPAP. **B**. Without the presence of LRPPRC or LRPPRC/SLIRP, mtPAP is free to adenylate in a non-coordinated manner. This allows the enzyme opportunities to extend poly(A) tails further than observed *in vivo* (above). The mt-mRNA coding region is shown in black, and the poly(A) tail is colored red.

region of mt-mRNAs" (Chujo *et al.*, 2012). Extended poly(A) tails in the presence of LRPPRC/SLIRP were observed when using an RNA 40-mer corresponding to an upstream fragment of *MTND3*, further suggesting that the effect may not be constituted by mt-mRNA-specific 3' structure unwinding. However, our results do agree with one principle of the hypothesis presented by Chujo *et al.*, which is that the LRPPRC effects does not appear to be sequence-specific.

It is possible that LRPPRC, SLIRP, and mtPAP all interact in some fashion at the 3' end of RNA, and perhaps the increased stabilization that occurs from that interaction allows more efficient polyadenylation. In poly(A) reactions from the low-resolution *in vitro* assay, when other factors were absent, His-mtPAP generated the strongest signal for poly(A) that were similar to those observed physiologically but also generated tails significantly exceeding this range. One explanation is the enzyme is capable of much higher processivity and extensions, but this capability is curbed by protein-protein interactions *in vivo.* Without the length-limiting system present *in vitro*, the polymerase's intrinsic capacity for generating poly(A) tails can go to its limit. Another explanation is the "longer lengths" observed are merely an artifact of the polyacrylamide/urea gel electrophoresis. As this gel-type is strongly denaturing, it is unlikely that the RNA is aggregating or persisting in higher order structures.

A consistent effect observed was the disappearance or reduction of these presumably longer poly(A) tails upon introduction of LRPPRC or LRPPRC/SLIRP. The protein or complex may in fact act as a length-regulating factor, even as it affects poly(A) tail length within the physiological range. In a manner similar to CPSF's role in nuclear polyadenylation, the interaction of LRPPRC, SLIRP, and mtPAP may coordinate and control the extension of the poly(A) tail so that it "loops" out, or coils into a globular structure (Kuhn *et al.*, 2009). This is in contrast to mtPAP acting alone, which when untethered by protein-protein interaction, can extend much further. However this extension may be less processive and occur at a slower rate. Both of these scenarios are represented in Figure 6.28. The "looping" extension of the poly(A) tail may be mediated by the continuous contact between mtPAP and LRPPRC/SLIRP as nucleotides are added, and the physiological length is the number of nucleotides added to the 3' end that cause the contact to break. This could be from torsion of the poly(A) tail, or other disruptive forces that occur as tail length grows.

While there are other reports indicating that LRPPRC and/or SLIRP can fulfill other roles in mitochondria, such as stabilizing non-translated mt-mRNAs (Ruzzenente *et al.*, 2012), this discussion is limited to the observations made *in vitro*. There are

consistent effects observed with just the three proteins together which are difficult to resolve, independent of ancillary functions for the proteins in mitochondria and in other cellular compartments.

6.4.3 The role of SLIRP

A curiosity that persists is the role of SLIRP in polyadenylation. The results presented in this study clearly show that there is an additive effect on poly(A) length extension from SLIRP complexing with LRPPRC. However it is also true that LRPPRC appears to exert the vast majority of this effect. Both LRPPRC and SLIRP have been reported to possess RNA binding domains, and LRPPRC/SLIRP binds mt-mRNA coding regions (Baughman *et al.*, 2009; Sasarman *et al.*, 2010; Chujo *et al.*, 2012). It is possible that SLIRP is more involved with the RNA interactions, while LRPPRC interacts with mtPAP. Thus when complexed, the two roles of the factors synergistically promote polyadenylation. The complex has been reported to not bind poly(A) sequences (Chujo *et al.*, 2012). Again, the LRPPRC/SLIRP complex may be more analogous to the nuclear CPSF complex, as opposed to the canonical nuclear poly(A) binding protein PABPN1 (Kuhn *et al.*, 2009). However, while not part of this study, the unpublished results from Nils-Goran Larsson's lab indicate that SLIRP does not appear to shift the size of RNA substrates in EMSA gels, while LRPPRC and LRPPRC/SLIRP clearly cause shifts. This argues against SLIRP acting as more of an RNA binding mediator in the context of polyadenylation. His-mtPAP did not cause shifts in EMSA gels either, nor did it affect the shifts generated by LRPPRC/SLIRP (Figure 6.26).

If there is a mitochondrial poly(A) binding protein, it is not currently identified. It is quite possible this potential player in the process could alter the dynamics of polyadenylation yet more from that observed *in vitro*. The necessity of investigating what other factors may be involved with polyadenylation in mitochondria, and elucidating more specific aspects of potential LRPPRC and SLIRP interactions with mtPAP, was clear. Towards that end, experiments undertaken to explore mtPAP interacting partners are presented in the next chapter.

6.4.4 Oligoadenylation of mitochondrial mRNAs

The *in vitro* results using the mutant enzyme argue against the existence of a separate oligoadenylase generating the oligo(A) tails on mt-mRNAs. The oligo(A) tail was observed in experiments knocking out or down LRPPRC, and siRNA-mediated depletion of mtPAP. If a separate oligo(A) polymerase exists, and was generating the 5-10nt tails present *in vivo*, one might predict the N478D mtPAP would not be adding any further nucleotides, as the short tail observed would have been a product of another factor. This is clearly not the case, as the N478D His-mtPAP enzyme generates short oligo(A) tails that match the lengths (5-10nt) observed *in vivo* for the 1432A>G homozygous mutant fibroblasts.

Utilization of oligoadenylated RNA substrates by mtPAP did not show different polyadenylation profiles from those generated from RNA with a naked 3' terminus. The oligo(A) extension has previously been hypothesized to act as a primer for further polyadenylation by mtPAP. The results of this study do not support this assertion. None of the experiments with mtPAP polyadenylating oligo(A) RNA indicated higher activity, rate, or processivity.

A potential explanation of the various conditions leading to oligo(A) tails, could be the involvement of deadenylases. Overexpression of PDE12 led to reduction in poly(A) tail lengths on mt-mRNAs, and siRNA knock-down of hPNPase led to small extensions of the tails. Expression of a wild-type *PAPD1* transgene in fibroblasts caused extra extension of mt-mRNA poly(A) tails (Chapter 5). These data suggest that part of the regulation of mt-mRNA poly(A) tail length may partially be the result of opposing adenylase and deadenylase activities. Perhaps if mtPAP/LRPPRC/SLIRP interact at the 3' end of mt-mRNAs, they prevent deadenylases from degrading the tail. When mtPAP is knocked down, or mutated (as in the case of the N478D enzyme), a low level of activity remains. When LRPPRC is removed, the three proteins do not coordinate at the 3' end of mt-mRNA. Thus, mtPAP polyadenylates, then dissociates, allowing degradation to occur, or the deadenylating factor is capable of displacing mtPAP in the first place. This is speculation, but if true would reconcile multiple lines of evidence. More research into this area is necessary.

In summary, this series of in vitro experiments has provided insight into the enzymatic capabilities and substrate specificities of both the wild-type and N478D mutant mtPAP. In addition, the length extensions observed in the presence of LRPPRC and LRPPRC/SLIRP aid in clarifying the dynamic environment at play during mt-mRNA polyadenylation, and the effects these trans-acting factors can exert. While questions

remain, the results of this study are critical to furthering our understanding of post-transcriptional mechanisms and their downstream impact.

Chapter 7

Investigating mtPAP interacting factors

7.1 Introduction

Polyadenylation in the nucleus is a dynamic and multifaceted process, carried out by multi-component protein machinery. The nuclear poly(A) polymerase requires multiple factors to bind its RNA substrate at the right location, boost processivity, and coordinate extension (Mandel *et al.*, 2008; Kuhn *et al.*, 2009). The mitochondrial poly(A) polymerase appears to be capable of several of these tasks unaccompanied, however there are proteins that have been reported to interact with mtPAP and be important for function (Chujo *et al.*, 2012; Ruzzenente *et al.*, 2012; Kazak *et al.*, 2013). While many aspects of mitochondrial polyadenylation can be reconstituted *in vitro*, it is unlikely that the currently identified factors, i.e. mtPAP, LRPPRC, SLIRP, and PABPC5 act alone. However, from the current literature it is unclear how polyadenylation is coupled with mechanisms such as transcriptional processing or ribosome loading. While the vast majority of polyadenylation in the nucleus is physically separated by cellular structures from the translation machinery, this partitioning is not in place in mitochondria. It is possible, therefore, that transcriptional processing is more tightly coupled with the translation apparatus, and mtPAP could be functionally tied to one process or the other in novel ways not observed in the nucleus.

Towards this end, my experiments were designed with the aim of identifying factors that interact with mtPAP, and are potentially involved with polyadenylation events. Several lines of investigation were designed to provide details of possible interactions and associations. Recently, the existence of mitochondrial RNA granules (MRGs) has been reported (Jourdain *et al.*, 2013), marked by the presence of the protein GRSF1. Significant portions of RNA processing occur in these granules, with demonstrated interactions of GRSF1 and RNase P. This mitochondrial subcompartment presents an attractive location for investigating the localization of mtPAP. Experiments were designed to identify whether mtPAP is also present in the MRGs, and if so, this would provide details of some factors that the enzyme could physically encounter.

Due to the potential for polyadenylation in mitochondria occurring as an event tightly coupled with translation, associations with mtPAP and the mitochondrial ribosome were also examined. Direct binding partners of mtPAP were to be investigated through immunoprecipitation experiments. The *in vitro* data using recombinant wild-type and

mutant mtPAP had shown that longer poly(A) tails were generated in the presence of LRPPRC and the LRPPRC/SLIRP complex. This led to the hypothesis that these proteins may be directly interacting in some fashion in order to facilitate/regulate the poly(A) extensions observed. Thus, direct binding associations between mtPAP and LRPPRC and SLIRP were particularly examined, in order to find evidence supporting this potential model. As the effects on gene expression resulting from oligo(A) tails in fibroblasts had not explicitly revealed a role for the tail beyond stop codon completion, investigation of modulatory factors for polyadenylation was performed to increase our understanding of the molecular mechanisms involved. This chapter presents the results of these lines of inquiry.

7.2 Materials and methods

7.2.1 Immunoprecipitation

Isolated crude mitochondria were prepared as detailed in 2.2.6.2. 20ul of magnetic Dynabead Protein G beads (Novex) per IP reaction were washed 3x with 100mM Na-phosphate pH 8.1 buffer. The beads were then suspended in 70ul 100mM Na-phosphate pH 8.1 buffer, and 10ug of α-mtPAP mouse monoclonal antibody (GeneTex GTX70156) was added to the solution, to generate the Protein G-Ig complex. This mixture was rotated at room temperature for 1 hour. While the antibody and beads were incubating, crude mitochondria were lysed by suspension in 150ul chilled lysis buffer (50mM Tris 7.4, 150mM NaCl, 1mM EDTA, 1% Triton X-100, 1mM PMSF, 10mM $MgCl_2$), then incubated on ice for 30 minutes. The insoluble fraction of the mitochondrial lysate was then pelleted by centrifugation at 16,000*g* at 4°C, for 15 minutes. The supernatant was collected, and protein concentration determined via Bradford assay. The magnetic bead/antibody complexes were then washed 3x with chilled lysis buffer. Equal amounts of lysate protein (800ug) were added to immunoprecipitation reactions if several samples were to be analyzed. Mitochondrial supernatant was incubated with the magnetic bead/antibody complexes at 4°C, rotating, for 1 hour. The beads/antibodies/antigen complexes were then collected and washed 5x with chilled lysis buffer. To elute the target antigen and co-immunoprecipitants, the bead/antibodies/antigen complexes were suspended in 1x Laemmli buffer, and heated to 70°C for 10 minutes, shaking at 1000rpm in an Eppendorf thermomixer. Immunoprecipitation samples were then either stored at -80°C, or directly loaded onto 12% SDS-polyacrylamide gels for analysis by immunoblotting.

For investigating protein-protein interactions mediated by RNA, the co-IP procedure was carried out as detailed above, with the following alterations: In the samples that were to have RNA removed, the mitochondrial lysate (800ug) had 5ug of RNase A introduced and was incubated at 10°C for 15min. For RNA-protected samples, all buffers and solutions were made up with DEPC-treated H_2O, and the isolated mitochondria were lysed in 150ul chilled lysis buffer that included 100U of SUPERase-In (Invitrogen) RNase inhibitor. For washes of the bead/antibodies/antigen complexes, lysis buffer contained 20U SUPERase-In/ml.

7.2.2 Isokinetic sucrose gradients

Chilled, filter-sterilized gradient buffer was prepared (50mM Tris pH 7.2, 10mM MgOAc, 40mM NH_4Cl, 100mM KCl, 1mM PMSF, 50ug/ml Chloramphenicol). Solutions of 10% and 30% sucrose were prepared in gradient buffer (0.5g sucrose in 5ml buffer and 1.5g sucrose in 5ml of buffer). 0.5ml of 10% sucrose solution was pipetted into an ultracentrifuge tube (Beckman Coulter 343778), with 0.5ml 30% sucrose injected under the 10% sucrose fraction using a 1ml syringe and needle. This was done gently, allowing 2 distinct clear fractions to be formed. The ultracentrifuge tube was then plugged using a rubber plug, making sure not to contact sucrose solution. On a balanced Gradient Master 107 (Biocomp), the sucrose fractions were mixed, using the TL55 program, short sucrose 10%-30%, 55sec/0.85. Once mixed, the gradient was stored on a flat surface, undisturbed, at 4°C, for 1 hour. The Optima TLX ultracentrifuge (Beckman) was turned on, and allowed to cool to 4°C. During the centrifuge cooling period, cells were harvested from a confluent T75 flask and pelleted as detailed in 2.2.6.2. On ice, the cell pellets were lysed in 80ul lysis buffer (50mM Tris 7.4, 150mM NaCl, 1mM EDTA, 1% Triton X-100, 1mM PMSF, 10mM $MgCl_2$, 1x protease inhibitors). The lysate was incubated at 4°C, rotating, for 30 minutes. Then the non-soluble fraction of the cell lysate was pelleted by centrifugation at 4°C, for 10 minutes, at 12,000*g*. The supernatant was collected, and protein concentration determined via Bradford assay. The plug on the gradient was carefully removed, and 900ug of lysate carefully loaded on top of the sucrose gradient, making sure not to disrupt gradient. The tube was then placed in the ultracentrifuge. The ultracentrifuge was set to deliver 100,000*g* for 2 hours 15 minutes at 4°C (acceleration = 1, and deceleration = 4). Upon finishing centrifugation, 100ul fractions were taken from the gradient, starting at the top (10% sucrose) and moving towards the bottom (30% sucrose). In total, 11-12 fractions were typically collected. These fractions were then analyzed by SDS-PAGE and immunoblotting.

7.2.3 Mass spectrometry analysis of immunoprecipitated samples

Immunoprecipitation (IP) experiments were carried out using an α-mtPAP antibody (GeneTex GTX70156), as described above. The IP samples were then separated by 12% SDS-PAGE, and stained with Coomassie brilliant blue. Stained bands suspected of

corresponding to mtPAP and unknown proteins were carefully excised from the gel, deposited in microtubes, and stored at -20°C. Analysis by mass spectrometry of mtPAP co-immunoprecipitation samples was carried out by the Radboud Proteomics Centre in Nijmegan, the Netherlands.

7.2.4 Immunofluorescent microscopy

Analysis of mtPAP localization was performed by Alexis Jourdain at the University of Geneva. 143B.206 osteosarcoma cells were either transiently transfected with a FLAG-tagged mtPAP construct (pcDNA5/FRT/TO-mtPAPFLAG, see 5.2.1) and mtPAP detected using α-FLAG antibodies (Sigma F1804), or the endogenous mtPAP was detected using α-mtPAP antibodies (GeneTex GTX70156). The cells were fixed using 4% paraformaldehyde. Immunodetection was carried out in PBS + 0.1% Triton X-100 + 3% w/v BSA, with antibodies targeting the FLAG-tag, mtPAP, or GRSF1. Essentially as described in (Jourdain *et al.*, 2013).

7.2.5 Stable transfection of HEK293 Flp-In™ T-REx™ cells with FLAG-tagged mtPAP

HEK293 Flp-In™ T-REx™ (hereafter referred to as HEK293) cells were seeded in 6-well tissue culture plates (Corning) 1 day before performing transfections. These cells are normally cultured with 10ug/ml Blasticidin^S and 100ug/ml zeocin. These antibiotics were omitted for the transfection steps. For transfection, two aliquots were mixed of 1.8ug pOG44 (1.8ul of 1 ug/ul), which encodes the Flp recombinase, and 0.2ug (4ul of 50ug/ul) pcDNA5/FRT/TO-mtPAPFLAG in 100ul of DMEM, for a total of 2ug DNA.
The two aliquots were used to mix ratios of DNA:Superfect of 1:5 and 1:7.5

1:5 ratio - 2ug DNA (100ul) + 10ul SuperFect (Qiagen)
1:7.5 ratio - 2ug DNA (100ul) + 14ul SuperFect

To the DNA/SuperFect mix, 600ul of complete DMEM was added, mixed gently 5x by pipetting, and allowed to incubate at room temperature for 10 minutes. At this point cells were washed 1x with Dulbecco's A-PBS, then the DNA/SuperFect mix was added to the wells. The cells were incubated with the mix for 3 hours at 37°C. After the incubation, the

DNA/SuperFect mix was removed and replaced with fresh warmed complete DMEM. After 24 hours in complete DMEM, Hygromycin^{B} was introduced to the culture media at a final concentration of 100ug/ml. Stable transfectants were selected, generally over a 2 week period, and individual lines generated by isolating clonal colonies.

HEK293 cells expressing N478D mtPAP-FLAG were generated according to the same protocol, utilizing the 1432A>G mutated version of the pcDNA5/FRT/TO-mtPAP-FLAG construct. This mutation was introduced using the Quikchange II Site-Directed Mutagenesis kit (6.2.2) with Mut-mtPAPF and Mut-mtPAPR primers (2.2.4.4). Protein expression was induced by 1ug/ml of tetracycline introduced into the culture media. Confirmation of tagged-protein expression was completed by immunoblotting using α-FLAG antibodies.

7.3 Results

7.3.1 Identification of mtPAP interaction partners by immunoprecipitation and mass spectrometry

In order to explore the possibility of proteins directly binding to mtPAP, immunoprecipitation (IP) experiments were carried out, utilizing a mouse monoclonal antibody recognizing mtPAP. The initial cells used to establish these IP conditions and efficacy of the antibody for IP were HEK293 cells, as they are enriched in mitochondria relative to fibroblasts. Crude mitochondria were isolated from the HEK293 rather than whole cell lysate to enrich the levels of mitochondrial proteins in the input material for the IP. Controls for the IP consisted of beads coated with either a goat α-MNK1 antibody for an IgG control, or beads without antibody bound. Immunoblotting for mtPAP was carried to confirm effective immunoprecipitation by the α-mtPAP mouse monoclonal antibody. Once confirmed, the Coomassie staining and mass spectrometry was then performed as described below.

To parse the interactions mediated via binding to RNA transcripts, some mitochondrial lysates were incubated with RNase A prior to incubating with bead/antibody complexes. Non-RNase A treated lysates were processed in an RNA-protective fashion. This included usage of DEPC-treated H_2O and introduction of RNase inhibitors.

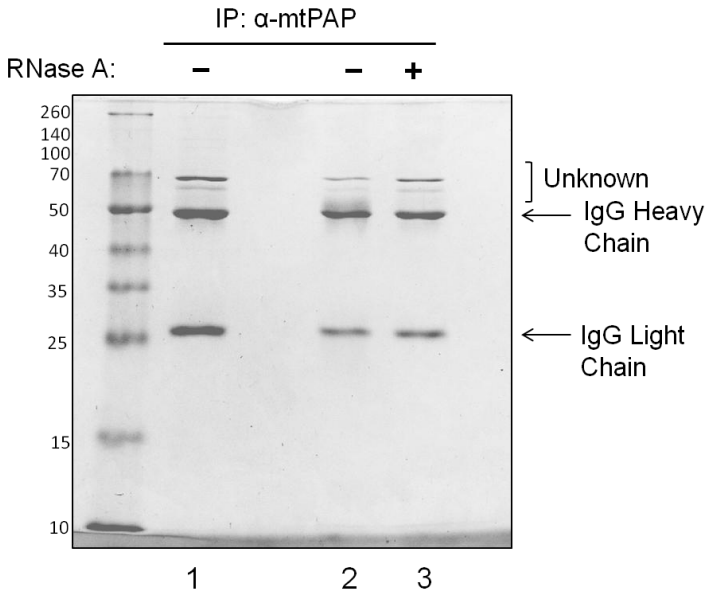

Figure 7.1. Coomassie staining of mtPAP co-IP samples
Coomassie Brilliant Blue stained 12% SDS-PAGE of proteins isolated from IP reactions using antibody against mtPAP. Preparation treated with RNase A is shown in lane 3, those processed in an RNA-protected manner are shown in lane 2. The gel was imaged using white light settings on the ChemiDoc MP (Bio-Rad).

The initial IP samples were separated via SDS-PAGE, and stained with Coomassie brilliant blue, in order to identify major protein

species present in the sample, as well as obtain an approximation of their abundance. These results are shown in Figure 7.1. Beyond the two stained bands corresponding to the IgG heavy and light chains of the α-mtPAP antibody, there were only two major bands observed at approximately between 60 and 70 kDa, in all co-IP samples. A band appeared at a slightly increased size, smearing up from the IgG heavy chain in a non-RNase A treated co-IP sample. These three bands, termed "smeared", "65kDa", and "70kDa", were carefully excised from the gel, placed into microtubes, and stored at -20°C. The gel slices were then sent to the Nijmegen Proteomics Facility at the Radboud University Nijmegen Medical Center for analysis via mass spectrometry.

The results of the analysis by mass spectrometry are shown in Table 7.1. The most

Table 7.1. Analysis of mtPAP co-immunoprecipitation by mass spectrometry.

GROUP	RANK	PROTEIN	emPAI 65 kDa	emPAI 70 kDa	emPAI Smear
1	1	gi|283436222|ref|NP_001164006.1| ATPase family AAA domain-containing protein 3A isoform 2 [Homo sapiens]	3.262158829	14.31740464	1.346228848
2	1	gi|75677353|ref|NP_114127.3| ATPase family AAA domain-containing protein 3B [Homo sapiens]	1.301807313	5.210169419	0.675474919
8	1	gi|194018490|ref|NP_001034300.2| ATPase family AAA domain-containing protein 3C [Homo sapiens]	1.11348904	4.956621435	0.496235656
3	1	gi|119395750|ref|NP_006112.3| keratin, type II cytoskeletal 1 [Homo sapiens]	1.894266125	1.768902684	1.030917621
6	1	gi|31542947|ref|NP_002147.2| 60 kDa heat shock protein, mitochondrial [Homo sapiens]	2.16227766	1.319447866	0
7	1	gi|190194365|ref|NP_060579.3| poly(A) RNA polymerase, mitochondrial precursor [Homo sapiens]	2.403414883	1.189906295	0.554137221
9	1	gi|55956899|ref|NP_000217.2| keratin, type I cytoskeletal 9 [Homo sapiens]	0.865663579	0.957341781	0.333521432
22	1	gi|136429|sp|P00761.1| TRYP_PIG Trypsin	1.335721469	0.832980711	0.832980711
5	1	gi|195972866|ref|NP_000412.3| keratin, type I cytoskeletal 10 [Homo sapiens]	1.371373706	0.77827941	1.487902367
4	1	gi|47132620|ref|NP_000414.2| keratin, type II cytoskeletal 2 epidermal [Homo sapiens]	0.843422992	0.715437896	0.910952975
15	1	gi|4508005|ref|NP_003440.1| tripartite motif-containing protein 26 [Homo sapiens]	0	0.479833198	0
12	1	gi|167466173|ref|NP_005337.2| heat shock 70 kDa protein 1A/1B [Homo sapiens]	0	0.458594012	0
35	1	gi|16751921|ref|NP_444513.1| dermcidin preproprotein [Homo sapiens]	0	0.389495494	0.389495494
16	1	gi|4757732|ref|NP_004199.1| apoptosis-inducing factor 1, mitochondrial isoform 1 precursor [Homo sapiens]	0	0.371686619	0
31	1	gi|24497605|ref|NP_057637.2| nuclear pore glycoprotein p62 [Homo sapiens]	0	0.258925412	0
21	1	gi|56237027|ref|NP_006537.3| insulin-like growth factor 2 mRNA-binding protein 1 isoform 1 [Homo sapiens]	0	0.216483949	0

significant protein identified in the "65kDa" and "70kDa" gel slices is ATAD3A, with ATAD3B and ATAD3C present to lesser extents. These proteins are most highly represented in the gel slice corresponding to 70kDa. In the "65kDa" gel slice, ATAD3A is also highly represented, and the next most abundant protein is mtPAP. This suggests a strong association of ATAD3 with mtPAP. Both mtPAP and ATAD3 have predicted masses of approximately 66kDa, and may be overlapping in terms of staining on the gel due to similar migration. The emPAI values obtained for other proteins identified in the

co-IP samples did not suggest significance. Mitochondrial HSP60 was indentified in the "65kDa" slice, but this was not investigated further. The "smear" gel slice was likely to be the result of keratin contamination from sample handling.

7.3.2 Immunoblot analysis of mtPAP co-immunoprecipitations

The limitation of using immunoblotting for identifying protein-protein interactions is the necessity of assuming what the targets may be and of there being sufficient amounts to be detectable. Since these experiments were initiated prior to performing mass spectrometry on co-IP samples, the priority factors to probe for were LRPPRC and

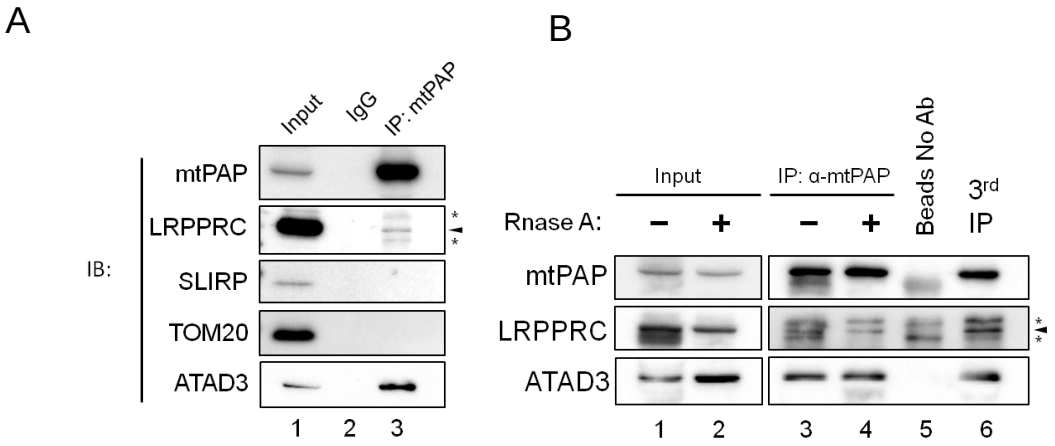

Figure 7.2. Immunoblot analysis of mtPAP co-immunoprecipitation.
Eluates from the immunoprecipitations with MNK-1 IgG control (lane 2) and mtPAP (lane 3) antibodies were decorated with antibodies as indicated. Specific band corresponding to LRPPRC is labeled with black arrow. Non-specific bands are labeled with asterisks. TOM20 was used as a control for input (lane 1) contamination.

SLIRP, based largely on the *in vitro* data with recombinant proteins, where these factors had been reported to interact with mtPAP, and the knockout experiments performed in transgenic mice. Once the mtPAP co-IP samples were analyzed by mass spectrometry, confirming the presence of ATAD3, this protein became the next priority. These resulting western data are shown in Figure 7.2 There was very weak signal at the 130 kDa size in the co-IP sample (Figure 7.2A, lane 3). The signal was significantly diminished compared to input, and sandwiched between two non-specific bands (marked by *). SLIRP was not detected in the co-IP sample, surprisingly, considering it is reported to show robust binding of LRPPRC. ATAD3 was also detected as immunoprecipitated by mtPAP (lane 3), in correspondence with the mass spectrometry data.

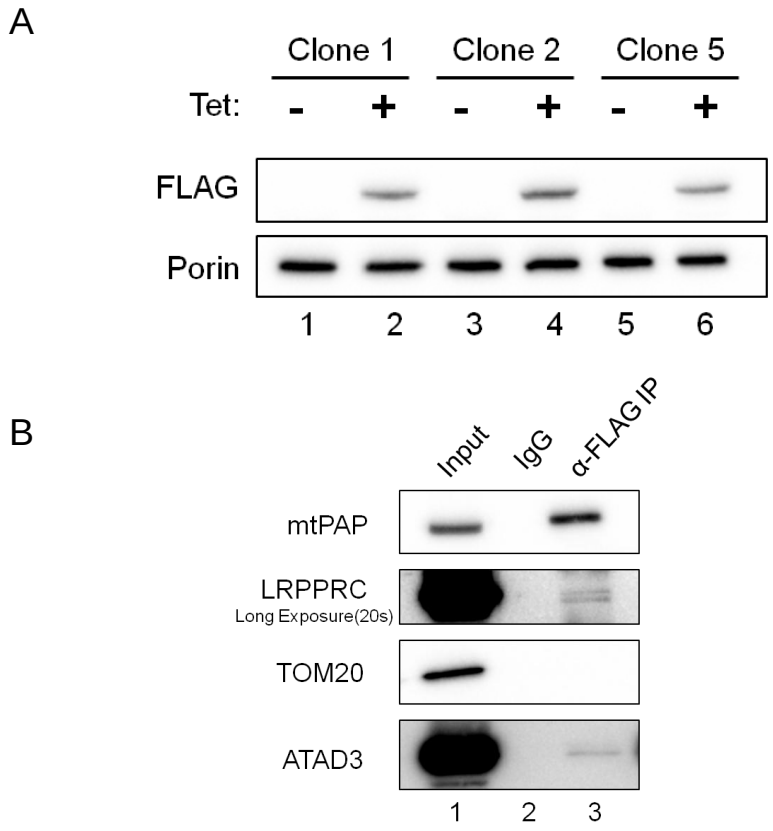

Figure 7.3. Expression and co-immunoprecipitation of mtPAP-FLAG
A.. Western analysis was performed to determine expression of FLAG-tagged mtPAP in clonal HEK293 cells transfected with pcDNA5/FRT/TO-mtPAP-FLAG following 3 days induction (tetracycline 1ug/ml). **B.** Mitochondria from "clone 2" were used for α-FLAG co-IP. Input (lane 1) and eluate (lane 3) were immunoblotted against mtPAP, LRPPRC, and ATAD3. TOM20 was used as a control for input contamination.

To examine whether potential interactions of LRPPRC and ATAD3 with mtPAP were mediated by RNA binding, RNase A-treated mitochondrial lysates were subjected to immunoprecipitation using the anti-mtPAP antibody, and analyzed by immunoblotting and compared to RNA-protected lysates. As shown in Figure 7.2B, neither the weak signal at 130kDa nor ATAD3 levels present in the co-IP samples changed upon RNase A treatment of the mitochondrial lysates. This suggested that if ATAD3 or LRPPRC possibly interact with mtPAP, these interaction may not be established through shared RNA binding.

To further confirm possible interactions between mtPAP, LRPPRC, and ATAD3, FLAG-tagged mtPAP was expressed in HEK293 cells, and the Sigma M2 α-FLAG monoclonal antibody used to immunoprecipitate mtPAP. It was expected that the initially observed interactions would be recapitulated using the FLAG-IP approach. However, previous attempts to use the α-FLAG antibody with FLAG-tagged mtPAP in the lentivirus-transduced fibroblasts (Chapter 5) produced poor results. As the system using HEK293 cells is well established in our lab, the FLAG-IP was carried out and analyzed by immunoblotting. Clones of the HEK293 line expressing tetracycline-inducible mtPAP-

FLAG were tested to determine expression levels (Fig 7.3A lanes 2, 4, 6). Good expression was identified in all 3 clones and clone 2 was selected for the FLAG-IP. The results, shown in Figure 7.3B, demonstrate interactions of LRPPRC and ATAD3 were not observed.

To rule out the possibility of the N478D mutation disrupting the potential interactions with either LRPPRC or ATAD3, co-IP experiments were performed using crude mitochondria isolated from control and 1432A>G mutant fibroblasts. The total input of mitochondrial lysate (Fig 7.4 lanes 1 and 2) was substantially less than used in the co-IP experiments utilizing HEK293 cells, with 250ug of fibroblast mitochondrial lysate versus 900ug HEK293 mitochondrial lysate. This likely had an impact on visualization of LRPPRC in the co-IP samples, as it could not be detected for the control (Fig 7.4 lane 4) and so it was not possible to determine if the level was affected in the mutant cell line (Fig 7.4 lane 3). ATAD3 is clearly present in the eluates of both the co-IP samples, and the level does not differ between wild-type or mutant fibroblasts (Fig 7.4 lanes 3 and 4) and not detectable in the IgG control (lane 5).

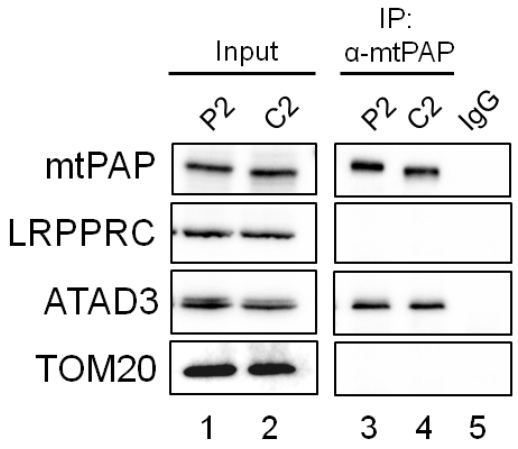

Figure 7.4. Wild-type versus N478D mtPAP co-immunoprecipitation
Mitochondrial lysate (250ug) was prepared from control (Lane 2) and homozygous 1432A>G (lane 1) fibroblasts. Eluates from immunoprecipitation reactions were probed for the presence of LRPPRC and ATAD3. TOM20 was used as a control for input contamination.

7.3.3 Investigating mtPAP associations with the mitochondrial ribosome

The processes of mitochondrial transcription and translation have been hypothesized to be tightly coupled, based on data from *S. cerevisiae* (Shadel, 2004). To investigate the possibility of mtPAP interacting with factors involved in translation, the sedimentation profile of mtPAP was examined, along with components of the mitochondrial ribosome. In addition, the previously indentified factors, LRPPRC and ATAD3, were examined. Any potential changes as a result of the N478D mutation were

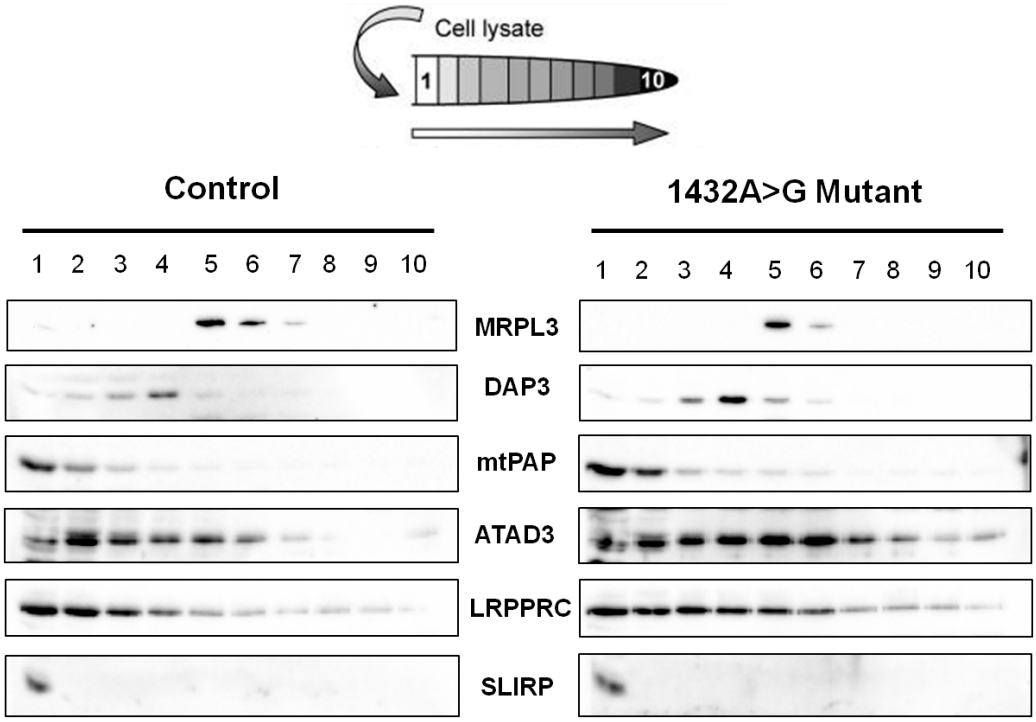

Figure 7.5. Migration of mtPAP in isokinetic sucrose density gradients
Fibroblast whole cell lysate (900ug) was separated through a 1ml 10-30% sucrose gradient. Fractions were analyzed by immunoblotting using MRPL3 and DAP3 as indicators of the large and small mitoribosomal subunits, respectively. The position in the gradient of mtPAP and the proteins identified as associated were also determined. The left panel corresponds to analysis of wild-type fibroblasts, and the right panel corresponds to analysis of the homozygous 1432A>G mutant fibroblasts.

also to be determined. The material used for the gradients was mitochondrial lysate isolated from control and 1432A>G mutant fibroblasts. The analysis of the sedimentation profiles consisted of immunoblotting fractions taken from the sucrose gradients.

Figure 7.5 shows that in both wild type and mutant cell lines mtPAP migrates primarily with the free fraction (fraction #1). No significant shift in fraction migration occurs as a result of the N478D mutation. DAP3 and MRPL3 were blotted as indicators of migration for the small and large subunits of the mitoribosome, respectively. Neither of these markers appeared to change migration status in the mutant fibroblasts. Further, the signal for wild-type and N478D mtPAP does not co-migrate with the markers for either the small or large subunits of the mitoribosome.

Both LRPPRC and ATAD3 show changes in their positions in the mutant fibroblasts compared to wild-type. In the control cells the majority of the signal for ATAD3 is in fraction 2, with the remaining signal spread between fractions 3 and 6. In the mutant cells, ATAD3 appears to be in complexes of higher molecular weights as the strongest signal has shifted to fractions 5 and 6. For LRPPRC, the majority of the wild type signal is in fractions 1-4, although there is very weak signal throughout all the fractions. In the mutant fibroblasts the signal is distributed in fractions 1-6. For both wild-type and mutant, SLIRP is only found within the free fraction (fraction 1).

These sucrose gradients did not visualize significant amounts of monosome, as is common for most cell lines. Thus, any changes resulting from the N478D mutation on assembly of the monosome could not be observed. The signals for MRPL3 and DAP3 are more intense for the mutant cells, due to exposure times necessary for visualization. This was consistent with the *de novo* protein synthesis data from wild-type and mutant fibroblasts, which also did not indicate any major uniform translation defects, making significant ribosome disruption unlikely as translation of all mtDNA-encoded peptides would be affected.

7.3.4 Localization of mtPAP in mitochondrial RNA granules

The discovery of mitochondrial RNA granules as discrete foci of RNA processing (Jourdain *et al.*, 2013) presented a logical location for mt-mRNA polyadenylation to take place . My host lab established a collaboration with Professor Jean-Claude Martinou's laboratory at the University of Geneva to carry out co-localization studies with mtPAP, and GRSF1 as a marker for the RNA granules. The immunofluorescence microscopy was performed by Alexis Jourdain, the lead author of the paper reporting the existence of the granules (Jourdain *et al.*, 2013). The pcDNA5/FRT/TO-mtPAPFLAG construct was sent to Professor Martinou's lab to be transiently expressed in 143B.206 osteosarcoma cells, as Mr Jourdain was most confident of identifying the localization of mtPAP using α-FLAG antibodies in these cells. The mouse monoclonal α-mtPAP antibody was also sent to their lab to also allow examination of the endogenous localization of mtPAP. It was hoped that these two approaches would ideally produce mutually supportive results.

The microscopy data for localization of wild-type endogenous and FLAG-tagged

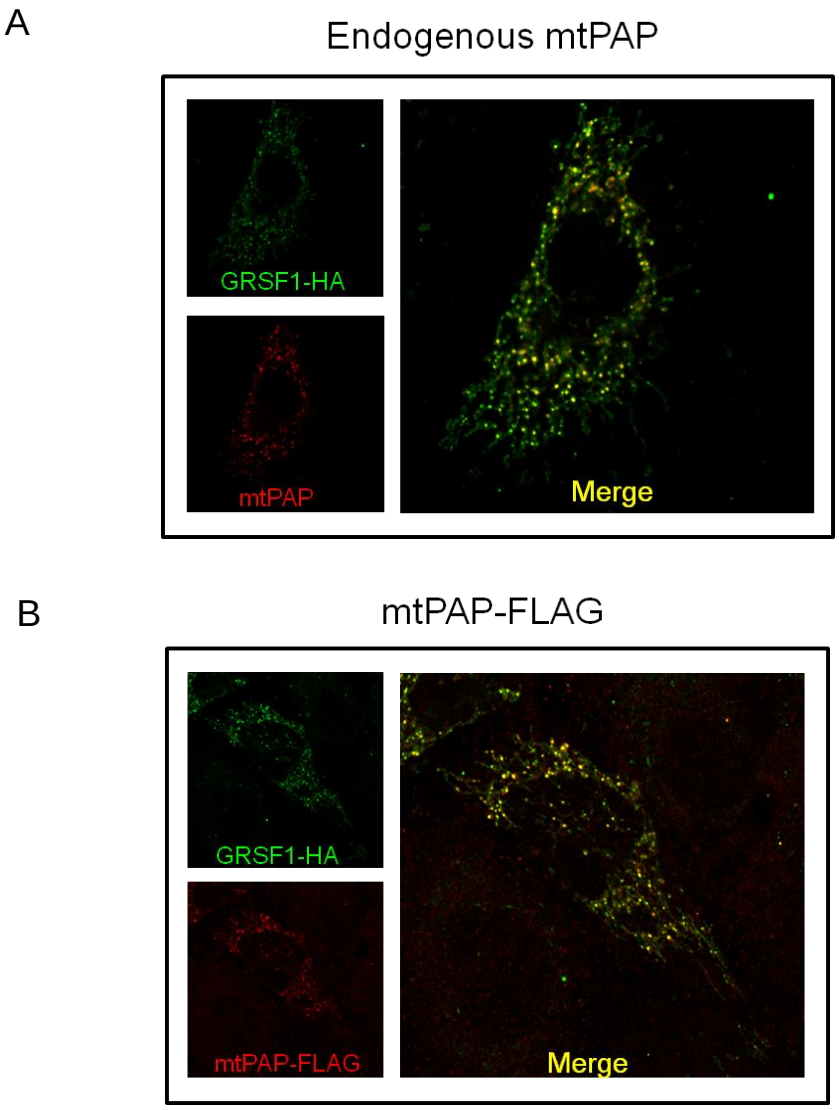

Figure 7.6. mtPAP is present in mitochondrial RNA granules.
A. Endogenous mtPAP was detected using α-mtPAP antibodies, and HA-tagged GRSF1 detected using α-HA antibodies, in 143B.206 cells. Fluorescent dye-conjugated secondary antibodies were used for visualization, and the signals merged to determine co-localization of mtPAP and GRSF1. **B.** 143B.206 cells were transiently transfected with the pcDNA5/FRT/TO-mtPAP-FLAG construct, and α-FLAG antibodies were utilized for detecting FLAG-tagged mtPAP. The FLAG signal was then merged with signal from HA-tagged GRSF1.

mtPAP are shown in Figure 7.6. Both the FLAG-tagged and endogenous mtPAP co-localize with GRSF1, indicating the presence of mtPAP in the mitochondrial RNA granules. To further support this evidence, both endogenous and FLAG-tagged mtPAP co-localized with FASTKD2, another marker of mitochondrial RNA granules (personal correspondence, unpublished data).

In continuing to evaluate the precise impact of the N478D mutation, the localization of mutant mtPAP was also examined. The 1432A>G mutation was introduced into the pcDNA5/FRT/TO-mtPAPFLAG construct, and this was sent to Professor Martinou's lab for transient expression in 143B.206 cells. As shown in Figure

7.7, the N478D FLAG-tagged mtPAP also appears to co-localize with GRSF1. However, the ability of the N478D mtPAP monomer to heterodimerize with the wild-type monomer is unknown. The presence of mtPAP in discrete mitochondrial foci does not seem to differ significantly with either the wild-type or N478D mtPAP-FLAG detected, so it is suggestive that the mutant enzyme is present in RNA granules as is the wild-type.

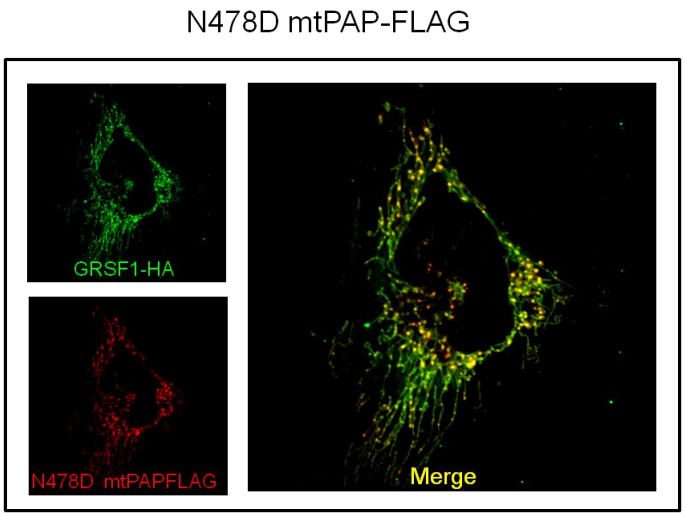

Figure 7.7. N478D mtPAP-FLAG co-localizes with mitochondrial RNA granules.
143B.206 cells were transiently transfected with a pcDNA5/FRT/TO-mtPAPFLAG construct harboring the 1432A>G mutation, and α-FLAG antibodies for detecting FLAG-tagged mtPAP. The FLAG image was then merged with the image from HA-tagged GRSF1.

7.4 Discussion

The most abundant protein found in the mtPAP co-IP samples was ATAD3. In addition to implications of involvement in chemoresistance and anti-apoptotic properties (Hubstenberger *et al.*, 2008; Fang *et al.*, 2010), this protein has been reported to be involved in multiple levels of mitochondrial gene expression. Reports have reported ATAD3 as associated with nucleoid, affecting ribosome and translation, and involvement in organelle fission machinery (He *et al.*, 2007; Gilquin *et al.*, 2010; He *et al.*, 2012). These reports also indicate that ATAD3 interacts with the mitochondrial inner and outer membranes. These varied reports of ATAD3 involvement make precise connections with mtPAP or polyadenylation difficult. ATAD3A appeared to be the dominant type of ATAD3 present in the co-IP samples, as opposed to ATAD3B and ATAD3C, although both of these were present at high levels in the IP, as judged by MS EMPAI values and western. ATAD3B has been reported as a negative regulator of ATAD3A (Merle *et al.*, 2012). A large amount of ATAD3A is present in mtPAP co-IP samples. As ATAD3A has been reported to oligomerize (Gilquin *et al.*, 2010), this may explain how such large amounts of the protein, relative to mtPAP, can be present in the co-IP samples. The reasons for the observed shift in position on the sucrose gradient in the presence of the N478D mtPAP are unclear. The possibility of a mutation causing increased interaction of ATAD3 with the mitoribosome is low, unless it normally associates with unincorporated subunits and these are increased in the presence of N478D mtPAP. However, there are no further data to support this hypothesis.

If the hypothesis that human mitochondrial transcription and translation are tightly coupled is true, perhaps ATAD3A serves as a linker for these processes. It may coordinate spatial localization of transcription and translation machinery, as it interacts with components of both, and is anchored to the inner mitochondrial membrane. The robust effect on *de novo* protein synthesis upon RNAi knock-down (He *et al.*, 2012) supports this. The fragmented morphology also reported with RNAi knock-down (Gilquin *et al.*, 2010) likely does not involve polyadenylation, and may simply reflect other roles that ATAD3 fulfills.

It is important to note the lack of ATAD3 signal in the FLAG-IP reactions. This may implicate ATAD3 as a non-specific interaction, rather than a physiologically relevant binding partner of mtPAP. An important experiment to perform would be immunoprecipitating ATAD3, and then blotting for the presence of mtPAP.

The hypothesized protein-protein interaction with LRPPRC was not supported by the IP and sucrose gradient data. The observed signal at 130kDa in HEK293 co-IP samples was not present at the levels expected for robust interaction with mtPAP. This does not conclusively disprove an interaction between LRPPRC and mtPAP, but if such an interaction exists, it may be very transient. The approach of excising Coomassie stained bands from co-IP samples separated by SDS-PAGE had the major limitation of not allowing examination of all the other proteins present at other points of migration through the gel. Analysis by mass spectrometry of the total co-IP sample would be more informative, particularly for identifying if LRPPRC is present at appreciable levels.

LRPPRC is clearly present in the free fraction of the sucrose gradient, like mtPAP. However, this is not evidence of a direct interaction, moreover LRPPRC is spread throughout several fractions of the gradient. Without visualization of the monosome, the impact of the N478D mutation on ribosome assembly is difficult to examine. The slight shift in position on the gradient observed in mutant fibroblasts may not be physiologically relevant. LRPPRC is commonly identified in mitochondrial protein immunoprecipitations. This may reflect *bona fide* interactions, or the 'sticky' nature of the protein generating a non-specific contaminant. While the model of direct interaction between LRPPRC/mtPAP is attractive, based on the *in vitro* polyadenylation data (Chapter 6), there is little published evidence to support it beyond those experiments.

The presence of mtPAP in mitochondrial RNA granules is not entirely unexpected, as it is logical to associate polyadenylation events spatially and temporally with transcript processing and maturation. This is what occurs in the human nucleus, with cleavage and polyadenylation intimately coupled. The localization experiments have also confirmed that the N478D mutation does not interfere with mtPAP being directed to the granules. This is consistent with the *in vitro* experiments using N478D mtPAP that suggested a potential defect in processivity of the enzyme rather than mis-localization. Future work should investigate whether RNA polymerase is present closely associated with the granules, perhaps with further co-IP and mass spectrometry analysis, with emphasis on searching for factors involved with transcription and maturation.

The localization to RNA granules also confirms mtPAP to be present and active in the mitochondrial matrix, as it is present with proteins that have been identified as residing in the matrix. The microscopy images appear to show mtPAP as present in discrete mitochondrial foci, rather than present diffusely in the matrix. If the enzyme were also fulfilling roles in the cytosol, a much more even distribution throughout the cell would be expected. This conflicts with a previous report that stated that mtPAP (then

referred to as TUTase 1) is present in the cytosol and responsible for oligouridylation of histone mRNA (Mullen and Marzluff, 2008). There remains a possibility that small, near-undetectable amounts of mtPAP are located in the cytosol, and responsible for oligouridylation of the histone mRNAs. However, a later report mentions, via unpublished data, that the effects of TUTase 1 on histone mRNAs was an indirect result of a cell growth defect (Su *et al.*, 2013). That report provides additional evidence that mtPAP may not be directly involved with cytosolic polynucleotide tails, and is probably exclusively a mitochondrial factor.

In conclusion, this chapter indicates that a novel candidate for interaction with MTPAP is ATAD3. In particular, the ATAD3A was the most abundant of the three ATAD3 isoforms. Characterization of this interaction is ongoing.

Chapter 8

Concluding remarks and future directions

The two major questions these studies aimed to address were: what is the role of the human mitochondrial poly(A) tail, and what is the impact of the mtPAP N478D mutation? Despite the rigorous investigations performed, neither of these questions have been completely resolved. However, over the course of this thesis work, major strides have been made in elucidating their answers. The results presented here represent the first report of the effects of a physiological, rather than an artificial loss of polyadenylation in human mitochondria, and how the loss of the mitochondrial poly(A) tail can cause the oxidative defects underlying the neurodegenerative pathologies reported as a consequence of a *PAPD1* mutation (chapters 4 and 5). The effect of LRPPRC enhancing the mtPAP polyadenylation activity was confirmed and clarified via the *in vitro* investigations (chapter 6). In addition, the novel interaction of mtPAP and ATAD3 was uncovered (chapter 7).

The establishment of fibroblast lines harboring the 1432A>G *PAPD1* mutation in culture was designed to allow a more physiologically relevant system for assessing the function of mitochondrial polyadenylation. Free from non-specific effects resulting from targeted intervention, the cells would ideally provide valuable mechanistic insights as to the role of the poly(A) tail in mitochondrial gene expression. As a result of the studies detailed in this thesis work, numerous insights have been made. The various perturbations of transcript and translation processes catalogued have presented a complex picture of the effects of truncating the poly(A) tail. Particular results stand out, in terms of raising more questions. The non-uniform changes with increases, decreases, or non-effect observed on mt-mRNA stability are perplexing. No single trend emerges from the specific impact on each of the transcripts. It is unclear whether the varying effects are a result of the tail performing multiple functions, or if the mt-mRNAs behave differently based on as yet unknown qualities.

For some transcripts there is also a disconnect between mt-mRNA levels and the steady state levels of the encoded polypeptide. There are differences in *de novo* protein synthesis and translation product turnover for different gene products. It is intriguing to speculate how the profound loss of a poly(A) extension at the 3' terminus of the mt-mRNA could affect its translatability and even more so the turnover of the resulting polypeptide. It is possible that small perturbations in translation processes can cause major defects, as reflected in the steady-state protein levels and assembly of the

respiratory complexes. These disconnects between transcript stability and protein synthesis represent major deficits in our understanding, mechanistically speaking. More work is necessary to dissect the molecular processes underlying these results. The data from complex IV gene expression stand out amidst the complicated results. From shortening of the poly(A) tail to decreased steady-state levels of the mRNA transcripts, to decreased protein synthesis, to decreased steady-state protein levels, culminating in a profound loss of fully assembled complex IV. This is the only complex to show such a linear progression of downstream effects from oligoadenylation of the mt-mRNAs, and presents a compelling argument for a role in transcript stabilization for the poly(A) tail in mitochondria.

The experiments performed here, particularly the transduction of the mutant patient fibroblasts with wild type *PAPD1*, confirmed the pathogenicity of the 1432A>G *PAPD1* mutation. As an extension of these observations, this work aimed to characterize the explicit impact of the mutation on the polymerase. Studying the characteristics of the recombinant mutant protein in isolation provided many clues as to the exact consequences of the defect. Gel filtration analysis revealed that the dimerization status of N478D mtPAP is not disrupted. The *in vitro* N478D mtPAP activity data generated supported the hypothesis that the mutation is disrupting activity, directly or indirectly, as western data from the fibroblast lines had established that the stability of the mutant protein was unaffected. No data indicated that the mutation affected any of the currently identified protein-protein interactions. My *in vitro* data indicated that the wild type protein was able to act on a naked RNA end and did not require an oligo(A) tail as a substrate, suggesting that another enzyme is not required to generate the oligo(A) tail as a prerequisite for a poly(A) extension. Wild type mtPAP was also able to extend from an oligo(A) tail. The mutant protein had similar recognition and was able to act on both naked and oligoadenylated 3' termini, although without the same level of extension activity. The reduced poly(A) tail length could therefore be through a defect in processivity, or changes in affinity for substrate. If the poly(A) polymerase disengages from the RNA transcript too easily, extension of the poly(A) tail could be compromised, as seen in the data from the mutant protein. The ability to isolate the exact structural or catalytic consequences of the mutation were beyond the scope of this work. What is clear is the N478D polymerase can still add to the 3' termini of RNA substrates, whether they are 'naked' or oligoadenylated but only in a severely compromised fashion. The lengths observed *in vitro* correspond to the lengths identified on the MPAT assay in the homozygous mutant fibroblasts. This provides evidence against the hypothetical oligo(A) polymerase in

mitochondria. It also leaves the question as to why the mutant cannot successively re-associate with the oligo(A) tail it generates to extend the 3' modification in an additive fashion.

Due to time restrictions, multiple avenues of investigation that were identified from results presented in this thesis were not explored. An aspect of transcriptional processing that was not investigated was the roles of the various nucleases may have in regulating the length of the poly(A) tail. hSUV3, PNPase, PDE12, and still undiscovered RNases may all play a role in regulating polyadenylation, as well as in regulating transcript stabilities. Depleting these factors in the mutant *PAPD1* cells may produce effects that are informative on which of the factors affect the poly(A) tails. This might be particularly informative in the patient fibroblasts transduced with the wild-type *PAPD1* transgene, where extra extension of the poly(A) tail was observed by MPAT assays. These putative RNase regulators of poly(A) tail length may act in concert with each other as well. There must be an *in vivo* system that monitors/regulates the particular length of the poly(A) tail. The *in vitro* data reported here suggests that mtPAP is capable of extensions longer than the approximately 45nt poly(A) tail found on mt-mRNAs. My data suggested that this might be modulated in the presence of the LRPPRC/SLIRP complex. However, as mentioned earlier, more work is necessary to rule out any assay artifact. This emphasizes the need for further experiments examining the processes governing poly(A) length.

While the patient fibroblasts proved to be valuable models for investigating mitochondrial polyadenylation, it is pertinent to note that the affected tissue in the patients was primarily neuronal. Investigating potential differences in how the mtPAP mutation impacts various cell types would be informative. Possible avenues of exploring this area include generating transgenic mice homozygous for the mutant *PAPD1* gene, or de-differentiating the patient fibroblasts, and then differentiating them into specific cell types of interest.

The identification, reported here, of ATAD3 interacting with mtPAP bears further exploration. The most pertinent experiment, as related to this body of work, would be assessing the poly(A) tail lengths in cell lines carrying ATAD3 mutations or cells depleted of ATAD3. This would reveal if interactions between the two proteins physiologically affects polyadenylation activity. Inclusion of recombinant ATAD3, particularly ATAD3A, in the *in vitro* poly(A) assays may also offer evidence of impact on poly(A) extension.

Several experiments remain to be performed to complete this area of work and allow manuscript preparation. Of critical importance is the enzymatic activity of complex V in homozygous 1432A>G *PAPD1* mitochondria. Depletion at steady-state of the ATP6 and putatively of ATP8 subunits would be expected to cause major assembly and activity issues for the complex, yet analysis via blue native PAGE suggests wild-type levels of assembly. A final experiment that I would like to perform is the immunoprecipitation of mtPAP from the *in vitro* reactions containing LRPPRC, to search for any evidence of protein-protein interaction.

In summary, this thesis work has shown that the shorter oligo(A) tails on human mitochondrial transcripts results in pathogenic molecular consequences, and revealed insights into the regulation of polyadenylation. These types of investigations are critical to fully elucidate the mechanisms governing transcript stability and translation effects in the presence of shortened poly(A) tails. Further studies based on the data generated for this thesis will allow progress to be made in understanding multifaceted mitochondrial disease states, and developing treatments for patients with defects in these specific pathways. The story still remains incomplete, and further research is required but the data presented here represents an advance in understanding the complexity of mitochondrial post-transcriptional maturation and gene expression.

Bibliography

Acin-Perez, R., Fernandez-Silva, P., Peleato, M. L., Perez-Martos, A. and Enriquez, J. A. (2008) 'Respiratory active mitochondrial supercomplexes', *Mol Cell*, 32(4), pp. 529-39.

Allen, J. F. and Raven, J. A. (1996) 'Free-radical-induced mutation vs redox regulation: costs and benefits of genes in organelles', *J Mol Evol*, 42(5), pp. 482-92.

Andersson, S. G. E., Zomorodipour, A., Andersson, J. O., Sicheritz-Ponten, T., Alsmark, U. C. M., Podowski, R. M., Naslund, A. K., Eriksson, A.-S., Winkler, H. H. and Kurland, C. G. (1998) 'The genome sequence of Rickettsia prowazekii and the origin of mitochondria', *Nature*, 396(6707), pp. 133-140.

Asin-Cayuela, J., Schwend, T., Farge, G. and Gustafsson, C. M. (2005) 'The human mitochondrial transcription termination factor (mTERF) is fully active in vitro in the non-phosphorylated form', *J Biol Chem*, 280(27), pp. 25499-505.

Bai, Y., Srivastava, S. K., Chang, J. H., Manley, J. L. and Tong, L. (2011) 'Structural Basis for Dimerization and Activity of Human PAPD1, a Noncanonical Poly(A) Polymerase', *Molecular Cell*, 41(3), pp. 311-320.

Barth, E., Stammler, G., Speiser, B. and Schaper, J. (1992) 'Ultrastructural quantitation of mitochondria and myofilaments in cardiac muscle from 10 different animal species including man', *J Mol Cell Cardiol*, 24(7), pp. 669-81.

Bastiaensen, L. A. K., Frenken, C. W. G. M., Ter Laak, H. J., Jaspar, H. H. J., Stadhouders, A. M., Ruitenbeek, W. and Veerkamp, J. H. (1982) 'Kearns syndrome: A heterogeneous group of disorders with CPEO, or a nosological entity?', *Documenta Ophthalmologica*, 52(2), pp. 207-225.

Baughman, J. M., Nilsson, R., Gohil, V. M., Arlow, D. H., Gauhar, Z. and Mootha, V. K. (2009) 'A computational screen for regulators of oxidative phosphorylation implicates SLIRP in mitochondrial RNA homeostasis', *PLoS Genet*, 5(8), p. e1000590.

Bernstein, P., Peltz, S. W. and Ross, J. (1989) 'The poly(A)-poly(A)-binding protein complex is a major determinant of mRNA stability in vitro', *Mol Cell Biol*, 9(2), pp. 659-70.

Bogenhagen, D. F., Rousseau, D. and Burke, S. (2008) 'The layered structure of human mitochondrial DNA nucleoids', *J Biol Chem*, 283(6), pp. 3665-75.

Borowski, L. S., Dziembowski, A., Hejnowicz, M. S., Stepien, P. P. and Szczesny, R. J. (2013) 'Human mitochondrial RNA decay mediated by PNPase-hSuv3 complex takes place in distinct foci', *Nucleic Acids Res*, 41(2), pp. 1223-40.

Bowmaker, M., Yang, M. Y., Yasukawa, T., Reyes, A., Jacobs, H. T., Huberman, J. A. and Holt, I. J. (2003) 'Mammalian mitochondrial DNA replicates bidirectionally from an initiation zone', *J Biol Chem*, 278(51), pp. 50961-9.

Bratic, A., Wredenberg, A., Gronke, S., Stewart, J. B., Mourier, A., Ruzzenente, B., Kukat, C., Wibom, R., Habermann, B., Partridge, L. and Larsson, N. G. (2011) 'The bicoid stability factor controls polyadenylation and expression of specific mitochondrial mRNAs in Drosophila melanogaster', *PLoS Genet*, 7(10), p. e1002324.

Brocks, J. J., Logan, G. A., Buick, R. and Summons, R. E. (1999) 'Archean molecular fossils and the early rise of eukaryotes', *Science*, 285(5430), pp. 1033-6.

Bruni, F., Gramegna, P., Oliveira, J. M., Lightowlers, R. N. and Chrzanowska-Lightowlers, Z. M. (2013) 'REXO2 Is an Oligoribonuclease Active in Human Mitochondria', *PLoS One*, 8(5), p. e64670.

Brzezniak, L. K., Bijata, M., Szczesny, R. J. and Stepien, P. P. (2011) 'Involvement of human ELAC2 gene product in 3' end processing of mitochondrial tRNAs', *RNA Biol*, 8(4).

Butow, R. A., Zhu, H., Perlman, P. and Conrad-Webb, H. (1989) 'The role of a conserved dodecamer sequence in yeast mitochondrial gene expression', *Genome*, 31(2), pp. 757-60.

Cai, Y. C., Bullard, J. M., Thompson, N. L. and Spremulli, L. L. (2000) 'Interaction of mitochondrial elongation factor Tu with aminoacyl-tRNA and elongation factor Ts', *J Biol Chem*, 275(27), pp. 20308-14.

Calvaruso, M. A., Smeitink, J. and Nijtmans, L. (2008) 'Electrophoresis techniques to investigate defects in oxidative phosphorylation', *Methods*, 46(4), pp. 281-7.

Calvo, S. E., Tucker, E. J., Compton, A. G., Kirby, D. M., Crawford, G., Burtt, N. P., Rivas, M., Guiducci, C., Bruno, D. L., Goldberger, O. A., Redman, M. C., Wiltshire, E., Wilson, C. J., Altshuler, D., Gabriel, S. B., Daly, M. J., Thorburn, D. R. and Mootha, V. K. (2010) 'High-throughput, pooled sequencing identifies mutations in NUBPL and FOXRED1 in human complex I deficiency', *Nat Genet*, 42(10), pp. 851-8.

Camara, Y., Asin-Cayuela, J., Park, C. B., Metodiev, M. D., Shi, Y., Ruzzenente, B., Kukat, C., Habermann, B., Wibom, R., Hultenby, K., Franz, T., Erdjument-Bromage, H., Tempst, P., Hallberg, B. M., Gustafsson, C. M. and Larsson, N. G. (2011) 'MTERF4 regulates translation by targeting the methyltransferase NSUN4 to the mammalian mitochondrial ribosome', *Cell Metab*, 13(5), pp. 527-39.

Catherman, A. D., Durbin, K. R., Ahlf, D. R., Early, B. P., Fellers, R. T., Tran, J. C., Thomas, P. M. and Kelleher, N. L. (2013) 'Large-scale top down proteomics of the human proteome: membrane proteins, mitochondria, and senescence', *Mol Cell Proteomics*.

Chan, D. C. (2006) 'Mitochondrial fusion and fission in mammals', *Annu Rev Cell Dev Biol*, 22, pp. 79-99.

Chen, H. W., Rainey, R. N., Balatoni, C. E., Dawson, D. W., Troke, J. J., Wasiak, S., Hong, J. S., McBride, H. M., Koehler, C. M., Teitell, M. A. and French, S. W. (2006) 'Mammalian polynucleotide phosphorylase is an intermembrane space RNase that maintains mitochondrial homeostasis', *Mol Cell Biol*, 26(22), pp. 8475-87.

Ching, E. and Attardi, G. (1982) 'High-resolution electrophoretic fractionation and partial characterization of the mitochondrial translation products from HeLa cells', *Biochemistry*, 21(13), pp. 3188-95.

Chinnery, P. F., Howell, N., Lightowlers, R. N. and Turnbull, D. M. (1997) 'Molecular pathology of MELAS and MERRF. The relationship between mutation load and clinical phenotypes', *Brain*, 120 (Pt 10), pp. 1713-21.

Chinnery, P. F., Thorburn, D. R., Samuels, D. C., White, S. L., Dahl, H.-H. M., Turnbull, D. M., Lightowlers, R. N. and Howell, N. (2000) 'The inheritance of mitochondrial DNA heteroplasmy: random drift, selection or both?', *Trends in Genetics*, 16(11), pp. 500-505.

Chomyn, A. (1996) 'In vivo labeling and analysis of human mitochondrial translation products', *Methods Enzymol*, 264, pp. 197-211.

Christian, B. E. and Spremulli, L. L. (2009) 'Evidence for an active role of IF3mt in the initiation of translation in mammalian mitochondria', *Biochemistry*, 48(15), pp. 3269-78.

Christian, B. E. and Spremulli, L. L. (2010) 'Preferential selection of the 5'-terminal start codon on leaderless mRNAs by mammalian mitochondrial ribosomes', *J Biol Chem*, 285(36), pp. 28379-86.

Chrzanowska-Lightowlers, Z. M. A., Pajak, A. and Lightowlers, R. N. (2011) 'Termination of Protein Synthesis in Mammalian Mitochondria', *Journal of Biological Chemistry*, 286(40), pp. 34479-34485.

Chujo, T., Ohira, T., Sakaguchi, Y., Goshima, N., Nomura, N., Nagao, A. and Suzuki, T. (2012) 'LRPPRC/SLIRP suppresses PNPase-mediated mRNA decay and promotes polyadenylation in human mitochondria', *Nucleic Acids Res*, 40(16), pp. 8033-47.

Colbeau, A., Nachbaur, J. and Vignais, P. M. (1971) 'Enzymic characterization and lipid composition of rat liver subcellular membranes', *Biochim Biophys Acta*, 249(2), pp. 462-92.

Cotney, J. and Shadel, G. S. (2006) 'Evidence for an early gene duplication event in the evolution of the mitochondrial transcription factor B family and maintenance of rRNA methyltransferase activity in human mtTFB1 and mtTFB2', *J Mol Evol*, 63(5), pp. 707-17.

Craven, L., Tuppen, H. A., Greggains, G. D., Harbottle, S. J., Murphy, J. L., Cree, L. M., Murdoch, A. P., Chinnery, P. F., Taylor, R. W., Lightowlers, R. N., Herbert, M. and Turnbull, D. M. (2010) 'Pronuclear transfer in human embryos to prevent transmission of mitochondrial DNA disease', *Nature*, 465(7294), pp. 82-5.

Crosby, A. H., Patel, H., Chioza, B. A., Proukakis, C., Gurtz, K., Patton, M. A., Sharifi, R., Harlalka, G., Simpson, M. A. and Dick, K. (2010) 'Defective Mitochondrial mRNA Maturation Is Associated with Spastic Ataxia', *The American Journal of Human Genetics*, 87(5), pp. 655-660.

Danovaro, R., Dell'Anno, A., Pusceddu, A., Gambi, C., Heiner, I. and Kristensen, R. M. (2010) 'The first metazoa living in permanently anoxic conditions', *BMC Biol*, 8, p. 30.

Davies, S. M., Rackham, O., Shearwood, A. M., Hamilton, K. L., Narsai, R., Whelan, J. and Filipovska, A. (2009) 'Pentatricopeptide repeat domain protein 3 associates with the mitochondrial small ribosomal subunit and regulates translation', *FEBS Lett*, 583(12), pp. 1853-8.

Dennerlein, S., Rozanska, A., Wydro, M., Chrzanowska-Lightowlers, Z. M. and Lightowlers, R. N. (2010) 'Human ERAL1 is a mitochondrial RNA chaperone involved in the assembly of the 28S small mitochondrial ribosomal subunit', *Biochem J*, 430(3), pp. 551-8.

Des Marais, D. J. (1998) 'Earth's early biosphere', *Gravit Space Biol Bull*, 11(2), pp. 23-30.

Dmochowska, A., Kalita, K., Krawczyk, M., Golik, P., Mroczek, K., Lazowska, J., Stepien, P. P. and Bartnik, E. (1999) 'A human putative Suv3-like RNA helicase is conserved between Rhodobacter and all eukaryotes', *Acta Biochim Pol*, 46(1), pp. 155-62.

Edmonds, M. and Abrams, R. (1960) 'Polynucleotide biosynthesis: formation of a sequence of adenylate units from adenosine triphosphate by an enzyme from thymus nuclei', *J Biol Chem*, 235, pp. 1142-9.

Elliott, H. R., Samuels, D. C., Eden, J. A., Relton, C. L. and Chinnery, P. F. (2008) 'Pathogenic mitochondrial DNA mutations are common in the general population', *Am J Hum Genet*, 83(2), pp. 254-60.

Emdadul Haque, M., Grasso, D., Miller, C., Spremulli, L. L. and Saada, A. (2008) 'The effect of mutated mitochondrial ribosomal proteins S16 and S22 on the assembly of the small and large ribosomal subunits in human mitochondria', *Mitochondrion*, 8(3), pp. 254-61.

Etheridge, R. D., Aphasizheva, I., Gershon, P. D. and Aphasizhev, R. (2008) '3' adenylation determines mRNA abundance and monitors completion of RNA editing in T. brucei mitochondria', *EMBO J*, 27(11), pp. 1596-608.

Falkenberg, M., Gaspari, M., Rantanen, A., Trifunovic, A., Larsson, N. G. and Gustafsson, C. M. (2002) 'Mitochondrial transcription factors B1 and B2 activate transcription of human mtDNA', *Nat Genet*, 31(3), pp. 289-94.

Fang, H. Y., Chang, C. L., Hsu, S. H., Huang, C. Y., Chiang, S. F., Chiou, S. H., Huang, C. H., Hsiao, Y. T., Lin, T. Y., Chiang, I. P., Hsu, W. H., Sugano, S., Chen, C. Y., Lin, C. Y., Ko, W. J. and Chow, K. C. (2010) 'ATPase family AAA domain-containing 3A is a

novel anti-apoptotic factor in lung adenocarcinoma cells', *J Cell Sci*, 123(Pt 7), pp. 1171-80.

Fernandez-Silva, P., Acin-Perez, R., Fernandez-Vizarra, E., Perez-Martos, A. and Enriquez, J. A. (2007) 'In vivo and in organello analyses of mitochondrial translation', *Methods Cell Biol*, 80, pp. 571-88.

Fung, S., Nishimura, T., Sasarman, F. and Shoubridge, E. A. (2013) 'The conserved interaction of C7orf30 with MRPL14 promotes biogenesis of the mitochondrial large ribosomal subunit and mitochondrial translation', *Mol Biol Cell*, 24(3), pp. 184-93.

Fuste, J. M., Wanrooij, S., Jemt, E., Granycome, C. E., Cluett, T. J., Shi, Y., Atanassova, N., Holt, I. J., Gustafsson, C. M. and Falkenberg, M. (2010) 'Mitochondrial RNA polymerase is needed for activation of the origin of light-strand DNA replication', *Mol Cell*, 37(1), pp. 67-78.

Gagliardi, D. and Leaver, C. J. (1999) 'Polyadenylation accelerates the degradation of the mitochondrial mRNA associated with cytoplasmic male sterility in sunflower', *EMBO J*, 18(13), pp. 3757-66.

Gallerani, R., di, I., Istituto di, C. and Saccone, C. (1976) 'Contemporaneous isolation of deoxyribonucleic acid-dependent ribonucleic acid polymerase and poly(A) polymerase from rat liver mitochondria', *Biochem J*, 157(2), pp. 295-300.

Gallie, D. R. (1991) 'The cap and poly(A) tail function synergistically to regulate mRNA translational efficiency', *Genes Dev*, 5(11), pp. 2108-16.

Galmiche, L., Serre, V., Beinat, M., Assouline, Z., Lebre, A. S., Chretien, D., Nietschke, P., Benes, V., Boddaert, N., Sidi, D., Brunelle, F., Rio, M., Munnich, A. and Rotig, A. (2011) 'Exome sequencing identifies MRPL3 mutation in mitochondrial cardiomyopathy', *Hum Mutat*, 32(11), pp. 1225-31.

Gebert, N., Joshi, A. S., Kutik, S., Becker, T., McKenzie, M., Guan, X. L., Mooga, V. P., Stroud, D. A., Kulkarni, G., Wenk, M. R., Rehling, P., Meisinger, C., Ryan, M. T., Wiedemann, N., Greenberg, M. L. and Pfanner, N. (2009) 'Mitochondrial cardiolipin involved in outer-membrane protein biogenesis: implications for Barth syndrome', *Curr Biol*, 19(24), pp. 2133-9.

Georgiades, K. and Raoult, D. (2011) 'The rhizome of Reclinomonas americana, Homo sapiens, Pediculus humanus and Saccharomyces cerevisiae mitochondria', *Biol Direct*, 6, p. 55.

Gilquin, B., Taillebourg, E., Cherradi, N., Hubstenberger, A., Gay, O., Merle, N., Assard, N., Fauvarque, M. O., Tomohiro, S., Kuge, O. and Baudier, J. (2010) 'The AAA+ ATPase ATAD3A controls mitochondrial dynamics at the interface of the inner and outer membranes', *Mol Cell Biol*, 30(8), pp. 1984-96.

Gohil, V. M. and Greenberg, M. L. (2009) 'Mitochondrial membrane biogenesis: phospholipids and proteins go hand in hand', *J Cell Biol*, 184(4), pp. 469-72.

Gohil, V. M., Nilsson, R., Belcher-Timme, C. A., Luo, B., Root, D. E. and Mootha, V. K. (2010) 'Mitochondrial and nuclear genomic responses to loss of LRPPRC expression', *J Biol Chem*, 285(18), pp. 13742-7.

Goto, Y. I., Nonaka, I. and Horai, S. (1990) 'A mutation in the tRNALeu(UUR) gene associated with the MELAS subgroup of mitochondrial encephalomyopathies', *Nature*, 348(6302), pp. 651-653.

Goujon, M., McWilliam, H., Li, W., Valentin, F., Squizzato, S., Paern, J. and Lopez, R. (2010) 'A new bioinformatics analysis tools framework at EMBL-EBI', *Nucleic Acids Res*, 38(Web Server issue), pp. W695-9.

Gray, M. W., Burger, G. and Lang, B. F. (1999) 'Mitochondrial evolution', *Science*, 283(5407), pp. 1476-81.

Hackstein, J. H., Akhmanova, A., Boxma, B., Harhangi, H. R. and Voncken, F. G. (1999) 'Hydrogenosomes: eukaryotic adaptations to anaerobic environments', *Trends Microbiol*, 7(11), pp. 441-7.

Hackstein, J. H., Tjaden, J. and Huynen, M. (2006) 'Mitochondria, hydrogenosomes and mitosomes: products of evolutionary tinkering!', *Curr Genet*, 50(4), pp. 225-45.

Hammarsund, M., Wilson, W., Corcoran, M., Merup, M., Einhorn, S., Grander, D. and Sangfelt, O. (2001) 'Identification and characterization of two novel human mitochondrial elongation factor genes, hEFG2 and hEFG1, phylogenetically conserved through evolution', *Hum Genet*, 109(5), pp. 542-50.

Hatchell, E. C., Colley, S. M., Beveridge, D. J., Epis, M. R., Stuart, L. M., Giles, K. M., Redfern, A. D., Miles, L. E., Barker, A., MacDonald, L. M., Arthur, P. G., Lui, J. C., Golding, J. L., McCulloch, R. K., Metcalf, C. B., Wilce, J. A., Wilce, M. C., Lanz, R. B., O'Malley, B. W. and Leedman, P. J. (2006) 'SLIRP, a small SRA binding protein, is a nuclear receptor corepressor', *Mol Cell*, 22(5), pp. 657-68.

Hayes, R., Kudla, J. and Gruissem, W. (1999) 'Degrading chloroplast mRNA: the role of polyadenylation', *Trends Biochem Sci*, 24(5), pp. 199-202.

He, J., Cooper, H. M., Reyes, A., Di Re, M., Sembongi, H., Litwin, T. R., Gao, J., Neuman, K. C., Fearnley, I. M., Spinazzola, A., Walker, J. E. and Holt, I. J. (2012) 'Mitochondrial nucleoid interacting proteins support mitochondrial protein synthesis', *Nucleic Acids Res*, 40(13), pp. 6109-21.

He, J., Mao, C. C., Reyes, A., Sembongi, H., Di Re, M., Granycome, C., Clippingdale, A. B., Fearnley, I. M., Harbour, M., Robinson, A. J., Reichelt, S., Spelbrink, J. N., Walker, J. E. and Holt, I. J. (2007) 'The AAA+ protein ATAD3 has displacement loop binding properties and is involved in mitochondrial nucleoid organization', *J Cell Biol*, 176(2), pp. 141-6.

Herrmann, J. M., Woellhaf, M. W. and Bonnefoy, N. (2013) 'Control of protein synthesis in yeast mitochondria: the concept of translational activators', *Biochim Biophys Acta*, 1833(2), pp. 286-94.

Hoch, F. L. (1992) 'Cardiolipins and biomembrane function', *Biochim Biophys Acta*, 1113(1), pp. 71-133.

Holt, I. J., Harding, A. E., Petty, R. K. and Morgan-Hughes, J. A. (1990) 'A new mitochondrial disease associated with mitochondrial DNA heteroplasmy', *Am J Hum Genet*, 46(3), pp. 428-33.

Holzmann, J., Frank, P., Löffler, E., Bennett, K. L., Gerner, C. and Rossmanith, W. (2008) 'RNase P without RNA: Identification and Functional Reconstitution of the Human Mitochondrial tRNA Processing Enzyme', *Cell*, 135(3), pp. 462-474.

Hornig-Do, H. T., Tatsuta, T., Buckermann, A., Bust, M., Kollberg, G., Rotig, A., Hellmich, M., Nijtmans, L. and Wiesner, R. J. (2012) 'Nonsense mutations in the COX1 subunit impair the stability of respiratory chain complexes rather than their assembly', *EMBO J*, 31(5), pp. 1293-307.

Huang, Y. and Carmichael, G. G. (1996) 'Role of polyadenylation in nucleocytoplasmic transport of mRNA', *Mol Cell Biol*, 16(4), pp. 1534-42.

Hubstenberger, A., Labourdette, G., Baudier, J. and Rousseau, D. (2008) 'ATAD 3A and ATAD 3B are distal 1p-located genes differentially expressed in human glioma cell lines and present in vitro anti-oncogenic and chemoresistant properties', *Exp Cell Res*, 314(15), pp. 2870-83.

Iborra, F. J., Kimura, H. and Cook, P. R. (2004) 'The functional organization of mitochondrial genomes in human cells', *BMC Biol*, 2, p. 9.

Jacob, S. T. and Schindler, D. G. (1972) 'Polyriboadenylate polymerase solubilized from rat liver mitochondria', *Biochem Biophys Res Commun*, 48(1), pp. 126-34.

Jiang, S. C. and Paul, J. H. (1998) 'Gene transfer by transduction in the marine environment', *Appl Environ Microbiol*, 64(8), pp. 2780-7.

Jourdain, A. A., Koppen, M., Wydro, M., Rodley, C. D., Lightowlers, R. N., Chrzanowska-Lightowlers, Z. M. and Martinou, J. C. (2013) 'GRSF1 regulates RNA processing in mitochondrial RNA granules', *Cell Metab*, 17(3), pp. 399-410.

Kaasik, A., Safiulina, D., Zharkovsky, A. and Veksler, V. (2007) 'Regulation of mitochondrial matrix volume', *American Journal of Physiology - Cell Physiolog*, pp. C157-C163.

Karlberg, O., Canback, B., Kurland, C. G. and Andersson, S. G. (2000) 'The dual origin of the yeast mitochondrial proteome', *Yeast*, 17(3), pp. 170-87.

Kazak, L., Reyes, A., Duncan, A. L., Rorbach, J., Wood, S. R., Brea-Calvo, G., Gammage, P. A., Robinson, A. J., Minczuk, M. and Holt, I. J. (2013) 'Alternative translation initiation augments the human mitochondrial proteome', *Nucleic Acids Res*, 41(4), pp. 2354-69.

Keller, R. W., Kuhn, U., Aragon, M., Bornikova, L., Wahle, E. and Bear, D. G. (2000) 'The nuclear poly(A) binding protein, PABP2, forms an oligomeric particle covering the length of the poly(A) tail', *J Mol Biol*, 297(3), pp. 569-83.

Khidr, L., Wu, G., Davila, A., Procaccio, V., Wallace, D. and Lee, W. H. (2008) 'Role of SUV3 helicase in maintaining mitochondrial homeostasis in human cells', *J Biol Chem*, 283(40), pp. 27064-73.

Kirby, D. M., Thorburn, D. R., Turnbull, D. M. and Taylor, R. W. (2007) 'Biochemical assays of respiratory chain complex activity', *Methods Cell Biol*, 80, pp. 93-119.

Kirches, E., Michael, M., Warich-Kirches, M., Schneider, T., Weis, S., Krause, G., Mawrin, C. and Dietzmann, K. (2001) 'Heterogeneous tissue distribution of a mitochondrial DNA polymorphism in heteroplasmic subjects without mitochondrial disorders', *Journal of Medical Genetics*, 38(5), pp. 312-317.

Kobayashi, M., Matsuo, Y., Takimoto, A., Suzuki, S., Maruo, F. and Shoun, H. (1996) 'Denitrification, a novel type of respiratory metabolism in fungal mitochondrion', *J Biol Chem*, 271(27), pp. 16263-7.

Koc, E. C. and Spremulli, L. L. (2002) 'Identification of mammalian mitochondrial translational initiation factor 3 and examination of its role in initiation complex formation with natural mRNAs', *J Biol Chem*, 277(38), pp. 35541-9.

Kolanczyk, M., Pech, M., Zemojtel, T., Yamamoto, H., Mikula, I., Calvaruso, M. A., van den Brand, M., Richter, R., Fischer, B., Ritz, A., Kossler, N., Thurisch, B., Spoerle, R., Smeitink, J., Kornak, U., Chan, D., Vingron, M., Martasek, P., Lightowlers, R. N., Nijtmans, L., Schuelke, M., Nierhaus, K. H. and Mundlos, S. (2011) 'NOA1 is an essential GTPase required for mitochondrial protein synthesis', *Mol Biol Cell*, 22(1), pp. 1-11.

Konovalova, S. and Tyynismaa, H. (2013) 'Mitochondrial aminoacyl-tRNA synthetases in human disease', *Mol Genet Metab*, 108(4), pp. 206-11.

Korhonen, J. A., Pham, X. H., Pellegrini, M. and Falkenberg, M. (2004) 'Reconstitution of a minimal mtDNA replisome in vitro', *EMBO J*, 23(12), pp. 2423-9.

Kotani, T., Akabane, S., Takeyasu, K., Ueda, T. and Takeuchi, N. (2013) 'Human G-proteins, ObgH1 and Mtg1, associate with the large mitochondrial ribosome subunit and are involved in translation and assembly of respiratory complexes', *Nucleic Acids Research*, 41(6), pp. 3713-3722.

Kruse, B., Narasimhan, N. and Attardi, G. (1989) 'Termination of transcription in human mitochondria: identification and purification of a DNA binding protein factor that promotes termination', *Cell*, 58(2), pp. 391-7.

Kuhn, U., Gundel, M., Knoth, A., Kerwitz, Y., Rudel, S. and Wahle, E. (2009) 'Poly(A) tail length is controlled by the nuclear poly(A)-binding protein regulating the interaction between poly(A) polymerase and the cleavage and polyadenylation specificity factor', *J Biol Chem*, 284(34), pp. 22803-14.

Kukat, C., Wurm, C. A., Spahr, H., Falkenberg, M., Larsson, N. G. and Jakobs, S. (2011) 'Super-resolution microscopy reveals that mammalian mitochondrial nucleoids have a uniform size and frequently contain a single copy of mtDNA', *Proc Natl Acad Sci U S A*, 108(33), pp. 13534-9.

Kurland, C. G. and Andersson, S. G. (2000) 'Origin and evolution of the mitochondrial proteome', *Microbiol Mol Biol Rev*, 64(4), pp. 786-820.

Lang, B. F., Gray, M. W. and Burger, G. (1999) 'Mitochondrial genome evolution and the origin of eukaryotes', *Annu Rev Genet*, 33, pp. 351-97.

Lightowlers, R. N. and Chrzanowska-Lightowlers, Z. M. (2013) 'Human pentatricopeptide proteins: Only a few and what do they do?', *RNA Biol*, 10(9).

Ling, M., Merante, F., Chen, H. S., Duff, C., Duncan, A. M. and Robinson, B. H. (1997) 'The human mitochondrial elongation factor tu (EF-Tu) gene: cDNA sequence, genomic localization, genomic structure, and identification of a pseudogene', *Gene*, 197(1-2), pp. 325-36.

Liu, L., Feng, D., Chen, G., Chen, M., Zheng, Q., Song, P., Ma, Q., Zhu, C., Wang, R., Qi, W., Huang, L., Xue, P., Li, B., Wang, X., Jin, H., Wang, J., Yang, F., Liu, P., Zhu, Y., Sui, S. and Chen, Q. (2012) 'Mitochondrial outer-membrane protein FUNDC1 mediates hypoxia-induced mitophagy in mammalian cells', *Nat Cell Biol*, 14(2), pp. 177-85.

Livak, K. J. and Schmittgen, T. D. (2001) 'Analysis of relative gene expression data using real-time quantitative PCR and the 2(-Delta Delta C(T)) Method', *Methods*, 25(4), pp. 402-8.

Lochmüller, H., Johns, T. and Shoubridge, E. A. (1999) 'Expression of the E6 and E7 Genes of Human Papillomavirus (HPV16) Extends the Life Span of Human Myoblasts', *Experimental Cell Research*, 248(1), pp. 186-193.

Lotz, C., Lin, A. J., Black, C. M., Zhang, J., Lau, E., Deng, N., Wang, Y., Zong, N. C., Choi, J. H., Xu, T., Liem, D. A., Korge, P., Weiss, J. N., Hermjakob, H., Yates, J. R., Apweiler, R. and Ping, P. (2013) 'The Characterization, Design, and Function of the Mitochondrial Proteome: From Organs to Organisms', *J Proteome Res*.

Ma, L. and Spremulli, L. L. (1995) 'Cloning and sequence analysis of the human mitochondrial translational initiation factor 2 cDNA', *J Biol Chem*, 270(4), pp. 1859-65.

Mandel, C. R., Bai, Y. and Tong, L. (2008) 'Protein factors in pre-mRNA 3'-end processing', *Cell Mol Life Sci*, 65(7-8), pp. 1099-122.

Mans, B. J., Anantharaman, V., Aravind, L. and Koonin, E. V. (2004) 'Comparative genomics, evolution and origins of the nuclear envelope and nuclear pore complex', *Cell Cycle*, 3(12), pp. 1612-37.

Martin, G., Keller, W. and Doublie, S. (2000) 'Crystal structure of mammalian poly(A) polymerase in complex with an analog of ATP', *EMBO J*, 19(16), pp. 4193-203.

Martin, M., Cho, J., Cesare, A. J., Griffith, J. D. and Attardi, G. (2005) 'Termination factor-mediated DNA loop between termination and initiation sites drives mitochondrial rRNA synthesis', *Cell*, 123(7), pp. 1227-40.

McDaniel, L. D., Young, E., Delaney, J., Ruhnau, F., Ritchie, K. B. and Paul, J. H. (2010) 'High Frequency of Horizontal Gene Transfer in the Oceans', *Science*, 330(6000), p. 50.

Mears, J. A., Sharma, M. R., Gutell, R. R., McCook, A. S., Richardson, P. E., Caulfield, T. R., Agrawal, R. K. and Harvey, S. C. (2006) 'A structural model for the large subunit of the mammalian mitochondrial ribosome', *J Mol Biol*, 358(1), pp. 193-212.

Mercer, T. R., Neph, S., Dinger, M. E., Crawford, J., Smith, M. A., Shearwood, A. M., Haugen, E., Bracken, C. P., Rackham, O., Stamatoyannopoulos, J. A., Filipovska, A. and Mattick, J. S. (2011) 'The human mitochondrial transcriptome', *Cell*, 146(4), pp. 645-58.

Merle, N., Feraud, O., Gilquin, B., Hubstenberger, A., Kieffer-Jacquinot, S., Assard, N., Bennaceur-Griscelli, A., Honnorat, J. and Baudier, J. (2012) 'ATAD3B is a human embryonic stem cell specific mitochondrial protein, re-expressed in cancer cells, that functions as dominant negative for the ubiquitous ATAD3A', *Mitochondrion*, 12(4), pp. 441-8.

Metodiev, M. D., Lesko, N., Park, C. B., Camara, Y., Shi, Y., Wibom, R., Hultenby, K., Gustafsson, C. M. and Larsson, N. G. (2009) 'Methylation of 12S rRNA is necessary for in vivo stability of the small subunit of the mammalian mitochondrial ribosome', *Cell Metab*, 9(4), pp. 386-97.

Mili, S. and Pinol-Roma, S. (2003) 'LRP130, a pentatricopeptide motif protein with a noncanonical RNA-binding domain, is bound in vivo to mitochondrial and nuclear RNAs', *Mol Cell Biol*, 23(14), pp. 4972-82.

Miller, C., Saada, A., Shaul, N., Shabtai, N., Ben-Shalom, E., Shaag, A., Hershkovitz, E. and Elpeleg, O. (2004) 'Defective mitochondrial translation caused by a ribosomal protein (MRPS16) mutation', *Ann Neurol*, 56(5), pp. 734-8.

Minczuk, M., He, J., Duch, A. M., Ettema, T. J., Chlebowski, A., Dzionek, K., Nijtmans, L. G., Huynen, M. A. and Holt, I. J. (2011) 'TEFM (c17orf42) is necessary for transcription of human mtDNA', *Nucleic Acids Res*, 39(10), pp. 4284-99.

Montoya, J., Christianson, T., Levens, D., Rabinowitz, M. and Attardi, G. (1982) 'Identification of initiation sites for heavy-strand and light-strand transcription in human mitochondrial DNA', *Proc Natl Acad Sci U S A*, 79(23), pp. 7195-9.

Mootha, V. K., Lepage, P., Miller, K., Bunkenborg, J., Reich, M., Hjerrild, M., Delmonte, T., Villeneuve, A., Sladek, R., Xu, F., Mitchell, G. A., Morin, C., Mann, M., Hudson, T. J., Robinson, B., Rioux, J. D. and Lander, E. S. (2003) 'Identification of a gene causing human cytochrome c oxidase deficiency by integrative genomics', *Proc Natl Acad Sci U S A*, 100(2), pp. 605-10.

Moraes, C. T., DiMauro, S., Zeviani, M., Lombes, A., Shanske, S., Miranda, A. F., Nakase, H., Bonilla, E., Werneck, L. C., Servidei, S. and et al. (1989) 'Mitochondrial DNA deletions in progressive external ophthalmoplegia and Kearns-Sayre syndrome', *N Engl J Med*, 320(20), pp. 1293-9.

Mullen, T. E. and Marzluff, W. F. (2008) 'Degradation of histone mRNA requires oligouridylation followed by decapping and simultaneous degradation of the mRNA both 5' to 3' and 3' to 5'', *Genes Dev*, 22(1), pp. 50-65.

Nagaike, T. (2005) 'Human Mitochondrial mRNAs Are Stabilized with Polyadenylation Regulated by Mitochondria-specific Poly(A) Polymerase and Polynucleotide Phosphorylase', *Journal of Biological Chemistry*, 280(20), pp. 19721-19727.

Nagaike, T., Suzuki, T., Tomari, Y., Takemoto-Hori, C., Negayama, F., Watanabe, K. and Ueda, T. (2001) 'Identification and characterization of mammalian mitochondrial tRNA nucleotidyltransferases', *J Biol Chem*, 276(43), pp. 40041-9.

Nagaike, T., Suzuki, T. and Ueda, T. (2008) 'Polyadenylation in mammalian mitochondria: Insights from recent studies', *Biochimica et Biophysica Acta (BBA) - Gene Regulatory Mechanisms*, 1779(4), pp. 266-269.

Nagele, E., Han, M., Demarshall, C., Belinka, B. and Nagele, R. (2011) 'Diagnosis of Alzheimer's disease based on disease-specific autoantibody profiles in human sera', *PLoS One*, 6(8), p. e23112.

Noer, A. S., Sudoyo, H., Lertrit, P., Thyagarajan, D., Utthanaphol, P., Kapsa, R., Byrne, E. and Marzuki, S. (1991) 'A tRNA(Lys) mutation in the mtDNA is the causal genetic lesion underlying myoclonic epilepsy and ragged-red fiber (MERRF) syndrome', *Am J Hum Genet*, 49(4), pp. 715-22.

Nolden, M., Ehses, S., Koppen, M., Bernacchia, A., Rugarli, E. I. and Langer, T. (2005) 'The m-AAA protease defective in hereditary spastic paraplegia controls ribosome assembly in mitochondria', *Cell*, 123(2), pp. 277-89.

Ojala, D., Montoya, J. and Attardi, G. (1981) 'tRNA punctuation model of RNA processing in human mitochondria', *Nature*, 290(5806), pp. 470-474.

Osinga, K. A., De Vries, E., Van der Horst, G. and Tabak, H. F. (1984) 'Processing of yeast mitochondrial messenger RNAs at a conserved dodecamer sequence', *EMBO J*, 3(4), pp. 829-34.

Osman, C., Voelker, D. R. and Langer, T. (2011) 'Making heads or tails of phospholipids in mitochondria', *J Cell Biol*, 192(1), pp. 7-16.

Park, C. B., Asin-Cayuela, J., Camara, Y., Shi, Y., Pellegrini, M., Gaspari, M., Wibom, R., Hultenby, K., Erdjument-Bromage, H., Tempst, P., Falkenberg, M., Gustafsson, C. M. and Larsson, N. G. (2007) 'MTERF3 is a negative regulator of mammalian mtDNA transcription', *Cell*, 130(2), pp. 273-85.

Pavlakis, S. G., Phillips, P. C., DiMauro, S., De Vivo, D. C. and Rowland, L. P. (1984) 'Mitochondrial myopathy, encephalopathy, lactic acidosis, and strokelike episodes: a distinctive clinical syndrome', *Ann Neurol*, 16(4), pp. 481-8.

Piechota, J., Tomecki, R., Gewartowski, K., Szczesny, R., Dmochowska, A., Kudla, M., Dybczynska, L., Stepien, P. P. and Bartnik, E. (2006) 'Differential stability of mitochondrial mRNA in HeLa cells', *Acta Biochim Pol*, 53(1), pp. 157-68.

Rabilloud, T., Kieffer, S., Procaccio, V., Louwagie, M., Courchesne, P. L., Patterson, S. D., Martinez, P., Garin, J. and Lunardi, J. (1998) 'Two-dimensional electrophoresis of human placental mitochondria and protein identification by mass spectrometry: toward a human mitochondrial proteome', *Electrophoresis*, 19(6), pp. 1006-14.

Rackham, O., Davies, S. M., Shearwood, A. M., Hamilton, K. L., Whelan, J. and Filipovska, A. (2009) 'Pentatricopeptide repeat domain protein 1 lowers the levels of mitochondrial leucine tRNAs in cells', *Nucleic Acids Res*, 37(17), pp. 5859-67.

Reyes, A., Kazak, L., Wood, S. R., Yasukawa, T., Jacobs, H. T. and Holt, I. J. (2013) 'Mitochondrial DNA replication proceeds via a 'bootlace' mechanism involving the incorporation of processed transcripts', *Nucleic Acids Res*, 41(11), pp. 5837-50.

Rodenburg, R. J. (2011) 'Biochemical diagnosis of mitochondrial disorders', *J Inherit Metab Dis*, 34(2), pp. 283-92.

Rorbach, J., Gammage, P. A. and Minczuk, M. (2012) 'C7orf30 is necessary for biogenesis of the large subunit of the mitochondrial ribosome', *Nucleic Acids Res*, 40(9), pp. 4097-109.

Rorbach, J., Nicholls, T. J. and Minczuk, M. (2011) 'PDE12 removes mitochondrial RNA poly(A) tails and controls translation in human mitochondria', *Nucleic Acids Res*, 39(17), pp. 7750-63.

Rorbach, J., Richter, R., Wessels, H. J., Wydro, M., Pekalski, M., Farhoud, M., Kuhl, I., Gaisne, M., Bonnefoy, N., Smeitink, J. A., Lightowlers, R. N. and Chrzanowska-Lightowlers, Z. M. (2008) 'The human mitochondrial ribosome recycling factor is essential for cell viability', *Nucleic Acids Res*, 36(18), pp. 5787-99.

Rossignol, R., Malgat, M., Mazat, J.-P. and Letellier, T. (1999) 'Threshold Effect and Tissue Specificity: IMPLICATION FOR MITOCHONDRIAL CYTOPATHIES', *Journal of Biological Chemistry*, 274(47), pp. 33426-33432.

Ruzzenente, B., Metodiev, M. D., Wredenberg, A., Bratic, A., Park, C. B., Camara, Y., Milenkovic, D., Zickermann, V., Wibom, R., Hultenby, K., Erdjument-Bromage, H., Tempst, P., Brandt, U., Stewart, J. B., Gustafsson, C. M. and Larsson, N. G. (2012) 'LRPPRC is necessary for polyadenylation and coordination of translation of mitochondrial mRNAs', *EMBO J*, 31(2), pp. 443-56.

Sacconi, S., Salviati, L., Nishigaki, Y., Walker, W. F., Hernandez-Rosa, E., Trevisson, E., Delplace, S., Desnuelle, C., Shanske, S., Hirano, M., Schon, E. A., Bonilla, E., De Vivo, D. C., DiMauro, S. and Davidson, M. M. (2008) 'A functionally dominant mitochondrial DNA mutation', *Hum Mol Genet*, 17(12), pp. 1814-20.

Sasarman, F., Brunel-Guitton, C., Antonicka, H., Wai, T. and Shoubridge, E. A. (2010) 'LRPPRC and SLIRP interact in a ribonucleoprotein complex that regulates posttranscriptional gene expression in mitochondria', *Mol Biol Cell*, 21(8), pp. 1315-23.

Sasarman, F. and Shoubridge, E. A. (2012) 'Radioactive labeling of mitochondrial translation products in cultured cells', *Methods Mol Biol*, 837, pp. 207-17.

Satoh, M. and Kuroiwa, T. (1991) 'Organization of multiple nucleoids and DNA molecules in mitochondria of a human cell', *Exp Cell Res*, 196(1), pp. 137-40.

Schaefer, A. M., McFarland, R., Blakely, E. L., He, L., Whittaker, R. G., Taylor, R. W., Chinnery, P. F. and Turnbull, D. M. (2008) 'Prevalence of mitochondrial DNA disease in adults', *Ann Neurol*, 63(1), pp. 35-9.

Schapira, A. H., Cooper, J. M., Dexter, D., Jenner, P., Clark, J. B. and Marsden, C. D. (1989) 'Mitochondrial complex I deficiency in Parkinson's disease', *Lancet*, 1(8649), p. 1269.

Schatz, G. (1996) 'The Protein Import System of Mitochondria', *Journal of Biological Chemistry*, 271(50), pp. 31763-31766.

Schmitz-Linneweber, C. and Small, I. (2008) 'Pentatricopeptide repeat proteins: a socket set for organelle gene expression', *Trends Plant Sci*, 13(12), pp. 663-70.

Serre, V., Rozanska, A., Beinat, M., Chretien, D., Boddaert, N., Munnich, A., Rotig, A. and Chrzanowska-Lightowlers, Z. M. (2013) 'Mutations in mitochondrial ribosomal protein MRPL12 leads to growth retardation, neurological deterioration and mitochondrial translation deficiency', *Biochim Biophys Acta*, 1832(8), pp. 1304-12.

Shadel, G. S. (2004) 'Coupling the mitochondrial transcription machinery to human disease', *Trends Genet*, 20(10), pp. 513-9.

Shadel, G. S. and Clayton, D. A. (1997) 'Mitochondrial DNA maintenance in vertebrates', *Annu Rev Biochem*, 66, pp. 409-35.

Sharma, M. R., Koc, E. C., Datta, P. P., Booth, T. M., Spremulli, L. L. and Agrawal, R. K. (2003) 'Structure of the mammalian mitochondrial ribosome reveals an expanded functional role for its component proteins', *Cell*, 115(1), pp. 97-108.

Sicheritz-Pontén, T., Kurland, C. G. and Andersson, S. G. E. (1998) 'A phylogenetic analysis of the cytochrome b and cytochrome c oxidase I genes supports an origin of mitochondria from within the Rickettsiaceae', *Biochimica et Biophysica Acta (BBA) - Bioenergetics*, 1365(3), pp. 545-551.

Slomovic, S., Laufer, D., Geiger, D. and Schuster, G. (2005) 'Polyadenylation and degradation of human mitochondrial RNA: the prokaryotic past leaves its mark', *Mol Cell Biol*, 25(15), pp. 6427-35.

Slomovic, S. and Schuster, G. (2007) 'Stable PNPase RNAi silencing: Its effect on the processing and adenylation of human mitochondrial RNA', *Rna*, 14(2), pp. 310-323.

Small, I. D. and Peeters, N. (2000) 'The PPR motif - a TPR-related motif prevalent in plant organellar proteins', *Trends Biochem Sci*, 25(2), pp. 46-7.

Soleimanpour-Lichaei, H. R., Kuhl, I., Gaisne, M., Passos, J. F., Wydro, M., Rorbach, J., Temperley, R., Bonnefoy, N., Tate, W., Lightowlers, R. and Chrzanowska-Lightowlers, Z. (2007) 'mtRF1a is a human mitochondrial translation release factor decoding the major termination codons UAA and UAG', *Mol Cell*, 27(5), pp. 745-57.

Soll, J. and Schleiff, E. (2004) 'Protein import into chloroplasts', *Nat Rev Mol Cell Biol*, 5(3), pp. 198-208.

Su, W., Slepenkov, S. V., Slevin, M. K., Lyons, S. M., Ziemniak, M., Kowalska, J., Darzynkiewicz, E., Jemielity, J., Marzluff, W. F. and Rhoads, R. E. (2013) 'mRNAs containing the histone 3' stem-loop are degraded primarily by decapping mediated by oligouridylation of the 3' end', *Rna*, 19(1), pp. 1-16.

Swerdlow, R. H., Burns, J. M. and Khan, S. M. (2010) 'The Alzheimer's disease mitochondrial cascade hypothesis', *J Alzheimers Dis*, 20 Suppl 2, pp. S265-79.

Szczesny, R. J., Borowski, L. S., Brzezniak, L. K., Dmochowska, A., Gewartowski, K., Bartnik, E. and Stepien, P. P. (2010) 'Human mitochondrial RNA turnover caught in flagranti: involvement of hSuv3p helicase in RNA surveillance', *Nucleic Acids Res*, 38(1), pp. 279-98.

Szklarczyk, R. and Huynen, M. A. (2010) 'Mosaic origin of the mitochondrial proteome', *Proteomics*, 10(22), pp. 4012-24.

Taylor, S. W., Fahy, E., Zhang, B., Glenn, G. M., Warnock, D. E., Wiley, S., Murphy, A. N., Gaucher, S. P., Capaldi, R. A., Gibson, B. W. and Ghosh, S. S. (2003)

'Characterization of the human heart mitochondrial proteome', *Nat Biotechnol*, 21(3), pp. 281-6.

Temperley, R. (2003) 'Investigation of a pathogenic mtDNA microdeletion reveals a translation-dependent deadenylation decay pathway in human mitochondria', *Human Molecular Genetics*, 12(18), pp. 2341-2348.

Temperley, R., Richter, R., Dennerlein, S., Lightowlers, R. N. and Chrzanowska-Lightowlers, Z. M. (2010a) 'Hungry Codons Promote Frameshifting in Human Mitochondrial Ribosomes', *Science*, 327(5963), p. 301.

Temperley, R., Wydro, M., Lightowlers, R. N. and Chrzanowska-Lightowlers, Z. M. (2010b) 'Human mitochondrial mRNAs--like members of all families, similar but different', *Biochim Biophys Acta*, 1797(6-7), pp. 1081-5.

Tomecki, R. (2004) 'Identification of a novel human nuclear-encoded mitochondrial poly(A) polymerase', *Nucleic Acids Research*, 32(20), pp. 6001-6014.

Towpik, J. (2005) 'Regulation of mitochondrial translation in yeast', *Cell Mol Biol Lett*, 10(4), pp. 571-94.

Tsaousis, A. D., Kunji, E. R., Goldberg, A. V., Lucocq, J. M., Hirt, R. P. and Embley, T. M. (2008) 'A novel route for ATP acquisition by the remnant mitochondria of Encephalitozoon cuniculi', *Nature*, 453(7194), pp. 553-6.

Tsuboi, M., Morita, H., Nozaki, Y., Akama, K., Ueda, T., Ito, K., Nierhaus, K. H. and Takeuchi, N. (2009) 'EF-G2mt is an exclusive recycling factor in mammalian mitochondrial protein synthesis', *Mol Cell*, 35(4), pp. 502-10.

van Meer, G., Voelker, D. R. and Feigenson, G. W. (2008) 'Membrane lipids: where they are and how they behave', *Nat Rev Mol Cell Biol*, 9(2), pp. 112-24.

Veltri, K. L., Espiritu, M. and Singh, G. (1990) 'Distinct genomic copy number in mitochondria of different mammalian organs', *Journal of Cellular Physiology*, 143(1), pp. 160-164.

von Heijne, G. (1986) 'Why mitochondria need a genome', *FEBS Lett*, 198(1), pp. 1-4.

Wang, D. D., Shu, Z., Lieser, S. A., Chen, P. L. and Lee, W. H. (2009) 'Human mitochondrial SUV3 and polynucleotide phosphorylase form a 330-kDa heteropentamer to cooperatively degrade double-stranded RNA with a 3'-to-5' directionality', *J Biol Chem*, 284(31), pp. 20812-21.

Wang, Z., Cotney, J. and Shadel, G. S. (2007) 'Human mitochondrial ribosomal protein MRPL12 interacts directly with mitochondrial RNA polymerase to modulate mitochondrial gene expression', *J Biol Chem*, 282(17), pp. 12610-8.

Wanrooij, P. H., Uhler, J. P., Simonsson, T., Falkenberg, M. and Gustafsson, C. M. (2010) 'G-quadruplex structures in RNA stimulate mitochondrial transcription termination and primer formation', *Proc Natl Acad Sci U S A*, 107(37), pp. 16072-7.

Wanschers, B. F., Szklarczyk, R., Pajak, A., van den Brand, M. A., Gloerich, J., Rodenburg, R. J., Lightowlers, R. N., Nijtmans, L. G. and Huynen, M. A. (2012) 'C7orf30 specifically associates with the large subunit of the mitochondrial ribosome and is involved in translation', *Nucleic Acids Res*.

Warburg, O. (1956) 'On the origin of cancer cells', *Science*, 123(3191), pp. 309-14.

Wells, J., Henkler, F., Leversha, M. and Koshy, R. (1995) 'A mitochondrial elongation factor-like protein is over-expressed in tumours and differentially expressed in normal tissues', *FEBS Lett*, 358(2), pp. 119-25.

Wenz, T., Luca, C., Torraco, A. and Moraes, C. T. (2009) 'mTERF2 regulates oxidative phosphorylation by modulating mtDNA transcription', *Cell Metab*, 9(6), pp. 499-511.

Weraarpachai, W., Antonicka, H., Sasarman, F., Seeger, J., Schrank, B., Kolesar, J. E., Lochmuller, H., Chevrette, M., Kaufman, B. A., Horvath, R. and Shoubridge, E. A. (2009) 'Mutation in TACO1, encoding a translational activator of COX I, results in cytochrome c oxidase deficiency and late-onset Leigh syndrome', *Nat Genet*, 41(7), pp. 833-7.

Williams, H. G., Benstead, J., Frischer, M. E. and Paul, J. H. (1997) 'Alteration in plasmid DNA following natural transformation to populations of marine bacteria', *Mol Mar Biol Biotechnol*, 6(3), pp. 238-47.

Wydro, M., Bobrowicz, A., Temperley, R. J., Lightowlers, R. N. and Chrzanowska-Lightowlers, Z. M. (2010) 'Targeting of the cytosolic poly(A) binding protein PABPC1 to mitochondria causes mitochondrial translation inhibition', *Nucleic Acids Res*, 38(11), pp. 3732-42.

Xin, H., Woriax, V., Burkhart, W. and Spremulli, L. L. (1995) 'Cloning and expression of mitochondrial translational elongation factor Ts from bovine and human liver', *J Biol Chem*, 270(29), pp. 17243-9.

Xu, F., Ackerley, C., Maj, M. C., Addis, J. B., Levandovskiy, V., Lee, J., Mackay, N., Cameron, J. M. and Robinson, B. H. (2008) 'Disruption of a mitochondrial RNA-binding protein gene results in decreased cytochrome b expression and a marked reduction in ubiquinol-cytochrome c reductase activity in mouse heart mitochondria', *Biochem J*, 416(1), pp. 15-26.

Xu, F., Addis, J. B., Cameron, J. M. and Robinson, B. H. (2012) 'LRPPRC mutation suppresses cytochrome oxidase activity by altering mitochondrial RNA transcript stability in a mouse model', *Biochem J*, 441(1), pp. 275-83.

Xu, F. and Cohen, S. N. (1995) 'RNA degradation in Escherichia coli regulated by 3' adenylation and 5' phosphorylation', *Nature*, 374(6518), pp. 180-3.

Yasukawa, T., Reyes, A., Cluett, T. J., Yang, M. Y., Bowmaker, M., Jacobs, H. T. and Holt, I. J. (2006) 'Replication of vertebrate mitochondrial DNA entails transient ribonucleotide incorporation throughout the lagging strand', *EMBO J*, 25(22), pp. 5358-71.

Ziebarth, T. D., Gonzalez-Soltero, R., Makowska-Grzyska, M. M., Nunez-Ramirez, R., Carazo, J. M. and Kaguni, L. S. (2010) 'Dynamic effects of cofactors and DNA on the oligomeric state of human mitochondrial DNA helicase', *J Biol Chem*, 285(19), pp. 14639-47.

Appendices

Appendix A:

Additional *in vitro* polyadenylation time courses

I.

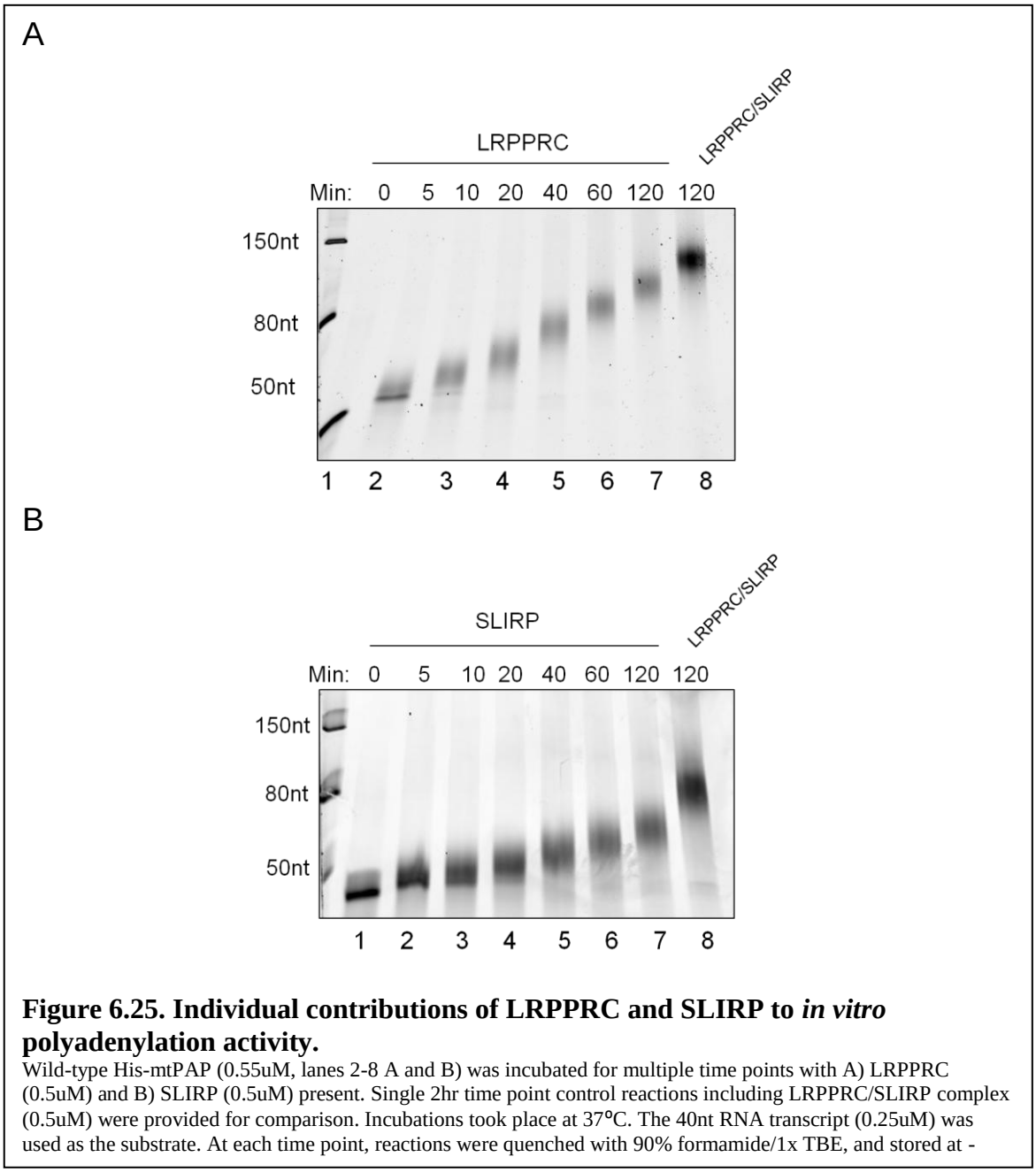

Figure 6.25. Individual contributions of LRPPRC and SLIRP to *in vitro* polyadenylation activity.

Wild-type His-mtPAP (0.55uM, lanes 2-8 A and B) was incubated for multiple time points with A) LRPPRC (0.5uM) and B) SLIRP (0.5uM) present. Single 2hr time point control reactions including LRPPRC/SLIRP complex (0.5uM) were provided for comparison. Incubations took place at 37°C. The 40nt RNA transcript (0.25uM) was used as the substrate. At each time point, reactions were quenched with 90% formamide/1x TBE, and stored at -

II.

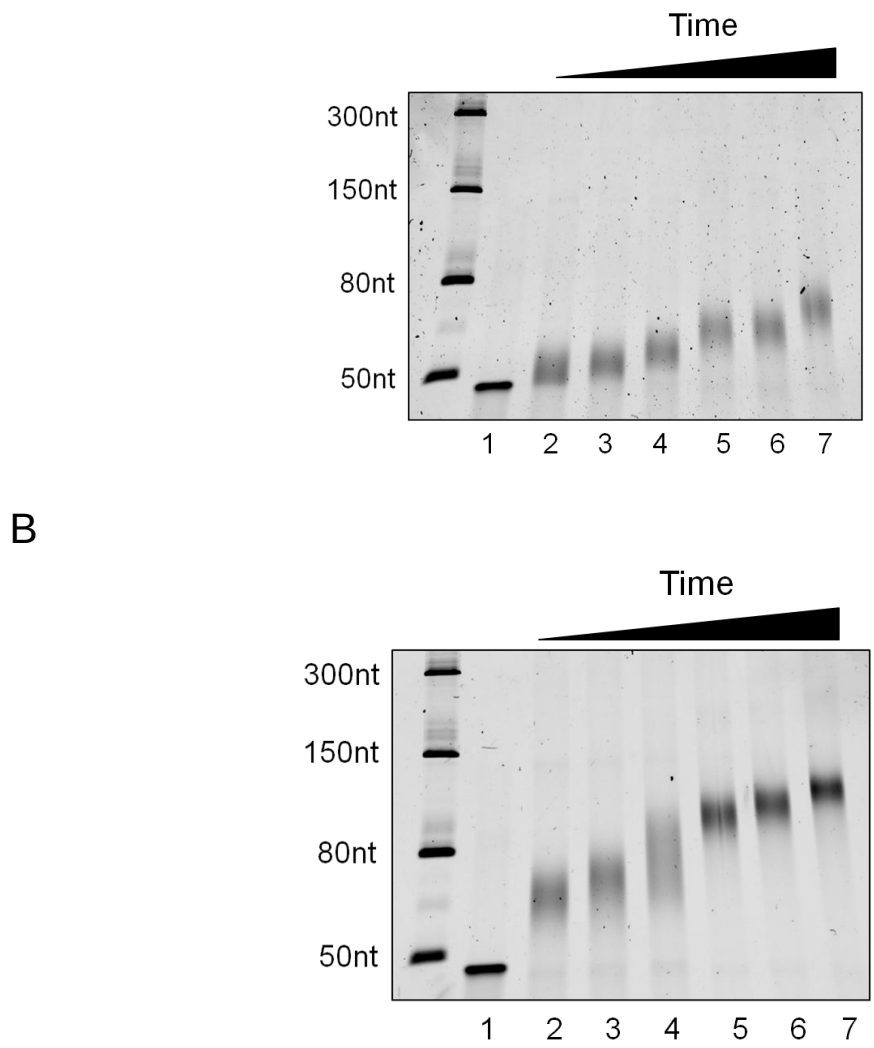

Figure 6.26. Polyadenylation time courses using oligo(A) RNA substrate.
Wild-type His-mtPAP (0.55uM) was incubated for the same time points as in Figure 6.24 without (A) and with (B) LRPPRC/SLIRP complex (0.5uM) present. Oligoadenylated 48nt RNA substrate was present at 0.25uM. Incubations took place at 37°C. At each time point (0 to 120min), reactions were quenched with 90% formamide/1x TBE, and stored at -20°C. Samples were later thawed, then separated through a 15% polyacrylamide/8.3M urea gel, and stained with SYBR gold. Stained products were visualized by scanning with a Typhoon FLA 9500 instrument.

Appendix B

I.

pcDNA™5/FRT/TO Vector

Map of pcDNA™5/FRT/TO

The figure below summarizes the features of the pcDNA™5/FRT/TO vector. Note that the hygromycin resistance gene lacks a promoter and its native ATG start codon. Transfection of the pcDNA™5/FRT/TO plasmid alone into mammalian cells will **not** confer hygromycin resistance to the cells. **The complete nucleotide sequence for pcDNA™5/FRT/TO is available for downloading from www.invitrogen.com or by contacting Technical Support (see page 12).**

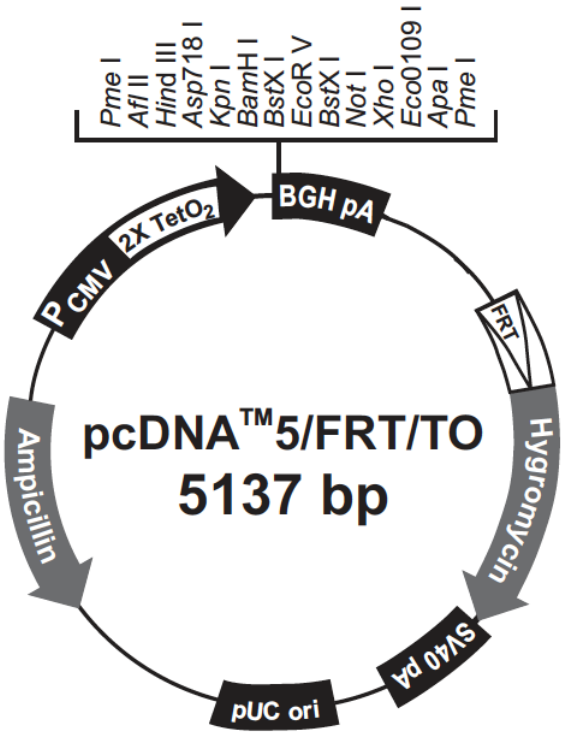

Comments for pcDNA™5/FRT/TO
5137 nucleotides

CMV promoter: bases 232-958
TATA box: bases 804-810
Tetracycline operator (2X $TetO_2$) sequences: bases 820-859
CMV forward priming site: bases 769-789
Multiple cloning site: bases 968-1077
BGH reverse priming site: bases 1089-1106
BGH polyadenylation signal: bases 1095-1319
FRT site: bases 1603-1650
Hygromycin resistance gene (no ATG): bases 1658-2678
SV40 early polyadenylation signal: bases 2810-2940
pUC origin: bases 3323-3996 (complementary strand)
bla promoter: bases 5002-5100 (complementary strand)
Ampicillin (*bla*) resistance gene: bases 4141-5001 (complementary strand)

II.

pcDNA™6/TR

Map of pcDNA™6/TR

The figure below summarizes the features of the pcDNA™6/TRvector. **The sequence of pcDNA™6/TR is available for downloading from our website site (www.invitrogen.com) or from Technical Support (see page 10).** See the next page for a description of the features of the vector.

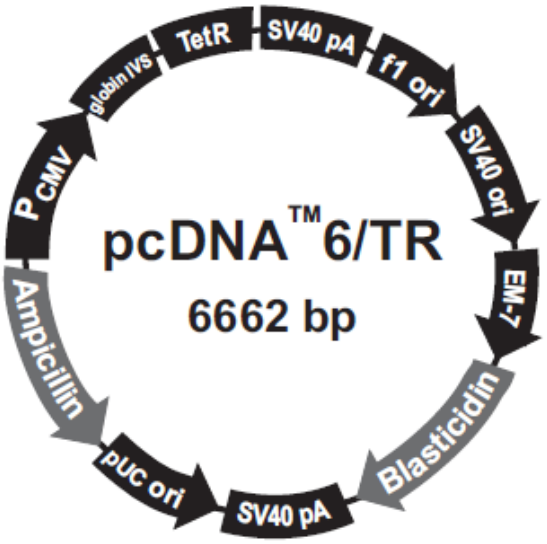

Comments for pcDNA™6/TR
6662 nucleotides

CMV promoter: bases 232-819
Rabbit β-globin intron II (IVS): bases 1028-1600
TetR gene: bases 1684-2340
SV40 early polyadenylation sequence: bases 2346-2477
f1 origin: bases 2897-3325
SV40 promoter and origin: bases 3335-3675
EM-7 promoter: bases 3715-3781
Blasticidin resistance gene: bases 3782-4180
SV40 early polyadenylation sequence: bases 4338-4468
pUC origin: bases 4851-5521
bla promoter: bases 6521-6625 (complementary strand)
Ampicillin (*bla*) resistance gene: bases 5666-6526 (complementary strand)

III.

Lentiviral vector backbone, with *PAPD1* (accession number: NM_018109.1) cloned in (Cat #: LP-W1687-Lv121, Lot #: GC10312K1105).

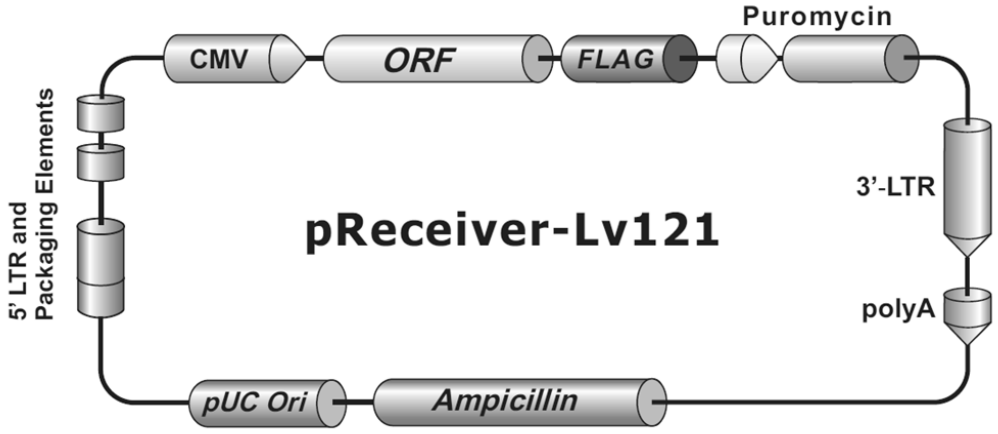

IV.

pET-28a-c(+) Vectors

TB074 12/98

	Cat. No.
pET-28a DNA	69864-3
pET-28b DNA	69865-3
pET-28c DNA	69866-3

The pET-28a-c(+) vectors carry an N-terminal His•Tag®/thrombin/T7•Tag® configuration plus an optional C-terminal His•Tag sequence. Unique sites are shown on the circle map. Note that the sequence is numbered by the pBR322 convention, so the T7 expression region is reversed on the circular map. The cloning/expression region of the coding strand transcribed by T7 RNA polymerase is shown below. The f1 origin is oriented so that infection with helper phage will produce virions containing single-stranded DNA that corresponds to the coding strand. Therefore, single-stranded sequencing should be performed using the T7 terminator primer (Cat. No. 69337-3).

pET-28a(+) sequence landmarks	
T7 promoter	370-386
T7 transcription start	369
His•Tag coding sequence	270-287
T7•Tag coding sequence	207-239
Multiple cloning sites	
(*Bam*H I - *Xho* I)	158-203
His•Tag coding sequence	140-157
T7 terminator	26-72
lacI coding sequence	773-1852
pBR322 origin	3286
Kan coding sequence	3995-4807
f1 origin	4903-5358

The maps for pET-28b(+) and pET-28c(+) are the same as pET-28a(+) (shown) with the following exceptions: pET-28b(+) is a 5368bp plasmid; subtract 1bp from each site beyond *Bam*H I at 198. pET-28c(+) is a 5367bp plasmid; subtract 2bp from each site beyond *Bam*H I at 198.

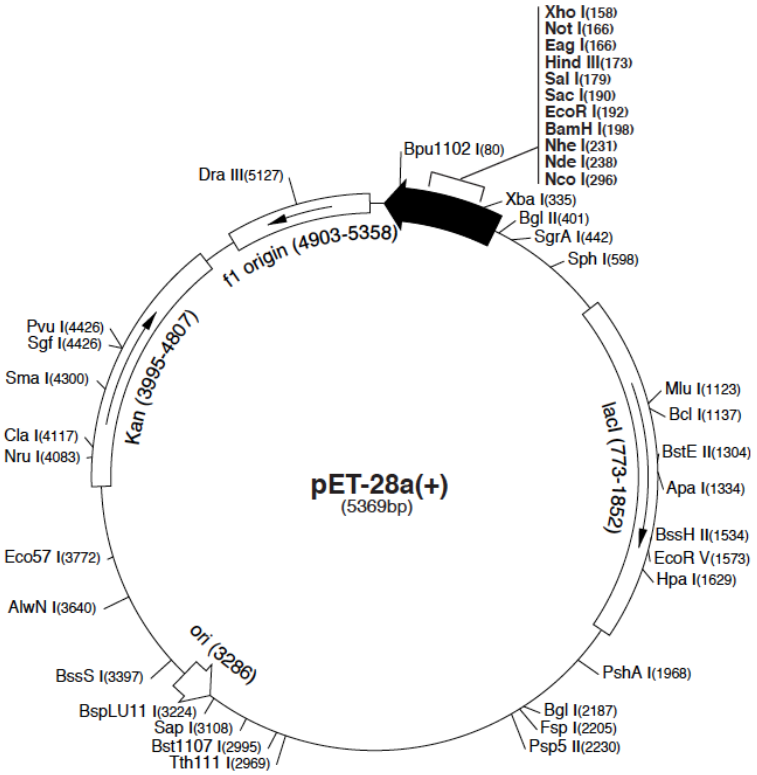

pET-28a-c(+) cloning/expression region

V.

pOG44 Vector

Map of pOG44

pOG44 is a 5785 bp vector that expresses a temperature-sensitive Flp recombinase (flp-F70L) under the control of the human CMV promoter as previously described (O'Gorman *et al.*, 1991). The vector contains a synthetic intron to enhance expression of the *FLP* gene. Note that the vector does not contain an antibiotic resistance marker to allow stable selection in mammalian cells. The following figure summarizes the features of the pOG44 vector. **The sequence for pOG44 is available from www.lifetechnologies.com or by contacting Technical Support (see page 9).**

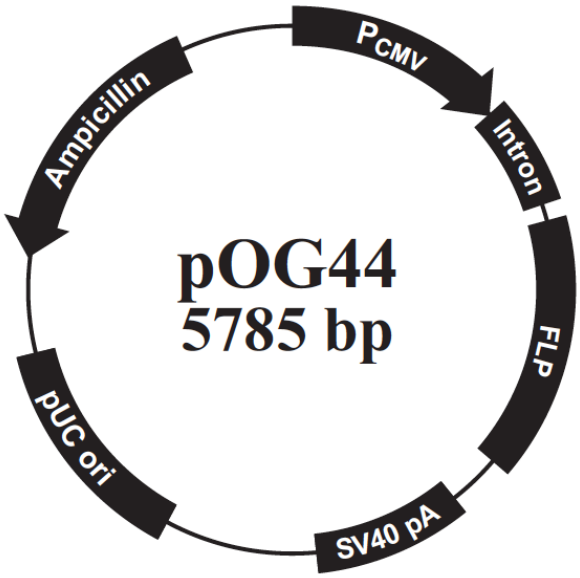

Comments for pOG44
5785 nucleotides

CMV promoter: bases 234-821
Synthetic intron: bases 871-1175
FLP ORF: bases 1202-2473
SV40 late polyadenylation signal: bases 2597-2732
pUC origin: bases 3327-3993 (complementary strand)
bla promoter: bases 4999-5097 (complementary strand)
Ampicillin (*bla*) resistance gene: bases 4138-4998 (complementary strand)

Appendix C

MTCO1 MPAT results pre and post WT *PAPD1* expression

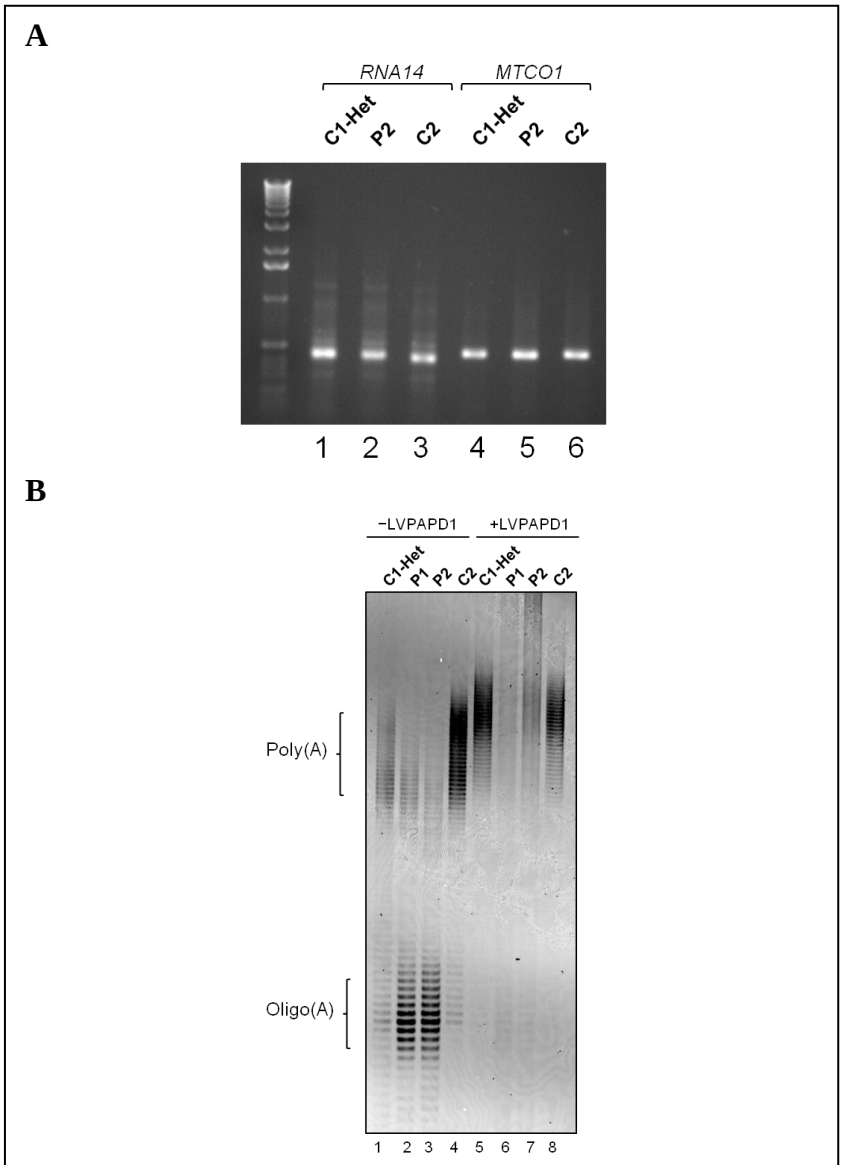

MTCO1* MPAT results pre and post expression of WT *PAPD1

A. Initial gene-specific PCR results for*RNA14* and *MTCO1*. **B.** Results of the *MTCO1* MPAT analysis performed on RNA extracted from fibroblasts pre and post treatment with LVPAPD1.